DISS. ETH NO. 27518

Globally Consistent Assessment of Climate-related Physical Risk.

A Conceptual Framework and its Application in Asset Valuation

A thesis submitted to attain the degree of

DOCTOR OF SCIENCES of ETH (Dr. sc. ETH Zurich)

presented by

SAMUEL EBERENZ

MSc ETH Atmos Clim Sc, ETH ZURICH

born September 26, 1988

citizen of Germany

accepted on the recommendation of

Prof. Dr. David N. Bresch

Dr. Oliver Marchand

Dr. Katja Frieler

2021

Ice melts like words off a page

John Malloy, Jessica Noviello & Jen Walsh,

The Seasons of Research (2021)

Summary

Climate change poses increasing risks to what is valuable to humans around the globe. Changing, often intensifying, weather and climate extremes can increasingly be attributed to anthropogenic climate change, and change is projected to accelerate throughout the 21st century. Against this backdrop, risk awareness is growing across sectors and so is the demand for research and tools supporting efforts to mitigate climate change and adapt to its adverse consequences. Over the past decades, more and more global-scale climate impact data and models have become available, including archives of reported disaster impacts, storm track datasets, and global gridded crop models simulating yield responses to climate variables. The risk modeling platform CLIMate ADAptation (CLIMADA), implemented in the programming language Python, provides a modular open-source and -access platform for the probabilistic, event-based assessment of climate-related impact and risk. The underlying conceptual framework describes risk as a function of hazard, exposure, and vulnerability. Hazard is represented by the intensity and frequency of weather and climate events. Exposures constitute the presence of people, ecosystems, or assets that can be affected by a hazard. Vulnerability, implemented in CLIMADA in the form of 'impact functions', relates hazard intensity to the degrees of damage experienced by the respective type of exposure. CLIMADA is a growing modeling platform, and the three studies in this thesis aim to bring it to global consistency. The studies constituting this thesis were conducted within a joint research and development project with an implementing partner in the financial sector applying the results directly for forward-looking asset valuation. The main objective of this collaboration was to develop, evaluate, and implement climate risk modeling configurations with a global scope for the assessment of physical climate impacts and related economic risk. The implementing partner has not only integrated the model components as developed in the present thesis, engagement with academia also helped him to design and implement a more consistent risk assessment framework well beyond the scope if this collaboration. In Chapter One of this thesis, both the applied and scientific context of the project are introduced, providing insight in the conceptual framework and its application.

Chapter Two enables the spatially explicit modeling of direct impacts to economic assets by providing a globally consistent asset value exposure layer. The method proposed and implemented makes use of the spatial correlation of economic activity and asset values in a country with both nightlight intensity and population density. The so-called LitPop ('[night] Li[gh]t Population') method combines satellite-based nightlight data and population data to disaggregate country-level asset value estimates to a sub-national high-resolution grid. The disaggregation skill is evaluated both quantitatively and qualitatively, comparing varying weights for nightlight

intensity and population count. A global gridded data set of disaggregated asset values in US dollars for the year 2014 is provided alongside the paper at a resolution of 30 arcsec (approx. 1 km globally).

In Chapter Three, LitPop exposure data is combined with a hazard set based on track data of hundreds of historical tropical cyclones (TCs) that made landfall in 53 countries between 1980 and 2017. The objective of the study is the calibration of the vulnerability component for TC risk modeling. For this purpose, wind speed footprints are modeled for each TC event. This allows the fitting of regional impact functions by comparing simulated with reported damage values for 473 reported events matched to individual TC tracks. Chapter Three is concluded with an explorative case study of TC damage in the Philippines, where the calibration comes with a large spread in fitted impact function parameters.

With Chapter Four, attention is shifted from TC impacts to a sectoral risk perspective, for a global, country-level assessment of historical and twenty-first century risk to crop production. This study is based on global gridded crop yield simulations for maize, rice, soybean, and wheat. It uses an unprecedented ensemble of transient yield simulation output from eight global gridded crop models driven by bias-corrected output from five global climate models, as facilitated by the Inter-Sectoral Impact Model Intercomparison Project (ISIMIP). Applying two complementary risk metrics, crop yield simulations are used to calculate the annual probability of projected crop production falling short of a given threshold, by country. Country-specific 21st century crop production risk is assessed by comparing these probabilities for historical and future levels of global warming, considering model agreement as a measure of robustness.

The three main chapters are followed by a summary of key findings: quantitative estimates of exposure value distribution, TC vulnerability, and crop production risk per country. This is followed by discussions of the cascading uncertainties intrinsic to complex risk modeling chains, and practical implications of the thesis within the context of the joint research and development project as well as beyond. To make the resulting data and tools available for research and application – also beyond the scope of this project – the work in this thesis pays special attention to using scientific data and tools licensed for both academic and commercial use. At the same time, methods developed here are published open-source and -access, both as part of the CLIMADA repository and as peer-reviewed research papers. As for an outlook, future research is proposed with the potential to mitigate some of the entailed uncertainties, expand TC risk modeling from historical to future risk, and build on the findings presented here, further integrating output from climate and impact models in the probabilistic risk modeling framework of CLIMADA for globally consistent multi-hazard climate risk modeling.

Zusammenfassung

Der Klimawandel stellt eine zunehmende weltweite Bedrohung für Umwelt und Mensch dar. Veränderungen der Intensität und Häufigkeit von Wetter- und Klimaextreme können bereits heute vermehrt auf den anthropogenen Klimawandel zurückgeführt werden und es wird prognostiziert, dass sich der Wandel im Laufe des 21. Jahrhunderts weiter beschleunigen wird. Vor diesem Hintergrund wächst auch das Bewusstsein für die Risiken des Klimawandels in Wissenschaft, Politik und Wirtschaft. Mit der zunehmenden Dringlichkeit und dem Ruf nach effektivem Klimaschutz sowie Anpassung an die negativen Folgen des Klimawandels steigt auch der Bedarf nach angewandter Forschung und Entwicklung in dem Gebiet. In den letzten Jahrzehnten sind mehr und mehr Daten und computergestützte Modelle zur Quantifizierung von Klimafolgen auf globaler Ebene verfügbar geworden, darunter etwa Archive mit gemeldeten Schäden durch Naturkatastrophen, Daten zu Verlauf und Intensität tropischer Stürme, und global gerasterte landwirtschaftliche Ertragsmodelle, welche die Auswirkungen von Klimavariablen auf den Anbau von Getreide und Sojabohnen simulieren. Die Risikomodellierungsplattform CLIMADA (CLIMate ADAptation), implementiert in der Programmiersprache Python, bietet eine modulare open-source und -access Plattform für die probabilistische, ereignisbasierte Bewertung von wetter- und klimabedingten Auswirkungen und Risiken. Der zugrundeliegende konzeptionelle Rahmen beschreibt Risiko als eine Funktion von Gefährdung (hazard), Exposition (exposure) und Verwundbarkeit (vulnerability). Die Gefährdung wird dabei durch die Intensität und Häufigkeit von Wetter- und Klimaereignissen repräsentiert. Die Exposition stellt das Vorhandensein von Bevölkerung, Ökosystemen oder Vermögenswerten dar, die von einer Gefahr betroffen sein können. Die Vulnerabilität, die in CLIMADA in Form von Schadensfunktionen (impact functions) implementiert ist, setzt die Intensität der Gefährdung mit dem Grad des Schadens in Beziehung, welchen die jeweilige Art der Exposition erfährt, wenn sie von einer Naturkatastrophe betroffen ist. Die drei hier vorgestellten wissenschaftlichen Studien leisten einen Beitrag dazu, relevante klimabezogene Naturgefahren in CLIMADA globale konsistent abzubilden und Risiken zu quantifizieren. Die Studien wurden im Rahmen eines Innovationsprojekts gemeinsam mit einem Implementierungspartner aus dem Finanzsektor durchgeführt, der die Ergebnisse direkt in seiner Finanzmodellierung anwendet. Das Hauptziel dieser Zusammenarbeit ist die Entwicklung, Evaluierung und Implementierung von Klimarisikomodellen für die Bewertung weltweiter physischer Klimaauswirkungen und dem damit verbundenen wirtschaftlichen Risiko. Im ersten Kapitel dieser Arbeit stelle ich sowohl den angewandten als auch den wissenschaftlichen Kontext der Doktorarbeit vor und gebe einen Einblick in den

konzeptionellen Rahmen, die verwendeten Daten und Modelle, sowie deren Anwendung.

Im zweiten Kapitel wird die räumlich explizite Berechnung eines global konsistenten, hochaufgelösten Expositionsdatensatzes beschrieben. Die sogenannte LitPop-Methode nutzt die räumliche Korrelation von wirtschaftlichen Aktivitäten und Vermögenswerten in einem Land mit der von Satelliten aufgezeichneten Helligkeit nächtlicher Beleuchtung und der Bevölkerungsdichte. Die Methode kombiniert satellitengestützte Nachtlicht- und Bevölkerungsdaten, um Vermögenswertschätzungen auf Länderebene auf ein subnationales hochauflösendes Raster zu disaggregieren. Die Qualität der Disaggregation wird sowohl quantitativ als auch qualitativ evaluiert, indem unterschiedliche Gewichtungen für die Nachtlichtintensität und die Bevölkerungsdichte verglichen werden. Neben der Methode wird ein globaler gerasterter Datensatz mit disaggregierten Vermögenswerten in US-Dollar für das Jahr 2014 mit einer Auflösung von 30 Bogensekunden (ca. 1 km global) öffentlich zur Verfügung gestellt.

In Kapitel Drei werden die LitPop-Expositionsdaten mit einem Gefährdungsdatensatz kombiniert, der auf Sturmdaten von Hunderten tropischen Wirbelstürme (TCs) basiert, die zwischen 1980 und 2017 in 53 Ländern auf Land getroffen sind und Schaden angerichtet haben. Das Ziel der Studie ist die Kalibrierung der Vulnerabilitätskomponente für die ereignisbasierte TC-Risikomodellierung mit CLIMADA. Zu diesem Zweck wurden Fussabdrücke der maximalen Windgeschwindigkeit für jeden Sturm modelliert. Dies ermöglicht das Anpassen regionaler Schadensfunktionen im Vergleich simulierter zu gemeldeten Schadenswerten für 473 Ereignisse, die einzelnen Stürmen zugeordnet sind. Das Kapitel wird mit einer explorativen Fallstudie zu Taifun-Schäden auf den Philippinen abgerundet, anhand derer die grosse Streuung der kalibrierten Schadensfunktionen diskutiert wird.

Im vierten Kapitel verlagert sich der Fokus weg von den Folgen tropischer Stürme hin zu einer sektoralen Risikoperspektive. Ziel der Studie ist eine globale Bewertung der Risiken für die landwirtschaftliche Produktion auf Länderebene im 21. Jahrhundert. Diese Studie basiert auf globalen gittergestützten Ertragssimulationen für Mais, Reis, Soja und Weizen. Sie verwendet ein neues Ensemble von acht globalen gitterbasierten Erntemodellen, die mit Klimadaten von fünf globalen Klimamodellen angetrieben werden. Dieses Ensemble entstand im Rahmen des Inter-Sectoral Impact Model Intercomparison Projects, Runde 3b (ISIMIP3b). Das länderspezifische Ernterisiko im 21. Jahrhunderts wird durch den Vergleich der Wahrscheinlichkeit von Ernteausfällen für historische und zukünftige Niveaus der globalen Durchschnittstemperatur evaluiert, wobei die Übereinstimmung zwischen den einzelnen landwirtschaftlichen Modellen als Mass für die Robustheit der Ergebnisse herangezogen wird.

Auf die drei Hauptkapitel folgt eine Zusammenfassung der wichtigsten Ergebnisse, gefolgt von Diskussion von Unsicherheiten und Limitierungen, sowie praktischer Implikationen der Doktorarbeit im Rahmen des angewandten Forschungs- und Entwicklungsprojekts – und darüber hinaus. Um die resultierenden Daten und auch über den Rahmen dieses Projekts hinaus verfügbar zu machen, liegt ein besonderer Fokus dieser Arbeit darauf, dass vorrangig wissenschaftliche Daten und Methoden verwendet werden, die sowohl für die akademische als auch für die kommerzielle Nutzung lizenziert sind. Ausserdem werden die hier entwickelten Methoden open-source und -access veröffentlicht, sowohl in wissenschaftlichen Publikationen als auch online als Teil des CLIMADA-Repository.

Publications

This thesis includes two published peer-reviewed articles and one manuscript in preparation:

Chapter 2: Eberenz, Samuel, Dario Stocker, Thomas Röösli, and David N. Bresch. **Asset Exposure Data for Global Physical Risk Assessment**. *Earth System Science Data* 12, no. 2 (April 9, 2020): 817–33. DOI: 10.5194/essd-12-817-2020.

Chapter 3: Eberenz, Samuel, Samuel Lüthi, and David N. Bresch. **Regional Tropical Cyclone Impact Functions for Globally Consistent Risk Assessments**. *Natural Hazards and Earth System Sciences* 21, no. 1 (January 29, 2021): 393–415. DOI: 10.5194/nhess-21-393-2021.

Chapter 4: Eberenz, Samuel, Carmen Steinmann, Jonas Jägermeyr, Wim Thiery, and David N. Bresch. **Complementary metrics pivotal in assessing 21st century crop production risk**, *in preparation.*

As lead author in all these papers I defined the research questions and objectives, led the code development and data analysis; as well as wrote and revised the manuscripts throughout the peer-review process. Both thesis supervisors and co-authors provided guidance, support, technical contributions, and feedback throughout this process.

Contents

Acknowledgements

My gratitude goes to all those who made this thesis and the work leading to it possible. It was David N. Bresch and Oliver Marchand, both now examiners of this thesis, who engaged with me and the idea for this dissertation and supported me in writing the initial funding proposal. Katja Frieler introduced me to the ISIMIP project and accepted to become the external examiner. I am grateful for the contributions by my co-authors Dario Stocker, Thomas Röösli, Samuel Lüthi, Carmen Steinmann, Wim Thiery, Jonas Jägermeyr, and David, for their support navigating in an interdisciplinary research field throughout the process of writing and revising our publications. Juli, Chris, Thomas, Malu, Simona, and David proofread parts of the manuscript with great patience and accuracy. Simona also kept me up to date with tropical cyclone literature. Stef and Nando advised me on formatting and layout of the manuscript.

For more than three years, I have always felt at home in the Weather and Climate Risk research group at ETH Zürich, thanks to the wonderful persons sharing much more than just office space with me, namely Adrian, Alessio, Alice, Arun, Beni, Benoît, Bin Bin, Carmen, Chahan, Chris, Christian, Clémence, Danny, Dario, Ediz, Eveyln, Franzi, Gabriela, Gregor, Inga, Ingo, Jamie, Jan, Jan, Kaspar, Laura, Mannie, Luise, Marie, Marius, Maurice, Olivier, Qinhan, Rachel, Sam, Sarah, Simona, Theresa, Thessa, Ursula, Valentina, Veronica, and Zélie. Particular thanks go to Sarah and Sandro for their competence and patience with regard to administrative and technical challenges. I also want to thank Gabriela for bearing with me when I learnt my first words in Python. Carmen supported me with great skill and patience when building a whole data analysis module in that language together. Starting in early 2020, Thomas and I have cultivated a weekly exchange during shared walks, both live and per telephone, throughout the ups and downs of paper writing, peer-review processes, and life in the pandemic. What quickly became a tradition, provided me with inspiration, reflection, and foothold throughout the last year of my doctorate.

My gratitude also goes to everyone at Carbon Delta for their open, warm, and welcoming attitude towards me and the collaboration – I'd like to mention especially those I have had the pleasure engaging with directly: Andrew, Anja, Asli, Boris, Caroline, David, David, Elke, Josip, Justin, Kerstin, Olli, Patric, Pedro, Phanos, Roman, Saijai, Sara, Stefan, and Zélie.

I am also deeply grateful to my family and friends who supported me in countless ways over the past years, especially Caro, Doro, Hanne, Iris, Isabel, Johannes, Julian, Karena, Lea, Lukas, Malu, Martin, Meret, Murr, Soraya, Stef, Tim, Verena, and Xenia. Without you, this thesis would not exist.

This thesis is dedicated to my niece Livia 珍

Figures

Tables

Abbreviations

AAD: annual average damage

CD: Carbon Delta AG

CLIMADA: CLImate ADAptation, a probabilistic climate and weather impact model

CMIP: Coupled Model Intercomparison Project

ΔGMT: global mean temperature (GMT) above pre-industrial levels

EDR: event damage ratio

EM-DAT: Emergency Events Database

FAO: Food and Agriculture Organization of the United Nations

GC6: Global Gridded Crop Model Intercomparison – Coupled Model Intercomparison Project round 6 (GGCMI-CMIP6)

GCM: global climate model / general circulation model

GDP: gross domestic product

GGCM: global gridded crop model

GGCMI: Global Gridded Crop Model Intercomparison

GMT: global mean temperature

GRP: gross regional product

IBTrACS: International Best Track Archive for Climate Stewardship

IPCC: Intergovernmental Panel on Climate Change

IQR: interquartile range

ISIMIP: Inter-Sectoral Impact Model Intercomparison Project

kcal: kilocalorie

LitPop: lit population (approach to disaggregate asset exposure data)

NGFS: Network for Greening the Financial System

nGRP: normalized gross domestic product

NRD: normalized reported damage

PCAF: Partnership for Carbon Accounting Financials

P: probability

P_h: probability of yearly crop production to fall short of the historical 2.5th percentile

P_r: probability of yearly crop production to fall more than 10% short of the mean

PR: probability ratio

RCM: regional climate model

RCP: Representative Concentration Pathway

RD: reported damage

RMSF: root-mean-squared fraction

T: return period

SASB: Sustainability Accounting Standards Board

SBTi: Science-Based Targets initiative

SED: simulated event damage

SSP: Shared Socioeconomic Pathway

TC: tropical cyclone

TCFD: Task Force on Climate-related Financial Disclosures

TDR: total damage ratio

UNDRR: United Nations Office for Disaster Risk Reduction

UNEPFI: United Nations Environment – Finance Initiative

UNFCCC: United Nations Framework Convention on Climate Change

WCR: Weather and Climate Risks

1. Introduction

some of the anthropoi
computerised their ancestors' theories
to a degree – or more –
making everyone look ahead
with uncertainty

anthropo-obscenity (2021)

1.1 Preamble

In 2018, the same year I began with the work for this thesis, the school strike for climate started an international protest movement, popularizing the term "climate crisis" across public and scientific discourse. The term was previously coined by Al Gore and other environmental activists in the first decade of the 21st century (Paglia, 2018). According to Paglia (2018), referring to climate change as a global crisis implies that climate change puts core values and assets of the human civilization at risk and there is an urgency to act upon it. In other words, the perception of anthropogenic climate change as a crisis is all about its consequences for humans and what is valuable to them. Discussing in full depth the diagnosis and attribution of anthropogenic climate change, as well as the urgency to mitigate greenhouse gas emissions, would go beyond the scope of this introduction. They are nonetheless the starting point for any research on climate risks and should therefore not go unmentioned. When reading recent publications in climate science, I personally enjoy comparing how the authors summarize these key questions in their introductions. My current favorite summary was crafted by Rosenzweig et al. (2017): "These key questions are now answered: climate change is happening and is being driven primarily by humans". The authors underpin this statement by referring to the "unequivocal" scientific findings assembled by the Intergovernmental Panel on Climate Change (IPCC) since the early 1990s (e.g., IPCC, 2013). Further scientific efforts have added evidence and nuance to these findings, for instance by attributing recent climatic extreme events and their impacts to climate change and its anthropogenic sources (e.g., Cramer et al., 2014; Herring et al., 2020; James et al., 2019; Otto, 2017; Hansen et al., 2016; Rosenzweig and Neofotis, 2013) and projecting that a further increase in global mean temperature will lead to more severe and wide spread impacts (e.g., Lange et al., 2020; Masson-Delmotte et al., 2018; Oppenheimer et al., 2014) as has to be expected in any complex system once excited beyond critical thresholds. This being said, the other side of climate crisis is the threat climate change poses to core values of human civilization. A threat that manifests when changing weather and climate patterns impact the lives, well-being, and livelihoods of humans, but also the socio-economic and ecological systems they value and depend upon. With this thesis, my hope is to make a small contribution to the understanding and quantification of these impacts, and contribute to the development and application of tools for the assessment of climate-related risks and how they might evolve over the 21st century. The work presented here was conducted as part of a collaboration with a company assessing climate risk in the financial sector, thriving to enable the implementing partner to render the impacts of climate change to this key sector more transparent (see Sections 1.3 and 1.5). As a joint research and development project, the project's aim was always two-fold, both to contribute to private and public efforts addressing the climate crisis. The results and methods of this study are or will be published open-access to help advance climate impact science and to make the results available both to public and private actors beyond the specific scope of this project. In the following, first an overview of the context, aim, and focus of this thesis is given with regard to the broader context (Section 1.2) and in cooperation with the project's implementing partner (1.3). Subsequently, the scientific background, including definitions, methods, and model types of climate risk modeling in general and specific for this thesis will be introduced (1.4). After that, I will provide an overview of the implementation of the outcomes from the three main studies, as well as additional data and methods used in the applied context of this project (1.5). The three papers constituting the main body of the thesis are found in Chapters Two to Four, followed by discussion and outlook.

1.2 Climate change in the financial sector

> *"In the past year, people have seen the mounting physical toll of climate change in fires, droughts, flooding and hurricanes. They have begun to see the direct financial impact as energy companies take billions in climate-related write-downs on stranded assets and regulators focus on climate risk in the global financial system. They are also increasingly focused on the significant economic opportunity that the transition will create, as well as how to execute it in a just and fair manner. No issue ranks higher than climate change on our clients' lists of priorities. They ask us about it nearly every day."*
>
> (Fink, 2021)

In reaction to climate change and the risks it poses, there is an increasing focus on measures to address climate change across disciplines in research, public discourse, but also the private sector, as illustrated by above quote from the 2021 letter to CEOs from Larry Fink, head of the multinational investment management corporation

BlackRock. Actions taken to avert or limit the climate crisis are often categorized either as mitigation or adaptation measures. The term mitigation of climate change (or climate protection) refers to all actions aiming to "reduce the sources or enhance the sinks of greenhouse gases" (IPCC, 2014b), with the goal to essentially limit climate change. The term adaptation describes the "process of adjustment to actual or expected climate and its effects", according to the IPCC's 5th assessment report's glossary. More specifically, adaptation aims at avoiding or moderating any kind of harm or adverse effects inflicted by climate change, but can also include exploiting associated "beneficial opportunities" (IPCC, 2014b).

The financial sector is widely recognized to play a critical role both for mitigation of and adaptation to climate change (e.g., Bloomberg et al., 2017; Kidney et al., 2017), at the latest since the Paris Agreement of 2015. I will illustrate this by example of institutional climate initiatives related to finance. While there are uncountable initiatives and civic movements from local to global scale that made substantial contributions to raise awareness of climate change in the financial sector and beyond, it is the work of the United Nations Framework Convention on Climate Change (UNFCCC) and, more sector specific, the Task Force on Climate-related Financial Disclosures (TCFD) with its focus on climate-related risks that has been most relevant in setting the scene for this thesis. Therefore, the main attention in the following is on these initiatives, and especially the terms and recommendations coined by the TCFD (Fig. 1) – and how this motivates the research and development presented in this thesis.

Figure 1: Core elements of climate-related financial disclosures, from Annex: Implementing the Recommendations of the Task Force on Climate-related Financial Disclosures (TCFD, 2017, p.11). One of the TCFD's goals is to "enable stakeholders to understand better the concentrations of carbon-related assets in the financial sector and the financial system's exposures to climate-related risks" (TCFD, online). The TCFD's recommendations rest on four pillars: governance, strategy, risk management, and metrics and targets. The scientific work presented here contributes to a science-based assessment of climate-related physical risks, to inform metrics, targets, and climate change mitigation and adaptation efforts in the financial sector and beyond.

Policy makers as well as non-governmental and private institutional actors across sectors have widely referred to the Paris Agreement to motivate novel climate initiatives. The Paris Agreement is an international agreement negotiated in 2015 at the 21st Conference of the Parties of the UNFCCC, signed by 194 countries and the European Union (status October 2020). According to Falkner (2016), the Paris Agreement introduced a new logic of international climate agreements: The focus on voluntary national greenhouse gas emission reduction targets embedded in a framework of international comparison implies a logic of 'naming and shaming', putting a large emphasize on domestic responsibility: "For the Paris Agreement to make a difference, the new logic of 'pledge and review' will need to mobilize international and domestic pressure and generate political momentum behind more substantial climate policies worldwide" (Falkner, 2016). Finance is widely recognized as a crucial sector both for global climate change mitigation and adaptation efforts. This is due to both the huge greenhouse gas footprint of investments and the need to mobilize private capital for 'climate friendly' investments, including an efficient allocation of capital both for climate mitigation and adaptation (Maltais and Nykvist, 2020). As a consequence, a multitude of initiatives have emerged with the goal to transform the finance sector, to ensure it contributes to achieving a sustainable economy, more specifically, an economy operating with greenhouse gas emissions that are within the boundaries required to keep global mean temperatures below a critical threshold, i.e., the thresholds agreed upon in the Paris Agreement of global mean temperatures 1.5 and 2°C above pre-industrial levels. In the following, I will briefly introduce several institutional climate initiatives in the financial sector most relevant for a better understanding of the context of this thesis.

The *United Nations Environment – Finance Initiative (UNEPFI)* was founded in 1992 in the context of Rio Climate Summit by members of the finance sector recognizing "that economic development needs to be compatible with human welfare and a healthy environment" and committing to sustainable development, management, and fostering public awareness and communication with regard to environmental and social aspects (UNEPFI, 1992). The UNEPFI hosted *United Nations-convened Net-Zero Asset Owner Alliance* (UNEPFI, 2019) was launched in 2019 and comprises 29 institutional investors representing nearly $ 5.0 trillion assets under management (state August 2020). Member organizations commit to transition their portfolios to net-zero greenhouse gas emissions by 2050 and align them with a 1.5° target formulated in the Paris Agreement (UNEPFI, 2019).

Focused on accounting as one specific aspect of financial reporting and accountability, the *Partnership for Carbon Accounting Financials* (PCAF, 2015) is another network of finance sector actors founded at the 2015 Paris Climate Summit with a focus on harmonizing approaches for carbon accounting. On the level of central banks, the *Network for Greening the Financial System* (NGFS) brings together eight central banks committed to support financing the transformation to a green, low-carbon economy and contributing to reaching the 2°C target of the Paris Agreement (NGFS, 2017). Other relevant sectoral initiatives and non-profit organizations aiming to "establish and improve industry specific disclosure standards" (SASB, online) with focus on climate change are the *Sustainability Accounting Standards Board* (SASB, online), *CDP* (CDP, online), and the *Science Based Targets initiative* (SBTi, 2019).

But what is it that is actually required to realize this multitude of commitments? Eventually, it is the real economy in which the financial sector is invested that emits greenhouse gases and needs to be transformed to mitigate global warming. For actors in an abstract system like the finance sector to enable necessary transformations without changing the rules of the system altogether, the sector depends on steering investments to where they actually make a difference. Climate-aware financial products, such as 'green bonds', are a relatively new asset class with a strong growth on the financial markets over the last decade (Kidney et al., 2017; Maltais and Nykvist, 2020). 'Green bonds' follow voluntary guidelines pinned down in the Green Bond Principles (ICMA Group, 2018) and are supposed to give investors the possibility to invest their money more sustainable, e.g., avoid investment in greenhouse gas emission intensive companies, among others. This asset class is claimed to be intended to contribute to sustainable transition by increasing transparency of information regarding ecological impacts of investments, which also indirectly supports the implementation of climate policies and lowering the cost of capital for low-carbon projects (Shishlov et al., 2016). To ensure that 'green' financial products actually invest where they make a difference, the financial sector depends on inter-comparable information on the risks and opportunities of the real economy with regard to climate change relevant transformations. Hosted by the *Linux Foundation Climate Finance Foundation* (LFCF), the project OS-CLIMATE puts emphasis on the access to technical solutions and transparent tools for this purpose. OS-CLIMATE has the goal to develop an open-source platform and tools to assess and manage both climate-related risk and solutions for the finance sector across multiple sectors globally, in cooperation with leading technology companies (OS-CLIMATE, 2020; The Linux Foundation, 2020). This is just one example for science-based, transparent tools, and impact-oriented metrics becoming more and more relevant for the financial sector in order to build trust in emerging 'green' financial products and monitor their impact with regard to climate change mitigation and adaptation. One of the most prominent sectoral publications with regards to the disclosure of climate relevant information are the recommendations of the *Task Force on Climate-related Financial Disclosures* (TCFD), building on the conviction that "increasing transparency makes markets more efficient and economies more stable and resilient" (Bloomberg et al., 2017). The recommendations are based on acknowledging the risk anthropogenic climate change poses across economic sectors and thereby for investors. The TCFD diagnoses an apparent lack of transparent and consistent corporate climate risk reporting, making it "difficult for investors to know which companies are most at risk from climate change, which are best prepared, and which are taking action" (Bloomberg et al., 2017). To counteract this, the report "establishes recommendations for disclosing clear, comparable and consistent information about the risks and opportunities presented by climate change." According to the TCFD, climate-related risk can be classified as either 'physical' or 'transition risk'. Transition risk entails 'policy and legal risk', 'technology risk', 'market risk', and 'reputation risk', with all of them mostly related to the mitigation of climate change and climate litigation. In contrast, physical risk refers to risk related to the changed climate system itself, such as intensified weather and climate extremes. The TCFD's concept of physical risk is discussed in more detail in Section 1.4.1. To also consider possible positive impacts of climate change for organizations, the TCFD recommends managing risks and opportunities in a combined framework, as they interplay in determining the financial consequences of climate change, e.g., impacts on revenue, expenditures, assets and liabilities, and capital and financing. With regard to risk disclosure, the TCFD recommends to report in pertinent risk metrics on governance structures, strategies, and risk management plans (Bloomberg et al., 2017; TCFD, 2017).

The focus on both transition and physical risk sets the stage for risk assessments in the financial sector that are not only considering investments (e.g., in greenhouse gas intensive industries) as drivers of environmental changes but also assets at risk from these changes. However, the assessment of climate-related risks, both with regard to transition and physical risk, is non-trivial and the forward-looking quantification of these risks requires an adequate level of science-based impact modeling – an endeavor beyond the know-how and resources of most organizations, except a few leading insurance and risk modeling companies. Making data and science-based tools for the assessment and disclosure of climate-related risk available for the public is not only supposed to help investors increase the climate-resilience of their portfolios and increase transparency of and trust in derived (financial) products, but can also support the mitigation and adaptation efforts of public sector organizations, non-profit organizations, as well as small or medium-sized corporates lacking resources for research and development themselves. While this can be said both for transition and physical risks, the focus of this thesis lies on the latter and the no less relevant topic of transition risk will not be discussed here further.

For physical risk, impact modeling based on the climate sciences needs to bridge the gap from a predominantly natural science discipline to the assessment of climate-related risks of public and private assets, including companies and investment portfolios. The output from climate research entails empirical weather and climate data, global and regional climate model output, but also derived insights about physical processes, trends, statistical relationships between variables, among others. An interdisciplinary and cascading approach is required to build on the massive corpus provided by the climate sciences, to condense methods and information relevant for applied risk assessments. Therefore, the priority for the work documented in this thesis has always been to bridge the gap between science and application in a pragmatic, yet scientifically rigorous way. For this, the work documented here has been in close cooperation with fellow researchers and an implementing partner, applying the outcomes directly for global assessments of physical climate risk.

1.3 A joint research and development project

This thesis is part of a joint research and development project of the Weather and Climate Risks (WCR) group at ETH Zurich with Carbon Delta AG, a Zurich based environmental fintech and data analysis firm. In 2019, during the joint project, Carbon Delta became part of the financial services provider MSCI Inc. (Carbon Delta, 2019). Throughout this thesis, I will refer to the firm as "Carbon Delta" or "implementing partner", both for the period before and after October 2019.

The joint project has been funded by Innosuisse (formerly Commission for Technology and Innovation, CTI), with two 18-month innovation project phases, titled "Integrating tropical cyclone risk in investment management strategies globally" (project no. 26792.1 PFES-ES, 2018/2019) and "Integrating climate change related water scarcity risks in investment management strategies" (project no. 37861.1 IP-SBM, 2020/2021). The topics of the joint research project are the direct economic impact of tropical cyclones across sectors (phase 1) and the impact of climatic conditions on the agricultural and power producing sector (phase 2), with a focus on crop yields and low extremes of surface water discharge (river low flow, see Section 1.5.2). The choice of hazards and sectors was based both on economic relevance and available resources in the scientific domain: Tropical cyclones are particularly distinct and destructive extreme events with a long tradition in the impact modeling community (e.g., Cardona et al., 2014; Emanuel, 2011a; Gettelman et al., 2017) – yet challenging to assess consistently on a global level (Ward et al., 2020). The second phase was co-designed with specific input regarding needs from the sector side, focusing on the two economic sectors most affected by changes in extreme temperatures and water availability: agriculture and power production (Bokern, 2019). Both phases of the project therefore address economically relevant hazard types and economic sectors, yet they comprise very different methodological requirements and scientific challenges, as will be seen in the three main chapters of this thesis. The cooperation with a globally oriented financial analyst proved to be well suited for the research side of the project, too, not least because the global scope of the assessment fits well with the global focus of recent climate impact research (e.g., Rosenzweig et al., 2017; Ward et al., 2020).

The aim of the joint project is research and the co-development of globally consistent hazard and vulnerability components within the climate risk modeling framework CLIMADA, for application both by the implementing partner and in research. Thereby, the focus lies on hazards with potentially high exposure of companies listed on global stock markets. To reach this aim, both phases of the project contribute to the development of science-based methods for the globally consistent modeling of current and future weather and climate risks measured in monetary terms. On the side of the implementing partner, the risk estimates modeled both on the level of single companies as well as aggregated over investment portfolios provide the basis for the calculation of their product Climate Value-at-Risk (CVaR). "Value at risk quantifies the size of loss on a portfolio of assets over a given time horizon, at given probability. Thus, [...] VaR from climate change can be seen as a measure of the potential for asset-price corrections due to climate change" (Dietz et al., 2016). Accordingly, Carbon Delta's CVaR product "provides forward looking and return-based valuation assessments to measure the potential impact of climate change on company valuations" (Carbon Delta, online). The CVaR methodology is based on dividend discounting (Dietz et al., 2016), a stock pricing approach originating from discounted dividend model of Gordon (1959, 1962). Dividend discounting essentially provides a solution to the question "what is the right price for a stock?" based on discounted dividends expected from the stock in the future (Kamstra, 2003). Therefore, dividend discounting requires estimates of risks and opportunities to a company over the coming decades. It should always be kept in mind that results of dividend discounting are highly dependent on the assumed discounting rate which is a strategic, political, and ethical choice rather than a scientific one (e.g, Nordhaus, 2019; Rendall, 2019). As a basis for the calculation of CVaR, the focus lies on future changes in stock values caused by a company's exposure to climate change, both in terms of transition and physical risk (see Section 1.4.1). For an isolated assessment of climate-related risk, other factors such as market dynamics and company specific adaptation levels are assumed to stay fixed at a current level (ceteris paribus assumption). This focus on climate-related impacts has been guiding choices and assumptions across all studies contributing to physical risk assessments undertaken as part of this thesis. While addressing substantially different types of risk, both phases of the collaboration aim at the quantification of the difference in risk due to climate change between the present and future decades, i.e. the "Delta" in Carbon Delta. This set-up assumes that the current risk posed by weather and climate extremes to companies is either explicitly or implicitly 'priced in' with regard to the companies' current valuation. It should be noted that this assumption of the current risk level builds on an idealized understanding of the knowledge of financial markets (e.g., Knorr Cetina and Preda, 2006), and can also be misinformed, because climate risk is often unknown or uncertain even for the current level of global warming. What is more, historical records often do not offer the sample size to map out the probability space of extreme events and related impacts. With the quantification of both current and future (projected) risk, the studies presented here contribute both to a re-evaluation of current risk levels as well as to a forward-looking valuation at higher projected levels of global warming.

1.4 Scientific background

1.4.1 Climate risk: concept and terminology

The work presented here is all about the quantification of climate-related economic risks. It is important to clarify what concept of risk is applied and how it is calculated, or modeled, in the studies presented here and also in risk assessments typically making use of the results. The definition of climate risk used throughout this work is shown in Box 1, together with related definitions and concepts. These definitions are based on the risk framework for IPCC reports defined in the IPCC Special Report on Extremes (IPCC, 2012) and the Fifth Assessment Report of the IPCC (Oppenheimer et al., 2014), as summarized and augmented by Zscheischler et al. (2018).

Risk: "The 'effect of uncertainty on objectives' (ISO, 2009, 2018; Lark, 2015). According to the IPCC (Oppenheimer et al., 2014), risk is the potential for consequences when something of value is at stake and the outcome is uncertain, recognizing the diversity of values. Risks arise from the interaction between hazard, vulnerability and exposure and can be described by the formula:

$$Risk = (probability\ of\ events\ or\ trends) \times consequences \tag{1.1}$$

where consequences are a function of the intensity of hazard (event or trend), exposures, and vulnerability. Here, we use the term risk to refer to environmental and societal impacts from weather and/or climate events." (Zscheischler et al., 2018)

Exposure: "The presence of people, livelihoods, species or ecosystems, environmental functions, services, and resources, infrastructure, or economic, social, or cultural assets in places and settings that could be adversely affected" (IPCC, 2012; Oppenheimer et al., 2014; Zscheischler et al., 2018)

Vulnerability: "The propensity or predisposition to be adversely affected" (IPCC, 2012; Oppenheimer et al., 2014). "Vulnerability encompasses a variety of concepts and elements including sensitivity or susceptibility to harm and lack of capacity to cope and adapt." (Zscheischler et al., 2018)

Hazard: "The potential occurrence of a natural or human induced physical event or trend or physical impact that may cause loss of life, injury, or other health impacts, as well as damage and loss to property, infrastructure, livelihoods, service provision, ecosystems and environmental resources" (Oppenheimer et al., 2014). In this thesis, "the term hazard usually refers to climate-related physical events or their physical impacts." (Zscheischler et al., 2018)

Weather and climate events: "Events at spatial and temporal scales varying from local weather to large-scale climate modes." (Zscheischler et al., 2018)

Impacts: "The effects of physical events on natural and human systems" (Zscheischler et al., 2018).

Box 1: Definitions of climate risk and related terms; adapted from Zscheischler et al. (2018).

When calculating a measure of physical climate risk following Equation (1.1), "consequences" are represented by quantifiable impacts of a weather and climate event. In the studies presented here, for example, these impacts are damage inflicted on physical assets by tropical cyclones and reported in monetary terms (Chapters Two and Three), or the deviation of crop production from a baseline value, as expressed in tons, kcal, or monetary value per year (Chapter Four). The "probability of events" in Equation (1.1) can be derived from a statistically modeled distribution, or estimated as a frequentist probability from the occurrence frequency of simulated or observed events. Depending on the underlying research agenda, various risk figures can be calculated within this framework, e.g., the **annual average impact** (AAI, Chapter Three) or the estimated impact occurring with a given **return period** (T, Chapter Four). The **exceedance frequency** is the inverse of the return period, that is, the frequency at which event impacts exceed a certain value (see Aznar-Siguan and Bresch, 2019).

The definition of risk applied here is also compatible with the perspective on climate-related risk adapted in the recommendations of the TCFD (c.f. Chapter 1.3). The TCFD classifies climate-related risk as either 'physical' or 'transition risk'. 'Climate risk' as defined in Box 1 corresponds to the 'physical risk' in the TCFD's framework, as can be seen from the TCFD's definitions:

Transition risk: "Transitioning to a lower-carbon economy may entail extensive policy, legal, technology, and market changes to address mitigation and adaptation requirements related to climate change. Depending on the nature, speed, and focus of these changes, transition risks may pose varying levels of financial and reputational risk to organizations." (Bloomberg et al., 2017).

In contrast, **physical risk** refers to risk posed by the (changed) climate system itself, like extreme weather and climate events, requiring adaptation efforts to be managed effectively. "Physical risks may have financial implications for organizations, such as direct damage to assets and indirect impacts from supply chain disruption" (Bloomberg et al., 2017). The TCFD further subdivides physical risk into 'acute' and 'chronic' risk: "Physical risks resulting from climate change can be event driven (acute) or longer-term shifts (chronic) in climate patterns" (Bloomberg et al., 2017). While the TCFD's focus is on the additional risk from climate change, it is apparent that physical risk due to climate change can hardly be quantified without an understanding of the climate-related physical risk that exists independently of climate change. The requirement to understand current risk is a constant companion of any effort to assess future climate risks. This can also be seen in the studies presented here. Chapters Two and Three focus on physical risk under current climate as a prerequisite of future risk assessments. The risk posed by tropical cyclones (Chapter Three) is clearly event driven and thus a form of acute risk in the TCFD's definition of the term. Only in Chapter Four, we actually assess consequences of climate change in future climate projections. For the assessment of the impacts of climate change on crop production, the signal seen in mean trends can be considered as drivers of chronic risk. However, sometimes the line between acute and chronic risk is blurred, for instance when analyzing years of extreme crop losses triggered by acute climatic extreme events. Therefore, special attention to risk terminology is required when assessing historical and future risks of crop failure. The TCFD also differentiates direct and indirect (or higher order) impacts with regard to physical risk. In this thesis, direct impact denotes the direct physical effects of an event, while higher-order impacts "include those that spill over from the area of impact to areas that suffered no physical harm" (Lyubchich et al., 2020), including contingent business interruption. This differentiation might seem straight forward on first glance. In practice however, the differentiation of direct and indirect impacts is not always unequivocal. For example, there can be inaccuracies with regard to whether numbers in damage reports are representing only 'pure' direct impacts or also include certain indirect effects. This can contribute to uncertainties in model calibration, as we will see for the case of tropical cyclone impact functions in Chapter Three.

The breakdown of risk to the components 'hazard', 'exposure', and 'vulnerability' (Box 1) offers a methodological path to disentangle the complexity of quantifying risk. Based on this and adding the authority of the IPCC, it comes to no surprise that the climate risk framework introduced by the IPCC and followed here has been widely adapted for climate risk assessments (Ward et al., 2020). The studies presented here also follow this framework in approaching risk: In Chapter Two, the focus is on the exposure component of acute physical risk, introducing a method to estimate the global distribution of asset exposure data based on publicly available input data sets. In Chapter Three, vulnerability is explored in its most basic mathematical form, an impact function mapping hazard intensity to a damage degree. In the study on crop production risk in Chapter Four, exposure and vulnerability are kept constant and the hazard is varied based on future climate projections. Here, the modeling of hazard intensity and vulnerability are rather complex and quickly exceed the scope of a single research project. Therefore, the impacts are derived from existing simulations of crop yield under changing climate, provided by a crop model intercomparison project. Hence, Chapter Four focuses on the computation and interpretation of meaningful statistics of model-based climate impacts on country-level crop production. More detail on models and data sources involved in this thesis can be found in Sections 1.4.2 and 1.5 and in the specific studies presented in Chapters Two to Four.

The quantification of weather and climate risk requires a quantification of impacts and probabilities of weather and climate events. Here, we differentiate 'modeled' or 'simulated' impact from 'reported' impact: Impact numbers can be either taken from surveys and reports, such as reported storm damage values as used as a basis for impact model calibration in Chapter Three, or simulated within an impact modeling framework. Based on the definition of "impacts" above, we here refer to **impact models** as mathematical models, usually implemented on a computer, to approximate the impact of weather and climate events based on the input of hazard intensity, exposure, and vulnerability. In the following section, weather and climate impact models are introduced in more detail.

1.4.2 Global scale climate impact and risk models

The first prominent endeavors to model aggregated economic impacts of global warming on a global scale have been so-called integrated assessment models (IAMs) developed by Nordhaus and colleagues since 1977, when they started constraining an energy supply and demand model with limits to atmospheric carbon dioxide concentrations ([CO_2]) (Newbold, 2010). According to Nordhaus and Boyer, IAMs "integrate in an end-to-end fashion the economics, carbon cycle, climate science, and impacts in a highly aggregated model that allow[s] a weighing of the costs and benefits of taking steps to slow greenhouse warming" (Newbold, 2010; Nordhaus and Boyer, 2000 p. 5). As for the modeling of climate impacts in IAMs, 'highly aggregated' means that the impacts, that is, the economic costs of global warming, are usually modeled directly as a function of global mean temperatures: "In aggregate models, damage is often represented as a quadratic function of global mean temperature"

(Nordhaus, 2017). While IAMs are considered pioneering work with regard to the integration of climate change in economic modeling and decision making, they have been widely criticized for modeling cost and benefits from global warming based on assumptions and aggregated damage functions with limited empirical evidence, – a simplification that does not live up to the complexity of the climate system and the risk posed by diverse natural hazard types in a non-linear system (e.g., Ackerman et al., 2009; Frisch, 2013), as most IAMs are "poor at handling discontinuous change" (Rosenzweig et al., 2017).

More recent versions of IAMs, but also alternative approaches in modeling (economic) climate impacts are attempting to better represent the complexity of the climate system, i.e., the relationship of global mean temperatures and weather and climate extremes, as well as the diversity of economic sectors and how they are affected by climate change (e.g., Carleton and Hsiang, 2016). This is attempted mainly by stepping down one or two steps from the high aggregation level of early IAMs with regard to the representation of hazard, exposure, and vulnerability; to acknowledge and better represent these complexities in climate impact models. This entails an explicit representation of different hazard types (and how they change in a warming climate), as well as the exposure and impact functions associated to different sectors and asset types. Here, sectors are not necessarily limited to economic sectors, but can include social, cultural, and ecological spheres, depending on the purpose of the model, i.e., the risk indicator to be estimated. Spatially explicit climate impact models with a global scope "have been used to identify regions that are affected disproportionately by climate change" (Oppenheimer et al., 2014), and recent developments move towards rendering impact assessment tools more readily available for public use, as well as towards a better representation of multi-hazard and compound risks (Oppenheimer et al., 2014), the latter requiring further interdisciplinary efforts for an adequate representation (Zscheischler et al., 2018).

According to a review article on global scale natural hazard risk assessments by Ward et al. (2020), "efforts to assess and map natural hazard risk at the global scale have been ongoing since the mid-2000s, starting with the natural disaster hotspots analysis of Dilley et al. (2005). This was followed [in 2009] by the global risk assessments for an increasing number of natural hazards in the biennial Global Assessment Reports (GARs) of the United Nations Office for Disaster Risk Reduction (UNDRR)". Ward et al. (2020) provide an overview over scientific literature on global-scale natural hazard risk assessments per hazard type with particular attention to the spatial resolution of the risk components (hazard, exposure, vulnerability), risk indicators, type of risk assessment, implemented measures of disaster risk reduction, and the time horizon of future risk assessments. Common risk indicators used in recent climate risk assessments are affected people and fatalities, direct and indirect economic damage, affected GDP, and area affected (Ward et al., 2020). The following climatic hazard types were typically assessed in the papers reviewed by Ward et al.: River floods, coastal floods, tropical cyclones, droughts and wildfires. Embracing the diversity of hazard types and sectors affected makes it increasingly difficult and beyond the scope of single research and model development efforts to model global climate impacts in an end-to-end fashion. Therefore, the increased complexity of climate impact models bears the risk of ending up with a fragmented landscape of climate impact models, each highly specialized on one or two hazard types and sectors. The present study is both indebted to and contributing to efforts in defragmenting the landscape of global-scale climate impact modeling, especially within the CLIMate ADAptation (CLIMADA) project and the Inter-Sectoral Impact Model Intercomparison Project (ISIMIP), both introduced further below.

One differentiates roughly two types of spatially explicit computerized models with a global scale that are referred to as climate 'impact' or 'risk models': event-based probabilistic risk models and gridded sectoral impact models. The first impact model type discussed here is an event-based impact modeling platform, simulating the impact (e.g., damage, but also potential benefits) of weather and climate extreme events such as storms, bush fires, floods, etcetera, to exposed populations or assets (e.g., Aznar-Siguan and Bresch, 2019; Cardona et al., 2012a). Evolving from so called 'natural catastrophe models' developed in the insurance industry, among others, event-based impact models are typically designed based on the risk concept introduced in Section 1.4.1: They are built in a modular fashion, organizing the risk modeling chain along the risk components hazard, exposure, and vulnerability (Aznar-Siguan and Bresch, 2019). The hazard component is thereby structured as event sets, with each event represented by a spatial distribution of hazard intensity (e.g., footprint of maximum wind speed of a storm event), and a time information such as occurrence date, frequency, or probability. The exposure component represents the spatial distribution of population, assets, or ecosystems potentially affected by an extreme event (c.f. Chapter Two of this dissertation). The vulnerability component is represented with so called impact functions f_{imp}, parameterizing "to what extent a [particular type of] exposure will be affected by a specific hazard" (Aznar-Siguan and Bresch, 2019), see Equation 1.3 below. Impact functions are sometimes also referred to as damage functions or vulnerability curves[1]. Chapter Three of this thesis is all about a globally consistent parameterization of an impact function for tropical cyclone wind damages to exposed assets. When a frequency, or

[1] The term 'damage function' is also used in the IAM community, however with a different scope as summarized in the beginning of this subsection. The term 'vulnerability curve' is most widely used in the (re)insurance industry. To avoid confusions, the term 'impact function' will be used throughout this thesis.

frequentist probability, is provided for each event, the risk formula provided in Equation (1.1) can be reformulated as follows, adopting the terminology from Aznar-Siguan and Bresch (2019):

$$Risk = probability \times \; severity, \tag{1.2}$$

with

$$\begin{aligned} severity = \; & F(hazard\ intensity, exposure, vulnerability) \\ = \; & exposure \cdot f_{imp}(hazard\ intensity) \end{aligned} \tag{1.3}$$

The separation of probability and severity in Equation (1.2) allows for straight-forward probabilistic risk computations exploiting any given estimates of the probability of events. Linking impact severity with probability estimates, event-based impact modeling platforms are frequently referred to as 'probabilistic'. Event-based multi-hazard impact modeling platforms include CAPRA (Cardona et al., 2012a), CLIMADA (Aznar-Siguan and Bresch, 2019; Bresch and Aznar-Siguan, 2021), HAZUS (Schneider and Schauer, 2006), and RISKSCAPE (King and Bell, 2006). Among these probabilistic multi-hazard impact modeling platforms, CLIMADA, implemented in the interpreted, high-level and general-purpose programming language Python is, to the author's knowledge, the only platform with a global scope that is open-source, licensed for both academic and commercial use, and available from a public code repository (Aznar-Siguan and Bresch, 2019; CLIMADA-Project, 2019). Therefore, CLIMADA is used as a framework for modeling throughout this thesis. Furthermore, all three publications forming the main part of this thesis also contribute directly to the development and calibration of the hazard, exposure, and vulnerability components of the CLIMADA versions 1.2 to 2.0 (Bresch et al., 2020; e.g., CLIMADA-Project, 2019). The core functionality of CLIMADA is computing "the impact of a hazard on its corresponding exposures and impact functions [...] and storing all the resulting risk assessment metrics" (Aznar-Siguan and Bresch, 2019) in a spatially explicit fashion. Resulting risk metrics of probabilistic risk assessments include estimates of annual expected impact (AAI), and return periods (or frequencies) of impacts to exceed a certain value at a certain location or spatially aggregated, typically visualized as impact exceedance frequency curves (Aznar-Siguan and Bresch, 2019). Additional tools to utilize these risk metrics for assessing the potential benefit of adaptation measures in the context option appraisal studies are implemented in CLIMADA v.1.4.1+ (Bresch and Aznar-Siguan, 2021).

The second type of climate impact models introduced here is a more broadly defined group of models simulating quantifiable and socio-economically or ecologically relevant impact from weather and climate variables. These models are sometimes referred to as 'sectoral' climate impact models, as they typically focus on one sector or area of interest, such as water, fishery, or agriculture. In contrast to event-based probabilistic impact models, sectoral impact models are typically process-based, that is, representing physical, chemical, and biological processes with numerical algorithms. For example, sectoral impact models include hydrological models simulating the response of hydrological variables such as surface water discharge or soil moisture to atmospheric (and socio-economic) drivers. Typically, the input and output data from process-based sectoral impact models are spatially gridded at equidistant timesteps, e.g., yearly crop yields for agriculture or daily and gridded daily surface water discharge for the hydrological sector. The input data are often output from global (GCMs) or regional (RCMs) climate models, or from observation-based reanalysis data sets. Typical resolutions are 50 km globally, 10 km regionally and often at 6h time-intervals.

The Inter-Sectoral Impact Model Intercomparison Project (ISIMIP) strives to harmonize, evaluate, benchmark, and publish climate impact simulations from sectoral climate impact models (ISIMIP, online; Rosenzweig et al., 2017; Warszawski et al., 2014). As summarized by Warszawski et al. (2014), ISIMIP is the first project to offer "a framework to compare climate impact projections in different sectors and at different scales": "The [ISIMIP] project builds on earlier climate change risk assessments at the global scale, such as the UK Fast Track project (Parry et al., 1999), the Climate Impact Response Functions (Füssel et al., 2003) initiative, and the more recent investigation by Arnell et al. (2013) covering climate impacts in six sectors (water availability, river flooding, coastal flooding, agriculture, ecosystems, and energy demands) using a coherent set of climatic and socioeconomic scenarios. However, all existing cross-sectoral impact studies use only one impact model per sector, and are thus unable to formally assess uncertainties beyond those stemming from climatic and socio-economic input data. In contrast, there are sector-specific multi-impact-model studies, such as Cramer et al. (2001) and Sitch et al. (2008) in the biomes sector, WaterMIP (Haddeland et al., 2011) in the water sector, and the Agricultural Model Intercomparison and Improvement Project AgMIP (Rosenzweig et al., 2013) in the agriculture sector. In this context, ISIMIP is intended to address the lack of a cross-sectoral multi-model assessment of impacts of climate change. The project serves the dual purpose of facilitating process understanding and model development in the scientific community, as well as providing quantitative results that are readily available to stakeholders and society in general." (Warszawski et al., 2014). According to Rosenzweig et al. (2017), "the overarching goal [of ISIMIP] is to use the knowledge gained to support adaptation and mitigation decisions that require regional or global perspectives within the context of facilitating transformations to enable sustainable development, despite inevitable climate shifts and disruptions. [...] The results are consistent multi-model assessments of sectoral risks and opportunities that enable studies that integrate across sectors, providing support for implementation of the Paris Agreement". The sectors assessed in the second round of ISIMIP are diverse: water (hydrological modeling), lakes, biomes, regional forests, permafrost, agriculture (crop modeling), temperature-related mortality (health), coastal systems, marine ecosystems and fisheries, and terrestrial biodiversity (Frieler et al., 2017a; ISIMIP, online, www.isimip.org). The large diversity in sectors makes it clear that from the perspective of the risk framework introduced above, there are sectors defined from an exposure perspective (e.g., forests or coastal systems), and others more defined from a hazard perspective (e.g., water sector). This also determines how output from sectoral impact models is used for downstream climate risk modeling: For example, gridded flood height data derived from hydrological model output as provided by ISIMIP have been integrated in the CLIMADA framework as a hazard intensity and combined with impact functions and exposure in the form of a spatial distribution of asset values to assess flood risk (Sauer et al., in press).

1.4.3 Empirical impact data for model calibration and evaluation

As weather and climate impact modeling becomes a broadly applied tool in research and climate risk assessments, there is a growing requirement for robust yet practicable model calibration and evaluation. In the context of the ISIMIP project, the evaluation of model performance and uncertainty are an integral aspect of the project design. Simulations driven by historical climate data allow testing the skill of impact models to reproduce historical impacts. This requires publicly available archives of systematically collected impact data. For example, Müller et al. (2017) used country level crop production statistics provided by the Food and Agriculture Organization's statistical database FAO-Stat (FAO, 2019) combined with scientific datasets containing gridded yield estimates for the evaluation of process-based crop models. In the insurance sector, companies usually calibrate impact functions of their natural catastrophe models with the data on (insured) damages they collect on their insurance portfolios. This kind of damage data is usually considered as a trade secret and not available to the public. There are however larger re-insurers as well as research groups collecting impact data and making global data sets available to research and the wider public on an aggregated level: NatCatSERVICE (Munich Re, 2018), SIGMA (Swiss Re Institute, 2020), and EM-DAT (Guha-Sapir, 2018). The demand for globally harmonized impact data sets has been increasing over recent years, including for information with regard to the attribution of impacts to anthropogenic climate change (Otto et al., 2020). Yet, the collection and quality control of globally harmonized impact data remains a challenge, not the least because of its political dimension: "Reported damage data are expected to come with considerable uncertainties, partly due the heterogeneity of data sources, the blending of direct and indirect economic damages, as well as political and structural reporting biases (Guha-Sapir and Below, 2002; Guha-Sapir and Checchi, 2018). Further uncertainty is introduced by the lack of international standards for reported damage datasets, leading to inconsistencies between data providers (Bakkensen et al., 2018b)." (Eberenz et al., 2021b) In the context of this thesis, we are using estimates of gross domestic (GDP) and regional (GRP) product from various official sources for the evaluation of asset value downscaling in Chapter Two. For the calibration of tropical cyclone impact functions in Chapter Three, we are using direct economic damage from tropical cyclones reported per event by EM-DAT in Chapter Three. In Chapter Four, the focus is less on developing a new model component as in Chapters Two and Three, but rather on showcasing the use of climate crop model ensemble output for a global crop production risk assessment. We therefore refrain from getting into crop model evaluation ourselves, referring gratefully to the model evaluations and uncertainty assessments provided by broader the crop modeling community (i.e., Müller et al., 2017, 2021). However, we use crop production statistics from FAO-Stat (FAO, 2019) to bias-adjust baseline crop production values per country.

1.5 Implementation: How the outcomes of this thesis are applied in practice

The results from Chapters Two and Three contribute to the first applied subproject with Carbon Delta (Section 1.5.1), Chapter Four to the second subproject (Section 1.5.2). For both projects, there have been joint research and development efforts beyond the work of Chapters Two to Four, to which the author of this thesis contributed as well. While these will not be elaborated in depth, they will be summarized to contextualize the studies with the applied side of this thesis. As part of the collaboration, an interface was co-designed and implemented to integrate CLIMADA in the risk modeling pipeline of the implementing partner.

1.5.1 Integrating tropical cyclone risk in investment management strategies globally

As part of this project, CLIMADA as a free and open-source probabilistic risk assessment platform, was integrated into the implementing partner's physical climate risk modeling chain. By doing so, tropical cyclone (TC) risk is modeled globally on a company level, both under recent and projected future climate conditions. For the TC risk simulation, the following risk components are combined:

Hazard: Just as for the calibration study presented in Chapter Three, the TC hazard set is derived from global historical TC storm tracks as provided by International Best Track Archive for Climate Stewardship (IBTrACS) (Knapp et al., 2010) and gridded maximum wind speed is calculated per track as a proxy for hazard intensity: "TC hazard intensity is represented by wind fields, i.e. the geographical distribution of the 1-min sustained wind speed per TC event, referred to as "wind speed" or "hazard intensity" in the following. Wind speed was simulated at a horizontal resolution of 10 x 10 km from historical TC tracks as a function of time, location, radius of maximum winds, and central and environmental pressure, based on the revised hurricane pressure-wind model by Holland (2008). Please also refer to Geiger et al. (2018) for a detailed description and illustration of the wind field model and its limitations" (Eberenz et al., 2021b). To increase the sample size for a probabilistic TC risk assessment and to close potential geographic gaps in the exact location of TC landfalls, the historical hazard event set was expanded by synthetic tracks. Per historical storm track, nine synthetical tracks were derived using a random walk algorithm as implemented in CLIMADA v.1.4 (Bresch et al., 2020) and described by Aznar-Siguan and Bresch (2019): "Synthetic tracks are obtained from historical ones by a direct random-walk process, starting at slightly perturbed initial locations of the tracks (Kleppek et al., 2008). Moreover, in order to take the decay of wind intensities after landfall into account, we statistically build an exponential decay coefficient of the wind speed (and corresponding increasing pressure) and apply it to the synthetic tracks after landfall." With nine synthetic tracks derived from each historical track, the hazard event set size is thus increased by a factor of ten.

Exposure: During research and development of the TC risk model, the globally consistent dataset of gridded asset exposure data LitPop, described in greater detail in Chapter Two, was used as exposure component. This applies both to the calibration of TC impact functions (Chapter Three) and the assessment of risk on an aggregated global level. For the modeling of TC impacts as input for the computation of CVaR, the implementing partner uses their own database of exposed locations per company, including geographical data, estimates of asset type and value, and revenue share per location.

Vulnerability: Impact functions calibrated for nine world regions are used to map wind speed to damage rates. They are the results of the calibration study presented in Chapter Three: "To better account for regional differences, a TC impact model was calibrated by fitting regional impact functions. The impact functions were calibrated within the CLIMADA risk modeling framework, using reported direct economic damage estimates from the EM-DAT dataset as reference data. For calibration, two complementary optimization approaches were applied, one aiming at minimizing the deviation of single event damages from the reported data and one aiming at minimizing the deviation for total damage aggregated over 38 years of data" (Eberenz et al., 2021b). The calibration process required a globally consistent asset exposure data set, which was developed as a prerequisite for the calibration study in Chapter Two. For the implementation at company level, the rather conservative impact functions based on an optimization of the total damage ratio (TDR) are applied as a best estimate of aggregate vulnerability. The risk assessment can be further complemented with the more sensitive impact functions based on an optimization of the root-mean-squared fraction (RMSF) to explore the range of resulting risk estimates under assuming above-average vulnerability.

Future climate. For projecting the risk increase due to changing TC characteristics in a future climate, we again perturbate the hazard set containing both historical and synthetical TC events. As mentioned already in the research plan submitted for this PhD project, this approach is rather straight forward but comes with considerable uncertainties: "Only few of the available climate risk assessments consider future hazard scenarios, even though this is crucial to prevent maladaptation (Gallina et al., 2016). It is also an essential ingredient to Carbon Delta's approach of estimating additional risk from climate change. The focus on additional risk assumes that current risk to the market value of companies is already implicitly priced-in on the financial markets. It is widely acknowledged that climate change causes a change in relevant properties of meteorological extreme events like TCs. However, there are still large uncertainties and inconsistencies between different studies concerning the response of TCs to climate change (IPCC, 2012; Knutson et al., 2010; Walsh et al., 2016). Nevertheless, the IPCC found agreements between studies on expected trends in TC intensity and frequency for certain ocean basins (IPCC, 2012). In a more recent downscaling experiment, Knutson et al. (2015) estimated trends per basin that are well inside the range of likely trends reported by the IPCC. It seems reasonable to use all statistically significant trends from Knutson et al. (2015) to create a future hazard set based on probabilistic TC tracks with adjusted event intensities and frequencies. We emphasize that the result is not a prediction but a plausible scenario of future TC risk with large epistemic uncertainties attached" (Eberenz, 2019).

1.5.2 Integrating climate change related water scarcity risks in investment management strategies

Two economic sectors most vulnerable to water scarcity are agriculture and the energy sector (Bokern, 2019). Since these two sectors and their dependency on water are very different, it was decided early in the project to treat them separately. The author of this thesis has contributed to research and development with regard to both sectors, however his main scientific contribution is the assessment of current and future global crop production risks as presented in Chapter Four.

Agriculture:

For the agriculture sector, the definitions of hazard, exposure, and vulnerability, respectively, are not as obvious as in the case of TCs. In the case of agriculture, crop models are used to simulate the impact from various climate-related drivers on crop yields. Risk to crop production can be defined rather narrowly as the "potential for reduced food production" (Challinor et al., 2018). Baseline mean gridded crop production can be considered here as the exposure component, and climate and weather variables as representations of the hazard. From this perspective, the crop models have the function of modeling (either process-based or statistically) the complex responses of crop yield to variations in climate and weather variables. From the perspective of event-based impact models using impact functions, the crop models than fulfill the same functionality as the impact functions in event-based models – a comparison best illustrated by emulators derived from process-based crop models, essentially linking crop yield responses to changes of temperature, water availability, nitrogen supply, and atmospheric CO_2 concentrations in a functional form (e.g., Franke et al., 2020a). When adapting a broader definition of agricultural risk however, the crop yield responses simulated by crop models can also be seen as the hazard component of a risk assessment that needs to be combined with more socio-economic representations of exposure and vulnerability to essentially assess the socio-economic risk induced by climate-related variations in crop production (e.g., Meza et al., 2019). In the global crop production risk assessment presented in Chapter Four of this thesis, we follow the narrower definition of climate-related crop production risk, exploiting the output from eight process-based crop models from the Global Gridded Crop Model Intercomparison – Coupled Model Intercomparison Project round 6 (GC6), experiment facilitated by ISIMIP round 3b (ISIMIP3b, ISIMIP, 2020a, 2020b). For GC6, crop models were run to simulate yearly crop yield for historical periods and the 21st century, based on harmonized forcing data and experimental parameters as specified in the ISIMIP3b protocol (ISIMIP, 2020b). For the assessment of crop production risk, future and historical gridded crop yields from global crop model ensemble simulations were combined with land-use data to derive time series of yearly crop production per country (c.f. Chapter Four). For this purpose, simulated yearly crop production values per country are pooled according to the level of global warming before calculating quantitative risk estimates. The main output from the analysis are two complementary risk metrics, both describing the change in probability of years experiencing extreme crop production losses with climate change – and a quantification of extreme events per country. As elaborated in the outlook section of Chapter Four, the results of this study can be further used as input data for assessments of downstream risk, such as food security or market risks, by combining the crop production risk estimates with socio-economic vulnerability indicators or impact functions. On the applied end of this thesis, our implementing partner will be using timeseries of fractional crop yield and/or the crop production risk metrics introduced in Chapter Four for estimating downstream crop production risk of companies in the food production value chain. In the following, the implementation is outlined following the categories hazard, exposure, vulnerability.

Hazard: As explained above, simulated crop yield variations can be used as input for the hazard component of a risk assessment. In the context of the implementation at Carbon Delta, this makes sense, since the focus is on downstream risk due to climate-related crop production losses. The specific hazard data applied here are yearly crop production estimates per country in metric tons. Country production is aggregated by integrating simulated gridded crop yield in tons per hectare and year over area. In the applied context, the individual model runs are pooled to obtain a large set of 'year events' for a probabilistic risk assessment. In the first implementation, we are using the output from three crop models as provided in ISIMIP2b (Frieler et al., 2017a) instead of the eight crop models of ISIMIP3b assessed in Chapter Four. Reason being that the ISIMIP3b output for the agricultural sector has not yet been made available for public use in early 2021. However, the data analysis framework as implemented within the CLIMADA risk modeling platform v.1.5.1 and available on GitHub (CLIMADA-Project, 2019), was designed in a flexible fashion for a seamless transition to input data from ISIMIP3b as soon as the data becomes available for public use. The crop risk module in CLIMADA was developed by the author of this thesis together with Carmen Steinmann.

Exposure and vulnerability: In the joint research and development project, the modeling of risk downstream of historical and future crop production time series is taken forward by the implementing partner. The goal is to map country level production risk to food-processing economic sectors and individual companies depending on purchasing staple crops for their revenue – an endeavor not further elaborated in this thesis. In the risk framework, the exposure component can be represented by information on international trade flows of agricultural commodities. For each individual company, crop bought by the company as input to their activity can then be attributed to crop producing countries. Like this, the hazard component in the form of crop production statistics on country-level can be mapped to individual companies. The vulnerability of each company is determined by the dependency of business activity on each modeled crop type. For example, a company producing popcorn in Switzerland from maize grown in Italy and Mexico is exposed with a high vulnerability to maize production failure in Italy and Mexico. If available, commodity markets and trade simulations or parameters can be further added to refine the exposure profile and account for more flexible market dynamics.

Future climate: The availability of both historical and future (21st century) climate crop simulations is inherent in ISIMIP's experimental setup (Frieler et al., 2017a; ISIMIP, 2020b), where sectoral impact models are driven by the bias-corrected and harmonized output from selected GCMs. For ISIMIP2b, climate forcing is provided in the form of GCM simulations from the Coupled Model Intercomparison Project round 5 (CMIP5, Taylor et al., 2012), both for the low-greenhouse-gas-emission

Representative Concentration Pathway (RCP) RCP2.6 and no-mitigation RCP6.0 (Frieler et al., 2017a). In the first version of the crop hazard set, ISIMIP2b climate-crop simulations from both RCPs and three crop models are implemented. For ISIMIP3b, the climate forcing comes from a more recent generation of climate models provided by CMIP6 (ISIMIP, 2020b; Jägermeyr et al., under review), entailing simulations following two emission scenarios: the Shared Socioeconomic Pathway SSP1 combined with RCP2.6 (here SSP126), and SSP5 with RCP8.5 (here SSP585). As summarized in Chapter Four, these trajectories "represent two plausible and contrasting trajectories for the 21st century (O'Neill et al., 2016). SSP126 represents a sustainable development (Riahi et al., 2017) with stringent mitigation, reducing greenhouse gas emissions to essentially zero by the end of the century (Pachauri et al., 2015). SSP585 represents a fossil-fueled development (Riahi et al., 2017) with rising emissions throughout the century (Pachauri et al., 2015)" (Section 4.2.1).

Energy sector:

In the subproject focusing on the energy sector, CLIMADA is used to simulate the impact of historical and future low river flow events on river cooled thermoelectric power plants, i.e., coal, oil, and gas-fired power plants and nuclear power plants, as well as hydroelectrical power plants. The approach is briefly outlined here for completeness, but forms no further part of this thesis. The CLIMADA hazard module 'LowFlow' is publicly available within v.1.5.1 of the CLIMADA repository on GitHub (CLIMADA-Project, 2019). The author of this thesis contributed in the development of the conceptual model together with David Bokern, as well as the implementation, and calibration of the river low flow impact model together with Zélie Stalhandske and Patric Kellermann.

Hazard: For the hazard component, low river flow events were identified that are connected in space and time, based on daily surface water discharge data simulated by an ensemble of four hydrological models driven by four different climate models for ISIMIP2b. The climate forcing is the same as for agriculture with ISIMIP2b described above. An algorithm was developed to identify distinct low flow events, based on the concept of low river flow used by Marx et al. (2018), among others. For event definition, grid cells were counted as experiencing low flow when the discharge falls below the 2.5th percentile of discharge during a historical reference period. To contribute to a low flow event, daily discharge needs to fall below this historical threshold during a minimum required amount of days per month. Distinct events were defined in space and time by clustering neighboring grid cells and consecutive months experiencing low flow. Like this, low flow hazard intensity per grid cell is defined as the number of days below the historical threshold during a given event.

Vulnerability: Impact functions for thermo- and hydroelectric power plants were fitted based on selected historical events with reported impact data available.

Historical low flow hazard events for calibration were derived from discharge simulations from ISIMIP2a. The aim of the calibration is for the model to best represent historical impacts on electrical power production. In ISIMIP2a, hydrological models were driven by historical climate data from re-analysis datasets. The resulting impact functions relate hazard intensity (days below threshold in consecutive months) to impact (percentage reduction in annual power production).

Exposure: For model development and calibration, the publicly available Global Power Plant Database was used (WRI, 2018), providing coordinates, utility type, and production capacities of power plants worldwide. Of the thermoelectric power plants, only those count as exposed to low river flow that use river water for cooling. River cooling is used in approximately two thirds of global thermoelectric power plants (van Vliet et al., 2016). Installations were filtered by distance to rivers, to exclude plants using alternative cooling mechanisms and water sources. For the modeling of low river flow impacts as input for the computation of CVaR, the implementing partner uses their own database of potentially exposed utility locations, including geographical coordinates, estimates of asset type and value, and revenue share per location.

Future climate: As in the case of agriculture, the hydrological models contributing to ISIMIP2b were driven by bias-corrected climate model output from CMIP5 (Taylor et al., 2012), both for RCP2.6 and no-mitigation RCP6.0 (Frieler et al., 2017a). Like this, low river flow hazard sets for the 20th (historical radiative forcing) and 21st century (RCP2.6 and RCP6.0) are available from three hydrological models driven by four GCMs.

2. Asset exposure data for global physical risk assessment

Samuel Eberenz[1,2], Dario Stocker[1,2], Thomas Röösli[1,2], David N. Bresch[1,2]

Published in Earth System Science Data, 12, 817–833, 2020,
DOI: 10.5194/essd-12-817-2020.

ABSTRACT. One of the challenges in globally consistent assessments of physical climate risks is the fact that asset exposure data are either unavailable or restricted to single countries or regions. We introduce a global high-resolution asset exposure dataset responding to this challenge. The data are produced using "lit population" (LitPop), a globally consistent methodology to disaggregate asset value data proportionally to a combination of nightlight intensity and geographical population data. By combining nightlight and population data, unwanted artefacts such as blooming, saturation, and lack of detail are mitigated. Thus, the combination of both data types improves the spatial distribution of macroeconomic indicators. Due to the lack of reported subnational asset data, the disaggregation methodology cannot be validated for asset values. Therefore, we compare disaggregated gross domestic product (GDP) per subnational administrative region to reported gross regional product (GRP) values for evaluation. The comparison for 14 industrialized and newly industrialized countries shows that the disaggregation skill for GDP using nightlights or population data alone is not as high as using a combination of both data types. The advantages of LitPop are global consistency, scalability, openness, replicability, and low entry threshold. The open-source LitPop methodology and the publicly available asset exposure data offer value for manifold use cases, including globally consistent economic disaster risk assessments and climate change adaptation studies, especially for larger regions, yet at considerably high resolution. The code is published on GitHub as part of the open-source software CLIMADA (CLIMate ADAptation) and archived in the ETH Data Archive with the link http://doi.org/10.5905/ethz-1007-226 (Bresch et al., 2019). The resulting asset exposure dataset for 224 countries is archived in the ETH Research Repository with link: https://doi.org/10.3929/ethz-b-000331316 (Eberenz et al., 2019).

[1] Institute for Environmental Decisions, ETH Zurich, Switzerland

[2] Federal Office of Meteorology and Climatology MeteoSwiss, Switzerland

2.1 Introduction

The modeling of climate risks on a global scale requires globally consistent data representing hazard, vulnerability, and exposure, as defined by the Intergovernmental Panel on Climate Change (IPCC, 2012, 2014a) among others. While natural hazard data can be derived from general circulation models, there is a lack of consistent exposure data on a global scale. Exposure is frequently defined as an inventory of elements at risk from natural hazards (Cardona et al., 2012b; UNISDR, 2009). For the modeling of physical risk as the direct economic impacts of disasters, exposure should specifically represent the spatial distribution of physical asset stock, i.e. buildings and machinery. While aggregate estimates of asset values are available at country level, open data on the spatial distribution of asset values are scarce. Proprietary asset exposure data (e.g. owned by insurance companies) are usually not publicly available.

Due to the lack of comprehensive asset stock inventories, large-scale asset exposure maps are often estimated top-down, using downscaling techniques (De Bono and Mora, 2014; Gunasekera et al., 2015; Murakami and Yamagata, 2019). On a country aggregate level, estimates of total asset values can be derived from socioeconomic flow measures, such as gross domestic product (GDP), since the two indicators exhibit strong correlations (Kuhn and Ríos-Rull, 2016). Annual values of socioeconomic flow variables, particularly GDP, are often more readily available than asset values. Assuming that human presence and activity are proxies of economic output, downscaling of GDP has been based on geographical population data (Kummu et al., 2018) and on population combined with land use, road networks, and locations of airports (Murakami and Yamagata, 2019). High-resolution yearly GDP maps based on these approaches are publicly available (Geiger et al., 2017; Kummu et al., 2018). Global asset exposure data were produced for the Global Assessment Report 2013 of the United Nations Office for Disaster Risk Reduction (UNISDR), following a downscaling approach (De Bono and Mora, 2014). However, the data's use beyond the scope of the Global Assessment Report is limited, because the data represent urban areas only and the methodology is not easily reproducible and thus not adaptable. For future quantitative risk assessments, more recent exposure data would be desirable. An alternative methodology to model global asset exposure based on the combination of diverse datasets was presented by Gunasekera et al. (2015). The authors combined data on built-up areas, building typologies, and construction cost with sector-specific asset data and GDP disaggregated proportionally to population density. Unfortunately, the source code and resulting exposure data have not been made publicly available. Reproducing these previously mentioned exposure modeling efforts is beyond the scope of most economic disaster risk assessments and climate change adaptation studies.

In recent years, the use of nightlight intensity from satellite imagery has seen a marked increase in science in general and especially for the disaggregation of socioeconomic indicators (Elvidge et al., 2012; Gettelman et al., 2017; Ghosh et al., 2013; Mellander et al., 2015; Pinkovskiy, 2014; Sutton et al., 2007; Sutton and Costanza, 2002). Being publicly available and updated regularly, global nightlight images have been proven to be a useful source of information and are commonly used in scientific contexts for the estimation of unavailable GDP or growth data (Henderson et al., 2012). However, there are some technical limits to the usage of nightlight satellite imagery (Han et al., 2018), especially saturation and blooming. As luminosity can only be distinguished up to a certain brightness, saturation may lead to very bright spots being underrepresented. In state-of-the-art nightlight products from the Suomi National Polar-orbiting Partnership's Visible Infrared Imaging Radiometer Suite (VIIRS), there are 256 shades of brightness, from the minimum zero (no light emission) to the maximum 255 (NASA Earth Observatory, 2017; Román et al., 2018). Any pixel brighter than what would entail a value of 255 will also appear at this value (Elvidge et al., 2007). Brightness can exude from bright pixels to neighboring pixels, causing the brightness in the latter to be overestimated, leading to blooming. This issue occurs in particular in large urban areas and on specific surfaces, such as sand and water (Elvidge et al., 2004; Small et al., 2005). As a consequence of saturation, socioeconomic indicators scale rather exponentially than linearly with nightlight intensity (Sutton and Costanza, 2002; Zhao et al., 2015, 2017). To counteract the saturation effect, Gettelman et al. (2017) and Aznar-Siguan and Bresch (2019) used exponentially scaled nightlight intensity as a basis for GDP disaggregation for tropical cyclone risk assessments. Saturation and blooming can also be mitigated by combining nightlights with other data types: Sutton et al. (2007) combined the areal extent of lit area with population data to estimate GDP at a subnational level. Zhao et al. (2017) enhanced nightlight intensity values with population data to get a more accurate estimation of spatial economic activity in China. This is based on the observation that there is also an exponential relationship between nightlight intensity and population density. The authors showed that the product of nightlight intensity and gridded population count (called "lit population" by the authors), is a better proxy for economic activity in China than nightlight intensity alone.

Here, we are using and expanding the lit population approach presented by Zhao et al. (2017) to define and implement a globally consistent methodology for asset exposure disaggregation, named LitPop hereafter. This paper presents global gridded asset exposure data and documents and evaluates the underlying LitPop methodology. The resulting asset exposure dataset for 224 countries is made available online at the ETH Research Repository (Eberenz et al., 2019). It is suitable to provide the globally consistent asset exposure base for modeling physical risks. The methodology is published on GitHub as part of the open-source event-based probabilistic impact model CLIMADA (CLIMate ADAptation) (Aznar-Siguan and Bresch, 2019; CLIMADA-Project, 2019) and archived in the ETH Data Archive (Bresch et al., 2019).

Information on input data, methodology, and the evaluation approach is provided in Section 2.2. Subsequently, the resulting global asset exposure data are presented and evaluation results are shown in Section 2.3. The advantages and limitations of the methodology are discussed in Sections 2.4. Please refer to Section 2.5 for data and code availability.

2.2 Data and methods

2.2.1 Overview

The core functionality of the LitPop methodology is the spatial disaggregation of national total asset values to obtain a gridded asset exposure product. Gridded nightlight intensity (Section 2.2.2) and gridded population data (Section 2.2.3) are combined to compute a digital number at grid cell level. Physical asset stock values (i.e. produced capital, Section 2.2.4.1) are then disaggregated proportionally to the digital number per grid cell (Section 2.2.5). This results in the gridded asset exposure dataset presented here. Instead of the physical asset stock, GDP (Section 2.2.4.2) or gross regional product (GRP, Section 2.2.4.3) can be distributed to obtain GDP per grid cell. Because of a lack of subnational produced capital data, GDP and GRP are used to evaluate the methodology by assessing the subnational disaggregation skill for varied combinations of the input data, as described in Section 2.2.6. A detailed overview of the input data is provided in Table 1; the disaggregation approach is illustrated in Fig. 2.

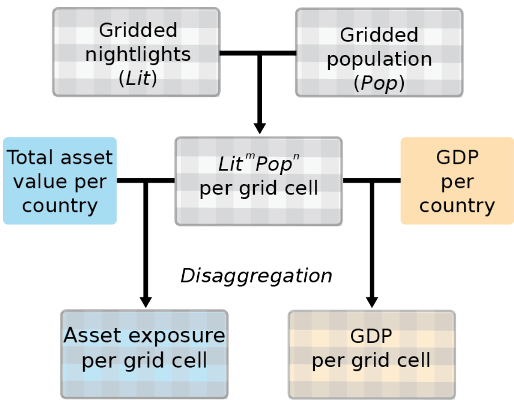

Figure 2: Work flow of the LitPop downscaling: gridded nightlights (Lit) and population (Pop) data are combined to compute gridded digital number $Lit^m Pop^n$ (Eq. 2.1). Then, total asset value per country (i.e. produced capital or nonfinancial wealth) is disaggregated proportionally to $Lit^m Pop^n$ to obtain gridded asset exposure data (Eq. 2.2). GDP is disaggregated in the same way and compared against reported GRP for the evaluation of the downscaling approach.

Table 1: Overview of input dataset, including information on usage, resolution, reference year, data source, and references. The reference year indicates the year for which the data used were provided. *) For GDP, the value of 2014 in current US dollars was used for 203 countries. For 21 countries without GDP data available for 2014, the closest available data points from the years 2000 to 2017 were used instead.

Input data	Usage	Spatial resolution	Reference year	Data source	Description
Gridded night-lights (Lit)	Disaggregation	15 arcsec	2016	NASA's Black Marble nighttime lights (NASA Earth Observatory, 2017; Román et al., 2018)	Section 2.2
Gridded population (Pop)	Disaggregation	30 arcsec (224 countries)	2015	Gridded Population of the World (GPW) (Center for International Earth Science Information Network (CIESIN), 2017)	Section 2.3 and Table S1
Produced capital	Estimation of total asset value	140 countries	2014	World Bank wealth accounting (World Bank, 2019a)	Section 2.4.1 and Table S1
GDP-to-wealth ratio	Estimation of total asset value	84 countries	2017	Global Wealth Report (Credit Suisse Research Institute, 2017)	Section 2.4.1 and Table S1
GDP	Estimation of total asset value and evaluation	224 countries	2014*	World Bank Open Data portal (World Bank, 2019b)	Section 2.4.2 and Table S1
GRP	Evaluation	507 regions in 14 countries	2012–2017	Various sources; see Table A1	Section 2.4.3 and Table A1

2.2.2 Satellite nightlight data

The nightlight intensity products used here are nighttime lights of the Black Marble 2016 annual composite of the VIIRS day-night band (DNB) at 15 arcsec resolution (Román et al., 2018), downloaded from the NASA Earth Observatory (2017). The processed datasets of luminosity by human activity based on VIIRS mark a distinct improvement over previous technologies, allowing for a greater range of light to be recorded (Carlowicz, 2012). The sun-synchronous satellite passes each place on Earth twice a day, at approximately 01:30 and 13:30 local time. Nightlight intensity on a scale from 0 to 255 is a variable derived from raw measurements. To isolate luminosity from sustained human activity, the Black Marble nightlight product includes corrections for Lunar artifacts, cloud, terrain, atmosphere, snow, airglow, stray light, and seasonal effects (Carlowicz, 2017; Lee et al., 2014; Román et al., 2018). The data are provided for 2012 and 2016 at a resolution of 15 arcsec, which corresponds to around 500 m at the Equator. The open-source code developed here can be adapted easily to use other versions and sources of nightlight data. This could be of interest for near-time applications in the future, as daily nightlight images could be available in the future (Carlowicz, 2017).

2.2.3 Gridded population data

The Gridded Population of the World (GPW) dataset is a spatially explicit representation of the world's population. It is based on two sets of inputs: nonspatial population data and cartography data. Using census data or population figures by the official national statistics offices, it uniformly distributes the numbers at the smallest available administrative unit to the corresponding cartographic shape, without taking into account any ancillary sources (Doxsey-Whitfield et al., 2015). The data quality for each country strongly depends on the underlying level of availability of population data. For example, for Canada, population data are available down to the fifth subnational administrative unit, of which 493 185 exist. The information for Canada is hence a lot more fine-grained than for instance for Jamaica or Uzbekistan, where population numbers are only recorded at the first subnational administrative unit (Socioeconomic Data and Applications Center (SEDAC), 2017). The level of detail and number of subnational administrative units resolved per country are listed in Table S1. While modeling is kept at a minimum in the GPW dataset, values are inflated or deflated from the latest year with data available to 2000, 2005, 2010, 2015, and 2020 (Center For International Earth Science Information Network (CIESIN), Columbia University, 2017).

GPW was selected for the LitPop methodology because, unlike other spatial population datasets, it does not incorporate nightlight satellite data or other auxiliary data sources (Leyk et al., 2019). This allows us to enhance nightlight data with a completely independent dataset. Moreover, it is released under the Creative Commons license. From GPW, the Population Count v4.10 data at the highest available resolution, 30 arcsec, are used, because they are the closest to NASA's nightlight dataset, in terms of both spatial resolution and available time steps.

2.2.4 Socioeconomic indicators

2.2.4.1 Total asset value per country

The World Bank's produced capital stock (World Bank, 2018) is one of the most comprehensive global estimates of the value of manufactured or built assets per country. It has been used as an indicator of exposure to natural disaster in the UNISDR's Global Assessment Report 2013 (De Bono and Mora, 2014). Produced capital accounts for machinery, equipment, and physical structures (World Bank, 2018). It also includes a fixed scale-up of 24% to account for the value of built-up land.

Produced capital values are currently available for 140 countries and five time steps: 1995, 2000, 2005, 2010, and 2014 from the World Bank wealth accounting (World Bank, 2019). Per default, the scale-up for built-up land is subtracted, assuming that there is no direct damage to the value of the land itself in the case of disaster. While not universally true, this assumption is based on the focus of the asset exposure data for the purpose of assessing direct impact to tangible structures. For applications considering the impact on the value of land, the linear scale-up can be reapplied before utilization of the asset exposure data.

Out of a total of 250 countries we considered for the production of this dataset, produced capital numbers for 2014 are available for 140 countries. For these 140 countries, produced capital for 2014 was used here as total asset value for disaggregation. For additional 87 countries, total asset values were set to non-financial wealth. Non-financial wealth was computed from the country's GDP and the GDP-to-wealth ratio estimates derived from the Credit Suisse Research Institute's Global Wealth Report (Credit Suisse Research Institute, 2017). This approach has previously been followed by Geiger (2018). We compared produced capital and non-financial wealth for 140 countries (Table S1) and found that non-financial wealth can be used as a conservative approximation of produced capital. For 59 of the 87 countries with neither produced capital nor non-financial wealth data available, an average GDP-to-wealth ratio of 1.247 was applied. In summary, the whole dataset contains gridded asset exposure data for a total of 224 countries, ignoring 26 countries and areas due to lack of data. Missing countries and areas (with currently assigned ISO 3166-1 alpha-3 codes) are Aland Islands, Antarctica, Bonaire, British Indian Ocean Territory, Sint Eustatius and Saba, Bouvet Island, Cocos (Keeling) Islands, Christmas Island, Guadeloupe, French Guiana, French Southern Territories, Heard Island and McDonald Islands, Holy See, Kosovo, Libya, Martinique, Mayotte, Pitcairn, Palestine, Reunion, South Georgia and the South Sandwich Islands, South Sudan, Svalbard and Jan Mayen, Syrian Arab Republic, Tokelau, United States Minor Outlying Islands, and Western Sahara. An overview over the utilized data per country, including, produced capital (were available), GDP-to-wealth ratios, and GDP for 2014 is provided in Table S1.

2.2.4.2 GDP

GDP is a well-established indicator of macroeconomic output. For most countries in the world, annual values are available dating back several decades. National GDP data in current US dollars in 2014 or the nearest available year are retrieved from the World Bank Open Data portal (World Bank, online).

While GDP is not a direct measure of physical asset values, it is used here both for scaling asset values in time to fill data gaps and for the evaluation of the LitPop methodology. The underlying assumption is that within a country, GDP and wealth are correlated, i.e. a higher GDP value is equivalent to higher asset values. This correlation has been established in empirical studies (Kuhn and Ríos-Rull, 2016).

2.2.4.3 GRP

The subnational equivalent to GDP is often referred to as GRP. GRP can be used to improve the downscaling of GDP, especially for countries with considerable regional differences. As described in Section 2.2.6 below, we use GRP data from 14 countries to evaluate the LitPop methodology by assessing its skill to disaggregate national

GDP to a subnational level. As there is no unified data source for GRP, it was gathered manually from government sources and OECD.Stat (Organisation for Economic Co-operation and Development, 2019). The countries used for evaluation are Australia, Brazil, Canada, Switzerland, China, Germany, France, Indonesia, India, Japan, Mexico, Turkey, the USA, and South Africa. The aim of the selection was to include countries from as wide a range as possible of income groups and world regions. Since the selection of countries was limited by the availability of GRP data, the selection has a bias towards industrialized and newly industrialized OECD member states. According to World Bank income groups, these countries include eight countries from the high-income group (World Bank income group 4), four countries from the upper-middle-income group (3), two countries from the lower-middle-income group (2), and no countries from the low-income group (1). Income groups and data sources per country are listed in Table A1 in the Appendix.

2.2.5 Disaggregation of asset exposure

To produce a high-resolution asset exposure map, the total asset value per country is disaggregated proportionally to a function of nightlight luminosity and population count. This approach is closely adapted from the work of Zhao et al. (2017). In their paper, historic GDP is disaggregated proportionally to a digital number computed from a multiplicative function of nightlights and population with the aim to make spatial GDP predictions for China. The underlying idea is to enhance brightness values with spatial population data to get a more accurate estimation of spatial economic activity. The work flow of the asset exposure disaggregation is described here in detail and illustrated in Fig. 2.

In a first step, the two gridded input datasets are interpolated linearly to the same resolution of 30 arcsec. Then, the combination of the two aforementioned datasets is conducted for each grid cell:

$$Lit^m Pop^n{}_{pix} = \left(NL_{pix} + \delta\right)^m \cdot Pop_{pix}{}^n \quad , \tag{2.1}$$

where the digital number value $Lit^mPop^n{}_{pix}$ per grid cell (pix) is computed from the grid cell's nightlight intensity $NL_{pix} \in [0, 255]$, population count $Pop_{pix} \in \mathbb{R}^+$, and the exponents $m, n \in \mathbb{N}$. For all $n > 0$, the added δ is equal to 1 to ensure that non-illuminated but populated grid cells do not get assigned zero values. In the case that nightlight data are used on their own without population data ($n = 0$), δ is set to zero.

In a second step, gridded Lit^mPop^n is taken as a relative representation of economic stocks at each grid cell. It is used to linearly disaggregate total asset values of a country to a geographical grid. More precisely, the value of $Lit^mPop^n{}_{pix}$ relative to the sum of Lit^mPop^n over all pixels within the boundaries of the country determines how much of a total value is assigned to each grid cell:

$$I_{pix} = I_{tot} \cdot \frac{Lit^m Pop^n{}_{pix}}{\sum_{pix\_i}^{N}\left(Lit^m Pop^n{}_{pix\_i}\right)} \tag{2.2}$$

where I_{pix} denotes the asset value per grid cell. The given value of a country's total asset value I_{tot} is distributed to each grid cell pix proportionally to the $Lit^m Pop^n$ share of the grid cell. N denotes the total number of grid cells (iterator pix_i) inside the boundaries of the country.

Changing the exponents m and n determines with which power the two input variables contribute to the disaggregation function. The exponents m and n do not only weight relatively between *Lit* and *Pop* but they also determine the contrast in the distribution between all grid cells within a country. The larger the exponent, the more value is concentrated on grid cells with large values of *Lit* or *Pop*. The aim of the evaluation described in Section 2.2.6 is to compare disaggregation skill of varied combinations of m and n and select the most adequate combinations for subnational disaggregation.

I_{tot} can represent either asset value or GDP, depending on the context. For the creation of gridded asset exposure data, I_{tot} represents asset value, i.e. produced capital or nonfinancial wealth. For the evaluation presented in Section 2.2.6, I_{tot} represents the flow variable GDP instead, as in the study of Zhao et al. (2017).

2.2.6 Evaluation

Gridded population and nightlight intensity can both be used as proxies for the spatial distribution of asset exposure. Both proxies have limitations: an asset distribution proportional to population density assumes that physical wealth is distributed equally among the population and that assets are located exactly where people live. As already mentioned in Section 2.2.3, for many developing countries, gridded population data have a coarse resolution. Nightlight-based models, on the other hand, are mainly limited by saturation and blooming as described in the Introduction. By combining nightlight intensity and population count, we expect to combine their skills while reducing the limitations mentioned above.

The LitPop approach's skill in disaggregating asset exposure cannot be assessed directly due to the lack of reference asset value data on a subnational level. Therefore, GDP and GRP are used instead for an indirect evaluation of the methodology. GDP and GRP are used to assess the subnational disaggregation skill, comparing varying combinations of the exponents m and n in $Lit^m Pop^n$.

The disaggregation skill is assessed as follows: (i) national GDP is disaggregated to the grid level. (ii) The resulting gridded GDP is then re-aggregated for each subnational region (i.e. district, state, or canton) to obtain modeled GRP. (iii) Based on the comparison of normalized modeled and reported reference values of GRP, skill metrics are computed per country. In total, we use reported GRP data for 507 regions in 14 countries to evaluate the model's ability to distribute national GDP to subnational regions.

To ensure comparability of skill metrics between different countries, GRP is normalized:

$$nGRP_i = \frac{GRP_i}{GDP}, \tag{2.3}$$

where $nGRP_i$ denotes the normalized GRP of subnational region i. Given that $\mathrm{GDP} = \sum_i^N(\mathrm{GRP_i})$, it follows from Equation 2.3 that $\sum_i^N(\mathrm{nGRP_i}) = 1$. Here, N is the set of all subnational units in the country.

To assess the disaggregation skill per country, three skill metrics are computed from nGRP: The Pearson correlation coefficient ρ (Equation 2.4) is computed to measure the linear correlation between the modeled $nGRP_{mod}$ and the reference value $nGRP_{ref}$. ρ is computed from the covariance (cov) and the standard deviations $\sigma_{\mathrm{mod}} = \sigma(\mathrm{nGRP_{mod}})$ and $\sigma_{\mathrm{ref}} = \sigma(\mathrm{nGRP_{ref}})$:

$$\rho = cov(nGRP_{i,mod}, nGRP_{i,ref})/(\sigma_{mod} \cdot \sigma_{ref}) \tag{2.4}$$

The correlation coefficient ρ is a widely used metric and straightforward to interpret and communicate: a value of 1 indicates a perfect positive linear correlation between the two variables while a value of 0 indicates that there is no linear correlation. However, ρ is no direct measure of the deviations of $nGRP_{mod}$ from $nGRP_{ref}$ and yields no information regarding the slope β of the linear relationship. Therefore, it only represents a potential skill and needs to be evaluated in combination with a measure of the slope. The slope of the linear regression conveys the information, whether there is a systematic over- or underestimation of regions with relatively large GRP in the disaggregated data.

$\beta = \rho \cdot \sigma_{mod}/\sigma_{ref}$ is calculated to complement the analysis: β larger (lower) than 1 implies an overestimation (underestimation) of the GRP of regions with relatively large GRP and an underestimation (overestimation) of regions with relatively low GRP by the downscaling within one country. Together, ρ and β allow for an evaluation of the linear fit between modeled and reference data.

Complementarily, the root-mean-squared fraction (RMSF) is a relative error metric, weighting the relative deviation for each region equally, independently of the absolute values. Therefore, RMSF (Equation 2.5) puts equal weight on all subnational administrative units in a country, even if their GRP and thus their absolute difference between modeled and reference values are small. A RMSF of 1 indicates perfect fit. A RMSF value of 2 means that on average the modeled GRP deviates by a multiplicative factor of 2 from the reference value.

$$RMSF = exp\left(\sqrt{\frac{1}{N}\sum_i^N \left[\log\left(\frac{nGRP_{i,mod}}{nGRP_{i,ref}}\right)\right]^2}\right) \quad (2.5)$$

For evaluation, the three skill metrics are calculated for varying combinations of nightlight and population data for the disaggregation of GDP. The resulting skill metrics are compared for each combination and country.

2.3 Results

2.3.1 Global gridded asset exposure

We applied the LitPop methodology with the exponents $m = n = 1$ to compute gridded asset exposure data for 224 countries and areas worldwide (Fig. 3). Total physical asset values of 2014 were disaggregated proportionally to Lit^1Pop^1 to a grid with the spatial resolution of 30 arcsec (approximately 1 km). Total asset values in the dataset sum up to $2.51*10^{14}$ (251 trillion) current US dollars in 2014. The 140 countries with produced capital data used as total asset value (see Section 2.2.4.1) contribute USD 245 trillion (97.6 %) to the total asset exposure. The remaining 84 countries where asset values were estimated from GDP and a GDP-to-wealth ratio instead contribute the remaining USD 6 trillion. In total, the 224 countries contribute around 99.9% to recorded global GDP. All numbers are based on the national values assembled in Table S1. Data sources are summarized in Table 1.

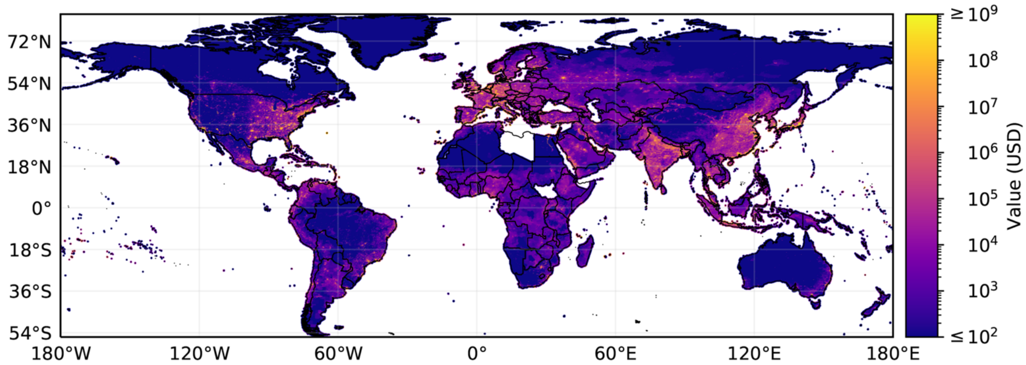

Figure 3: World map showing gridded asset exposure values scaled to a resolution of 600 arcsec. The actual resolution of the underlying gridded data is 30 arcsec (~1 km). To obtain this dataset, national total asset values were disaggregated proportionally to the distribution of Lit^1Pop^1 for 224 countries and areas. A total of 26 countries and areas without data are left blank, including Libya, South Sudan, and Syria. The color map is logarithmic and limited to USD 100 (lower bound) and USD 1 000 000 000 (upper bound). Borders and coast lines are based on Cartopy (Met Office, 2010).

In the following subsections, the LitPop methodology is evaluated both quantitatively and qualitatively: The results of the quantitative assessment of disaggregation skill introduced in Section 2.2.6 are presented in Section 2.3.2, providing justification for the selected combination of the exponents m and n for the global dataset. Differences between asset exposure distribution based on Lit^1, Pop^1, and Lit^1Pop^1 are shown by example of detail maps of two metropolitan areas (Section 2.3.3). Finally, limitations of the LitPop methodology are discussed by the example of GDP disaggregation in Mexico (Section 2.3.4).

2.3.2 Evaluation

To evaluate the performance of the LitPop methodology, we compute and compare the disaggregation skill with regards to GDP for varying exponents m and n in Lit^mPop^n (Eq. 2.1 and 2.2). Here, we show the comparison based on 14 countries with a total of 507 regional GRP data points available. The 14 countries make up 67% (USD 168 trillion) of the total dataset's exposure and 64.5% (USD 52 trillion) of global GDP in 2014. Ten combinations of m and n are assessed: Lit^1Pop^1, Lit^1, Lit^2, Lit^3, Lit^4, Lit^5, Pop^1, Pop^2, Lit^2Pop^1, and Lit^3Pop^1. These exponent combinations were selected based on examples in the literature and then explored iteratively, stopping at combinations with decreased skill compared to lower-order combinations. For each country and exponent combination, the median and the spread of three skill metrics are compared: ρ, β, and RMSF (Fig. 4 and Tables A2 and A3).

For ρ (Fig. 4a), Lit^1Pop^1 shows the best overall median of ρ (0.94) with the lowest interquartile range (IQR) of 0.09. The IQR is used here as a measure of variability of the skill metrics, as it signifies the difference between the 25th and the 75th percentiles of the resulting skill metric. The same holds for β of Lit^1Pop^1 (median=1.03, IQR=0.12, Fig. 4b). In contrast, β is on average well below 1 for combinations exclusively based on Lit (i.e., Lit^m). A value of β below 1 indicates an underestimation of the GRP of regions with relatively large GRP and an overestimation of smaller regions. This can possibly be attributed to the saturation problem of nightlight intensity data, given that large regions with relatively large GRP usually accommodate more metropolitan areas where saturation occurs the most. This interpretation is supported by the relatively low asset values attributed to London and Mumbai metropolitan areas by Lit^1 shown in Section 2.3.3.

For purely population-based disaggregation, we found a median of β below 1 for *Pop*[1]and well above 1 for *Pop*[2] (Fig. 4b). This suggests that disaggregation proportional to *Pop*[1] underestimates the asset values in urban agglomerations, while it is overestimated by *Pop*[2]. For the metric RMSF, *Pop*[1] (median=1.37, IQR=0.37) and *Lit*[4] (median=1.64, IQR=0.36) perform best, while *Lit*[1]*Pop*[1] has a median RMSF of 1.67 and an IQR of 1.29 (Fig. 4c).

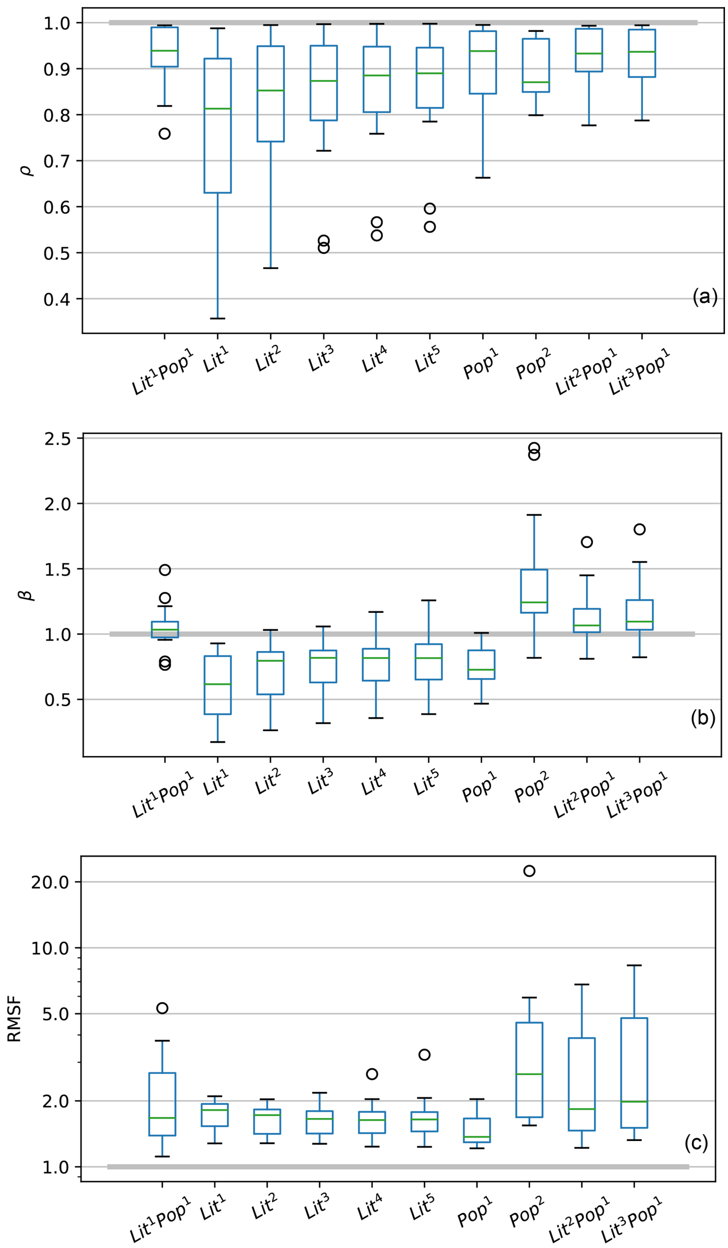

Figure 4: Box plots showing the skill metrics ρ (a), β (b), and RMSF (c) for variations in Lit^mPop^n. The metric value of 1, indicating perfect skill, is demarcated by the solid grey line. The plots are based on data from 14 countries and show the median (green), the first and third quartiles (IQR, blue box), data points outside the IQR but not more than 1.5·IQR distance from either the first or the third quartile (black whiskers), and outliers (black circles). RMSF is plotted on a logarithmic scale. Underlying metric values per country are listed in Table A2. Median and IQR per skill metric and combination of exponents are shown in Table A3

Within the set of combinations exclusively based on *Lit* (n=0), the skill metrics β and RMSF perform best for Lit^4 (Fig. 4b,c), with median ρ improving for larger values of *m*, however changing little from Lit^4 to Lit^5 (Fig. 4a).

Based on the comparison of the disaggregation skill with varying exponents *m* and *n*, there are two candidates for the most adequate functionality: Lit^1Pop^1 (best ρ and β) and Lit^4 (best RMSF and best performance for n=0). The skill metrics of linear regression, ρ and β, give a better representation of the disaggregation skill for the absolute values than RMSF which is based on the relative deviation per data point. Prioritizing a better distribution of total values over relative performance, we conclude that Lit^1Pop^1 can be considered the most adequate combination of *Lit* and *Pop* for the subnational downscaling of GDP. For countries with a lack of highly resolved population data, alternative datasets could be produced based on Lit^4 alone.

2.3.3 Detailed maps for metropolitan areas

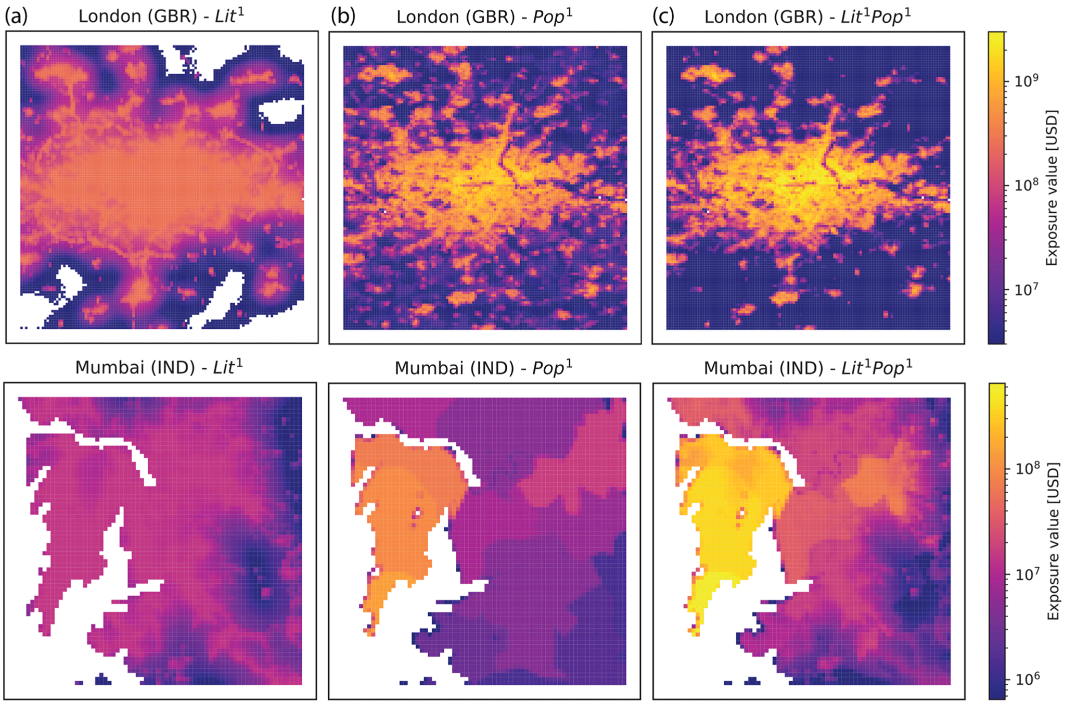

Figure 5: Maps of disaggregated asset exposure value. Values are spatially distributed proportionally to nightlight intensity of 2016 (Lit^1, a), population count as of 2015 (Pop^1, b), and the product of both (Lit^1Pop^1, c) for metropolitan areas in the United Kingdom (GBR) and India (IND). The maps are restricted to the wider metropolitan areas of London (51–52° N, 0.6° W–0.4° E) and Mumbai (18.8–19.4° N, 72–73.35° E). The color bar shows asset exposure values in current USD in 2014 per pixel of approximately 1 km^2.

Saturation and blooming in nightlight intensity data cause disaggregation based on nightlights alone to misrepresent actual value distribution, especially in urban areas. This can be seen in Fig. 5, showing maps of the distribution of national produced capital disaggregated proportionally to Lit^1 (a), Pop^1 (b) and Lit^1Pop^1 (c) for two wider metropolitan areas. London (top row) and Mumbai (bottom) were chosen as examples. Comparable maps for Mexico City and New York are shown in Fig. A1 in the Appendix.

The general exposure value level in the metropolitan areas shown in Fig. 5 are largest for *Lit^1Pop^1* (Fig. 5c), highlighting a larger concentration of values in urban areas with this approach. The value distribution based on *Lit^1* (Fig. 5a) does not show many details within the urban area. This effect is partially caused by saturation: the light radiation in the depicted areas is of such high intensity, that the nightlight data do not offer any way to distinguish different levels of human activity. We can also observe the blooming effect, with the luminosity of bright parts crowding out to neighboring pixels, causing them to appear brighter than their underlying light sources would warrant. This latter effect can be particularly illustrated over the Thames River and Bow Creek in the northeastern part of London: The unpopulated river area is resolved by *Pop^1* (Fig. 5b top) but not by *Lit^1* (Fig. 5a top). By taking population density into account, the *Lit^1Pop^1* dataset enhances contrast and detail in urban areas (Fig. 5b, c). In addition, bright objects can be overrepresented by *Lit^1*: in Fig. 5a (top), the M25 London Orbital Motorway around London clearly stands out, with some pixels even at the same value as in central London.

As seen in the case of Mumbai, the *Lit^1Pop^1* based asset exposure map of the metropolitan area in Fig. 5c (bottom) shows much higher total values than those based on nightlights or population alone. This means that for *Lit^1Pop^1*, a larger proportion of the national produced capital of India is attributed to the metropolitan area of Mumbai compared to *Lit^1* and *Pop^1* alone.

2.3.4 Example Mexico

The skill metrics for the subnational disaggregation of GDP in the country Mexico show low values of ρ compared to most other countries for all tested values of *m* and *n* (ρ=0.76 for *Lit^1Pop^1*, see Table A2a). The example of Mexico is presented here to illustrate limitations and uncertainties of the disaggregation approach. Figure 6 shows the data behind the evaluation for Mexico, i.e. modeled and reference *nGRP* for all 32 districts of Mexico. The corresponding plot data can be found in Table S2 in the Supplement. While the LitPop methodology performs well for most of the districts with relatively low GRP, it fails to reproduce reference *nGRP* for the main (capital) metropolitan region consisting of the districts México and Mexico City (Distrito Federal).

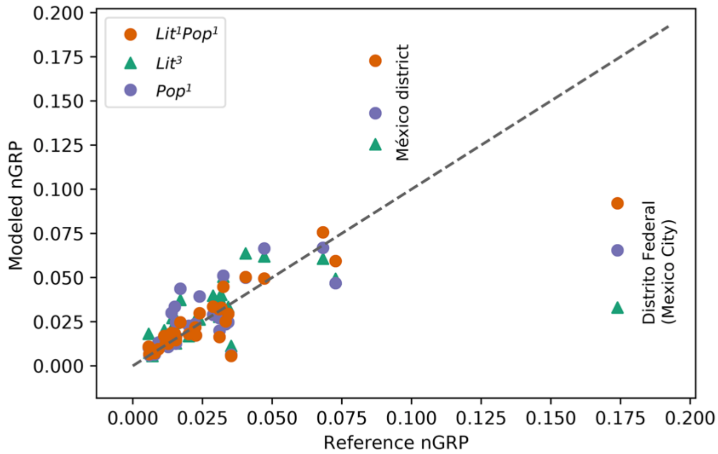

Figure 6: Normalized gross regional product (nGRP) for the 32 districts of Mexico. Reference values are shown on the horizontal axis and modeled values on the vertical axis.

The two districts with the largest GRP of the highly centralized country are Distrito Federal (the Mexico City district) with a reference *nGRP* of 17.4% and the México district (8.7%), surrounding Distrito Federal. Asset exposure maps of the metropolitan region are shown in Fig. A1 in the Appendix. The disaggregation of GDP underestimates *nGRP* for the Mexico City district while overestimating the value for México for all evaluated combinations of *m* and *n* (*nGRP* values for Lit^1Pop^1, Lit^3, and Pop^1 are shown in Fig. 6). The overestimation of the México district's *nGRP* indicates that the district has an over-proportional nightlight intensity and population count compared to a relatively low reference *nGRP*. Both districts combined sum up to modeled *nGRP* values of 11.2% (m=1) to 17.6% (m=5) for Lit^m, 20.8% for Pop^1, and 26.5% for Lit^1Pop^1 (Table S2), the last agreeing well with a combined reference *nGRP* of 26.1%.

2.4 Discussion

The LitPop methodology allows for the creation of globally consistent and spatially highly resolved estimates of gridded asset exposure value. According to Pittore et al. (2017), efforts towards improving exposure data should aim at global consistency, continuous integration of new data and methods, and a careful validation of models and data. Here, we will discuss the advantages and limitations of the LitPop methodology with regard to the following key criteria: global consistency, disaggregation skill, scalability and flexibility, openness, replicability and reproducibility, and low entry threshold.

Global consistency. Based on globally available input data, the LitPop methodology was applied across countries from different continents and income groups. While the presented asset exposure dataset is not complete, it provides data for 224 countries contributing 99.9 % of global GDP. Therefore, LitPop-based asset exposure data can be used as a basis for globally comparable economic risk assessments. However, the evaluation of the methodology's disaggregation skill presented here is limited to an assessment of disaggregation skill for 14 OECD countries. It should be noted that due to lack of data we were not able to evaluate the method's performance for low-income countries (World Bank income group 1). Therefore, the application of the asset exposure data for local assessments in countries within low-income groups should be treated with caution. Another caveat to global consistency is the fact that the quality and resolution of the underlying population dataset vary between countries, as discussed in greater detail in the next paragraph. As a consequence of these limitations, asset exposure data should be validated against local data before application for local risk assessments, especially in low-income countries.

Assessment of disaggregation skill. For the gridded exposure dataset presented here, the LitPop methodology is used to disaggregate total asset values. Due to a lack of subnational reference asset values, the LitPop methodology's performance for the downscaling of asset stock values could not be evaluated directly. The assessment of disaggregation skill was instead based on the flow variables GDP and GRP. Given a correlation between stocks and flows within each country, this approach represents an indirect evaluation of the methodology for asset exposure downscaling. Evaluating 14 countries, we found that the LitPop methodology generally performs well in disaggregating GDP to the subnational level. The skill metrics ρ and β showed that Lit^1Pop^1 distributes GDP better to the subnational level than the other combinations of nightlight and population data assessed. For RMSF, Pop^1 and Lit^4 perform best on average. We selected Lit^1Pop^1 as a basis for the disaggregated asset exposure dataset presented here. This decision is based on two considerations: (1) giving ρ and β priority over RMSF because they are measures of absolute deviation between variables (compared to RMSF that is a measure of relative deviation per data point) and (2) the fact that Lit^1Pop^1 combines the advantages of both input data types and mitigates their disadvantages, i.e., with regard to saturation, blooming, and detail. For countries without a high detail level in the population data available, asset exposure based on Lit^mPop^n is more or less equivalent to that based on Lit^m alone. For regional application in these countries, evaluation results suggest that disaggregation proportional to Lit^4 could distribute asset values best in the absence of detailed population data.

Scalability and flexibility. Subject to data availability, the LitPop methodology can be used to estimate the distribution of physical asset values for any target year at a wide range of resolutions. The data sources used here cater to resolutions up to 30 arcsec. While the GPW dataset provides population data for the previous 2 decades, the NASA nightlight images are currently only available for 2012 and 2016. The methodology includes a scaling of exposure data proportionally to current GDP for years without any data available. The methodology can potentially be adapted to a variety of applications by an appropriate choice of the socioeconomic indicator that is disaggregated. The World Bank's produced capital data are used here as the default total asset value per country. Alternatively, GDP can be used as an estimator of economic output. GDP multiplied by a factor derived from the country-specific income group can also be used to estimate asset values (Aznar-Siguan and Bresch, 2019; Geiger et al., 2017). This was done for countries without produced capital numbers available. Since the CLIMADA repository is open-source, the LitPop methodology can be amended to include alternative data sources and versions of gridded nightlight, population and total asset values, or other socioeconomic indicators to expand and update the asset exposure data. The LitPop methodology was developed to provide globally consistent asset exposure data for global-scale physical risk modeling. While it could be used for other applications as well, the limitations of its scope should be noted. The LitPop methodology does not account for differences in infrastructure types and vulnerability. In addition, gridded data may cause poor scoping of areas most vulnerable, or those with more exposed population. The example of Mexico (Section 2.3.4) illustrates the limitations of the LitPop methodology when it comes to the disaggregation of GDP within a metropolitan area: While the disaggregation of GDP proportional to Lit^1Pop^1 nicely reproduces the summed *nGRP* of the metropolitan area, the methodology fails to reproduce the distribution of *nGRP* between the two districts that make up the metropolitan area. Therefore, the use of the asset exposure data for local applications should be treated with care. The use for local or sector-specific applications is limited without the addition of sector-specific datasets. For risk assessments with a local focus as well as in countries of low income, we would advise using more local approaches and bottom-up methods for identifying and analyzing the vulnerability component. Additionally, the asset exposure data could be further refined by including auxiliary data, such as road networks and land cover (Geiger et al., 2017; Murakami and Yamagata, 2019), or mobile phone cell antenna density (Brönnimann and Wintzer, 2018). In order to include sector-specific assets not represented by the LitPop methodology, i.e. power plants or mines in unpopulated areas, additional sector-specific asset inventories should be included (Gunasekera et al., 2015). For a globally consistent approach, sectoral data should however be included with caution, as such datasets are prone to regional or national biases.

Openness, replicability, and low entry threshold. The LitPop methodology was developed in the programming language Python 3 and published on the code hosting service GitHub as well as in a permanent repository (see Section 2.5). The CLIMADA repository is developed open-source and makes use of open-access data to enable unrestricted use for applications beyond academia. In addition to the dataset provided, the LitPop-module can be used both to apply the computed asset exposure data for direct application in event-based risk assessments with CLIMADA and to export gridded asset exposure data to standard formats for use in other applications. While Lit^1Pop^1 is the default, Lit^mPop^n with custom exponents can be chosen as a basis for disaggregation. The documentation of CLIMADA is hosted on Read the Docs (https://climada-python.readthedocs.io/en/stable/, last access: 4 April 2020). It includes an interactive tutorial of CLIMADA and the LitPop module (climada-python.readthedocs.io/en/stable/tutorial/climada_entity_LitPop.html, last access: 4 March 2021), with guidance on how to compute and export LitPop-based asset exposure data.

2.5 Data and code availability

Asset exposure data at a resolution of 30 arcsec for 224 countries, as well as normalized Lit^1 and Pop^1 for the 14 countries used for evaluation are archived in the ETH Research Repository with link https://doi.org/10.3929/ethz-b-000331316 (Eberenz et al., 2019). The LitPop methodology is openly available as a module of CLIMADA (CLIMADA-Project, 2019) at GitHub under the GNU GPL license (Free Software Foundation, Inc., 2007). CLIMADA v1.2.0 was used for this publication, which is permanently available at the ETH Data Archive with link http://doi.org/10.5905/ethz-1007-226 (Bresch et al., 2019). The scripts reproducing the published dataset, as well as all figures in the present publication and the main results are published in the CLIMADA-papers repository on GitHub with link https://github.com/CLIMADA-project (Aznar-Siguan et al., 2020).

2.6 Conclusion

The open-source LitPop methodology was developed to provide a geographical distribution of physical asset exposure values that can be used to model first-order economic impacts of weather and climate events and other natural disasters. It uses publicly available data sources to calculate gridded asset exposure estimates. The global consistency, flexibility and openness, and the integration in the CLIMADA repository offer value for manifold use cases for economic disaster risk modeling and climate change adaptation studies. However, the methodology could not be evaluated directly against subnational asset data, and the evaluation based on GDP was limited to 14 OECD countries. Therefore, the asset exposure data are not suitable for applications with a local or sector-specific focus without further validation. Future research and development could focus on the integration of more highly resolved population data and other ancillary data sources as they become available globally. Validation against subnational asset value and empirical asset stock inventories yields the potential to evaluate and further improve the accuracy of asset exposure downscaling, for both global and regional applications. Regional validation could further inform the choice of the most appropriate downscaling functionality for different income groups and world regions.

3. Regional tropical cyclone impact functions for globally consistent risk assessments

Samuel Eberenz[1,2], Samuel Lüthi[1,2], David N. Bresch[1,2]

Published in Natural Hazards and Earth System Sciences, 21, 393–415, 2021,
DOI: 10.5194/nhess-21-393-2021.

ABSTRACT. Assessing the adverse impacts caused by tropical cyclones has become increasingly important as both climate change and human coastal development increase the damage potential. In order to assess tropical cyclone risk, direct economic damage is frequently modeled based on hazard intensity, asset exposure, and vulnerability, the latter represented by impact functions. In this study, we show that assessing tropical cyclone risk on a global level with one single impact function calibrated for the USA – which is a typical approach in many recent studies – is problematic, biasing the simulated damage by as much as a factor of 36 in the north West Pacific. Thus, tropical cyclone risk assessments should always consider regional differences in vulnerability, too. This study proposes a calibrated model to adequately assess tropical cyclone risk in different regions by fitting regional impact functions based on reported damage data. Applying regional calibrated impact functions within the risk modeling framework CLIMADA (CLIMate ADAptation) at a resolution of 10 km worldwide, we find global annual average direct damage caused by tropical cyclones to range from USD 51 up to USD 121 billion (value in 2014, 1980–2017) with the largest uncertainties in the West Pacific basin where the calibration results are the least robust. To better understand the challenges in the West Pacific and to complement the global perspective of this study, we explore uncertainties and limitations entailed in the modeling setup for the case of the Philippines. While using wind as a proxy for tropical cyclone hazard proves to be a valid approach in general, the case of the Philippines reveals limitations of the model and calibration due to the lack of an explicit representation of sub-perils such as storm surge, torrential rainfall, and landslides. The globally consistent methodology and calibrated regional impact functions are available online as a Python package ready for application in practical contexts like physical risk disclosure and providing more credible information for climate adaptation studies.

[1] Institute for Environmental Decisions, ETH Zurich, Switzerland

[2] Federal Office of Meteorology and Climatology MeteoSwiss, Switzerland

3.1 Introduction

Tropical cyclones (TCs) are highly destructive natural hazards affecting millions of people each year (Geiger et al., 2018; Guha-Sapir, 2018) and causing annual average direct damage in the order of USD 29 to 89 USD billions (Cardona et al., 2014; Gettelman et al., 2017; Guha-Sapir, 2018). Climate change and coastal development could significantly increase the impact of TCs in the future (Gettelman et al., 2017; Mendelsohn et al., 2012). Increasing risks from TCs and other extreme weather events pose a challenge to exposed populations and assets but also to governments and investors as actors in globally connected economies. Governments, companies, and investors increasingly express the need to understand their physical risk under current and future climatic conditions (Bloomberg et al., 2017). Thus, quantitative risk assessments require a globally consistent representation of the economic impact of TCs and other natural hazards.

Probabilistic risk models can provide the quantitative basis for risk assessments and adaptation studies. Since the mid-2000s, there have been increasing scientific efforts in developing and improving global-scale natural hazard risk assessments (Cardona et al., 2014; Gettelman et al., 2017; Ward et al., 2020). Risk from natural hazards is frequently modeled as a function of severity and occurrence frequency, which can be computed by combining information on hazard, exposure, and vulnerability (IPCC, 2014a). Global- and regional-scale TC risk models often represent hazard as the spatial distribution of the maximum sustained surface wind speed per TC event (Aznar-Siguan and Bresch, 2019; Ward et al., 2020). In past studies, wind fields modeled from historical TC tracks were used to assess economic risk in the Global Assessment Report (GAR) 2013 (Cardona et al., 2014; UNDRR, 2013) and to quantify affected population (Geiger et al., 2018), among others. For the assessment of future risk, historical TC records can be complemented with events simulated in downscaling experiments based on the output of global climate models (Gettelman et al., 2017; Korty et al., 2017), or synthetic resampling algorithms (Bloemendaal et al., 2020). The exposure component can be represented by the spatial distribution of people, assets or economic values potentially affected by TCs (Geiger et al., 2018; Ward et al., 2020). For the modeling of direct economic damage, exposure is usually derived from building inventories for local risk assessments (Sealy and Strobl, 2017), or estimated by spatially disaggregating national asset value estimates (De Bono and Mora, 2014; Eberenz et al., 2020; Gettelman et al., 2017).

The vulnerability of an exposed value to a given hazard can be represented by impact functions, also called damage functions or vulnerability curves, relating hazard intensity to impact. Impact functions for the assessment of direct economic damage caused by TCs usually relate wind speed to relative damage (Emanuel, 2011b). For the USA, TC impact functions are available specific to different building types

(Federal Emergency Management Authority [FEMA], 2010; Yamin et al., 2014), as well as on an aggregate level (Emanuel, 2011b). Emanuel et al. (2012) found a lack of sensitivity of simulated TC damage to the exact shape of the impact function for the USA. However, due to global heterogeneities in the tropical cyclone climatology (Schreck et al., 2014), building codes, and other socioeconomic vulnerability factors (Yamin et al., 2014), it is inadequate to use a single universal impact function for global TC risk assessments. Bakkensen et al. (2018b) used reported damage data to calibrate TC impact functions for China, highlighting both the potential of this approach and the considerable uncertainties related to the quality of reported damage data. Still, there is a lack of globally consistent and regionally calibrated impact functions. Due to this lack, impact functions calibrated for the USA have been used in a variety of local and regional studies outside the USA, i.e. the Caribbean (Aznar-Siguan and Bresch, 2019; Bertinelli et al., 2016; Ishizawa et al., 2019; Sealy and Strobl, 2017), China (Elliott et al., 2015b), and the Philippines (Strobl, 2019). A similar impact function has also been applied for modeling TC damages on a global level (Gettelman et al., 2017).

For GAR 2013, building-type specific impact functions from FEMA were assigned to exposure points based on global data based on development level, complexity of urban areas, and regional hazard level at each location (De Bono and Mora, 2014; Yamin et al., 2014). However, the impact functions were not calibrated regionally against reported damage data. Furthermore, the required complexity in exposure data exceeds the scope of many risk assessments.

Can globally consistent TC impact modeling be improved by calibrating the vulnerability component on a regional level?

This article addresses this question by calibrating regional TC impact functions in a globally consistent TC impact modeling framework, as implemented within the open-source weather and climate risk assessment platform CLIMADA (CLIMate ADAptation, Aznar-Siguan and Bresch, 2019). This study contributes to reaching the goal of consistent global TC risk modeling and a better connection of global and regional impact studies. The objectives of this study are to (1) calibrate a global TC impact model by regionalizing the impact function; (2) assess the annual average damage (AAD) per region and compare the results to past studies, and (3) evaluate the robustness of the calibration and discuss the limitations and uncertainties of both the model setup and the calibration. To inform the discussion of uncertainties, we complement aggregated calibration results (Section 3.3) with an event-level case study for the Philippines (Section 3.4). While the attribution of vulnerability to regional drivers is outside the scope of this study, the results can serve as a starting point for further research disentangling the socio-economic and physical drivers determining vulnerability to TC impacts locally and across the globe.

3.2 Data and methods

To regionally calibrate TC impact functions, simulated damage is compared to reported damage, as illustrated in Figure 7. In a first step, direct economic damage caused by TCs is simulated in the impact modeling framework CLIMADA (Fig. 7a-d; Section 3.2.1 to 3.2.2.2) with one single default impact function applied globally to start from (Section 3.2.2.3). Then, damage data points per country and TC event are assigned to entries of reported damage (Fig. 7e-f; Section 3.2.3.1). For the matched events, the ratio between simulated and reported damage is calculated (Fig. 7g; Section 3.2.3.2). For calibration, countries are clustered into regions, and two complementary cost functions are optimized based on the damage ratios, by regionally fitting the slope of the impact function (Fig. 7h; Section 3.2.3.3).

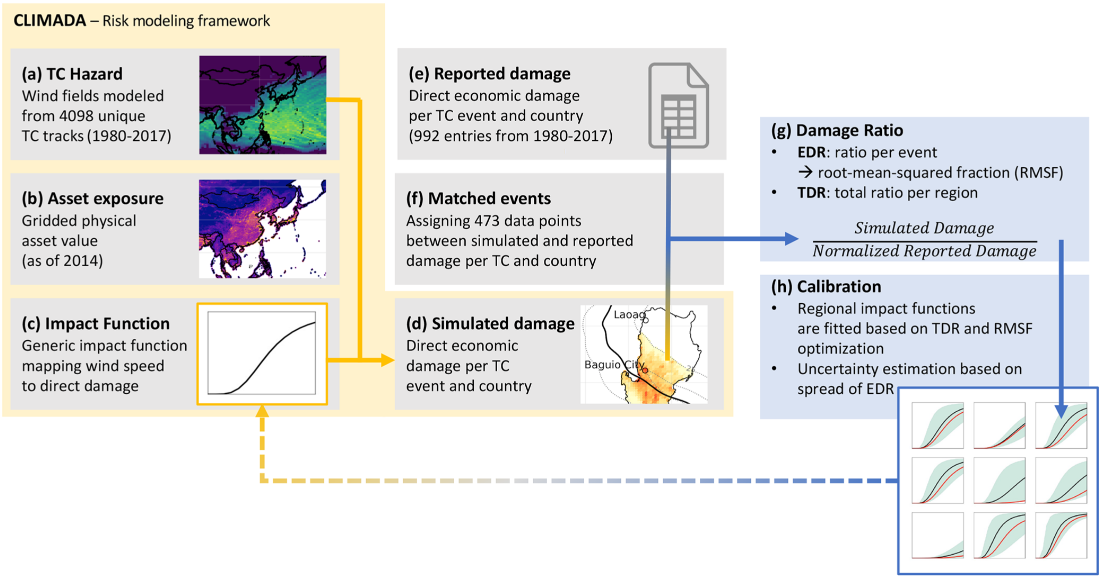

Figure 7: Schematic overview of the data and methods applied to calibrate regional tropical cyclone (TC) impact functions in a globally consistent manner. From left to right: TC event damages are first simulated within the CLIMADA framework based on TC hazard (a), asset exposure (b), and a default impact function (c), c.f. Section 3.2.1 to 3.2.2.3. Resulting simulated damages (d) are compared to reported damage data from EM-DAT (e) for 473 matched TC events (f) by means of the damage ratio (g), c.f. Section 3.2.2.4 to 2.3.2. During calibration (h), steps (c) to (g) are repeated several times with varied impact functions for each region, optimizing the cost functions TDR and RMSF (c.f. Section 3.2.3.3) . The result is a set of best fitting impact functions for nine world regions (Section 3.3.2). Finally, the calibrated impact functions are plugged into CLIMADA once more (dashed arrow)to compute annual average damage (AAD) per region (Section 3.3.3).

3.2.1 CLIMADA – spatially explicit TC risk modeling

The CLIMADA (CLIMate ADAptation) impact modeling framework has been developed at ETH Zurich as a free, open-source software package (Aznar-Siguan and Bresch, 2019). It is written in Python 3.7 and made available online on both GitHub (CLIMADA-Project, 2019) and the ETH Data Archive (Bresch et al., 2019). Here, CLIMADA was used for the preprocessing of hazard and exposure data, and for the spatially explicit computation of direct damage on a global grid at 10 km resolution. The setup works equally well at a higher chosen resolution, but the given uncertainties especially in calibration data and computational constraints justify the chosen resolution. In the CLIMADA framework, damage is defined as the product of exposed assets and a damage ratio. The damage ratio is an impact function multiplied by hazard intensity.

In our case, damage per TC event and country is simulated as follows: for each grid cell and event, damage is calculated as the product of total exposed asset values and the mean damage ratio. The mean damage ratio (0 to 100%) results from plugging the hazard intensity (maximum sustained wind speed) into the impact function. Finally, damage per event is aggregated over all grid cells within the country. Please refer to Section 3.2.1 and 3.2.2.3 in Aznar-Siguan and Bresch (2019) for a more detailed description of impact calculation.

3.2.2 Data

3.2.2.1 TC Hazard

TCs typically inflict damage due to strong sustained surface winds, storm surge inundation, and torrential rain (Bakkensen et al., 2018a; Baradaranshoraka et al., 2017; Park et al., 2013). Next to maximum wind speed, storm size is an important factor controlling TC impacts (Czajkowski and Done, 2013). Since the severity of surge and rain is to a certain extent correlated to wind speed and storm size (Czajkowski and Done, 2013), the latter is often taken as a proxy hazard intensity (Emanuel, 2011b; Gettelman et al., 2017). Here, TC hazard intensity is represented by wind fields, i.e., the geographical distribution of the 1 min sustained wind speed at 10 m above ground per TC event, referred to as "wind speed" or "hazard intensity" in the following. Wind speed was simulated at a horizontal resolution of 10 km x 10 km from historical TC tracks as a function of time, location, radius of maximum winds, and central and environmental pressure, based on the revised hurricane pressure–wind model by Holland (2008). Please also refer to Geiger et al. (2018) for a detailed description and illustration of the wind field model and its limitations.

Historical TC tracks were obtained from the International Best Track Archive for Climate Stewardship (IBTrACS) (Knapp et al., 2010). As data quality and global coverage improved after approximately 1980 (Geiger et al., 2018), 4098 historical TC tracks from 1980 to 2017 were selected based on data completeness criteria with regards to data fields provided within IBTrACS following the approach described by Geiger et al. (2018) and Aznar-Siguan and Bresch (2019). Out of the 4098 TCs, a total number of 1'538 landfall events with the potential of causing damage were identified. Potential damage is given if at least one grid cell of a TC's wind field with an intensity of 25.7 m s^{-1} (~50 kn) or more coincides with an asset exposure value larger than zero. A world map showing the maximum intensity per grid cell for all tracks is shown in the Supplement (Fig. S1).

3.2.2.2 Asset exposure

Asset exposure for the assessment of direct economic risk is represented by the spatially explicit monetary value potentially impacted by a hazard. Here, we use gridded asset exposure value at a resolution of 10 km x 10 km. The dataset is based on the disaggregation of national estimates of total asset value (TAV, Table B3) proportional to the product of nightlight intensity and population count (Eberenz et al., 2020). Following the approach in GAR 2013 (De Bono and Mora, 2014), the TAV per country is represented by the produced capital stock of 2014 from the World Bank Wealth Accounting (World Bank, 2019). Out of the 62 countries used for calibration, 32 come with produced capital estimates. For the remaining 30, an estimate of non-financial wealth is used as a fallback (Eberenz et al., 2020), based on the gross domestic product (GDP) of 2014 from the World Bank Open Data portal (World Bank, online) combined with an GDP-to-wealth factor from the Global Wealth Report (Credit Suisse Research Institute, 2017). The asset exposure dataset utilized here and a detailed overview over limitations and data availability per country are documented in Eberenz et al. (2020).

3.2.2.3 Impact function

In CLIMADA, vulnerability is represented by impact functions. They are used to compute damage for each TC event at each exposed location by relating hazard intensity to relative impact. Since no directly wind-induced damage is expected for low wind speeds, TC impact functions for the spatially explicit modeling of direct damages can be constrained by a minimum threshold V_{thresh} for the occurrence of impacts and an upper bound of 100% direct damage (Emanuel, 2011b). Empirical studies suggest a high power-law function for the slope, i.e., the increase in damage with wind speed (Pielke, 2007). An idealized sigmoidal impact function satisfying these constraints was proposed by Emanuel (2011b):

$$f = \frac{v_n^3}{1 + v_n^3} \quad \text{, with} \quad v_n = \frac{MAX[(V - V_{thresh}), 0]}{V_{half} - V_{thresh}} \tag{3.1}$$

Equation (3.1) defines the impact function f as a function of wind speed V. The function takes two shape parameters as inputs: V_{thresh} and V_{half}. A lower threshold V_{thresh} of 25.7 m s^{-1} (50 kn) was proposed for the USA by Emanuel (2011b) and empirically supported for China (Elliott et al., 2015b). The slope parameter V_{half} signifies the wind speed at which the function's slope is the steepest and a damage ratio of 50% is reached (Fig. 8). It should be noted that the effects of varying V_{thresh} and V_{half} on resulting impacts are not linearly independent.

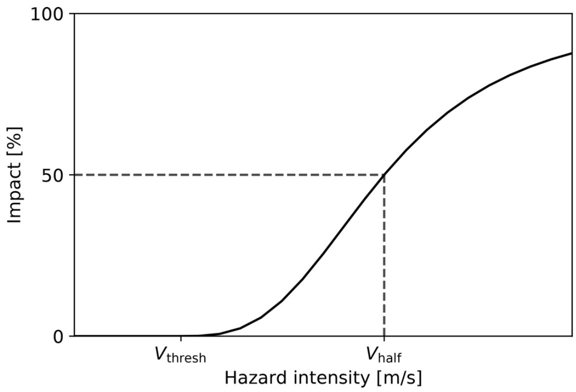

Figure 8: Idealized TC impact function based on Emanuel (2011b). V_{half} is the hazard intensity (i.e. maximum sustained wind speed) at which the relative impact reaches 50% of the exposed asset value. No impact occurs for an intensity below V_{thresh}.

Based on the reference data provided by FEMA (2010), V_{half} for damage to buildings can range from 52 to 89 m s^{-1} depending on building type and surface roughness (Elliott et al., 2015b). Applying FEMA impact functions that were verified with reported damage data for US hurricanes Andrew [1992], Eric [1995], and Fran [1996], Sealy and Strobl (2017) estimated V_{half} to range from 71.7 to 77.8 m s^{-1}, depending on building type, with a mean value of 74.7 m s^{-1}.

In a comparison of calibration results based on a sigmoidal impact function with a more complex 12-step staircase function, Lüthi (2019) found no improvement of calibration skill with the more complex function. Therefore, a sigmoidal function is applied in this study. The default impact function with V_{thresh} = 25.7 m s^{-1} and V_{half} = 74.7 m s^{-1} is used for a first, uncalibrated, simulation of global TC damages, and as a starting point for calibration. While V_{half} is fitted during the calibration process, the lower threshold V_{thresh} is kept constant throughout the study. This is based on the finding by Lüthi (2019) that the variation in more than one of the linearly dependent parameters most likely results in an overfitting during calibration with physically implausible values for V_{thresh} in some world regions.

On the chosen 10 km x 10 km grid, single buildings are not resolved. Therefore, damage is aggregated over several buildings in a grid cell and not all buildings are expected to be damaged to the same degree. However, the wind-speed-dependent impact function is also implicitly accounting for the damage caused by storm surge and torrential rain, when calibrated against reported damage data. For these two reasons, we allow for values of V_{half} lower and larger than the literature range for pure wind-induced building damage in the calibration. To find the functional slope best fit to simulate the direct economic damage of TCs in a region, V_{half} is varied step-wise with $V_{half} > V_{thresh}$ (c.f. Section 3.2.3.3, Calibration of regional impact functions).

3.2.2.4 Reported damage data

Reported damage data for historical TC events are required on a global level to calibrate TC impact functions.

Reported damage estimates for disasters worldwide are available from the International Disaster Database EM-DAT (Guha-Sapir, 2018). EM-DAT provides data per event and country, including disaster type and subtype, date of the event, and impact estimates. The main data sources of EM-DAT are UN agencies, governmental and non-governmental agencies, reinsurance companies, research institutes, and the press.

EM-DAT provides one entry per country and event. Therefore, one meteorological TC can be listed in EM-DAT several times, with one entry for each country affected. In the following, each of these entries per storm and country will be referred to as single 'TC events'. For instance, Hurricane Irma comes with 17 events in EM-DAT (disaster no. 2017-0381) as it impacted 16 Caribbean countries and the USA. From 1980 to 2017, there are 1650 TC events reported in EM-DAT of which 991 come with a reported monetary damage value.

The EM-DAT database provides total damage per event and country in current US dollars. In contrast, the asset exposure data used for the modeling of damage are kept fixed at the USD value of 2014 (Section 3.2.3). To allow for a comparison of reported and simulated damages that is independent of economic development, reported damage values need to be normalized to a reference year. For instance, Weinkle et al. (2018) applied two normalization methodologies for hurricane damage in the continental USA for 1900-2017, adjusting reported impact for inflation, per-capita wealth, and the population of affected counties (Collins and Lowe, 2001; Pielke et al., 2008). Due to a lack of global time series of wealth data, reported damage is normalized by means of GDP scaling. This is based on a less prerequisite approach applied in Munich Re's NatCat, in which recorded damages are normalized proportionally to regionalized GDP (Munich Re, 2018). This normalization approach assumes that time series in current GDP serve as a first order approximation of economic development, implicitly accounting for inflation, changes in wealth per capita and population. To obtain estimates of normalized reported damage (NRD) per event E, reported damage (RD) is scaled proportionally to the affected country's change in GDP between the year of occurrence y and the year 2014:

$$NRD_E = RD_E * \frac{GDP_{2014}}{GDP_y} \tag{3.2}$$

We found that GDP scaling removes the significant positive trend from the yearly impacts in the USA (p-values of 0.04 before and 0.14 after normalization). This is in agreement with the findings of existing normalization studies for past TC impacts in the USA (Pielke et al., 2008; Weinkle et al., 2018).

3.2.3 Methods

3.2.3.1 Event matching: assigning reported damage data to simulated TC events

For the comparison of simulated and reported TC damage, reported events from EM-DAT per TC and country need to be assigned to TC tracks from IBTrACS. Tracks were matched based on the country affected and timestamps (Lüthi, 2019). (1) In a first step, the impacted countries per TC track are determined, i.e., in which countries a storm does make landfall. (2) Subsequently, the best-fitting tracks are assigned to the reported events based on an iterative comparison of start dates provided in the datasets. Given that countries are hit by several TCs in a relatively short time, the assignment certainty varies. Finally, (3) tracks with a low assignment certainty are double-checked manually for removal or reassigning.

In total, we matched 848 EM-DAT events to their respective tracks. These events account for 913 billion USD in reported economic damage out of the total 959 billion USD from the 991 EM-DAT events (95 %). For 534 of the 848 assigned events, there is economic damage larger than zero simulated in CLIMADA with the respective TC track. Generally, the difference between simulated and reported damage per matched event spans several orders of magnitude. Extreme outliers are likely to be associated with either a mismatch or flawed values of reported damage. Therefore, we exclude 61 extreme outliers from calibration, i.e. all events that come with a deviation of more than a factor of 1000 between normalized reported damage and simulated damage with the default impact function.

Eventually, a total of 473 assigned events remain for analysis and referred to as ‘matched events’ in the following. These matched events, representing damage per TC and country, are based on 376 TC tracks making landfall in 53 countries (one TC can make landfall in several countries). The total reported damage from these 473 matched events accounts to 91 % of the sum of all TC-related reported damage from 1980 to 2017 in EM-DAT (76 % after normalization). Damage simulated for the 376 TCs with the default impact function amount to 58 % of the total global simulated damage from all 4098 TC tracks.

3.2.3.2 Damage ratios: event damage ratio and total damage ratio

For the analysis of regional differences in TC vulnerability, event damage is simulated with CLIMADA for all matched events with the default impact function (Section 3.2.4). The event damage ratio (EDR) is computed per matched event E as the ratio of simulated event damage (SED) over normalized reported damage (NRD):

$$EDR_E = \frac{SED_E}{NRD_E} \tag{3.3}$$

An EDR of 1.0 indicates a perfect fit between SED and NRD. An EDR greater (smaller) than 1.0 indicates an overestimation (underestimation) of the simulations as compared to reports. As there are considerable deviations between the distribution of EDRs between countries, the median of EDRs per country is used to define calibration regions in Section 3.2.3.3.

To compare the aggregated damage on a global or regional level, we use total damage ratio (TDR) defined as the sum of simulated damages divided by the sum of normalized reported damages:

$$TDR_R = \frac{\sum_{E=1}^{N} SED_E}{\sum_{E=1}^{N} NRD_E}, \tag{3.4}$$

where N is the number of matched events E in a region R.

The distribution of EDRs and TDRs before calibration, as well as TDRs after calibration, is shown per region in Figs. 12 and S4 and per country in Fig. S2.

3.2.3.3 Calibration of regional impact functions

As a first step towards the regional calibration of the TC impact model, distinct calibration regions were defined based on three criteria regarding (1) geography, (2) data availability, and (3) patterns in damage ratios before calibration. (1) We clustered countries by hemispheric ocean basins. This results in five high-level regions: North Atlantic and East Pacific oceans (NA), North Indian Ocean (NI), Oceania (OC), South Indian Ocean (SI), and north West Pacific (WP). This first geographical separation is applied to account for differences in TC characteristics and data sources between the ocean basins (Schreck et al., 2014). The five basins are then subdivided based on (2) a minimum desired number of 30 data points (matched TC events) per region and (3) the median EDRs per country. Applying criterion 2, three countries come with a sufficient amount of data points to be calibrated for themselves: China (N=69), the Philippines (N=83), and the USA (N=43, including three events in Canada). Applying criterion 3, the remaining countries in WP are further subdivided into two regions: South East Asia with median EDR < 1.2 and the rest of the north West Pacific with EDR > 5 (see Fig. S2d). In summary, the nine calibration regions are the Caribbean with Central America and Mexico (NA1), the USA and Canada (NA2), North Indian Ocean (NI), Oceania with Australia (OC), South Indian Ocean without Australia (SI), South East Asia (WP1), the Philippines (WP2), mainland China (WP3), and the north West Pacific (WP4) (see Fig. 9 and Table B1).

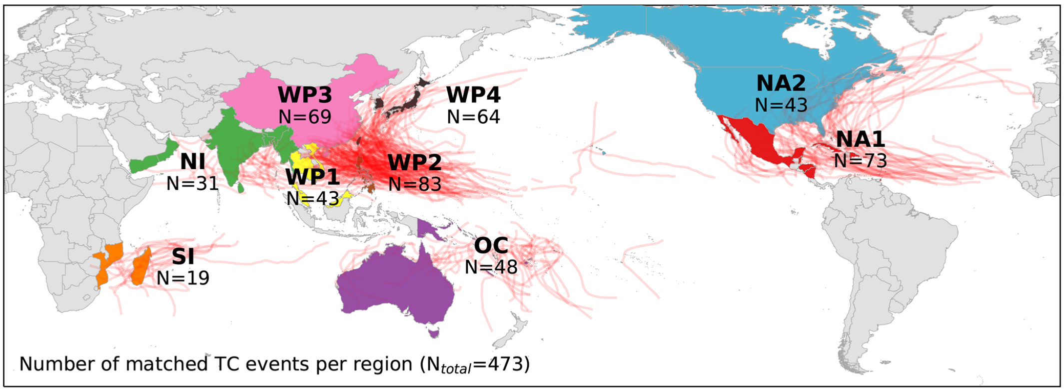

Figure 9: World map highlighting the 53 countries used for calibration, color coded per calibration region. The tracks of 376 TCs used for calibration are plotted as red lines. The number of resulting matched events N is displayed per region. Regions by color: red: the Caribbean with Central America and Mexico (NA1); blue: the USA and Canada (NA2); green: North Indian Ocean (NI); purple: Oceania with Australia (OC); orange: South Indian Ocean (SI); yellow: South East Asia (WP1), brown: the Philippines (WP2), rose: China Mainland (WP3); black: rest of North West Pacific Ocean (WP4). The countries per region are listed in Table B1.

Regional impact functions are calibrated following two complementary approaches based on (1) minimizing the spread of EDRs and (2) the optimization of TDRs. For the first calibration approach, the root-mean-squared fraction (RMSF) is introduced as a cost function:

$$RMSF = exp\left(\sqrt{\frac{1}{N}\sum_{E=1}^{N}[\ln{(EDR_E)}]^2}\right) \tag{3.5}$$

Input variables are the number of events N and the natural logarithm of EDR (cf. Eq. 3.3). The RMSF is a measure of the spread in EDRs, i.e., the relative deviation between modeled and reported damage for all matched events in a region. In the computation of RMSF, each event E has the same weight, independent of the absolute damage values. The natural logarithm ensures that an overestimation is penalized the same as an underestimation. RMSF is optimized by identifying the impact function associated with the lowest value of RMSF. A value of 1 would indicate perfect fit of all events. For the second calibration approach, TDR is optimized. A TDR larger than 1 implies that the summed simulated damage exceeds the reported values and vice versa. Therefore, TDR is optimized by identifying the impact function associated with a TDR as close to 1 as possible. As TDR is a ratio of damage aggregated over several events, the TDR approach is biased towards better representing events with large absolute damage values. In both calibration approaches, the slope of the generic impact function (Fig. 8) is calibrated by fitting the parameter V_{half} in Eq. (3.1). An increase in V_{half} corresponds to a flattening of the function and thus lower resulting simulated damage (cf. Fig. 8). For the fitting of V_{half}, damage is simulated for all matched events and an array of V_{half} ranging from 25.8 to 325.7 m s^{-1} in increments of 0.1 m s^{-1}. For each increment, EDR is computed for all matched events. Consequently, the values of the cost functions RMSF and TDR are computed for each region and increment of V_{half}. Subsequently, the value of V_{half} associated with optimal results for each cost function is identified. V_{half} optimized per region is used to calculate fitted impact functions per region. The calibrated impact functions are used to compute the annual average damage (AAD) per region, allowing for the comparison of results with other studies in Section 3.3.3.

3.3 Results

3.3.1 Damage ratio with default impact function

The comparison of TC damage simulated globally with a default impact function (Eq. 3.1 with V_{half}=74.7 m s^{-1}) reveals (1) interregional differences and (2) considerable uncertainties in CLIMADA's ability to reproduce the reported damage values per event. The distribution of uncalibrated EDRs per region is shown in Fig. 10. EDRs per matched event are shown in Fig. B1, and the distribution of EDRs per country is shown in Fig. S2.

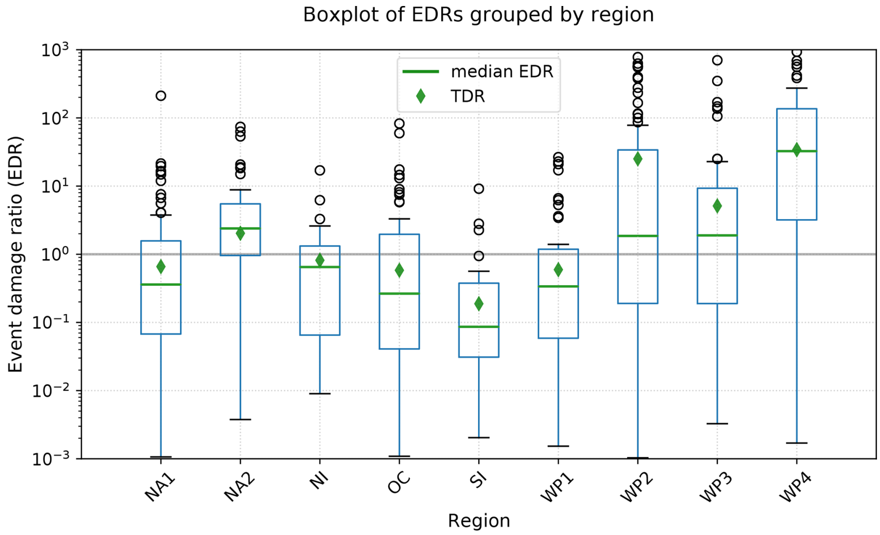

Figure 10: Spread of event damage ratio (EDR, boxplot) and total damage ratio (TDR) per region before calibration (V_{half}=74.7 m s^{-1}) per region. The plots are based on data from 473 TC events affecting 53 countries. The EDR boxplots show the median (green line), the first and third quartiles (IQR, blue box), data points outside the IQR but not more than 1.5·IQR distance from either the first or the third quartile (black whiskers), and outliers (black circles). The additional markers show TDR before calibrated (green diamond). The regions are the Caribbean with Central America and Mexico (NA1); the USA and Canada (NA2); North Indian Ocean (NI); Oceania with Australia (OC); South Indian Ocean (SI); South East Asia (WP1), the Philippines (WP2), China Mainland (WP3); rest of North West Pacific Ocean (WP4).

3.3.1.1 Inter-regional differences

Both the ratios EDR and the cost functions RMSF and TDR show interregional differences with regard to the deviation of the damages simulated with the default impact function from reported damage (Figs. 10 and 12). For most regions, total simulated and normalized reported damage deviates less than 1 order of magnitude (Table B2). The outliers are the regions WP4 (TDR = 35.6; Hong Kong, Japan, Macao, South Korea, Taiwan) and WP2 (TDR = 25.9; the Philippines). For those two regions, the large value of TDRs reveals a mean overestimation of simulated damage as compared to reported damage. In regions with TDR < 1, the uncalibrated model potentially underestimates the damages caused by TCs. These regions are the Indian Ocean (SI and NI), South East Asia (WP1), Oceania with Australia (OC), and the Caribbean (NA1). The region SI (Madagascar and Mozambique) shows the overall lowest TDR of 0.2, indicating an underestimation of damage by a factor of 5.

3.3.1.2 Intra-regional uncertainties

The EDR values within each region show a large spread over several orders of magnitudes (Fig. 10). There is no significant correlation between EDR and NRD (Fig. B3), suggesting that the over- and underestimation of simulated event damage is not related to TC severity. The largest spread, as expressed by the RMSF, can again be found in the regions WP4 and WP2 (Fig. 12c). The lowest RMSF was found in the regions NI, NA2, and NA1, i.e., the North Indian and North Atlantic basins. While the large interregional differences show the need for a regional calibration of impact functions, the spread of EDRs within some regions point towards uncertainties and limitations of the modeling setup that will not be removed by calibrating the impact function alone.

3.3.2 Regional impact functions

We calibrated regional impact functions to address interregional differences in TDRs. The resulting impact functions calibrated with two complementary approaches are shown in Fig. 11. The resulting impact functions vary between the regions both in slope and level of uncertainty, with V_{half} ranging from 46.8 to 190.5 $\mathrm{m\,s^{-1}}$ (Fig. 12a and Table B2). In addition to the regional impact functions, global impact functions were fitted based on all 473 data points combined, resulting in V_{half} ranging from 73.4 (RMSF optimization, i.e., RMSF = min.) to 110.1 $\mathrm{m\,s^{-1}}$ (TDR optimization, i.e., TDR = 1). Applying the regional impact functions, TDR calculated for all regions combined is 4.7 for the default impact function and 2.2 for the RMSF optimized impact functions (Fig. 12b). With the calibration based on TDR optimization, the bias in aggregated simulated damages can be removed, i.e., an impact function is fitted that leads to TDR = 1. This does not mean that the simulated damage of each single event is equal to the reported damage. In fact, there is a large spread in the values of V_{half} that would fit best for individual events. This uncertainty is visualized by the interquartile range (IQR) of the array of impact functions fitted to the individual events per region (shading in Fig. 11). For the individual fitting per event, the value of V_{half} is determined by what would be required to obtain an EDR equal to 1. The sensitivity of TDR and RMSF per region to changes in V_{half} is visualized in the Supplement. Regions with a large uncertainty, i.e., a large spread of EDRs, generally show a relatively low robustness of the cost functions (Fig. S3). On a globally aggregated level, calibration reduces the spread of EDRs to a certain degree, placing more than half of events in the EDR range from 10^{-1} to 10.

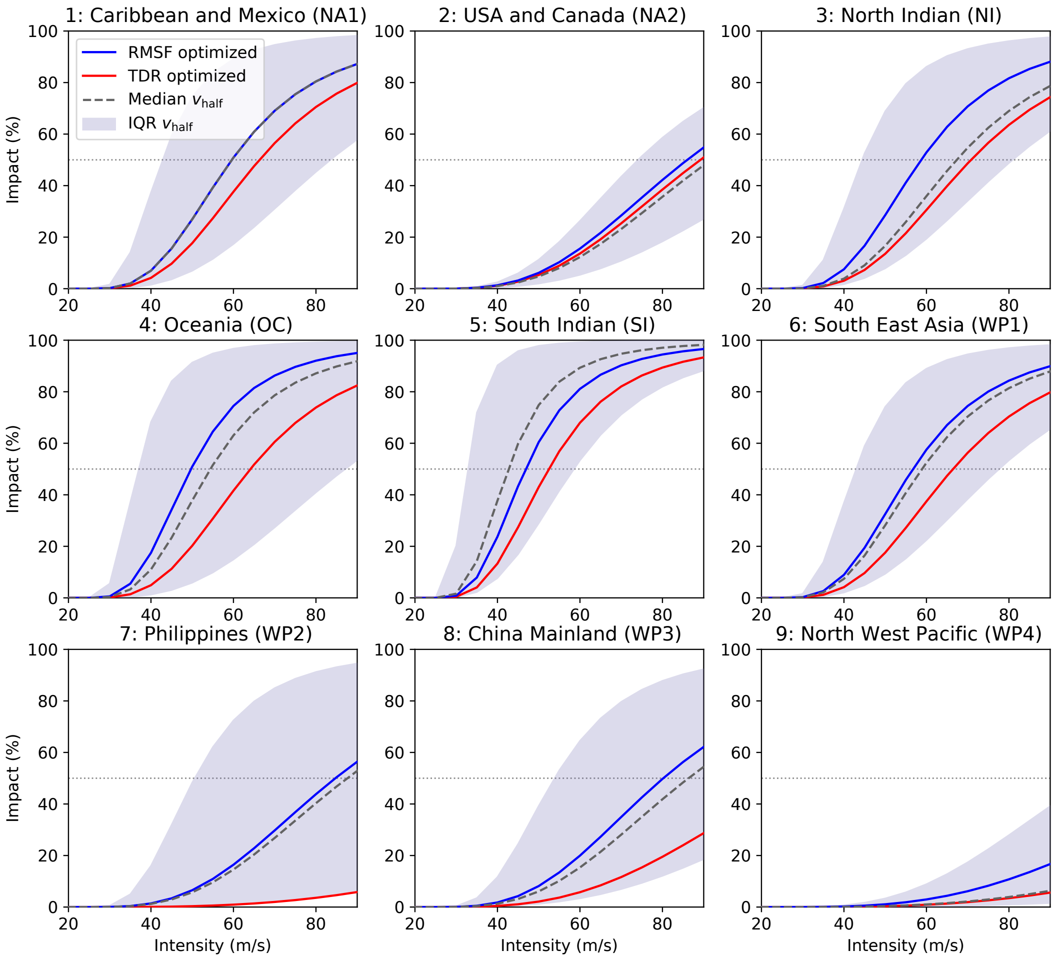

Figure 11: Regional impact functions for nine calibration regions, based on complementary calibration approaches: RMSF optimized (blue), TDR optimized (red), and the median V_{half} obtained from fitting impact functions for each individual event to obtain an EDR of 1 (dashed). The shading demarcates the range containing 50% of the individually fitted impact functions per region, i.e. the interquartile range (IQR).

The comparison of complementary calibration approaches gives an indication of the robustness of the calibration per region. In all regions, the calibrated impact functions based on both approaches lie within the interquartile range of the individually fitted curves (Fig. 11). However, the difference between V_{half} for the two approaches ranges from $3\,m\,s^{-1}$ (region NA2) to $104\,m\,s^{-1}$ (WP2). The largest uncertainties were found in the fitting of V_{half} for regions WP2–4 in the north West Pacific. In these regions, the TDR optimization fits values of V_{half} that are much larger than for the RMSF optimization (Fig. 12a). This corresponds to rather flat impact functions as shown in the bottom row of Fig. 11. Since TDR gives larger weight to events with large damage values, these results indicate that these events are systematically overestimated by the model in the regions WP2–4. The flat calibrated impact functions partly compensate for this overestimation. As a further indication of large uncertainties, TDR optimization in these three regions returns RMSF values that are larger than with the uncalibrated impact function (Fig. 12c). Possible reasons for the uncertainties in the model are explored in a case study for the Philippines in Section 3.4 and further discussed in Section 3.5.

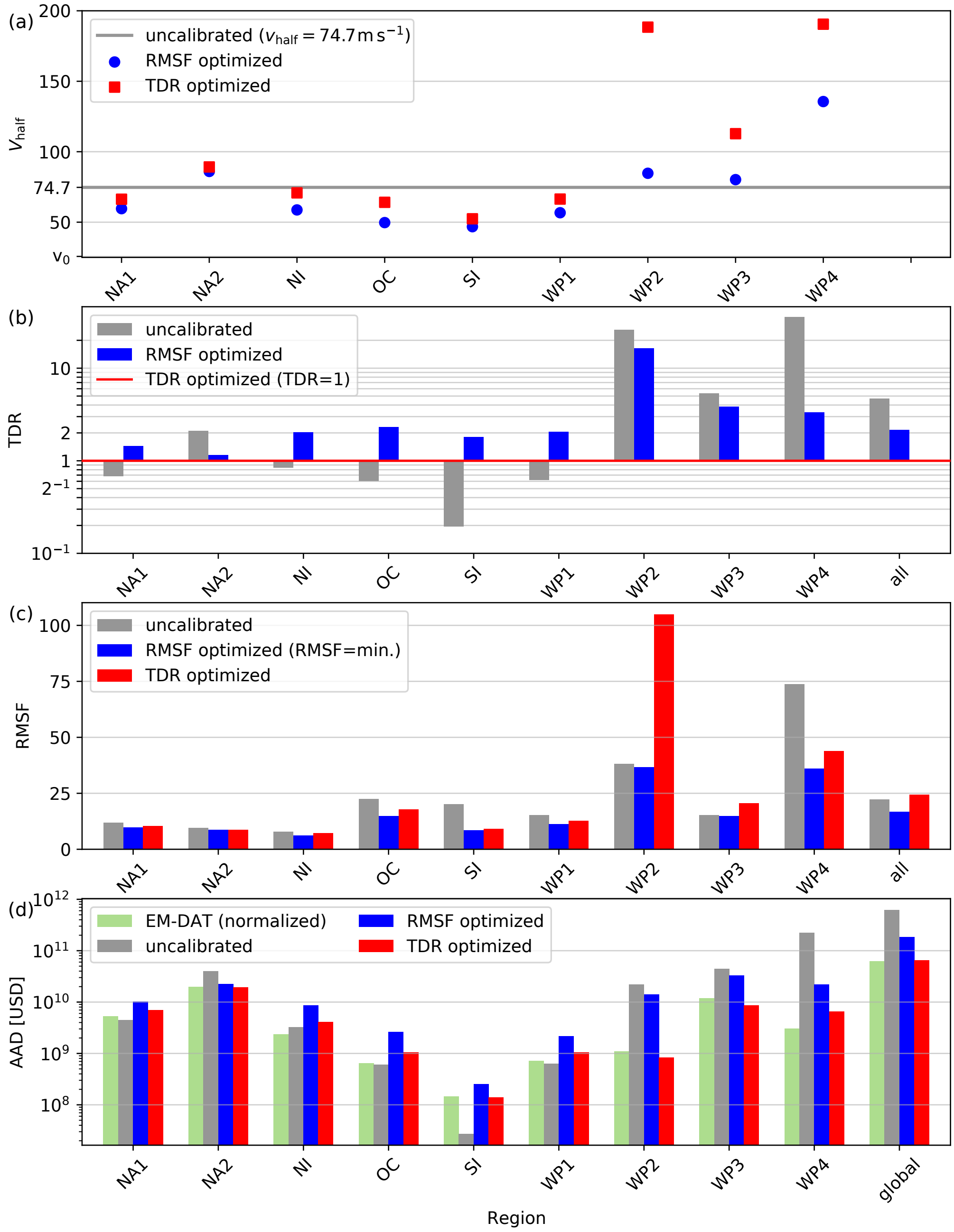

Figure 12: Calibration results and cost functions for nine calibration regions and all regions combined, each shown before (grey) and after calibration (blue and red): (a) V_{half}: fitted impact function parameter; (b) TDR: ratio of total simulated and normalized reported damage; (c) RMSF: root-mean-squared fraction; and (d) AAD: normalized reported (green) and simulated annual average damage (AAD). AAD is computed from all events available in EM-DAT (N=1650, green) and IBTrACS (N=4098), not just the 473 matched events used for calibration (a-c). Please refer to Tables 2 and B2 for numerical values. The regions are the Caribbean with Central America and Mexico (NA1); the USA and Canada (NA2); North Indian Ocean (NI); Oceania with Australia (OC); South Indian Ocean (SI); South East Asia (WP1), the Philippines (WP2), China Mainland (WP3); rest of North West Pacific Ocean (WP4).

3.3.3 Annual average damage AAD

Despite considerable interannual variability of TC occurrence and impacts, AAD is often used as a reference value for the mean risk per country or region. Here, we compare AAD computed with the regionalized TC impact model to values from EM-DAT and the literature (Table 2). AAD from EM-DAT represents values normalized to 2014 based on all 991 damaging events reported in the database from 1980 to 2017. Based on the calibrated impact functions, direct damage is simulated based on the full set of TC tracks ($N=4096$) and all countries. AAD values per country are provided in the Supplement. The computation of global AAD considers all countries, not only those used for calibration. Thereby, the regionally calibrated impact functions are used for other countries in the same region (cf. Table B1). AAD in countries not attributed to any region is calculated with impact functions calibrated globally. The resulting AAD for the calibration regions and the global aggregate are shown in Fig. 12d and Table 2. The standard deviation of AAD is generally of the same order of magnitude as AAD (Table 2).

Table 2: Annual average damage (AAD) from calibrated CLIMADA, as well as AAD from EM-DAT (normalized to 2014), GAR 2013, and Gettelman et al. (2017). Total AAD and the standard deviation of annual damage (in brackets) per region is given in billions of current US dollars ($B). AAD relative to total asset value (TAV; cf. Table B3) is provided in per mill (‰, italics). TAV values per region and study are reported in Table B3. Please note that both GAR 2013 and Gettelman et al. (2017) included synthetic TC tracks in their analysis which are based on historical tracks. The last row (world, bold) considers all countries. AAD values by country are provided in the Supplement. * USA and Bermuda without Canada.

Region	AAD EM-DAT	AAD-calibrated CLIMADA: RMSF optimized		AAD-calibrated CLIMADA: TDR optimized		AAD GAR 2013		AAD (Gettelman et al., 2017)	
	$B (2014)	$B (2014)	‰ of TAV	$B (2014)	‰ of TAV	$B (2005)	‰ of TAV	$B (2015)	‰ of TAV
NA1	5.3 (14.2)	10.3 (16.1)	*2.2*	6.9 (11.7)	*1.5*	4.6	*2.1*	9.5 (17.8)	*0.3–1.1*
NA2	19.7 (43.1)	22.4 (32.5)	*0.4*	19.4 (28.2)	*0.3*	11.8	*0.5*	11.0 (15.5)	*0.2**
NI	2.3 (3.8)	8.6 (13.9)	*1.4*	4.1 (6.7)	*0.6*	0.3	*0.2*		
OC	0.7 (0.8)	2.6 (3.6)	*0.4*	1.1 (1.6)	*0.2*	0.1	*0.1*		
SI	0.1 (0.3)	0.3 (0.6)	*5.7*	0.1 (0.4)	*3.2*	0.0	*2.8*		
WP1	0.7 (1.2)	2.2 (3.4)	*1.0*	1.1 (1.6)	*0.5*	0.0	*0.0*		
WP2	1.1 (1.8)	14.0 (34.6)	*22.3*	0.8 (2.3)	*1.3*	2.0	*11.0*		
WP3	11.9 (14.8)	32.9 (39.4)	*1.0*	8.6 (10.3)	*0.3*	9.0	*2.0*		
WP4	3.0 (4.0)	21.9 (24.3)	*0.8*	6.6 (7.3)	*0.2*	60.0	*3.1*		
Σ WP	16.8	71.0	*1.2*	17.0	*0.3*	71.1	*2.8*	61.4 (53.8)	*0.9–1.0*
Σ all	45.0 (54.8)	115.2 (72.4)	*0.8*	48.6 (33.2)	*0.3*	87.9	*1.6*		
World	**46.3 (55.6)**	**120.9 (73.9)**	***0.5***	**50.6 (33.6)**	***0.2***	**88.9**	***0.9***	**84.6 (63.9)**	***0.4–0.5***

For the years 1980 to 2017, we find aggregated global AAD to range from USD 51 up to USD 121 billion (value in 2014). In comparison, global AAD from EM-DAT is USD 46 billion. Values from GAR 2013 and Gettelman et al. (2017) range from USD 67.0 to USD 88.9 billion. It should be noted, however, that the two studies consider different time periods than our study (1950 to 2010 and 1979 to 2012, respectively), as well as deviant TAVs per country. Global TAV for 224 countries aggregates to USD 251 trillion compared to USD 156 trillion in Gettelman et al. (2017) and only USD 96 trillion in GAR 2013 (Table 2). Therefore, the comparison of AAD relative to TAV is a better measure to compare the results of the three studies. Relative to TAV, simulated global AAD amounts to 0.2 ‰–0.5 ‰ in our calibrated model as compared to 0.4 ‰–0.5 ‰ in Gettelman et al. (2017) and 0.9 ‰ in GAR 2013 (Table 2).

The aggregated region with the largest simulated AAD is East Asia (WP; USD 17–71 billion), followed by the USA with USD 19–22 billion and the North Indian Ocean with USD 4–9 billion. The regions WP2 and WP4 show the largest discrepancy in AAD simulated with the two alternative calibrated impact functions. This is consistent with the large uncertainties found in these regions during calibration (Section 3.3.1 and 3.3.2). In the most southern regions NI, SI, OC, and WP1, simulated relative AAD is consistently larger than in GAR 2013. This indicates that the calibration corrects for a systematic underestimation of TC vulnerability in these regions. For the Philippines (WP2), the largest AAD relative to TAV was simulated (22.3 ‰ with the RMSF optimized impact function). While the damage estimates simulated for WP2 come with large uncertainties, the range of relative AAD (1.3 ‰–22.3 ‰) encompasses the 11.0 ‰ for the Philippines in GAR 2013. The case of the Philippines will be further analyzed and discussed in Section 3.4.

3.4 Explorative case study: the Philippines

For a better understanding of the uncertainties involved in the TC impact function calibration, we exploratively examine simulated and reported damages of matched events in the Philippines (region WP2). The Philippines is the region with the least robust calibration results, with a large spread in EDRs and the largest discrepancy between the two calibration approaches. The difference in V_{half} between the two calibration approaches exceeds 100 m s^{-1} (Fig. 12a). Consequently, there is a large spread in simulated AAD ranging from USD 0.8 to USD 14 billion (Table 2). This corresponds to an underestimation of annual risk of USD 0.3 billion up to an overestimation of USD 21.2 billion as compared to normalized values from EM-DAT with an AAD of USD 1.1 billion.

The goal of this explorative case study is to better understand what drives these uncertainties in the TC impact model within the region, discuss the limitations of the calibrated model, and identify points for improvement for the future development of global TC impact models. Thereby, we assess the following hypotheses. (1) Potential differences between urban and rural exposures and vulnerabilities as considered in GAR 2013 (De Bono and Mora, 2014) are not fully resolved in the model. (2) The simplified representation of the TC hazard intensity with wind speed alone is not capable of adequately modeling the impact of TCs with over-proportional damage caused by sub-perils like storm surge and torrential rainfall (Baradaranshoraka et al., 2017; Park et al., 2013). In the following, we explore these hypotheses with the example of 83 matched TC events in the Philippines while keeping in mind that the model setup is not designed to represent single events perfectly due to the large inherent stochastic uncertainty. To explore these hypotheses, we review reports and the literature on TC impacts in the Philippines and examine the relationship between EDRs per event with the spatial distribution of the wind field and subsequent simulated damages associated with each single event.

3.4.1 Tropical cyclones in the Philippines

The Republic of the Philippines is one of the most TC-prone countries in the world (Blanc and Strobl, 2016). From 1951 to 2014, an annual average of 19.4 TCs entered the Philippine Area of Responsibility (Cinco et al., 2016) with six to nine TCs making landfall in the Philippines each year (Blanc and Strobl, 2016; Cinco et al., 2016). This is a relatively high frequency compared to five to eight landfalls in China (Zhang et al., 2009), and an average of three landfalls per year in the North Indian Ocean region (Wahiduzzaman et al., 2017) as well as in the USA (Lyons, 2004). The north and east of the Philippines are the regions most exposed to TC landfalls, with most TCs crossing the Philippines from east to west (Cinco et al., 2016; Espada, 2018). Rainfalls associated with TCs contribute around 35% of annual precipitation in the Philippines, with regional values ranging from 4 % to 50 % (Cinco et al., 2016).

In total, 83 matched TCs making landfall in the Philippines were used for calibration. For 11 of the 21 most damaging TC events, reports and scientific literature on associated sub-perils and impacts were reviewed (Table B4). In summary, TCs making landfall in the Philippines cause damage due to great wind speed, storm surge, and rain-induced floods and landslides. Meteorologically, the storm systems interact with the monsoon season affecting both the dynamics and the severity of torrential rain (Bagtasa, 2017; Cayanan et al., 2011; Yumul et al., 2012). TCs in the Philippines inflict damage on several sectors; it is most costly for housing and agriculture but also for schools, hospitals, power and water supply, roads, and bridges (Table B4). Single events were also reported to cause damage and business disruption to airports and ports (Typhoon Haiyan) and dikes (Nesat and Xangsane). This complexity of how and where TCs cause damage in the Philippines is in stark contrast to the relatively simple representation of hazard and exposure in our modeling setup. It is therefore not surprising that our calibrated TC impact model is over- and underestimating the damage of individual events, as illustrated for the Philippines by the wide spread of EDRs. In the following, we will take a closer look at events with over- and underestimated simulated damage to explore the two hypotheses above.

3.4.2 Urban vs. rural exposure

Most of the asset exposure value of the Philippines is concentrated around the metropolitan area of Manila (Metro Manila). Located around 14.5°N, 121.0°E

(Fig. 13a), Metro Manila is Philippine's political and socio-economic center (Porio, 2011). The typhoons Angela (1995), Xangsane (2006), and Rammasun (2014) are prominent TCs hitting the Metro Manila directly. In our analysis, these TCs come with particularly large EDRs, i.e., an overestimation of simulated vs. reported damages, even with calibrated impact functions (Table B4). All three typhoons show maximum sustained wind speeds in Manila greater than $50\,\mathrm{m\,s^{-1}}$ (Fig. 14b, e, f), corresponding to relative damage ranging from 6 % up to 37 % of asset exposure value with the calibrated impact function. These large relative damage values in combination with the concentration of asset exposure value in the Manila region are likely to explain the large EDRs of these events. The analysis of all 83 TC events used for calibration support this hypothesis, underpinning the crucial role the large asset exposure values in the Metro Manila plays for the wind-based simulated damage. An overestimation of simulated damages (e.g., EDR > 10) consistently coincides with large wind speeds over Metro Manila. Out of 19 TCs affecting Manila directly, we find 16 (84 %) with an EDR > 10 and zero occurrences of EDR < 0.1 (Fig. 14). In contrast, only 9 of 64 TCs not affecting Manila directly come with an EDR > 10. In summary, we found that simulated damage of an event would more usually substantially exceed normalized reported damage if the event hit Manila directly. This confirms hypothesis (1) in that a special treatment of the impact functions for urban areas could improve the TC impact model.

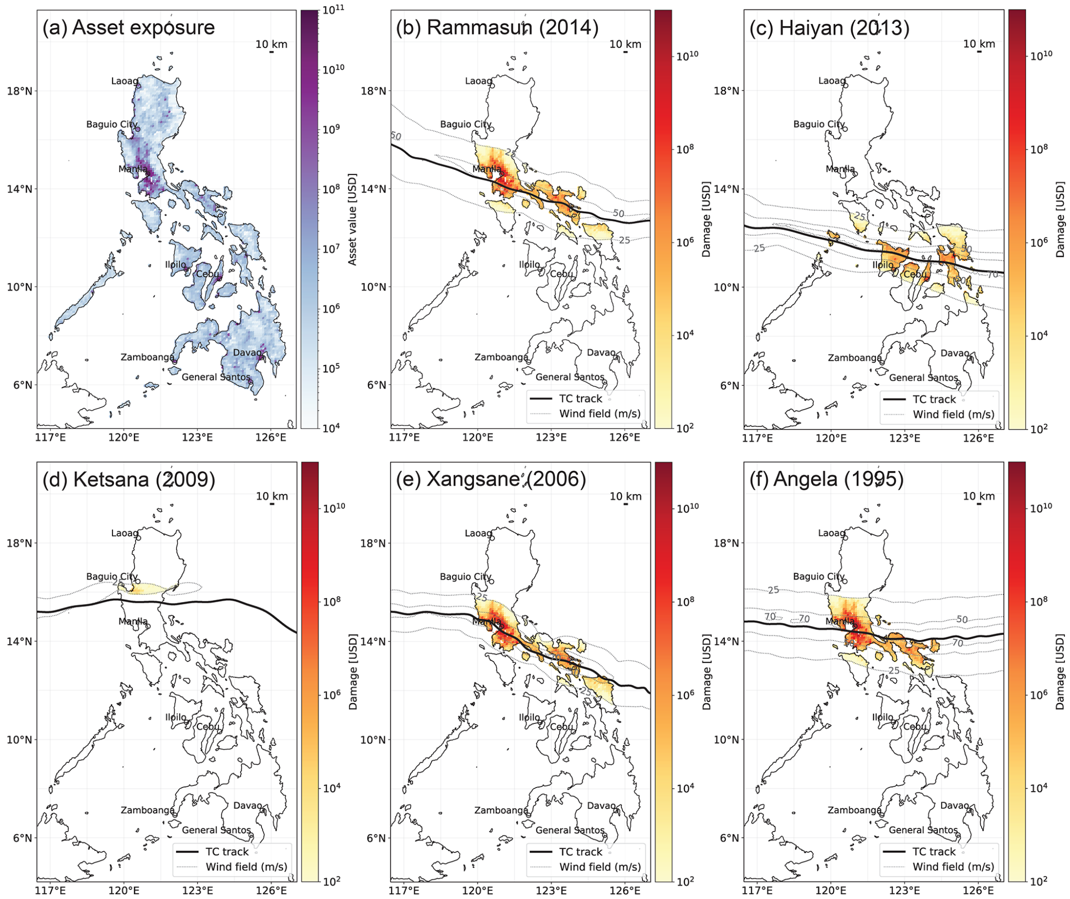

Figure 13: Maps of the Philippines showing (a) the spatial distribution of asset exposure value in the Philippines (US dollar value in 2014) based on Eberenz et al. (2020) and (b–f) mapped TC impacts for Typhoon Rammasun (b), Typhoon Haiyan (c), Tropical Storm Ketsana (d), Typhoon Xangsane (e), and Typhoon Angela (f). For each event, the map shows the TC track from IBTrACS (bold solid line), the spatial distribution of simulated maximum 1 min sustained wind speed at 10 m above ground in meters per second (m s^{-1}) (dashed lines at 25, 50, and 70 m s^{-1}), and simulated direct damage at a 10 km resolution (color shading). Coast lines and the location of major cities are marked on the map based on Cartopy (Met Office, 2010).

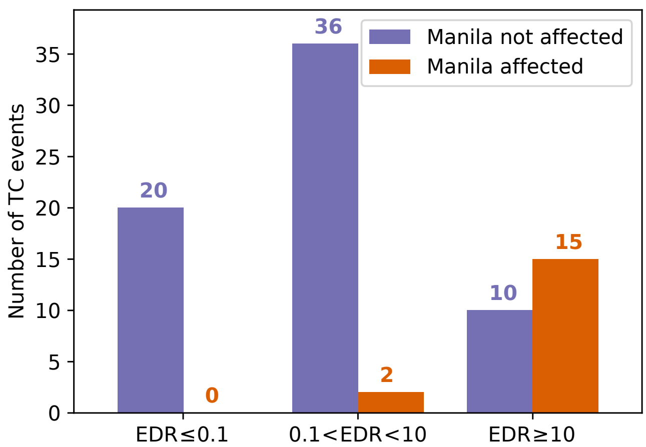

Figure 14: Distribution of the event damage ratios (EDRs) for 83 TCs making landfall in the Philippines from 1980 to 2017. The number of events for three ranges of EDRs are compared, differentiating whether Manila was directly affected by the TC's wind field (orange) or not (purple). Manila is considered to be affected if the hazard intensity exceeds 25 m s^{-1} at 14.5° N, 121.0° E.

3.4.3 Impact of storm surge and torrential rain

While urban vulnerability to strong winds in Metro Manila appears to be overestimated by the calibrated impact function, Metro Manila is known to be highly exposed and vulnerable to regular, large-scale flooding (Porio, 2011). The main drivers of flood vulnerability are its geographical setup, largely unregulated urban growth and sprawl, and substandard sewerage systems, especially in low-income areas (Porio, 2011). Tropical Storm Ketsana, locally known as Ondoy (2009) is an example with very low simulated damages coinciding with large reported damages associated with flooding in Metro Manila; Ketsana's EDR is 0.002, i.e., simulated damage is more than 2 orders of magnitude smaller than reported. The large reported damage (NRD = USD 401 million) was mainly due to floods and landslides. Torrential rainfall caused severe river flooding in Metro Manila and landslides around Baguio City resulting in severe damage (Abon et al., 2011; Cruz and Narisma, 2016; Nakasu et al., 2011; NDCC, 2009a). The flood damage was not resolved by the wind-based impact model with intensities well below 50 $m\,s^{-1}$ and affected neither Manila nor the northern Baguio City directly (Fig. 13d). Notably, even for TCs with large overestimations of simulated damage due to high wind speeds in Metro Manila, namely Fengshen and Xangsane, a substantial part of the reported damage was actually caused by pluvial flooding and landslides and not by wind alone (Yumul et al., 2008, 2011, 2012).

For the most severe TC in the recent history of the Philippines, Typhoon Haiyan (2013), normalized reported damage and simulated damage are on the same order of magnitude resulting in an EDR of 0.17. Haiyan, with sustained 1 min surface wind speeds up to 87.5 $m\,s^{-1}$, caused thousands of casualties and around USD 10 billions of economic damage in the Philippines (Guha-Sapir, 2018; Mas et al., 2015). Devastating wind and storm surge associated with Haiyan caused damage to multiple sectors, including ports and an airport. It should be noted that sector-specific impacts are not resolved in the impact model and that Haiyan did not affect Manila directly. Relatively large damage was simulated around Tacloban City, Leyte, which was actually devastated by Haiyan's storm surge. Large wind impacts were also simulated further west around the cities of Iloilo and Cebu (Fig. 13c) that were not as exposed to surge as Leyte province. The relatively good performance of the model in the case of Haiyan is thus not explained by a perfect location and representation of the impact in the model. It is rather based on overestimated urban wind damages partly balancing the lack of damages caused by storm surge.

3.4.4 Conclusions from the case study

The case of the Philippines reveals limitations of the model and calibration due to the lack of an explicit representation of sub-perils such as storm surge, torrential rainfall, and landslides (Section 3.4.3). The flood damage caused by Ketsana is a showcase example for severe damage associated with a TC with relatively low wind speeds, which is to say an event that cannot be adequately reproduced with a wind-based impact function. Adding to the stochastic uncertainty, the magnitude of rainfall during TC events in the Philippines is not only determined by the intensity of the TC event but also by the coinciding monsoon season, as in the case of typhoons Fengshen and Haiyan (Espada, 2018; IFRC, 2009; Yumul et al., 2012).

Next to a lack of representation of all components of hazard intensity, differences in exposure and vulnerability between urban and rural areas exposed to TCs are likely to contribute to the large spread in EDRs and subsequently uncertainty in the impact function calibration. This has been illustrated in Section 3.4.2; the large overestimation of simulated event damage of TCs affecting the Manila metropolitan area points towards relevant sources of epistemic uncertainty. On the one hand, a large share of exposed asset values in the model are concentrated in urban areas, while exposed agricultural assets in rural areas are neglected. On the other hand, one single impact function might not be sufficient to represent both urban and rural building vulnerability. Another factor contributing to the high simulated damages in Manila could be the wind field model. Manila is located in a bay on the west coast of the main island Luzon. Most TCs approach Luzon from the east. The wind field model adapted from Holland (2008) does not, however, take into account variations in topography and surface roughness. This could lead to an overestimation of simulated wind speeds downstream of elevated land, as in the case of Manila. A better representation of wind speed over land could mitigate this problem (Done et al., 2020).

3.5 Discussion

3.5.1 Relevance for TC risk assessments

In this study, we showed how the regionalization of impact functions improves the assessment of TC risk in numerous world regions, correcting an overestimation of aggregated TC damages by a factor of potentially up to 36 in the north West Pacific and an underestimation by a factor of 5 in the South Indian Ocean. To complement the global perspective, we explored the limitations of the TC impact modeling setup through the case study of TC events in the Philippines.

The calibration resulted in large regional differences in the slope of impact functions with considerable consequences for the magnitude of simulated damages. In

Section 3.3.2, we compared average simulated damage with regionalized impact functions to results from the literature. While the comparison is limited by differences in the model setups, we found that regional damage estimations relative to the exposed asset values generally agree well with the results of previous studies. However, the results for the north West Pacific region (WP4), consisting of Japan, South Korea, Macao, Hong Kong, and Taiwan, deviate substantially from GAR 2013. Simulated relative AAD in the region ranges from 0.2 ‰–0.8 ‰ as compared to 3.1 ‰ in GAR 2013. This difference implies that, besides the use of building-type-specific impact functions, the TC impact model of GAR 2013 substantially overestimates TC damages in WP4 compared to reported data. Consistent with this finding, the uncalibrated simulation showed the largest overestimation of aggregated damage in this region. Assuming that the order of magnitude of reported direct damage from EM-DAT is reasonable, the regionalization of impact functions presented here is an improvement for TC risk assessments in the region.

For calibration, two complementary approaches were employed: the optimization of aggregated simulated compared to reported damage (TDR) and the minimization of the spread of damage ratios of single events (RMSF).

Annual average simulated damage based on the TDR-optimized set of impact functions is generally closer to the values found in EM-DAT than the values based on RMSF optimization. This is not surprising since TDR is designed to represent aggregated damage per region. For the assessment of TC risk on an aggregated level, it is therefore most appropriate to employ the more conservative TDR-optimized model, even though single events can be massively underestimated with the flatter impact functions. Complementary, impact functions based on RMSF optimization and the spread of individual event fitting can be included in risk assessments for sensitivity analysis.

3.5.2 Uncertainties and limitations

The deviation between the results of the two calibration approaches indicates how robust the calibration is with regards to the model's ability to represent the correct order of magnitude of single event damage. Whereas the model setup returns reasonable risk estimates and consistent calibration results for Central and North America, we found an extensive spread in EDR and calibration results for other regions, especially in East Asia. While the correlation between simulated and reported event damage is improved by the calibration, the simulated damage of single TC events can deviate several orders of magnitude from reported damage (Figs. 10, B1, and B2). In the regions of the north West Pacific (WP2–4), the fitted impact functions are ambiguous with large discrepancies between the two calibration approaches. The low robustness found in these regions stems from multiple causes, including the stochastic uncertainty in TCs as natural phenomena, as well as epistemic uncertainties located in the hazard, exposure, and vulnerability components of the impact model. An additional source of uncertainties is located in the reported damage data used for reference. Future improvements in the TC impact model and a sound judgment of the limitations of the calibrated impact functions require better understanding of the epistemic uncertainties. In the following, we will discuss these uncertainties for the different components of the model.

The case of the Philippines provides insights into the uncertainties located in the model setup, both in the representation of hazard intensity and in differences between the structure and vulnerability of exposed assets in urban and rural areas (Section 3.4). The hazard is represented by wind fields modeled from TC track data, and the same impact functions are applied for urban and rural areas. These are considerable simplifications of the actual interaction of cyclones with the natural and built environment. To reduce these uncertainties, the hazard component could be improved by considering topography (Done et al., 2020) and complementing wind speed with sub-perils like storm surge, torrential rain, and landslides. For a better representation of urban assets, building-type-specific impact functions, and a differentiation of urban and rural exposure as applied for GAR 2013 (De Bono and Mora, 2014) could be beneficial. Furthermore, geospatial agricultural yield data could be added to the exposure data, although reported damage for calibration is mostly not available at such sectoral granularity. Next to the model setup, the reported damage data obtained from EM-DAT are another relevant source of uncertainty. Reported damage data are expected to come with considerable uncertainties partly due the heterogeneity of data sources, the blending of direct and indirect economic damages, and political and structural reporting biases (Guha-Sapir and Below, 2002; Guha-Sapir and Checchi, 2018). Further uncertainty is introduced by the lack of international standards for reported damage datasets, leading to inconsistencies between data providers (Bakkensen et al., 2018b). These uncertainties limit our understanding of the robustness of the calibration. For future calibration studies relying on reported damage data, calibration robustness could be increased by combining datasets from different sources in an ensemble of datasets (see Zumwald et al., 2020).

In this study, we did not explicitly quantify the uncertainties related to the model setup, the input data for hazard and exposure, and the reported data used as reference data for calibration. Rather, the robustness of the calibrated impact functions was judged based on the deviation between the two calibration approaches and the spread of impact functions fitted to the individual TC events. Based on the limitations discussed above, we conclude that the resulting array of regionalized impact functions should be applied with caution, being aware that the model setup is not suitable to represent single TC events adequately. However, the calibrated impact functions mark an improvement for the modeling of aggregated risk estimates, such as the annual average damage (AAD). Impact functions sampled from the range of calibration results can be applied for a more probabilistic modeling of TC impacts. It should also be noted that the impact functions calibrated for the years 1980–2017 cannot be expected to be stable in the future. Applying these impact functions for the assessment of future TC risk requires, ceteris paribus, an assumption with regard to vulnerability.

While the results of this study are not specific to the CLIMADA modeling framework, the precise shape and scaling of the calibrated impact functions are, however, to a certain degree specific to the choices and input data of the modeling setup: (1) the choice of free parameters in the impact function (c.f. Section 3.2.2.3 and Lüthi, 2019), (2) the TAVs (cf. Table B3; impact functions would scale differently with a different assumed inventory of exposed assets), (3) spatial resolution, and (4) the representation of hazard intensity. The regionalized impact functions presented here were calibrated for wind-based damage modeling on a spatially aggregated level. Model setups with an explicit representation of related sub-perils like storm surge or torrential rain require different (i.e., flatter) impact functions for the wind-induced share of TC damage, as well as additional impact functions for each sub-peril. Likewise, impact models with an explicit representation of building types and agricultural assets require a more differentiated set of impact functions. Considering the irreducible stochastic uncertainties in the system, it remains to be shown to which degree the large interregional differences in calibrated impact functions found in this study can be explained by regional differences in building types and standards, physical TC characteristics, or other factors.

3.6 Conclusion and outlook

In this article, the global assessment of TC risk was improved by regionalizing the vulnerability component of the TC impact assessment. To better account for regional differences, a TC impact model was calibrated by fitting regional impact functions. The impact functions were calibrated within the CLIMADA risk modeling framework using reported estimates of direct economic damage from the EM-DAT dataset as reference data. For calibration, two complementary optimization approaches were applied, one aiming at minimizing the deviation of single event damage from the reported data and one aiming at minimizing the deviation for total damage aggregated over 38 years of data. By fitting impact functions, we were able to reduce regional biases as compared to reported damage data, especially for countries in the north West Pacific and South Indian Ocean regions. The substantial overestimation of TC damages in the north West Pacific with the default impact function opens the question for the drivers of the apparently lower vulnerability in this region. Considering the inability of the model setup to directly represent the impacts from TC surge and pluvial flooding, one would rather expect aggregated calibrated impact functions to be steeper than the default wind impact function. Therefore, we suggest investigating interregional differences in other possible drivers, including building standards but also damage-reporting practices. A study combining the empirical evidence provided by reported damage data on the one hand with socio-economic indicators on the other hand would be desirable but rather challenging as this would add even more layers of complexity and cascading uncertainties to the calibration, especially on a global level.

The calibrated model comes with considerable uncertainties related both to the impact model setup and the reported damage data. The largest uncertainties were found for the north West Pacific regions, while the calibration produced consistent results for the North Atlantic regions. The spread of fitted impact functions within each region can be exploited to better account for these uncertainties in probabilistic risk assessments. Based on our findings, we recommend to always consider interregional differences in vulnerability for the application in global TC impact models. For model setups comparable to the one described here, we recommend the use of TDR-optimized functions for risk assessments on an aggregated level. The resulting simulated damage can complement reported damage data. Assuming that reported damages are more likely to underestimate actual impacts, it could be advisable to sample impact functions from the range between the complementary calibration results. For probabilistic impact modeling, a random sampling from the array of impact functions fitted to individual events could be considered. This becomes especially relevant for regions with large uncertainties attached to the calibration results, such as the north West Pacific and Oceania. Limitations of our research motivate future work. For TC impact models, we echo the call for a more refined representation of TC hazards as a combination of wind-, surge-, and rain-induced flood and landslide events. When modeling multiple TC sub-perils, aggregated reported damage data are not sufficient to constrain impact function calibration. This might be resolved by consulting socio-economic- and engineering-type data and knowledge. Furthermore, our case study for the Philippines suggests that model accuracy could be further improved by differentiating between urban and rural asset exposure, considering topography in wind speed estimations, and including exposed agricultural assets.

4. Complementary metrics pivotal in assessing 21st century crop production risk

Samuel Eberenz[1,2], Carmen B. Steinmann[1,2], Jonas Jägermeyr[3,4,5] ,
Wim Thiery[6], David N. Bresch[1,2]

Manuscript in preparation.

ABSTRACT. Agriculture is one of the economic sectors most vulnerable to climate change. Global gridded crop models (GGCMs) are used to simulate historical and future crop yield responses to a changing climate. Intercomparison efforts such as the Inter-Sectoral Impact Model Intercomparison Project (ISIMIP) allow for the analysis of agreement and divergence between models and parameters, as well as the projection of future crop production under a range of emission and land use scenarios. Recent studies project both regionally decreasing mean crop yields and increasing inter-annual variability with climate change for the 21st century, likely posing a serious threat to food security. To inform the development of science-based adaptation plans, it is crucial to assess the probability and severity of future climate-induced production losses. Based on the unprecedented climate-crop ensemble facilitated by ISIMIP3b, we assess country-level crop production risk with the risk modeling platform CLIMate ADAptation (CLIMADA). The modularized implementation with CLIMADA allows for the use of crop model outputs as hazard component for flexible assessments of crop production risk, with user-determined production layers as exposure. As risk metrics, we calculate probabilities of years with extreme crop production losses for maize, rice, soybean, and wheat. Two complementary thresholds allow for the assessment of losses both relative to historical and future mean production levels. We find that variability-driven risk increases most in countries with relatively low current risk levels. Maize is the only crop type analyzed with a worldwide substantially elevated risk in a 2°C world, driven by a decline in mean yields. For rice, soybean, and wheat, results are more differentiated with reduced risk projected for most countries at 2°C. At 4°C, globally aggregated crop production risk increases, due to both reduced production levels and more severe extreme events. The results come with considerable uncertainties and

[1] Institute for Environmental Decisions, ETH Zurich, Switzerland

[2] Federal Office of Meteorology and Climatology MeteoSwiss, Switzerland

[3] NASA Goddard Institute for Space Studies, New York, USA

[4] Columbia University Center for Climate Systems Research, New York, USA

[5] Potsdam Institute for Climate Impacts Research (PIK), Germany

[6] Department of Hydrology and Hydraulic Engineering, Vrije Universiteit Brussel, Belgium

opposing trends in some regions. Of the three major crop producing countries, China shows a future increase in risk for maize and wheat, and declining risk for rice and soybean. The USA shows elevated future crop production risk for all crop types, and India shows reduced risk levels, compared to historical climate. Overall, our results highlight substantially increased risk to crop production under warming projected for the mid to end 21st century and the need to assess crop yield projections more differentiated in future climate risk assessments, both geographically and with regard to the choice of risk metrics.

4.1 Introduction

Agriculture is among the economic sectors most vulnerable to meteorological and hydrological extremes (e.g., Bokern, 2019; Frieler et al., 2017b; Mbow et al., 2019). It is thus not surprising that the impacts on agriculture were among the first impacts of climate change to be studied (e.g. Adams, 1989; Kulshreshtha and Klein, 1989; National Research Council (U.S.). Carbon Dioxide Assessment Committee, 1983). Climate change is affecting crop yields in many ways, including changes in the mean and extremes of temperature and precipitation regimes, and rising atmospheric CO_2 concentration ([CO_2]) (e.g., Franke et al., 2020b, 2020a; Mbow et al., 2019). In state-of-the-art crop yield simulations, observed weather variations account for more than 50% of yield variations in many major crop producing countries (Frieler et al., 2017b). On a global level, climate variability accounts for roughly a third of observed crop yield variability (Ray et al., 2015). Climate change has likely already affected global aggregate food production (Gaupp et al., 2020; Ray et al., 2019). In a warming climate, the risk of multi-breadbasket failures, that is, the probability of simultaneous crop failure in multiple relevant production areas across the globe, are projected to increase (Gaupp et al., 2019; Tigchelaar et al., 2018). Climate change thus poses a threat to food security as source of income and livelihood, from local to global scales (e.g., Hurlbert et al., 2019; Mbow et al., 2019; Stevanović et al., 2016; Wiebe et al., 2015). Food supply instability risk is projected to reach high levels, i.e., significant and wide spread impacts, at 2°C of global warming, and very high levels at 4°C (Hurlbert et al., 2019).

For assessing the impact of future climate on crop production, with weather conditions outside the historical record, one depends on crop models. Crop models help to reduce complexity of different climate variables affecting crop yield. Both empirical and process-based modeling approaches are applied for the projection of crop yields under climate change (Blanc and Reilly, 2017). Process-based models consider non-linear effects of climate variables on crop yields (Blanc and Reilly, 2017), including variations in the phenological response of crops and the interaction between different weather variables as well as delayed effects such as water storage

(Frieler et al., 2017b). This makes process-based crop models best suited to simulate crop yield projections for climate scenarios outside the range of historical climate. On a global scale, process-based global gridded crop models (GGCMs) are widely used to study future crop yields under climate change conditions (e.g., Elliott et al., 2015a; Franke et al., 2020b; Jägermeyr et al., under review; Rosenzweig et al., 2014). The most relevant drivers of crop yield changes in GGCM projections are temperature, water availability, [CO_2], radiation components and nitrogen availability (Elliott et al., 2014; Franke et al., 2020a; Müller et al., 2017; Rosenzweig et al., 2014; Schleussner et al., 2018). Both GGCMs and the driving climate projections from global climate models (GCMs) contribute substantially to the uncertainty in climate-crop model ensembles (Müller et al., 2021). For the first half of the 21st century, uncertainties in climate-crop model ensembles are dominated by the differences of the GGCMs (Müller et al., 2021). While there have been considerable improvements in the parameterization of CO_2 effects in GGCMs (Jones et al., 2017), not all CO_2 effects are adequately represented (Blanc and Reilly, 2017; Vanuytrecht and Thorburn, 2017). The impact of elevated [CO_2] on mean crop yield trends is considered one of the most relevant sources of uncertainty in current GGCMs (Rosenzweig et al., 2014). Toward the end of the century, the uncertainty of the driving GCMs becomes dominant, contributing more than half of variance in climate-crop simulation ensembles, mainly due to the spread in the projected severity of climate change between the individual GCMs (Müller et al., 2021). Risk assessments based on GGCM ensembles should take into account that there are significant differences between models (Challinor et al., 2018; Jones et al., 2017; Rosenzweig et al., 2014) and simply increasing the ensemble size does not necessarily imply a better sampling of realistic possible outcomes (Challinor et al., 2018). However, the confidence in a climate-crop ensemble can be increased by a careful experiment design, model evaluation, and potentially subsequent emergent constraints (e.g., Eyring et al., 2019) and model weighing (Brunner et al., 2020). This includes a selection of ensemble members based on skill and spread (benchmarking), as well as a harmonization of the experimental setup (Challinor et al., 2018; Jägermeyr et al., under review; Müller et al., 2017).

For the 21st century, negative mean trends in crop yield are generally projected at low latitudes in response to moderate levels of global warming (Jägermeyr et al., under review; Rosenzweig et al., 2014; Schauberger et al., 2017). Lange et al. (2020) found that future warming increases the area fraction experiencing reduced crop production in many world regions, especially in low- and middle-income countries, while the land fraction affected by crop failure is projected to decrease in parts of Europe and Central Asia. Under a high-emission scenario, changes in mean yields of maize, rice, soybean, and wheat are projected to emerge from historical variability as early as in the 2030s in many main crop producing regions, changing the risk profile of these regions within the next decades (Jägermeyr et al., under review). These results stem from an analysis the time of emergence of the mean trend from historical variability based on the up-to-date largest harmonized and benchmarked multi-model ensemble simulations from process-based GGCMs. These harmonized crop yield simulations were facilitated by the Inter-Sectoral Impact Model Intercomparison Project ISIMIP (ISIMIP, 2020b; Rosenzweig et al., 2017) round 3b (ISIMIP3b) and the Agricultural Model Intercomparison and Improvement Project (AgMIP), within the Global Gridded Crop Model Intercomparison (GGCMI) project.

In a warming climate, not only mean yields are projected to change, but also the inter-annual variability. Generally, variability is projected to increase for the major staple crops in most world regions (e.g., Ostberg et al., 2018; Tigchelaar et al., 2018). Müller at al. (2021) found an increase in overall variance of crop yield projections with the radiative forcing. Among maize, rice, soybean, and wheat, Müller at al. (2021) found largest total variance for winter and spring wheat, and lowest variability for maize. Increases in variability can lead to more frequent or more severe production shocks, impacting food security, markets, and livelihoods. Yet, changes in variability are often not considered in climate impact assessments (Franke et al., 2020a). Both trends in mean crop yields and in interannual variability determine the probability of years with extreme reduced crop production values. Therefore, trends in both the mean and the variability of crop production can be analyzed to assess the risk climate variability and change pose for national and global crop production. In a study based on three GGCMs from ISIMIP phase 2b, Lange et al. (2020) assess the probability of crop yields in any given year to fall below the 2.5th percentile of a historical reference period, an approach that has also been applied for the assessment of meteorological extremes like heavy precipitation and heat (e.g., Fischer and Knutti, 2015). Using empirical crop models to assess global maize production risks under future warming, Tigchelaar et al. (2018) assessed the probability of relative crop yield losses of more than 10 % and 20 % below the present-day mean (Tigchelaar et al., 2018). The authors found an increase in the probability that the maize production in the top four producing countries falls more than 10% below present day mean from virtually 0% under present-day climate up to 7% in a 2°C warming above pre-industrial and 86% under 4°C warming (Tigchelaar et al., 2018).

The above studies all measure crop production risk as the probability of years below a threshold fixed from historical or detrended reference values. A change in these probabilities can be caused both by a mean trend shifting the whole distribution and by a change in variability. Year to year anomalies in GGCM simulated country level crop yield were assessed and compared to reported crop production statistics by Jägermeyr and Frieler (2018). For the analysis, the authors detrended the timeseries and calculated the relative deviation of crop yields as compared to two years before and two years after a year with a reported drought or heat wave. Like this, the study by Jägermeyr and Frieler (2018) put a focus on the aspect crop production risk induced by climate variability. A mean positive trend may mask increased occurrence of extremely low yields, a topic which is generally understudied in global crop projection studies. Risk metrics that are independent of the mean trend can help to fill this gap. Here, we use an extensive ensemble of crop yield simulations first described by Jägermeyr et al. (under review) for a global assessment of crop production risk for major staple crops, assessing probabilities of crop failure extremes both compared to historical levels as well as independent of the mean trend. We focus on quantifying the probability of reduced crop production due to projected climate change, as a narrowly defined form of food system risk (Challinor et al., 2018). The potential for reduced future crop yields will be referred to as 'crop production risk' throughout the study and can be measured with a probability (or a return period) associated with crop production to fall below a certain threshold within a specific time window. This approach allows both for a differentiated analysis of changes in the risk of crop production losses between countries, and for a quantification of impacts and associated probabilities in absolute terms.

4.2 Data and methods

For the assessment of crop production risk, country-level risk metrics are calculated based on gridded crop yield simulations from the GGCM intercomparison experiment GC6 (see Section 4.2.1), focusing on historical (0.5°C) and future (2°C and 4°C) levels of global warming. Putting forward two complementary metrics of crop production risk (Section 4.2.4), we assess future crop production risk with two complementary metrics. The first metric focusses on the probability of rare events of crop production loss under historical climate, using a percentile-based fixed historical threshold. The second metric focusses on the risk of production falling short of a threshold relative to the mean. The approach is described in detail in the following subsections. For postprocessing and calculation of risk metrics, crop yield data is loaded into the global climate risk assessment platform CLIMADA (CLIMate ADAptation, Aznar-Siguan and Bresch, 2019), where risk is represented as a function of hazard, exposure, and vulnerability. This allows for a flexible re-combination of various crop yield simulation and exposure layers for the calculation of risk metrics. Here, we represent hazard by normalized crop yield, that is, the relative deviation of simulated crop yield per grid cell from a historical mean value (Section 4.2.1). Exposure is represented by the baseline crop production, that is, gridded historical mean crop production per crop type. Historical baseline production is calculated by spatially integrating simulated historical mean yields over harvest area and bias corrected against crop production statistics on a country-level (Section 4.2.2). In this study, we are interested in the direct risk to crop production, therefore the vulnerability component is represented by an identity function, i.e., crop production per simulated year is calculated directly as the product of normalized crop yield (hazard) with the baseline production (exposure). Prior to the analysis, yearly crop production values are bias-adjusted, detrended, and clustered by crop model and level of global warming (Section 4.2.3). Two complementary metrics of crop production risk are introduced in Section 4.2.4.

4.2.1 Hazard: gridded normalized crop yields

The ensemble of climate-crop simulations used here comprises eight GGCMs driven by simulated climate from bias-adjusted climate projections (Cucchi et al., 2020; Lange, 2019) from the Climate Model Intercomparison project round 6 (CMIP6, Eyring et al., 2016). The experiment, referred to as GC6 (GGCMI-CMIP6) hereafter, has first been described by Jägermeyr et al. (under review). In the experimental setup of GC6 the focus is on the response of GGCMs to changes in climate and [CO_2], while neither technological nor genetical developments, nor adaptation through farm-level crop and water management are considered. The ensemble is used here to assess projected climate-change impacts for varying levels of global warmings.

The outputs from eight process-based GGCMs are considered here, each simulating one or more of the crop types maize (Zea mays L.), rice (Oryza sativa L.), soybean (Glycine max L. Merr.), as well as wheat (Triticum sp. L.), modeled separately as spring and winter wheat. These crop types make up for 90% of the current total nutritional cereal and soybean production worldwide (FAO, 2019; Jägermeyr et al., under review). The crop models are: AquaCrop-ACEA, CROVER, CYGMA1p74, EPIC-IIASA, LPJmL, PEPIC, PROMET, and SIMPLACE-LINTUL5+ (Table C2). The GGCMs were run in an harmonized experimental set-up and forced with harmonized and bias-adjusted output from a benchmarked set of 5 CMIP6 GCMs selected for ISIMIP3b (ISIMIP, 2020b, online; Jägermeyr et al., under review): GFDL-ESM4, IPSL-CM6A-LR, MPI-ESM1-2-HR, MRI-ESM2-0, UKESM1-0-LL (see Table C3 for further details). Selection criteria include structural independence, performance for historical periods, process representation, and a representative mean and spread of equilibrium climate sensitivity compared to the full CMIP5 ensemble of GCMs (Jägermeyr et al., under review). Each simulation of a GGCM driven by a specific GCM is referred to climate-crop simulation in the following.

For each of the 37 climate-crop model combinations, transient crop simulations for historical (1850-2014) and future (2015-2100) time periods are used. For future time periods, two potential development trajectories are analyzed here, the Shared Socioeconomic Pathway SSP1 (Riahi et al., 2017) in combination with the

Representative Concentration Pathway RCP2.6 (here SSP126), and SSP5 with RCP8.5 (here SSP585). These combinations of SSPs and RCPs represent two plausible and contrasting trajectories for the 21st century (O'Neill et al., 2016). SSP126 represents a sustainable development scenario (Riahi et al., 2017) with stringent mitigation, reducing greenhouse gas emissions to essentially zero by the end of the century (Pachauri et al., 2015). SSP585 represents a fossil-fueled development (Riahi et al., 2017) with rising emissions throughout the century (Pachauri et al., 2015). For the crop yield simulations, [CO_2] levels are transient, representing historical concentrations for the past and rising in accordance with respective RCP for the future. For the crop yield simulations used here, socio-economic drivers and parameters such as harvested area and potential adaptation efforts were kept constant at a 2015 level to isolate the climate change signal (Jägermeyr et al., under review). For some GGCMs, only a subset of driving GCMs and crop types was available for this study (Table C4): While simulations from all eight GGCMs were analyzed for maize, output from six GGCMs are available for rice, excluding AquaCrop-ACEA and SIMPLACE-LINTUL5+. seven for soybean, excluding AquaCrop-ACEA, seven for rice, excluding SIMPLACE-LINTUL5+. For the combined assessment, results from these two GGCMs were excluded. Therefore, the multi-crop assessment for all crop types combined is based on six GGCMs.

For the hazard component of the risk assessment, absolute values of gridded crop yield provided in tons per hectare and year are normalized by dividing simulated crop yield both for future and historical runs with the mean yield simulated for a historical reference period (1983-2013).

4.2.2 Exposure: baseline gridded crop production

To estimate current levels of crop production in tons per hectare, multi-model-mean yields simulated for the historical period 1983 to 2013 were multiplied with harvested area for rainfed and irrigated systems respectively for each crop type and grid cell. Here, we use gridded land-use data based on the HYDE 3.2 data set (Klein Goldewijk et al., 2017) and harmonized by Hurtt et al. (2020). Gridded irrigation ratios per crop type are based on the 'Farming the planet' datasets for the year 2000 (Monfreda et al., 2008; Ramankutty et al., 2008), as shown in Figure C2. These land-use data sets were used as provided as input data for ISIMIP3b (ISIMIP, 2020b; Jägermeyr et al., under review). Subsequently, the resulting gridded simulated production values were bias-adjusted per country to obtain the gridded baseline crop production used here as exposure layer. This was done in two steps. First, gridded production was normalized per country by dividing simulated gridded values by the country's total production. Then, normalized gridded values were multiplied with country-level reported yearly production quantity as provided by the United Nation's Food and Agricultural

Organization (FAO, 2019), averaged over the years 2008 to 2018. The aim of this bias adjustment with FAO data is to best represent current levels of crop production per country as a baseline for future risk assessment.

For the calculation of yearly production values, normalized crop yields per simulated year (see Section 4.2.1) are multiplied with the baseline crop production exposure to obtain gridded crop production in tons per year for each crop type and climate-crop simulation (Fig. 15a). For crop aggregation, production values in kcal per simulated year were summed for each country and risk metric. The countries with the highest yearly combined crop production in kcal per capita are Argentina, Paraguay, and the USA.

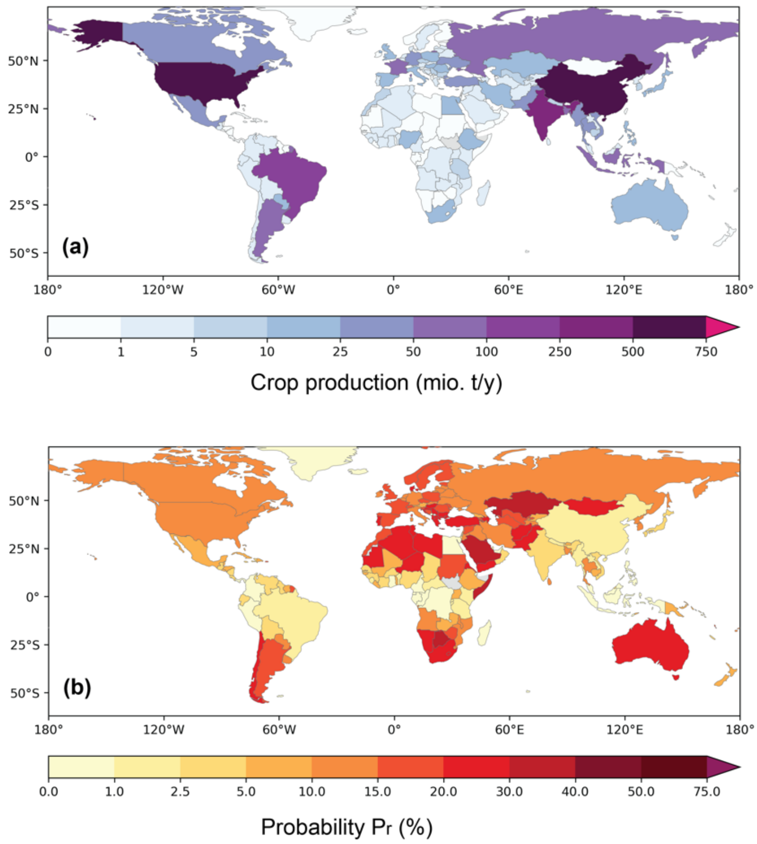

Figure 15: Multi-model median crop production statistics per country at 0.5°C global warming (historical reference bin, ΔGMT = 0.5°C 0.5°C, see Section 4.2.3). Mean yearly crop production is shown in purple in mio. tons per year for maize, rice, soybean, and wheat combined (a). Subplot (b) shows the probability P_r of crop production to fall more than 10% short of the mean in any given simulated year in the historical reference bin.

4.2.3 Global mean temperature bins and detrending

Due to differences in the climate sensitivity between individual GCMs, they simulate deviating rates of global mean temperature (GMT) increase for the same trajectories of [CO_2]. At the same time, Ostberg et al. (2018) found that simulated crop yields can be described in terms of GMT above pre-industrial levels (ΔGMT) to a large extend, with little path dependence. Therefore, GCM induced uncertainty can be reduced by assessing the change in crop production over the 21st century as a function of ΔGMT instead of time. For this purpose, we re-organize crop production data in bins of global warming, referred to as ΔGMT bins in the following. The detrending of crop yield timeseries allows for an analysis of the variability driven aspect of crop production risk by minimizing the effect of slowly changing factors such as agricultural management or CO_2 effects (e.g., Leng and Hall, 2019; Lu et al., 2017). Before binning, yearly crop production values are detrended to avoid a trend-induced spread in data points causing a distortion of variability within a ΔGMT bin. To this end, a second-order polynomial detrending is applied per country, for each time series of simulated yearly crop production per crop type, GGCM, and GCM. ΔGMT bins are formed per crop type and GGCM following the approach by Ostberg et al. (2018) and Lange et al. (2020), among others. First, ΔGMT is calculated for each model year as the deviation of GMT from pre-industrial GMT, that is, the mean over the full ISIMIP3b pre-industrial climate control period, for each GCM. Then, each ΔGMT bin is set to contain all simulated years with a range of ±0.5°C. Like this, yearly crop production values simulated are pooled across GCMs and scenarios (e.g., historical, SSP126, SSP585). Thus, risk metrics are calculated per GGCM, crop type, and ΔGMT bin, from these pooled data points, irrespective of the underlying GCM and scenario. With the pooling of the yearly crop production data across GCMs and scenarios, we increase the number of data points per ΔGMT bin for the purpose of the risk assessment. We do not pool across GGCMs because the spread of inter-annual yield variability within a climate-crop model ensemble was found to be dominated by the spread across GGCMs (Ostberg et al., 2018). Keeping the GGCMs differentiated thus avoids an artificial spread variability and allows for the use of crop model agreement to measure robustness. The total number of simulated years across the five climate models and three scenarios is 1685. The +0.5°C bin contains 601 years, the +2°C bin 357 years, and the +4°C bin 73 years.

As a basis for an un-biased calculation of the risk metrics, yearly crop production values are bias-adjusted after detrending and pooling. To this end, the mean before detrending is added to the detrended values for each combination of crop type, ΔGMT bin, GGCM, and GCM. The correction resets the mean to the value before detrending. By adjusting values to a common mean per bin and crop model, further offsets of the mean between the driving GCMs are removed. As a result of this correction, crop production values for each bin and GGCM have the same mean level as before detrending, while artefacts in the spread due to time dependent trends are removed (see Fig. C7-C16). These bias-adjusted detrended binned sets of yearly data points are further used for the calculation of risk metrics.

4.2.4 Risk metrics

To assess crop production risk, we make use of the global risk assessment platform CLIMADA (Aznar-Siguan and Bresch, 2019). The probabilities of yearly crop production falling below a given threshold are used as risk metrics. The pre-processed simulated yearly crop production data points within each bin are used for the computation of risk metrics, for each crop type and ΔGMT bin. While the risk metrics are calculated across a range of ΔGMT bins, the main focus is on the comparison of a historical reference ΔGMT bin to future ΔGMT bins, namely 2°±0.5°C and 4°±0.5°C bins, to a historical reference ΔGMT bin. Here, we focus on two complementary risk metrics, both representing the probability of simulated yearly production within a GMT bin to fall short of a defined threshold. The annual probability P can be both expressed as percentage or inversely, in the form of a return period (T) in years (see Aznar-Siguan and Bresch, 2019):

$$P = \frac{1}{T} \tag{4.1}$$

For any given combination of crop model and crop type, only ΔGMT bins with a minimum sample size of 30 simulated years available are considered for probability calculations with the relative threshold. Furthermore, crop production deviations are only calculated for T values that are smaller than the sample size of a given ΔGMT bin.

A frequently used approach to estimate the climate change influence on climate extremes and impacts is to calculate the ratio of probability of extreme events under a new situation (e.g. a climate affected by anthropogenic forcing) and the probability in a reference period (e.g., Fischer and Knutti, 2015; Stott et al., 2004, 2016; Thiery et al., 2020; Vogel et al., 2019). Here, the resulting probability ratio (PR) is a measure for the relative deviation of probability P of extreme crop losses in a given ΔGMT bin from the probability $P_{0.5°C}$ in the historical reference bin. PR is calculated as the ratio of assessed and reference probability:

$$PR = \frac{P}{P_{0.5°C}} \tag{4.2}$$

It should be noted that PR is infinite where the historical reference probability is equal to zero. If not declared otherwise, PR values provided in the results section are computed as the multi-model median of PR values computed for each individual crop model. This is relevant to keep in mind, because the multi-model median of PR is not exactly equal to PR calculated from multi-model median probabilities. Reason being that the result of calculating the ratio and the multi-model median is not indifferent of the order of the mathematical operations. The probability of severe crop losses increases for PR<1 and decreases for PR>1. In the results, we speak of high crop model agreement if more than 70% of crop models agree in the direction of probability change as compared to the reference period. The minimum required agreement of 70% ensures that a variety in crop model types need to agree, as the largest group of models, site-based GGCMs, constitute 5 out of 8 (62.5%) of models in the ensemble (see Table C2). For the calculation of probabilities, the number of years in a ΔGMT bin falling below a given threshold are counted. The two thresholds applied here are the fixed (historical) threshold and the relative threshold (Fig. 16), described in the following subsections.

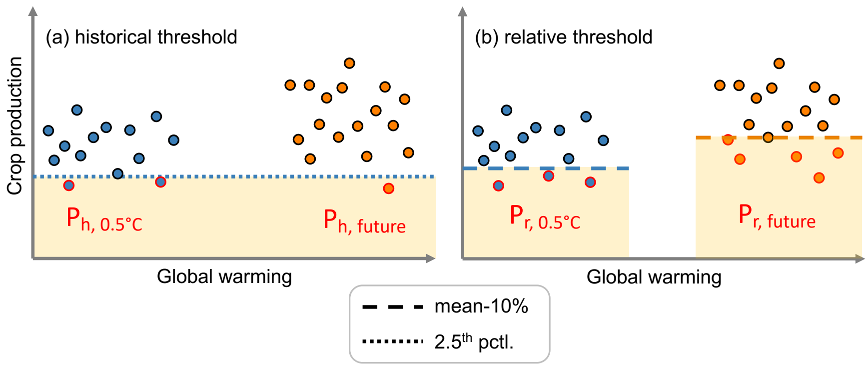

Figure 16: Illustration of the historical (a) and relative (b) threshold used for the calculation of the probability of years with low crop production extremes. P_h is the probability of any given year to fall below the 2.5th percentile of the historical 0.5°C global warming bin (historical threshold, dotted line). P_r is the probability of any given year to fall more than 10% short of the mean production at any given level of global warming (relative threshold, dashed lines). In the given example, $P_{h,\,future} < P_{h,\,0.5°C}$, while $P_{r,\,future} > P_{h,\,hist}$. Actual data points with thresholds are shown in Fig. C7-C16.

4.2.4.1 Fixed historical threshold and Ph

The first risk metric is the probability P_h of simulated yearly production within a ΔGMT bin to fall short of a fixed threshold defined from historical distribution of crop production (Fig. 16a). P_h can be interpreted as a measure of risk to absolute crop production, a compared to historical values. This fixed historical threshold is calculated as the n^{th} percentile of yearly production in the historical reference ΔGMT bin. The n^{th} percentile corresponds to the value that crop production falls short of with a return period (T) of 100/n years. The probability of crop production to fall short of the n^{th} percentile in the historical ΔGMT bin is n % by definition, i.e. 2.5% for the 2.5^{th} percentile. While P_h was calculated across a range of historical percentiles (1.667^{th} to 50^{th}), most results are shown here for the historical 2.5^{th} percentile used as a threshold (corresponding to T=40 years), following Lange et al. (2020). The historical threshold is also referred to as 'fixed' because once defined from the historical reference ΔGMT bin, it is fixed for all other ΔGMT bins. However, it should be noted that while the absolute values of the historical threshold are fixed across ΔGMT bins, they are not the same everywhere. The absolute production value of the historical threshold differs between locations (e.g., grid cells, countries) and crop models, depending on the distribution of crop production in the reference bin at each location and for each crop model (see dotted lines in Figures C7-C16). Here, the probability of crop production to fall short of the historical threshold, that is, the

2.5th percentile of the 0.5°C bin of global warming, is referred to as P_h in the results. PR_h is the ratio of P_h to $P_{h,0.5°C}$.

4.2.4.2 Relative threshold and Pr

An assessment based on a relative threshold can reveal the risk of reduced production due to increased variabilities otherwise masked by a dominant mean trend. The associated risk metric is the probability P_r of crop production losses greater than 10% (Fig. 16b). P_r is calculated as the fraction of years within a ΔGMT bin with simulated production falling more than 10% short of the mean production in the same ΔGMT bin. This means that the absolute value of the relative threshold changes across ΔGMT bins (dashed lines in Fig. 16b). This threshold is called 'relative' (or flexible) because it is defined relative to the mean within each ΔGMT bin – and independent of production levels in the historical reference ΔGMT bin. As a consequence, the crop production risk measured with P_r is expected to increase with an increase in variability, independently of the mean trend. This holds of course only, if there is no relevant counteracting change in skewness. Like this, the relative threshold complements the historical threshold, adding a more variability-based risk perspective to the assessment. For all four crop types and most crop models, the value of the relative threshold (mean-10%) globally aggregated for ΔGMT=0.5°C is very close to the 2.5th percentile used as a historical threshold, as seen in Figures C10 (maize), C12 (rice), C14 (soybean), and C16 (wheat). This is one reason for the choice of 10%. The other reasons are that mean-10% is straightforward to communicate and has been applied as a historical threshold by Tigchelaar et al. (2018). The probability that in any given modeled year, the production in a country or globally falls below the relative threshold, that is, a decline of 10% or more below the mean production at the same level of global warming, is referred to as P_r in the results. PR_r is the ratio of P_r to $P_{r,0.5°C}$. P_r for the ΔGMT=0.5°C is mapped per country in Fig. 15b.

4.3 Results

We analyzed simulated crop production per country to project probabilities of extreme crop losses for future levels of global warming. The total mean simulated historical production of all crops combined is 2.66 mio. tons/y, corresponding to 8.73 × 10^{15} kcal/y. The historical 2.5th percentile (i.e., extreme event occurring every 40 years) of global production is 8.34 × 10^{15} kcal/year (-4.5%), with higher globally synchronized losses possible for individual crop types (see Fig. 17, blue lines) and countries. For increased global mean temperatures, the probabilities P_h and P_r return partially consistent and partially diverging results per country and crop type. The key finding for P_h measured against an historical threshold is that globally aggregated projections for 2°C are mostly more optimistic than historically, with increased production levels resulting in reduced crop failure probability P_h. All crop types except maize contribute to this signal (see Fig. 17). At 4°C, an increase in P_h is projected, with reduced production levels for all crop types compared to 2°C. On a globally aggregated level, relative production deviations from the mean are not changing substantially, except for an increase in relative rice and wheat production losses for very rare events with return periods T > 30 years (Fig. 18). The probability of crop losses relative to the mean, P_r, provides differentiated insights for single countries and crop types. For maize production, PR_h and PR_r agree in most countries, for example projecting an increase in risk in the USA and a decrease in South Africa (see Section 4.3.2). For rice and soybean, decreasing P_h are generally contrasted with increasing P_r (see Section 4.3.3 & 4.3.4). For wheat, the outlook is very uncertain, however with increased relative loss potential projected for rare events with high return periods in a 4°C world (see Section 4.3.5).

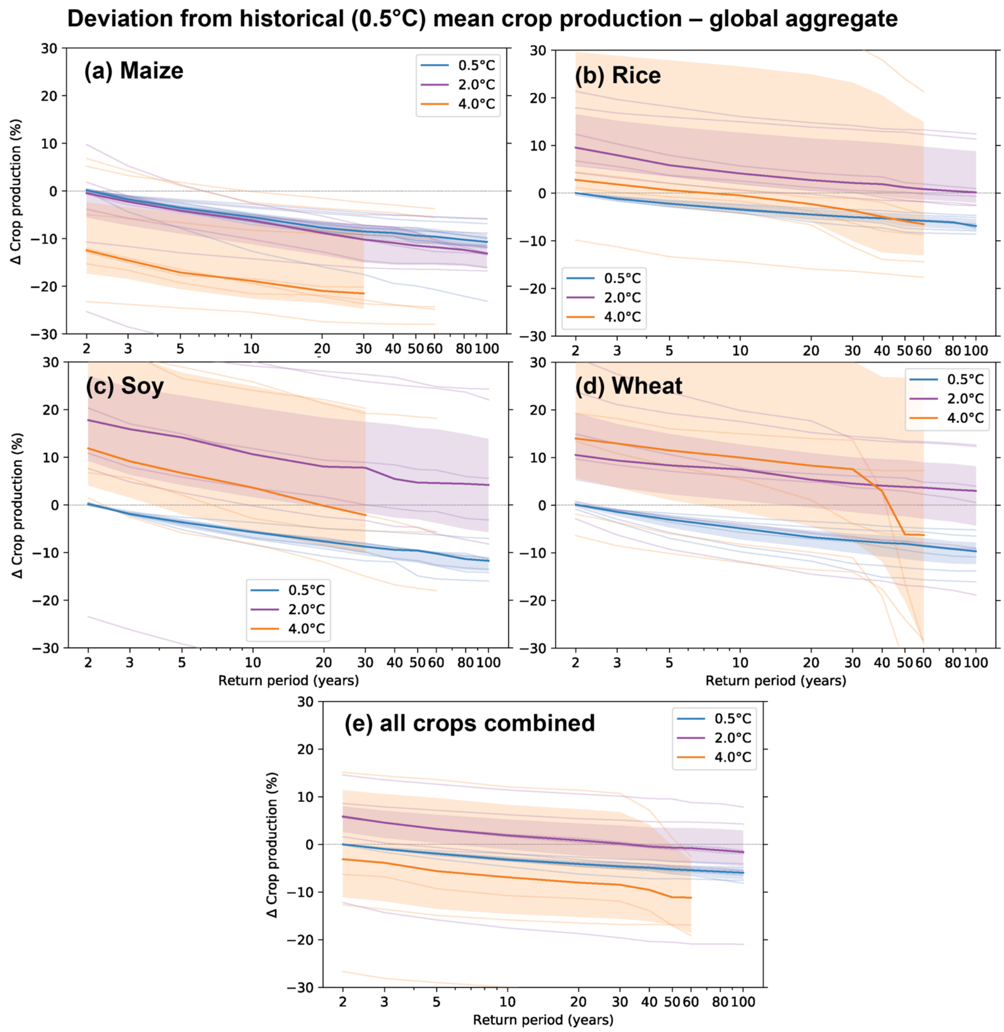

Figure 17: Globally aggregated deviation of crop production from the historical mean for a global warming of 0.5° (historical reference bin, blue), 2°C (purple) and 4°C (orange) for (a) maize, (b) rice, (c) soybean, (d) wheat, and (e) all four crops combined. Solid lines demarcate the multi-crop-model median, thin lines the individual crop models, and shading the inter-quartile range of the individual models. All projections assume that land-use and management remain unchanged. A return period of 40 years corresponds to the 2.5th percentile of crop production. Similar plots for major producing countries are shown in Fig. C17-C24.

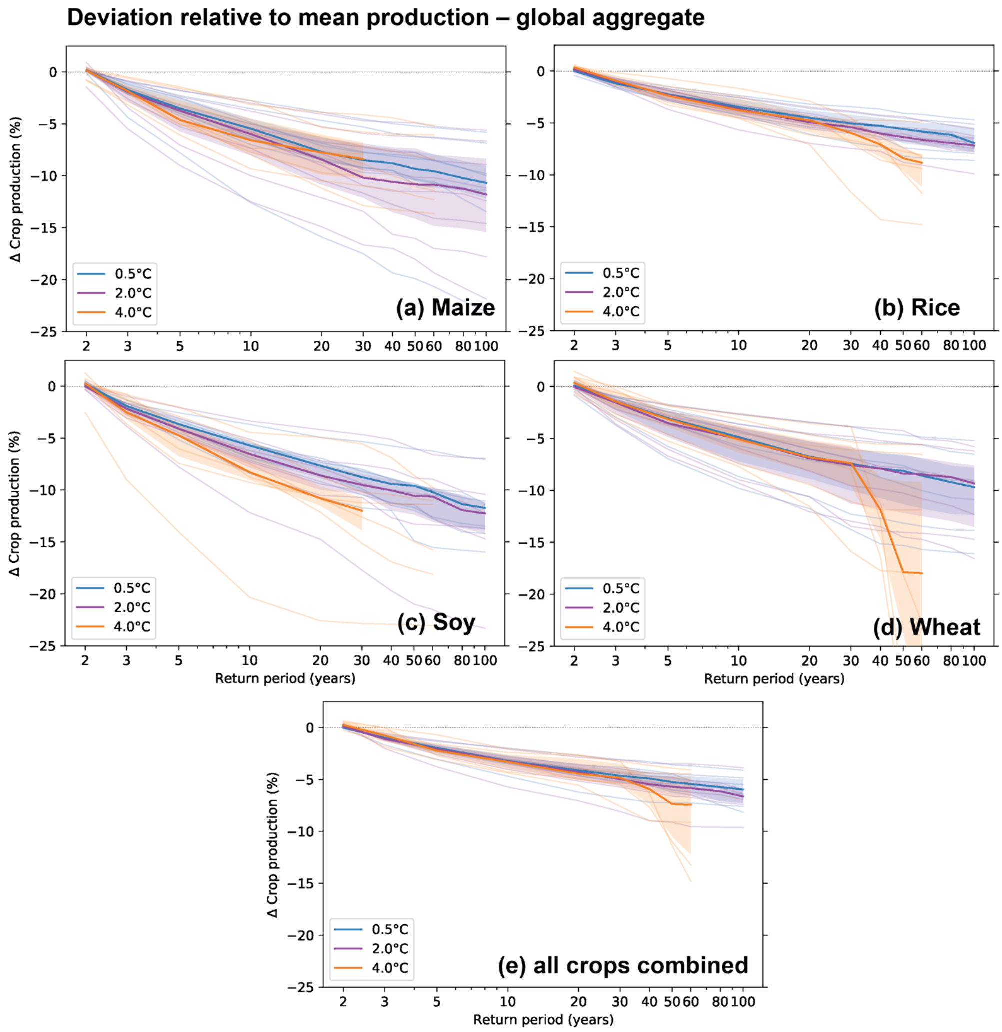

Figure 18: Globally aggregated deviation of crop production relative to the mean within each global warming bin for 0.5° (blue), 2°C (purple) and 4°C (orange) of global warming for (a) maize, (b) rice, (c) soybean, (d) wheat, and (e) all four crops combined. Solid lines demarcate the multi-crop-model median, thin lines the individual crop models, and shading the inter-quartile range of the individual models. All projections assume that land-use, management, and irrigation patterns remain unchanged. The relative threshold is defined as 10% below the mean production for each level of global warming (ΔGMT bins of width 1°C). Thus, the probability of falling below the relative threshold can be derived from these plots: The probability is the equal to the inverse of the return period where Δ crop production falls below -10%. A return period of 2 years corresponds to the median crop production. Similar plots for major producing countries are shown in Fig. C17-C24.

4.3.1 Multi-crop production risk

Historical threshold: Absolute global crop production levels for all four crop types combined are projected to increase at 2°C global warming by roughly 4 % to 6 % compared to historical levels across return periods (difference between purple and blue line in Fig. 17e). At 4°C global warming, the multi-model-median projects absolute global crop production to fall ~3 % short of historical levels, with increased losses for rare events (T > 40 years). Most crop models agree on an increase in P_h at 4°C, with a multi-model-median 16-fold probability increase (PR_h = 15.9) to P_h = 39.7% (Table 3a), however with a wide spread between individual models. The world map of PR_h changes fundamentally from 2 to 4°C of global warming (Fig. 19a-b). At

2°C, most countries show a decreased P_h compared to 0.5°C (Fig. 19a). However, there are also 50 countries already experiencing increased $RP_h > 1$ at 2°C, mostly situated in North and Central America, the Caribbean, equatorial Africa, and south-west Europe (Fig. 19a). At 4°C, P_h increases with $PR_h > 1$ for 106 countries (orange and red color in Fig. 19b), including most major crop producing countries except Argentina and India (Table 3a). The USA is the second largest producer of maize, rice, soybean, and wheat combined – and among the countries displaying the largest values of PR_h (Fig 5a,b). For the USA, most models agree on an increase in crop loss probability P_h against the historical threshold at 4°C (PR_h=13.4 and P_h =33.6%, Table 3a). Largest P_h at 4°C global warming is projected in Central America and western Africa, led by Sao Tome and Principe, Guatemala (both P_h = 100 %), El Salvador (99 %), Venezuela (98 %) Honduras (95 %) and Gabon (93 %). In contrast, a decrease of P_h to 0 % (i.e., a strong reduction in risk) at 4°C is projected for 28 countries. The most important crop producing countries with P_h = 0 % projected at 4°C are Argentina, Australia, Kazakhstan, South Africa, Ethiopia, and Japan.

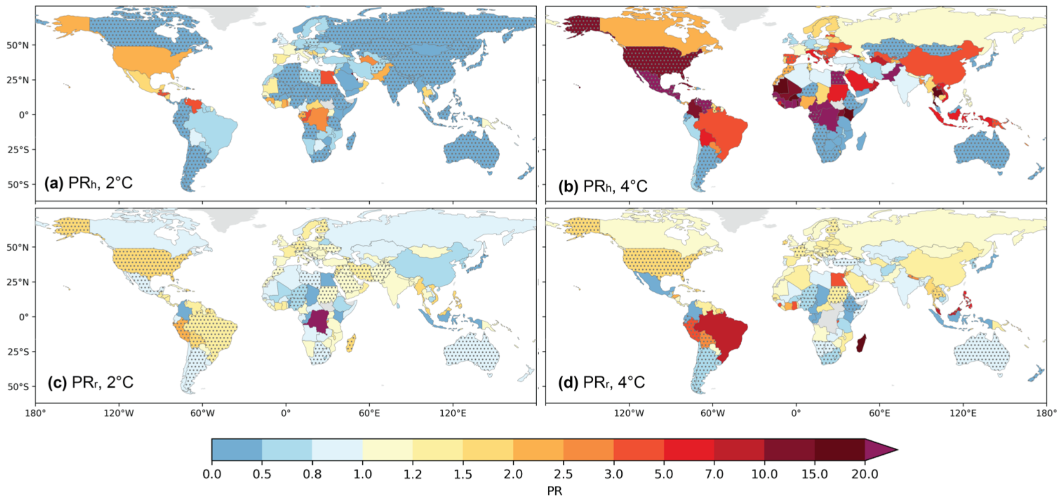

Figure 19: Multi-model median probability ratio (PR) per country for maize, rice, soybean, and wheat combined at a global warming level of 2°C (a, c) and 4°C (b, d) above pre-industrial levels, as compared to historical climate (0.5°C). PR is defined as the ratio of the probability of crop production to fall below a given threshold divided by the historical reference probability (0.5°C global warming). PR_h (a, b) is the factor of change in probability P_h that crop production in a given year falls below the 2.5th percentile of the 0.5°C bin (historical threshold). PR_r (c, d) is the factor of change in probability P_r that crop production in a given year falls more than 10% short of the mean of the given warming level (relative threshold). Blue colors (PR<1) indicate a decrease in probability. For PR>1 probability is increased compared to 0.5°C. Stippling indicates a crop model agreement above 70% on the sign of probability change.

Relative threshold: For all four crop types combined, the probability P_r of years with globally aggregated production to fall more than 10% short of the mean is almost zero across levels of global warming (Fig. 18e & Table 3b). For individual countries, the prospects with regard to P_r are more differentiated, with increases in some and decreases in other countries (Fig. 19c,d). Of the major crop producing countries, the strongest signal with high model agreement is again found for the USA, with an increase of P_r from 12.7 % at 0.5°C to 15.4 % (2°C) and 17.1 % (4°C) of global warming (Table 3b). The major crop producing countries where models agree on a decrease in P_r at 4°C are Argentina and France (Table 3b). The map of historical P_r shows considerable differences between regions (Fig. 15b). Above average crop loss probabilities are simulated for Argentina, Australia, southern and northern Africa, Europe, the Middle East, the Arabic peninsula, and central Asia. Low historical values of P_r are simulated for northern South America, Equatorial Africa, as well as East and South East Asia. It is interesting to note that several countries with decreasing P_r start off from relatively high historical levels of P_r already (Table 3b), including Argentina, South Africa, and Australia, where no increase in risk is projected across crop types and warming levels.

Table 3: Combined crop production risk changes. Baseline mean crop production and probability of crop production to fall short of the historical (a, P_h) and the relative (b, P_r) threshold for maize, rice, soybean, and wheat combined under historical (5°C) and future (2°C and 4°C) levels of global warming. Values are provided on a globally aggregated level and for twelve major crop producing countries. Multi-model median probabilities are shown with the inter-quartile range (IQR) of single crop model results provided in brackets. Blue shading marks a decrease in probability as compared to 0.5°C levels. Orange shading marks an increase in probability as compared to 0.5°C levels. The asterisk (*) implies more than 70% crop model agreement on the sign of probability change compared to 0.5°C of global warming. The countries are China (CHN), USA, India (IND), Brazil (BRA), Argentina (ARG), Indonesia (IDN), Russia (RUS), France (FRA), Ukraine (UKR), Canada (CAN), Bangladesh (BGD), and Vietnam (VTN). Similar results per crop type are shown in Table C1.

Country (ISO3)	**Mean production** 0.5°C		**Probability** (IQR in brackets) [%]					
			(a) P_h (historical threshold 2.5th pctl)			**(b) P_r** (relative threshold mean-10%)		
	10^{12} kcal/y	**mio. t/y**	**0.5°C**	**2.0°C**	**4.0°C**	**0.5°C**	**2.0°C**	**4.0°C**
global	**8728**	**2665**	**2.5**	**0.8* (1.5)**	**39.7* (91.4)**	**0.3 (0.2)**	**0.7 (0.7)**	**0.7 (2.4)**
CHN	1821	560	2.5	0.3* (1.6)	8.2 (77.4)	1.4 (3.5)	1.1 (0.8)	2.7 (2.1)
USA	1778	508	2.5	5.0 (8.4)	33.6* (71.9)	12.7 (6.4)	15.4* (8.9)	17.1* (7.9)
IND	854	279	2.5	0.1* (0.5)	2.1 (3.4)	4.1 (3.2)	3.6 (2.7)	4.8 (2.4)
BRA	575	169	2.5	1.3 (2.5)	11.0 (72.6)	1.9 (1.5)	2.5* (13.5)	7.5 (10.3)
ARG	300	88	2.5	0.1* (0.3)	0.0* (0.0)	16.1 (8.1)	19.7 (7.8)	15.1* (7.9)
IDN	269	91	2.5	0.1* (1.1)	15.8 (73.3)	0.2 (1.4)	0.0 (0.4)	0.0 (2.1)
RUS	240	71	2.5	0.8* (1.3)	2.7 (5.1)	10.2 (3.0)	9.7 (4.6)	8.9 (5.5)
FRA	172	51	2.5	2.7 (7.6)	2.7 (15.4)	17.9 (12.1)	19.0 (21.3)	16.4 (21.2)
UKR	162	47	2.5	1.5 (5.8)	8.9 (21.9)	14.2 (16.9)	17.6* (13.2)	26.0 (15.1)
CAN	155	46	2.5	0.0* (0.8)	6.2 (6.5)	12.0 (4.2)	13.6 (7.2)	13.0 (6.5)
BGD	150	53	2.5	0.7* (1.1)	6.8 (49.0)	12.0 (4.0)	9.4 (4.0)	13.0 (4.5)
VTN	135	47	2.5	1.1 (3.1)	15.1 (21.2)	3.0 (1.5)	4.8 (2.7)	4.1 (6.8)

Risk metric consistency: For all four crop types combined and considering crop model agreement, there are only 9 out of 167 countries analyzed with a consistently reduced value of both P_h and P_r projected for 2°C warming (Argentina, Australia, South Africa, Nigeria, Japan, South Korea, Libya, Lesotho, Niger; contributing 6.1 % of global production), and one country with a consistently increased risk at 2°C

(Burundi). For the remaining 157 countries (93.9 % of global production), risk projections for ΔGMT=2°C are either not consistent between P_h and P_r, or lacking crop model agreement. At ΔGMT=4°C, there are 11 countries with consistently optimistic prospects, that is, reduced probabilities (Argentina, Australia. South Africa, Ethiopia, Uruguay, Ecuador, New Zealand, Lesotho, Niger, Namibia, and Eritrea, 5.6 % of global production) opposed to three countries were models agree on an increase both in P_h and P_r, i.e., increased risk. These countries, accounting for 20.4% of the aggregated global production, are the USA, Georgia, and Slovenia. For 71 additional countries (74 % of global production), both P_h and P_r are projected to increase albeit with limited model agreement (Fig. 19b,d), most prominently for China and Brazil (Table 3).

4.3.2 Maize

Maize is the only crop type analyzed with a geographically widespread increase in risk projected for a global warming of 2°C above pre-industrial levels. This is also reflected by the increase in probability P_h for global maize production to falls below the historical 2.5th percentile to 5 % (PR_h =2) at 2°C and 82 % (PR_h =31) at 4°C global warming, with high model agreement on the increase in P_h (Table C1a). At 4°C global warming, global maize production is more than 10% below the reference levels across all return periods (Fig. 18a).

Just as for the global aggregate, the three largest maize producing countries, USA, China and Brazil, show a strong increase in P_h with high model agreement (Table C1a, Figure C5a). In addition, USA shows increased P_r with high model agreement, both at 2°and 4°C global warming (Table C1b). As will be further elaborated in the discussion, PR_r appears less relevant against the backdrop of considerable decreases in absolute maize production risk as indicated by PR_h in Figure C5a. Argentina and South Africa, both situated around mid-latitudes in the Southern Hemisphere, are the only two out of twelve major maize producing countries showing a decrease in P_h: More than 70% of crop models agree on a diminished P_h at 4°C global warming in these two countries (Table C1a). It should be noted however, that both countries show relatively large historical levels of P_r of 20-30%, suggesting large simulated inter-annual variability of maize production already under current climatic conditions.

4.3.3 Rice

Among the major rice producing countries, production outlooks in a warming climate are consistently most optimistic for China and Japan, and most pessimistic for Thailand and Pakistan (Table C1b). In the global aggregate, the absolute global rice production increases across return periods for 2°C of global warming as compared to 0.5°C (Fig. 17b). At 4°C, rice production is close to historical levels, projected to potentially fall below for large return periods (T > 50 years). These global projections are also reflected by the results for most single countries: For most of the twelve largest rice producing countries, except Thailand and Pakistan, a decrease in P_h is projected at 2°C of global warming (Table C1b). At 4°C, an increase in P_h is projected for half of the major producers, most prominently in Thailand and Pakistan, the two countries experiencing increased risk at 2°C already. However, there is generally no strong agreement among individual crop models regarding the sign of change in P_h at 4°C as compared to the historical reference bin (Table C1b). High model agreement on reduced P_h is projected for several countries in the southern hemisphere, including Argentina, South Africa, and Australia, as well as Japan and Russia in the north (Figure C5b).

Globally aggregated, the results show a small increase of rice production risk due to inter-annual variability for return periods larger 30 years (Fig. 18b) at 4°C. Global P_r remains close to 0% across all analyzed levels of global warming. For the largest rice producing country, China, there is a high model agreement on a decrease in P_r from 1.7 % at 0.5°C to 0 % at 4°C (Table C1b). A decrease in P_r is also projected for Japan. For all other major rice producing countries, however, an increase in crop production risk as measured by P_r is projected both for 2°C and 4°C global warming, with high model agreement in USA, Thailand, and Pakistan.

4.3.4 Soybean

Just as for rice, absolute global soybean production increases across return periods for 2°C of global warming as compared to 0.5°C (Fig. 17c), resulting in decreased P_h globally and in all major producing countries (Table C1c). At 4°C, global soybean production falls short of 2°C level but stays above historical values across return periods (Fig. 17c). Accordingly, the twelve major soybean producing countries show a decrease in P_h at 2°C (Table C1c), and most of these countries also show decreased risk still at 4°C. However, for the USA and Brazil, contributing approximately two thirds of global soybean bean production, P_r is projected to increase at 4°C, with a multi-model median P_h of 2.7% and 19.2% in the USA and Brazil, respectively (Table C1c), albeit with limited model agreement. At 4°C, increased P_h is also projected for Bolivia, Mexico, and further countries in Central America, Africa, and South East Asia (Figure C5c).

Outlooks for soybean production risk measured against the flexible mean are less optimistic (Fig. 18c). The increase in global P_r from 2 % at 0.5°C to 7 % at 4°C (Table. C1c) corresponds to a development from an expected return period of 50 years to 15 years of production values more than 10 % below the mean (orange line compared to blue line Fig. 18c). At 2°C, half of the major soy producing countries display increased P_r, including the three largest producers, USA, Brazil, and Argentina, with high model agreement (Table C1c). In contrast, India is the only major soybean producer where crop models agree on reduced P_r at 2°C. The results for 4°C show considerable increases in soybean production risk due to inter-annual variability for most countries. The largest increases in P_r are projected for most of the Americas, as well as Benin, Ivory Coast, Madagascar, and Thailand (Fig. C6c). Of the 12 largest soybean producing countries, only India, Uruguay, and Indonesia show model agreement on a decrease of P_r at 4°C (Table C1c).

4.3.5 Wheat

Just as for rice and soybean, absolute global wheat production is projected to increase across return periods for 2°C of global warming as compared to 0.5°C (Fig. 17c). At 4°C however, global wheat production drops substantially across individual crop models, around return periods of ca. 30 to 50 years (Fig. 17c). These return periods are reflected in the threshold-based assessment, as the 2.5th percentile corresponds to a return period of 40 years. The same signal is seen in wheat production risk due to inter-annual variability, with relative global production levels falling well below historical levels (Fig. 18c). This results in an increase in globally aggregated P_r from 1 % at 0.5°C to 2.7 % at 4°C global warming, however with limited model agreement (Table C1d and Fig. 18c). It cannot be ruled out however that the sharp drop in crop production for rare events (T > 30 years) at 4°C is a sampling artefact. All twelve largest wheat producing countries show a decrease in P_h at 2°C of global warming (Table C1d). Projections are diverging at 4°C: For the largest producer, China, models project an increase both in P_h and P_r. In contrast, decreasing wheat production risk is projected for the second largest producer, India, with high model agreement (Table C1d).

3.4 Discussion

3.4.1 Key findings

We applied two risk metrics that reflect two complementary risk perspectives regarding food security. P_h is a commonly applied risk metric (e.g., Fischer and Knutti, 2015; Lange et al., 2020; Vogel et al., 2019), using historical extremes as the baseline for the assessment of future risk. Therefore, P_h is partially determined by the mean trend in crop production, inheriting uncertainties in the mean trend due to the CO_2 fertilization effect. What is more, an increase in variability might be masked by a positive mean trend when P_h alone is considered in a risk assessment. To add a metric more independent of the mean trend, we therefore complemented the assessment of the historical threshold with a relative threshold. 'Relative' means that the threshold value is relative to the mean production, recalculated for each level of global warming. With P_h, we assess future crop failure risk under the assumption that current risk reduction methods and adaptation levels prevail into the future. With the perspective represented by P_r, we assume that with trends in mean production, there will be an adaptation to these trends, but not to changes in extremes relative to the mean (or at least not to the same degree). While an explicit assessment of these assumptions is outside the scope of this study, both approaches add value for the assessment of future crop production risk, as they can be used to answer different questions.

The historical threshold (2.5^{th} percentile of the 0.5°C world) highlights regions and crop types with reduced or elevated absolute levels of crop production in a warming climate compared to historically extreme years, with potential implications for the mean supply in food stocks, both globally and regionally. On a global level, P_h is generally projected to decrease at 2°C and increase at 4°C. P_h is often dominated by the mean trend, as illustrated by a comparison of results with Jägermeyr et al.'s study of mean trends that is based on the same climate-crop simulation ensemble (under review). Generally, a positive trend in mean crop yields is associated with decreasing P_h and vice versa, as can be seen by comparing crop-specific world maps of the mean trend with the country-level PR_h. For example, the global patterns of largely increasing P_h for maize match well with the decline in mean maize yields identified by Jägermeyr et al. (under review): Global mean production of rice, soybean, and wheat is projected to increase in absolute numbers for moderate levels of global warming. This agrees with decreased P_h projected for these crop types at 2°C global warming. In contrast, the probability P_h of years with higher production losses relative to the mean is elevated at 4°C of global warming for soybean and wheat. This signal is reflected on the global aggregate with increased relative losses at return periods larger than 30 years. While there is limited agreement between the individual crop models with regard to these aggregated changes, the results suggest that regional crop production is at a higher risk in a 4°C world than today, both with regard to P_h and P_r. Under the assumptions that crop production systems and markets are more easily adapting to long term mean trends than to changes in variability, the relative threshold adds a complementing perspective on crop production risks. A changing return period of years with a large loss of crop production relative to the mean essentially indicates a change in frequency of climate-related production shocks with potential impact on food security and markets. Thus, adapting to increased variability is a fundamentally different challenge than adapting to long-term trends in mean production and accompanying potential shifts in production areas.

The deviating results for P_h and P_r, especially at a moderate global warming level of 2°C, show that the choice of the risk metric matters and should be chosen carefully in the context of risk assessments. A considerable increase in risk measured relative to the historical threshold, as seen for maize in most countries, implies reduced absolute production levels due to climate change. Where these reductions are substantial, risk changes associated the changes in variability as measured by P_r can be considered less relevant against the backdrop of diminishing absolute production levels. But in many cases, the signal in P_h is not as unequivocal. Soybean production in the USA and wheat production in China are two examples where the two approaches produce contrasting results. According to Jägermeyr et al. (under review), the mean soybean production in USA is projected to remain largely unchanged over the 21st century. For wheat production in China there are even gains in mean production projected. In both cases, we found the probability P_h to decrease from 0.5°C to 2°C, and to be virtually equal to historical levels (2.7 % instead of 2.5 %) at 4°C of global warming (Table C1c,d). In contrast, the probability P_r of crop production to fall more than 10 % short of the mean is increased both at 2°C and 4°C in both cases, with high agreement between individual crop models (Table C1c,d). This additional information added by P_r complements the risk profile of the affected countries: For soybean production in the USA and wheat production in China, the models project an increase in production shock frequency with climate change. Masked by a positive mean trend, this signal was not detected by P_h.

The general increase in maize production risk projected for ΔGMT=2°C and 4°C is also consistent with the results by Tigchelaar et al. (2018, Table 1), but there are differences with regard to the change in probability for individual countries. While the two studies agree on considerable increases in the probability of production to fall short of an historical threshold (P_h) in the USA, China, Brazil, and other major maize producing countries, Tigchelaar et al. deviate from our results for Argentina and South Africa. Their assessment projects an increase in risk also for these two countries, in contrast to decreasing P_h projected here. Relative thresholds were not assessed by Tigchelaar et al. (2018). There are basic methodological differences that should be considered when comparing the two studies, as the maize yield projections by Tigchelaar et al. (2018) are based on empirical instead of process-based crop models.

It is also interesting to compare our resulting risk metrics to the assessment of historical drought risk to agricultural systems by Meza et al. (2019). In their study, the hazard component was based on climate indicators for the period 1980-2016 which lies within the range of ΔGMT=0.5°C ± 0.5°C chosen as historical reference here. The comparison of the world maps of both drought hazard and risk (Fig. 2 in Meza et al., 2019) with the world map of baseline $P_{r,\ 0.5°C}$ (Fig. 1b) shows considerable spatial agreement: Regions with above-average historical risk are North America, Argentina, southern Africa, the greater Mediterranean region, central Asia, and Australia. Noteworthily, most crop models in our study do not project a further increase in P_r for most of these countries with historically high risk. In both assessments, regions with low historical agricultural risk entail most of northern South America, equatorial Africa, as well as East and South East Asia. This agreement is noteworthy, considering the many methodological differences between the two studies, as their study is not based on GGCMs.

4.4.2 Uncertainties and limitations

The drops in rice and wheat production at 4°C for rare events (T > 30 years) shown in Fig3b,d could be sampling artefacts, due to a reduced the sample size at 4°C and the fact that not all driving climate models provide the same amount of data points for global mean temperatures > 3.5°C for the 21st century (Table C3). On a more general note, any risk assessment can only be as good as the input data. Besides all measures taken to either mitigate or communicate uncertainties, there are many remaining uncertainties that cannot be addressed sufficiently within the scope of this study. First, it is important to be aware that crop production projections are not to be confused with anything close to predictions of actual production amounts in the future. This is particularly so due to the experimental design that does not consider developments in technologies, genetics, land-use patterns, and farm-land management. While the large climate-crop model ensemble size allows for a more robust risk assessment than studies based on single GGCMs, many uncertainties in the modeling chain cannot be reduced nor fully accounted for by simply applying a large ensemble (Challinor et al., 2018; Müller et al., 2021). This is partly due to imbalances in the ensemble, with individual crop models often simulating opposite trends for globally aggregated yields (Fig. C7-C16). Other reasons include biases and processes that are imperfectly or incompletely represented by both climate and crop models. The question, whether the climate-crop model experiments used here are adequate for the purpose a crop production risk assessment cannot be finally answered. Parts of the uncertainties can be discussed based on evaluative studies from model intercomparison studies. This includes the fundamental question whether the relevant extremes are represented adequately both in the GGCMs and the forcing climate variables from GCM output. Ridder et al. (2021) found skill in CMIP6 climate models to simulate compound events of extreme heat and drought events, however not for all regions and ensemble members equally. The spread between climate models can partly be explained by the spread in climate sensitivity between individual GCMs, as well as amplified regional deviations (Eyring et al., 2016). Here, uncertainties in the driving climate models are partially accounted for by binning data points by level of global warming instead of time, attempting to mitigate differences in climate sensitivity. However, this approach is prone to a distortion of variability due to long-term trends that are not driven by global mean temperature, such as CO_2 effects. This was counter-acted with a detrending performed before binning and bias-adjusting the mean value per bin afterwards. The remaining spread between climate models was put up with for the risk assessment presented here, requiring the assumption that the five selected climate models represent a balanced sample of plausible climates within each bin of global mean temperature. According to Leng and Hall (2019), "large discrepancy exists among crop models in simulating yield loss risk under droughts not only in the magnitude but also in terms of its sensitivity to increasing drought severity. This could be due to the differences in model structure, representation of environmental stress, agricultural management, and CO_2 fertilization effect." For certain countries and crop types, however, we found a better agreement between individual models than for the global aggregate.

The uncertainty introduced by the crop model ensemble was dealt with in several ways. To mitigate the fact that the ensemble is most likely unbalanced (see Müller et al., 2021), the analysis focusses on multi-model median, a statistic less sensitive to outliers than the mean. Furthermore, we report inter-model agreement of 70% as a measure of robustness, requiring a minimum subset of crop models to agree on the sign of change in probability. Between the four crop types, highest rates of model agreement regarding probability changes at 2°C and 4°C were found for maize and lowest for rice (stippling in Fig. C5 & C6, asterisks in Table C1). This agrees to the findings by Müller et al. (2017) that recent generations of GGCMs perform best in reproducing temporal variability for maize and worst for rice. Uncertainties in the mean trend are partially mitigated by contrasting PR_h with the assessment of PR_r, a metric independent of the mean trend. Future intercomparison experiments and sensitivity analyses are required to better understand and reduce the level of uncertainty both with regard to the mean trend and extreme events, as they are both relevant for decision making.

4.4.3 Outlook

The approach presented here can be further refined, especially with regard to the bias adjustment of the exposure data, the detrending method, the definition of historical reference periods, and the choice of risk metrics.

Here, gridded baseline crop production was bias adjusted using country-level production statistics provided by the FAO. A bias correction on a grid point level has the potential to increase accuracy, especially for larger countries. For this, an approach similar to Jägermeyr et al. (2020) can be followed instead, using gridded production estimates from the Spatial Production Allocation Model 2005

(SPAM2005, IFPRI and IIASA, 2016), and identifying and filling gaps based on data from the dataset Monthly Irrigated and Rainfed Crop Areas around the year 2000 (MIRCA2000, Portmann et al., 2010) and Ray et al. (2012) yield data.

Detrending is instrumental to the risk assessment presented here, mainly to avoid an artificially increased variability due to a trend within the analyzed bin of data points. The choice of the detrending method can have an impact on the distribution of the detrended data. Here, we applied a 2nd order polynomial regression model for detrending. The robustness of risk assessments based on climate-crop model ensembles should be tested with regard to detrending in future studies. Specifically, results could be compared for detrending with polynomial and locally weighted regression, centered moving average, and spline smoothing models, that have shown high skill for detrending historical maize yield data in the USA (Lu et al., 2017).

The historical reference period was set to entail all simulated years with global mean temperature (GMT) between 0°C and 1°C above pre-industrial levels. This choice is based on the applied context of this study, focusing on future change in risk compared to historical levels. ΔGMT is currently starting to exceed ΔGMT =1°C, that is, the upper limit of this bin. For studies focusing more on climate change attribution, however, this reference bin is not ideal, because it covers a considerable degree of anthropogenic climate change signal already. For a climate change attribution study, a historical reference period could be set as ΔGMT ranging from 0°C ±0.5°C instead.

While the use of a historical percentile as threshold is common practice in climate impact and attribution studies, the relative threshold is less established. Here, the relative threshold was set to 10% below the mean because this value is straight-forward to communicate and interpret for a wide audience. The choice of 10 % was also based on Tigchelaar et al. (2018). Following up on the experience with applying a relative threshold here, further research could explore alternative statistics and metrics to assess the aspect of crop production risk that is variability-induced and independent of the mean trend. For example, future studies could compare and evaluate current and future risk based on internal variability as measured by the variance, coefficient of variation, skewness, or apply relative thresholds such as mean minus the standard deviation. Reciprocally, the historical threshold could be set to mean-10% instead of the 2.5th percentile, to increase consistency between the two probability metrics. Like this, the robustness of results to the choice of thresholds can be analyzed and risk metrics identified that are both statistically robust and meaningful to a broader audience.

Future rounds of model intercomparison projects (e.g., facilitated by ISIMIP) have the potential to improve the robustness of crop production risk assessments. Improvements can be achieved by further development of models and parameterizations, as well as broadened experimental design with varying management options to better inform adaptation efforts. The implementation in CLIMADA can be further used for adaptation options appraisal (Bresch and Aznar-Siguan, 2021). For example, the setup can be used to explore the potential of varying crop types, land-use patterns, and irrigation ratios for climate change adaptation. The use of normalized crop yields as hazard component allows to circumvent biases arising from potential offsets in absolute yields between the individual GGCMs. Another advantage of this modular design is that the hazard can easily be combined with alternative crop production exposure data for country- or even farm-level specific case studies and risk assessments. Like this, the flexibility of the implementation allows for a broad range of applications.

Moving beyond the narrow definition of agricultural risk as the 'potential for reduced food production' (Challinor et al., 2018), agricultural risk assessments can further explore socio-economic impacts of reduced crop production, i.e., on food supply (in-)stability (Hurlbert et al., 2019), income, political stability, or global and local markets. In order to build a risk assessment with a socio-economic dimension, the quantitative estimates of crop production risk per country could be linked with socio-economic vulnerability indicators, such as the governance strength indicator of adaptive capacity developed by Andrijevic et al. (2020). This would allow for an update and quantitative amendment of recent assessments of climate-related risks to the agricultural system and food security such as the study by Meza et al. (2019). Furthermore, the resulting crop production values and risk metrics can be used for downstream risk assessments, for example as input for trade network analysis, assessing country-level food reserves relative to domestic use (stocks-to-use ratio) as in Jägermeyr et al. (2020). Alternatively, vulnerability can be added directly to the risk assessment in the form of impact functions relating variations of normalized crop yield to impact measures such as people affected, direct economic damage, supply chains, or price shocks. For example, based on reports of economic costs of crop failure, impact functions can be calibrated to simulate the relationship of normalized crop yields to economic damages. It should be noted that with an assessment of 'downstream risk' associated to crop production losses, the definitions within the risk framework are shifted, with regard to what hazard, exposure, and vulnerability are. The crop production risk assessed here would rather have the status of a hazard, when combined with socio-economic vulnerability factors or trade analysis. In such a framework, exposure would not be defined as the baseline local crop production but rather people, companies, or states directly or indirectly affected by food supply instability.

Next to the multi-crop risk assessment presented here, future research could further explore crop production risk due to of compound extreme events. Soil moisture and heat memory implemented in state-of-the-art GGCMs allows for assessing the probability of repeated low production in consecutive years. Also, the setup can be further exploited to calculate the probabilities of concurrent crop failures in multiple breadbaskets under historical and future climatic conditions, building on recent studies by Gaupp et al. (2019, 2020), Lange et al. (2020), Vogel et al. (2019), and Zscheischler (2018, 2020), among others. For a better understanding of the drivers of crop production risk, simulated years of low production can be attributed to climatic extremes identified in the climate model output, for example droughts and heat waves, building on the methodology used by Jägermeyr and Frieler (2018) for historical events.

4.5 Conclusion

The combination of different risk metrics and consistency measures allows for a differentiated risk assessment on country level. This can be used to identify countries and regions with above- or below-average risk of crop production losses in a changing climate – both due to trends in the mean and the probability of extreme events relative to the mean. This study exploits a multi-crop-model ensemble to assess the climate-related risk to crop production for elevated levels of global mean temperature on a country level. While known caveats and uncertainties remain, the methodology allows for a differentiated risk assessment per country based on current state-of-art GCMs and GGCMs, producing quantitative estimates of the production value that is at risk. In the country-level risk assessment presented here, we used two complementary risk metrics to highlight countries and crop types for which models agree on future decreases or increases in the probability of low crop production extremes. Like this, we were able to identify hotspots of potential future crop failure risk based on state-of-the-art climate-crop simulations without ignoring the uncertainties entailed.

The results of this risk assessment are future projections of the risk climate change poses to today's levels of crop production. This assessment might inform adaptation strategies on a global level or serve as a starting point for more detailed adaptation studies both on a global and a country level. Across the globe, maize production is threatened by climate change already at global mean temperatures 2°C above preindustrial levels, as to be expected within the coming few decades. In many countries, projected increases in absolute crop yields for rice, soybean, and wheat are contrasted by increases in variability-induced risk. At 4°C global warming, partial yield increases for 2°C are diminished. Increased risk is projected for multiple main producing countries across crop types, especially for countries with low historical variability-induced risk. While some countries are projected to experience increasing crop yields in a warming climate, the projected changes in crop production risk could lead to both local food crisis and adverse distributional effects. Therefore, the results highlight the urgency to mitigate climate change, limiting global warming to levels of 2°C or below. For countries with an increase in crop production risk projected, adaptation of the agricultural sector to climate change should be addressed in a prioritized manner. Overall, our results highlight substantially increased risk to crop production under warming projected for the mid to end 21st century and the need to assess crop yield projections more differentiated in future climate risk assessments.

5. Discussion and outlook

5.1 Central findings

All three studies presented here share a common aim, to work towards globally consistent, yet regionally differentiated modeling of climate-related economic impacts and risks, both under current and future climatic conditions. Therefore, I will first briefly recap and discuss central findings of each chapter before moving to a discussion of generalizable insights beyond the scope of the single studies.

The central finding in Chapter Two (1st paper) is that socioeconomic indicators such as GDP or total asset values can be realistically disaggregated from country-level aggregates proportionally to a multiplicative combination of gridded nightlight intensity data (Lit) with gridded population density data (Pop). Evaluation of the LitPop method for 14 countries showed that the approach has skill in disaggregating country-level GDP to state or district level. A visual assessment of derived high-resolution asset value maps of metropolitan areas further suggests that the combination of Lit and Pop can mitigate known artifacts in nightlight products, such as blooming and saturation, given a sufficient resolution of population data. We concluded that combining Lit and Pop improves the subnational spatial disaggregation skill for GDP and correlated macroeconomic indicators compared to using only one of the two data types. The comparison of different exponents m and n in $Lit^m \cdot Pop^n$ generally returned the highest skill for m=1, n=1 ($Lit^1 \cdot Pop^1$). Providing both a high-resolution (30 arcsec) global asset exposure dataset and the underlying methodology open-source and documented has the potential to lower the entry-level for global-scale assessments of direct economic damage due to natural hazards. Still, the relatively straight-forward methodology comes with caveats and uncertainties. These include limitations of the evaluation due to missing data on sub-national levels, and the omittance of asset classes and critical infrastructure not correlated to population density and luminosity. Uncertainties and limitations are further summarized in Section 5.3 below.

The direct comparison of the simulated impact of several hundred tropical cyclone (TC) events with reported direct economic damage records around the globe in Chapter Three (2nd paper) resulted in a calibrated set of TC impact functions for nine world regions. The investigation revealed that a global impact function did not represent TC damage potential adequately around the globe. Before calibration, simulations overestimated TC damage potential considerably in the North West Pacific region, strongest for Taiwan, Hong Kong, Japan, Macao, and South Korea. In contrast, damage potential was underestimated for Madagascar and Mozambique in the South Indian Ocean and most South Pacific countries. On a sub-regional level, a case study for the Philippines provides insight on further potential for improvement of the TC impact modeling setup. This includes the potential to differentiate on the hazard side, i.e., to account for storm surge and pluvial flooding explicitly and to differentiate between urban and rural exposure and vulnerabilities (see outlook in Section 5.5.2). In conclusion, we postulate large potentials for further reducing the considerable uncertainties associated with the calibration of TC impact functions. Most prominently, we suggest differentiating rural and urban exposure types, simulating sub-perils such as storm surge and torrential rain explicitly, and improving and harmonizing quality standards for archiving and documenting reported damage data.

Central findings presented in Chapter Four (3rd paper) touch upon the potential and limitations of exploiting gridded global output from state-of-the-art climate-crop model ensembles for the assessment of 21st century crop production risk. While model uncertainties are considerable, with often contradictory results from individual crop models, we identified combinations of countries and crop types with high model agreement regarding future change in crop production risk. By juxtaposing both a fixed historical threshold and a relative threshold for the calculation of crop production loss probabilities, we highlighted cases where the more established historical threshold could not detect a signal of variability-induced increase in risk as detected by the relative threshold. For example, we found such a constellation for future soybean production in the USA and wheat production in China. Methodologically, we concluded that using a relative threshold adds value to the risk assessment. However, we propose further research and exploration of alternative measures of variability-induced crop production risk. A deepening reflection on the complementary risk metrics in relation to uncertainty can be found in Section 5.3.

Chapters Two to Four do not only contribute to the development of individual components of a global risk modeling framework, but also towards a better understanding of opportunities and challenges related to the combination of heterogeneous input data for global risk assessments, with the ambition to model risk globally consistent yet regionally differentiated. Furthermore, we discuss practical implications in the context of their immediate application and beyond in Section 5.4. One central aggregated finding is that the multitude of data and methodologies available today make it possible to spatially-explicitly represent hazard, exposure, and vulnerability – and thus representing relevant risk components at a global scale. The modularity of the risk framework also allows for a flexible representation of weather- and climate-related risks, acute and chronic, event-focused and annually aggregated, direct and indirect, including pre-conditioning and attribution – as further discussed below, based on the comparison of model configurations in Section 5.2 and the outlook for compound crop risk assessments in Section 5.5.3. This provides the basis for multi-hazard and multi-sectoral risk modeling on a global scale, moving far beyond the scope of traditional integrated assessment models. The increase in complexity about what is represented in spatially explicit risk model configurations comes however at cost, as multi-step modeling chains entail cascading uncertainties. Additional auxiliary data and local calibration can improve the representation of either single events or regional particularities in exposure and vulnerability. However, auxiliary input data inflate the complexity of the modeling setup even further, and are often not consistently available on a global scale. A deepening discussion of the uncertainties, how they are addressed in this thesis, and derived findings can be found in Section 5.3 below. The practical implications of this thesis constitute a relevant outcome of the research and development project and are discussed in Section 5.4 followed by outlook and future research in Section 5.5.

5.2 Comparison of risk model configurations

A comparison of the impact modeling setup presented in the three papers (Chapters 2-4) serves well as a starting point to reflect upon the broad range of opportunities a modular risk assessment framework as provided by CLIMADA offers for modeling weather and climate-related risks. Chapters Two and Three contribute to a globally consistent model for the impacts and risks posed by TCs (and comparable hazard types) on the built environment. In Chapter Four, we integrated climate-crop model output to assess climate impacts on country-level crop production risk for maize, rice, soybean, and wheat. The comparison of TC and crop production risk modeling can illustrate two very different manifestations of what we attempt to represent with climate-related physical risk models. By contrasting these two implementations from different perspectives, the wide range of how risk components can be defined for physical risk modeling within the framework of hazard, exposure, and vulnerability can be probed and discussed. The respective model configurations are discussed in detail in the corresponding chapters and Section 1.5. Here, we focus on comparing different aspects of these configurations.

The TC impact model is a single-hazard model, while crop production risk modeling requires a more complex representation of hazard and vulnerability motivated from the perspective of a particular economic sector exposed to climate-related risk. In Chapter Three, the TC hazard set was used to simulate direct economic damage in the form of impact to the built environment. The same hazard set could just as well be applied to model damages to human lives and livelihoods, to forests, power production – and also agricultural production. In contrast, the fractional crop yield used as hazard set in Chapter Four is tied to the agricultural sector, representing crop yield responses to climatic conditions. This implies several fundamental deviations of the crop production risk modeling setup compared to the implementation for TCs.

First of all, there is a conceptual difference between the two model configurations regarding the vulnerability component. For TC, vulnerability is represented by impact functions relating wind speed to damage. For crop production, the vulnerability of crop yields to climate variables is represented in a more complex way by the process-based crop models. In this configuration, an additional modulation via an impact function in CLIMADA would only make sense for the assessment of indirect impacts, not for simulating the direct response in crop production to climate variations (see outlook Section 5.5.3 for further elaboration). The second major difference stems from the definition of 'events' in the two different model configurations. The TC hazard consists of a set of clearly defined events, each representing a specific natural phenomenon: the cyclone's windspeed footprint, with a certain extent in space in time. Several TC events can occur in the same year and even affect the same location. Compound effects of consecutive TCs affecting the same area are not implemented in the current setup but could be accounted for by adjustments to exposure and impact functions after a TC hit, e.g., via post-processing of the impact set. On the contrary, normalized crop yield represents the compound modeled response of crop yields to various climatic conditions, including droughts and heat waves occurring within a given year, that is, all climatic conditions provided by the driving climate model output and considered in the process-based crop models. Memory effects in crop models also allow a partial representation of pre-conditioned events as defined by Zscheischler et al. (2020). The representation of compound events also hinges on proper representation in the driving climate simulations. A recent study analyses the representation skill of bivariate compound events in state-of-the-art climate models, specifically "the co-occurrence of heavy rain and strong wind, and heat waves and meteorological drought" (Ridder et al., 2021). The authors conclude that "[…] some CMIP6 models can be used to examine compound events, particularly over North America, Europe, and Eurasia" (Ridder et al., 2021), but still with large potential for improvement. It should be noted that the aggregated crop yield response is not attributed to the specific climatic drivers in Chapter Four. Each 'event' of normalized crop yield represents one year's climate-related deviation of the productive potential from a temporal mean, analyzed spatially explicitly, that is, for each grid cell individually. For this reason, this model configuration needs a definition of which event is considered disastrous under what local (grid cell or country-aggregate) conditions. This was achieved in Chapter Four by aggregating the modeled yearly absolute crop production per country and identifying years with production values below a given threshold. Another possibility would be a step or gradient in the impact function, however requiring further justification for choosing a threshold per grid cell. Another perspective on the different approaches to 'events' in the two implementations can be gained using the lenses of acute and chronic risk introduced in Section 1.4.1. While TC events fall under the category of acute physical risk (see Section 1.4.1), crop production risk as assessed here represents a combination of chronic and acute risk. The creeping character of changing climatic conditions over time can lead to chronic risk, while the variability-driven risk due to specific conditions in a simulated year can be considered an acute risk. However, the distinction of acute and chronic risk is blurred in the case of any long-term change in variability, putting the usefulness of these definitions in a scientific context to question. In conclusion, this comparison illustrates the flexibility of the risk framework applied here and highlights implications for experimental setup and the evaluation and analysis of respective results when defining hazard, exposure, and vulnerability with a certain degree of creativity.

5.3 Uncertainties

Climate risk modeling entails cascading uncertainties all along the modeling chain. The hazard component alone is constructed from input data that is either based on processed measurements (Zumwald et al., 2020), survey data and/or output from models (e.g., climate models, hydrological models, crop models, TC wind field models). The same holds for the exposure (e.g., remote sensing data and country-level asset value estimates) and vulnerability components (e.g., the shape and scaling of impact functions). The cascade of uncertainties can be illustrated by the example of the calibration of TC impact functions presented in Chapter Three. The calibration builds on TC wind footprints as hazard component and an estimate of gridded asset values as exposure component. Both input data sets are resulting from modeling endeavors themselves, with their own uncertainties. For calibration of the impact function, hazard and exposure are then combined with further – often highly uncertain – data, such as reported estimates of direct economic damage per event. Sensitivity analysis is a common approach to assess model uncertainties. For sensitivity analyses, input data and model parameters are sampled from a (plausible) range or distribution (Saltelli, 2002). The many steps involved in climate risk modeling make systematic uncertainty assessments rather extensive and require many assumptions with regard to parameters varied and their plausible ranges that need to be constrained in order to keep the assessment computationally tractable. Therefore, providing a rigorous sensitivity analysis for risk assessments building on multiple modeling chains is often not feasible. However, well designed uncertainty analyses focusing on relevant drivers are technically possible and beneficial to model developers and decision-makers interpreting model results. For crop yield simulations, a study of uncertainties of state-of-the-art climate-crop ensembles was published by Müller et al. (2021). The authors explored uncertainties in climate-crop ensembles such as the GC6 ensemble analyzed in Chapter Four, driven by climate models from both CMIP5 and CMIP6. The authors calculated the share of variance explained by the spread of both climate and crop models. Thereby, they differentiated by crop types and modeled year, as model uncertainty in transient climate simulations is not stationary over time. This kind of uncertainty analysis is pivotal for the experimental design and the discussion and interpretation of results. The study presented in Chapter Four benefited greatly from their findings, guiding methodological decisions such as the detrending and binning of years by global mean temperature to mitigate uncertainties due to differences in the climate sensitivity of climate models.

The focus of neither of the three studies presented in this thesis was on the systematic analysis of uncertainty. In all three studies, the main objective was to contribute a science-based component to an end-to-end climate risk assessment while making key uncertainties visible and providing guidance both for present usage and future, more systematic uncertainty assessments. The guiding principle was to provide users with results and methods that can be put into practical use in a straight-forward fashion – also outside the academic discourse – while informing them of uncertainties and most relevant assumptions entailed. This purpose is served in multiple ways, however with some common features that have proven both valuable and feasible in the context of the academic papers and the applied project. As a basis, uncertainties, limitations, and assumptions in the input data were discussed based on scientific literature. Based on this discussion, choices with regard to input data and methods were made, considering both fitness for purpose as well as availability and accessibility. In all three studies, uncertainties with regard to methodological choices are made visible by comparing results for several, preferably complementary choices. In the first two studies, the discussion of uncertainties and comparison of complementary metrics is complemented with regional case studies. In Chapter Two, limitations of the LitPop method are discussed along an example of the metropolitan area around Mexico City and a quantitative evaluation of skill metrics for 14 countries. In Chapter Three, possible reasons for large deviations in event damage ratios (EDRs) are discussed for the Philippines, based on studies with a regional focus, and analyses for single TC events. Both case study regions were chosen due to low robustness in results as diagnosed by a large spread between the complementary metrics discussed above.

The LitPop methodology presented in Chapter Two disaggregates country-level asset values to obtain a gridded layer of asset exposure estimates. The methodology is evaluated by comparing complementary skill metrics for a plausible range of exponents weighting the two input data sets (nightlight intensity and population count). Based on the quantitative evaluation, the local case study, and literature, we were able to identify the following drivers of uncertainty in the LitPop methodology. (1) The choice of the best estimate of national total asset values comes with uncertainty, scaling the resulting exposure values within each country in a linear fashion. (2) Due to limited data availability, the evaluation of disaggregation skill was limited to 14 countries and of these 14 countries, only two are lower-middle income countries and none are low income countries, biasing the evaluation to countries that are economically better off. (3) The level of detail of the gridded population data used as input varies between countries and the data is usually less detailed for low income countries that were also not evaluated, see (2). (4) For evaluation, disaggregation skill was assessed for gross domestic product (GDP) instead of asset value, due to lack of sub-national asset value data. While GDP and asset values can be expected to be strongly correlated within countries, the spatial distribution of the two indicators is not necessarily identical, potentially introducing biases to the evaluation. (5) While the evaluation and case study suggest that the methodology has skill both for urban and rural area, the performance on a local level was not validated.

For the calibration of regional TC impact functions (Chapter Three), two complementary cost functions based on the ratio of simulated to reported event damage were assessed. A comprehensive explanation is given for each cost function: The total damage ratio (TDR), on the one hand, integrates damage over time before the ratio is calculated, making the result more sensitive to outliers with large total damage. The root-mean squared fraction (RMSF), on the other hand, weights the relative ratio of each event equally, irrespective of the total damage caused by each event. The resulting impact functions based on minimizing TDR are more optimistic (or 'conservative'), simulating lower damage values than those calibrated by minimizing RMSF. Based on the two cost functions and resulting sets of impact functions, users in an applied context are thus well informed to make a choice tailored to the scope and aim of their particular application. Advanced users can build a robustness analysis on the alternative impact functions, or even based on the spread of individually fitted impact functions as provided in the study. The difference between results for the two complementary cost functions can be taken as an indicator of the robustness of the calibration in each region. Relevant drivers of uncertainties in the calibration of regional TC impact functions as identified in Chapter Three are: (1) Reported damage data comes with lack of transparency with regard to inconsistencies and potential biases that are not quantified. Inconsistencies in reported damage data can potentially be explained by the wide range of capacities, scope, and conflicting interests of data providers (governments, insurance companies, research institutes, NGOs, etc.) as well as the damage type represented (direct, indirect, insured, etc.). (2) The modeling setup uses maximum wind speed as hazard intensity, lacking an explicit representation of TC-related sub-hazards with high damage potential such as storm surge and torrential rain. (3) The exposure layer comes with the uncertainties summarized above, especially a potential under- or over-estimation of total asset values can bias the damage estimates and resulting impact functions. (4) Certain sectors exposed to TC impacts are not represented in the exposure layer, most notably agricultural production. (5) The TC tracks used as basis for the TC hazard are from different data providers with known inconsistencies in reporting standards. (6) The wind field model by Holland (2008) does not represent variations in topography and surface roughness explicitly. Furthermore, the wind field model was developed for hurricanes in the North Atlantic and might not be fully adequate for other ocean basins. All mentioned drivers of uncertainty in the TC impact function calibration are – for obvious reasons – also drivers of uncertainty in TC risk assessments.

In the assessment of crop production risk (Chapter Four), we do not analyze to which degree the projected changes in mean production and variability are represented adequately by the single crop models. But in the discussion of uncertainties, the study draws on comprehensive model uncertainty analyses such as those by Müller et al. (2017, 2021). Methodologically, the impact of crop model uncertainty on the resulting risk metrics is addressed by assessing the risk for each individual crop model. After that, the risk metrics per crop model are combined, communicating both the multi-model median as well as an indicator of model agreement. In this study, again, two complementary metrics are calculated. The probability (P) and probability ratio (PR) of years with extremely low crop production are computed based on two complementary thresholds. The historical threshold is fixed at the 2.5th percentile of yearly crop production in the subset of years driven with climate model output with global warming at historical levels (0.5°C ± 0.5°C above pre-industrial levels). The relative threshold is independent of historical production levels, set to 10 % below the mean production at a given level of global warming. Like this, the historical threshold puts an emphasis on changes in total production numbers while the relative threshold is used to identify changes in variability-induced changes in the probability of extreme events. Again, users of the study's result can either chose between the two metrics based on their priorities or combine them to obtain a differentiated profile of crop production risk as projected by the climate-crop model ensemble, that is an ensemble of global gridded crop models driven with climate data from a selection of global climate models. With this approach and a transparent discussion of known uncertainties, the study attempts to make best use of the available ensemble of state-of-the-art climate-crop simulations without concealing the considerable cascading uncertainties of the climate-crop-risk modeling chain. Major sources of uncertainty relevant for the crop production risk assessment setup and results presented in Chapter Four are (1) climate model uncertainties with regard to the representation of global and regional extremes, compound events, and climate variability under both historical and unpreceded levels of global warming and (2) crop model uncertainties, especially with regard to the parameterization and process-representation of climatic extremes and CO_2 effects (e.g., fertilization) with consequences on the robustness of projections of both mean yields and inter-annual variability on a global and regional level. (3) Imbalances and outliers in the climate-crop simulation ensemble have the potential to distort risk metrics and results. (4) The choice of risk metric, threshold value, and detrending method can have consequences on the outcome of the assessment of variability-induced crop production risk. The robustness of the results with regard to these choices has not yet been analyzed systematically. (5) The study rests on multiple assumptions with regard to agricultural management and technologies, including land-use, irrigation ratios, and crop types and varieties. The choice to keep such management factors constant at current levels is nonetheless a choice and the sensitivity of results to the underlying assumptions stands yet to be analyzed.

In conclusion, the general approach towards the cascading uncertainties entailed in any of the presented modeling chains is a pragmatic one. In all three main chapters, we attempted to discuss uncertainties based on literature and explorative case studies. Consequently, the studies were designed to address the most relevant known uncertainties and to communicate remaining uncertainties, both quantifiable and non-quantifiable ones, in a rather descriptive manner. While this approach does not replace more rigorous uncertainty analyses, I am convinced that it can provide guidance for users of the methods and results presented, model developers, as well as researchers conducting uncertainty analyses in the future. This guidance includes pinpointing relevant sources of uncertainty and provides a rationale for plausible parameter ranges and choices.

5.4 Practical implications

5.4.1 Use of results in an applied context

The spatially explicit and globally consistent modeling of climate risk offers potential to expand the disclosure of climate related physical risk as promoted by the TCFD (Bloomberg et al., 2017). This thesis contributes science-based open-source risk modeling tools, as well as discussions of their skills and limitations with relevance for this wider applied context. An overview of how the outcomes from this thesis and the whole PhD project are put into use in the particular context of the implementing partner is provided in Section 1.3. Here, practical implications from our findings are discussed beyond the scope of the joint research and development project. For this discussion, I am guided by the typology of users of climate services postulated by

Skelton et al. (2019). In their study, the authors classify users of the Swiss climate scenarios CH2011 into the three groups 'observers', 'sailors', and 'divers'. Here, I am adapting this typology to the context of the assessment and modeling of climate-related risk (Fig. 20), to organize the discussion of the practical implications of this thesis.

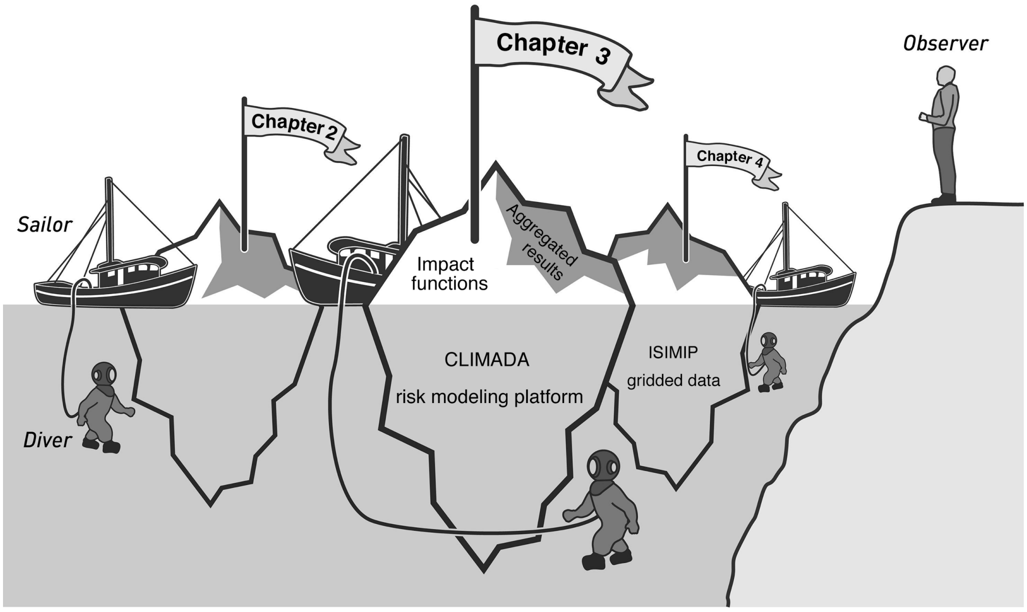

Figure 20: Conceptual illustration of Skelton et al. (2019)'s typology of climate scenario use, drawing on the metaphor of the iceberg, and adapted for the context of the assessment and modeling of climate-related risk and the studies presented in this thesis. Divers are interested in using the bulk of methodology and data accessible only to those with the skills, such as risk modeling platform CLIMADA and gridded simulated climate impact data from the ISIMIP project. Sailors make use of key results visible from the surface (and are supported by the raw data), such as asset exposure data from Chapter Two, calibrated impact functions from Chapter Three, or return periods of crop production loss from Chapter Four. Observers are interested in aggregated results (i.e., the iceberg), such as identifying country-specific information and interregional differences in TC vulnerability or crop production risk. Figure and caption adapted from Skelton et al. (2019, p.4), original illustration: S. Bösch, ETH Zurich.

All three studies presented in this thesis aim at applications geared towards the assessment and modeling of global-scale climate-related impacts and risks. To this end, the methodology and results presented in this thesis are useful in a straightforward manner across the user types illustrated in Figure 20. Observers aim to learn something relevant from the studies without getting into the water themselves, i.e. without engaging in data analysis or applying any methodology. They primarily benefit from aggregated quantitative results such as current and future crop production risk profiles per country (Chapter Four) or inter-regional vulnerability differences in damage inflicted by tropical cyclones (Chapter Three). These aggregate results can help to identify hotspots of tropical cyclone vulnerability or crop production risk in need of adaptation efforts at country scale. Sailors might make use of the global data set of gridded asset value estimates disaggregated with the LitPop-methodology (Chapter Two) that can easily be downloaded and integrated as an exposure layer for all kinds of spatially explicit risk assessments across platforms.

Both sailors and divers might also adapt the calibrated TC impact functions from and risk metrics for crop production risk in their own risk assessments. I consider users as divers if they use a full risk modeling platform such as CLIMADA or want to make use of gridded global climate-impact model ensemble output data from ISIMIP, such as crop yields or surface water discharge. Divers might make use of the modules and methodologies developed in this thesis and made available in the CLIMADA repository (see Section 'Code and data availability'). For example, CLIMADA's TC hazard module can be combined with the LitPop-based asset exposure data and the calibrated TC impact functions for both global and regional impact assessments, down to a resolution of a few kilometers (yet still globally consistent). Expert risk modelers can also explore the robustness of their probabilistic risk modeling setup by testing the range of parameter choices evaluated for the LitPop methodology (exponents m and n, see Chapter Two) and alternative impact functions based on the complementary cost functions in Chapter Three. Users who want to dive into the extensive output data from ISIMIP as a basis for the assessment of future climate-related risk can get guidance from the approach followed in Chapter Four to deal with a large set of climate-crop model simulations and cascading uncertainties. Again, a code basis is provided along with the study that can be adapted for similar assessments based on output from future rounds of ISIMIP, and also integrated into modeling chains for the assessment of downstream sectoral risk.

In conclusion, as one practical implication of this thesis, global TC risk modeling efforts should always consider inter-regional differences in TC vulnerability even on an aggregated level, and should not apply one single impact function globally. For assessments of future climate-related risks, such as crop production risk, this thesis can provide guidance for the choice of risk metrics and the post-processing of the output from global-scale climate-impact model ensembles. For applications like risk assessments on sub-regional scale, users should be aware that global consistency might come at cost of local accuracy, as discussed in Chapters 2 and 3. The exposure data, impact functions, and crop production risk estimates presented here are most likely inadequate to be used locally, especially at resolutions higher than few kilometers. However, they can be used for a first assessment of the general situation, e.g., to identify potential hotspots and to estimate the order of magnitude of impacts before assembling local data and knowledge for a more adequate local-scale risk assessment.

5.4.2 Joint research and development for climate risk modeling

As the urgency for action on climate change increases across sectors, more and more researchers as well as private sector actors engage in global-scale climate risk modeling. However, such efforts have proven to be resource intensive in terms of research, the development of tools and code, and computational costs. Purely academic studies are often not perceived as useful for direct implementation by practitioners, possibly due to the different focus of academic research questions, and sometimes also simply because data and methods are often not documented adequately nor licensed for use outside academia. On the other hand, the costliness of climate risk modeling puts it beyond the scope of many public authorities and smaller to mid-sized organizations and businesses, for example in the financial and insurance sector, who are nonetheless affected by climate risk. To address this gap between science and application, more and more resources in the form of code and data are and have been made available for climate risk assessments in recent years, both by research groups, scientific collaborative projects like ISIMIP and CLIMADA, but also by industry-led pre-competitive research and development projects such as the Oasis Loss Modelling Platform (Oasis LMF, online). This makes pre-competitive collaborations publishing results and methods, like the one presented here, pivotal for the joint cross-sectoral progress in addressing the multiple challenges posed by climate change. While the implementing partner benefits from the collaboration by shaping the focus and methodology of the research and being the first to make use of outcomes, the scientific community and further organizations benefit from open-access and open-source publication of results and methods that do not involve intellectual property of the implementing partner. With the collaboration accompanying this thesis, I made the experience that climate risk modeling efforts can benefit from joint research and development that moves collaboration beyond the level of mere consultancy or one-way knowledge transfer. One challenge in joint research and development are intellectual property and licensing aspects of both input and output data as well as co-developed tools. For this, it is crucial to generate scientific output intended for applied use available under a permitting license. Many projects have realized this requirement for their output to be impactful beyond academia, including CLIMADA which is published under the GNU General Public License[1] version 3 (Free Software Foundation, Inc., 2007), and ISIMIP's success in convincing most contributors to publish their data under the Creative Commons[2] license CC BY 4.0 putting no constraints on commercial use (Creative Commons, online). It is sometimes debated whether research funded with public money should be made available for commercial use just to be picked up by private sector actors and hidden behind pay-walls. While I don't want to rule out that there can be abuse, my experience is rather that added value by commercial utilization has the potential to act as a multiplier of the societal impact of scientific outcomes. What is more,

[1] https://www.gnu.org/licenses/gpl-3.0.en.html (last accessed February 19, 2021)

[2] https://creativecommons.org/licenses/by/4.0/ (last accessed March 1, 2021)

research groups can control the dissemination of their science by publishing research methods and results with elaborate licensing and a sufficient level of documentation and support, and by engaging in joint research and development projects. Still, joint research and development receiving public funding should always make a contribution to the public domain. At the same time, parts of the input to an applied risk modeling setup are likely to involve trade secrets and intellectual property of the implementing partner. The modular risk framework implemented in CLIMADA, like in most risk modeling platforms, allows for a clear definition of the individual risk components, such as hazard, exposure, impact functions, and also pre- and postprocessing as well as clear interfaces between single modules. The ambit of both partners can be defined along the boundaries of these modules, clarifying both competence and ownership between research and implementing partner. This can be illustrated by example of the TC impact model implemented alongside this thesis (see Section 1.5.1). Here, the hazard data is based on publicly available data and a scientifically published wind field model. Based on scientific literature, the initiation of the probabilistic historical and future hazards set was implemented in the open-source and open-access CLIMADA repository. The same is true for the calibrated impact functions presented in Chapter Three. These two parts of the TC impact model are thus published in the public domain and contribute to extending both academic debate and applied risk assessments, being available for use and further development beyond the scope of this project. The main competitive advantage of the implementing partner comes from combining these scientific hazard and vulnerability modules with their own exposure layer, i.e., their company asset location database. Being involved in the research design of this thesis, the results are directly applicable by the implementing partner, because the studies' outcomes directly meet their requirements for a globally consistent yet spatially explicit risk assessment. Implementing partners in research and development projects also benefit from the credibility added to their products as far as crucial ingredients are not only science-based but also embedded and published in the academic debate. For this to be possible, the research partner requires a high degree of freedom, but also time allocated, for conducting their research with all scrutiny required and accommodating the full peer-review process for publication. Implementing partners can move even further, allowing their research partners to use data sets considered to be trade secret on an aggregated or anonymized level, further increasing both the academic leverage and the transparency of and trust in their work. Framed carefully and complaisantly, pre-competitive joint research and development can lead to multiple co-benefits as well as transparency towards the wider public and particularly clients, as opposed to black box solutions developed completely in-house. Given the resource intensity and high degree of uncertainty entailed in climate risk modeling, customers should in fact be suspicious of claims for products to be 'science-based' when the underlying climate risk modeling is not transparent nor embedded in collaborative research and development with academia or pre-competitive platforms, and research outcomes shall be made available to the public with no strings attached.

5.5 Future research and outlook

5.5.1 Global asset exposure

We developed the nightlight-population (LitPop) method to provide a globally consistent asset value exposure layer for modeling natural hazard impact on assets such as the built environment and infrastructure. For the project's scope and further unrestricted use by developers and stakeholders working with the open-source and -access platform CLIMADA, one of the main requirements was that all input data is open-access and licensed for both academic and commercial use. Furthermore, the aim was not to produce a black box but rather a transparent, easily understandable, and reproducible methodology to ensure a low entry threshold for a wide variety of users. The main advantage of the LitPop method is that it can be updated relatively easily as new versions of gridded population data or nightlight intensity data become available. One major disadvantage are a lack of local precision and the inability to project the distribution of asset values to the future. Future projections of population distribution exist for a variety of shared socioeconomic pathways (SSPs) (Jones and O'Neill, 2016; Leyk et al., 2019), including efforts to incorporate climate change impacts (Rigaud et al., 2018). Annual global population data at 0.5° and 2.5' resolutions for the years 2006-2100 for a variety of SSPs and based on the population projections described in Jones and O'Neill (2016) are provided by ISIMIP as secondary input data (ISIMIP, online, https://www.isimip.org/gettingstarted/input-data-bias-correction/details/62/, last accessed 15 February 2021). The LitPop method can be improved and expanded based on such datasets, possibly replacing the GPW population dataset used in Chapter Two, which is flawed with varying spatial detail between countries. However, this could require an adaptation of the disaggregation method for future projections because nightlight intensity as used by LitPop is an intrinsically empirical variable and not available for the future. This also holds for many other auxiliary data sets such as street networks used in alternative approaches (e.g., Geiger, 2018; Murakami and Yamagata, 2019). In 2019, the Global Human Settlement Layer Data Package 2019 (GHS P2019) became available (Florczyk et al., 2019), providing global gridded data of built-up area and settlements from 1975 till 2015, under a fully open and free data and methods policy. Such data sources could be applied to substitute or refine LitPop-based exposure, especially for applications requiring a high degree of local representation. In the same direction, future research should also be aimed at evaluating the skill of the LitPop method with varying parameters, both locally and regionally, against ground-truth data, such as census data or detailed building registers, or alternative data sources such as GHS P2019. For risk modeling studies using LitPop-exposure attempting a systematic analysis of uncertainties, the following parameters and input variables could be varied within reasonable ranges with reference to Chapter Two: spatial resolution, exponents m and n in the disaggregation factor $Lit^m \cdot Pop^n$, total asset value per country, and source of nightlight and population data. Any such concerted effort towards a globally consistent projection of exposure, best including an occupational and sectorial split, would benefit many projects well beyond natural catastrophe risk assessment and climate change impact studies and hence well justify substantial resources to be put in this endeavor.

5.5.2 Tropical cyclone impact modeling

The field of TC hazard and impact modeling is progressing quickly these days and future research should keep up with developments in the private sector, especially regarding the representation of hazard intensity and the probabilistic and process-based modeling of historical and future TC events. There has been progress in improving wind field models (e.g., Done et al., 2020) and creating probabilistic event sets with statistical resampling techniques (Bloemendaal et al., 2020). While the dynamical downscaling of TC events from climate model output remains a challenge, there has been considerable progress over the past two decades in modeling current and future TC tracks and characteristics (e.g., Bhatia et al., 2018; Bloemendaal et al., 2020; Emanuel et al., 2006; Emanuel, 2013; Knutson et al., 2015; Lee et al., 2018, 2020; Roberts et al., 2020b, 2020a; Walsh et al., 2015, 2016). Relevant recent observed changes in TC characteristics are summarized as follows: "Some studies have suggested that changes in tropical cyclones are potentially detectable in the present day (Knutson et al., 2019). Observed changes in intensity (Elsner et al., 2008; Kossin et al., 2013), including the migration [geographical shift] of the location of maximum intensity (Altman et al., 2018; Kossin et al., 2014; Sharmila and Walsh, 2018), have been documented, with possible links to frequency (Kang and Elsner, 2015). Evidence for reductions in propagation speeds since 1949 has been suggested (Kossin, 2018) and also questioned (Lanzante, 2019; Moon et al., 2019), while changes in precipitation associated with individual TCs have also been proposed (Emanuel, 2017; Risser and Wehner, 2017; Van Oldenborgh et al., 2017). However, disentangling natural variability from anthropogenic forcing remains challenging (Knutson et al., 2019)" (Roberts et al., 2020b).

For the future, a review paper by Knutson et al. (2020) identified the following projected responses of TC characteristics to anthropogenic warming: (1) higher storm inundation levels due to sea level rise, (2) increased TC precipitation rates, (3) increase in global average TC intensity, (4) increase in proportion and frequency of high intensity TCs (category 4-5), (5) poleward expansion of the latitude of maximum TC intensity in the western North Pacific, (6) decrease in global TC frequency, and (7) a slowdown in TC translational speed (Knutson et al., 2020). For the applied part of the thesis presented here, we based a future TC hazard set on projected changes in event frequency and intensity from Knutson et al. (2015), see also Section 1.5.1. Frequency and intensity are two relevant characteristics prone to be affected by climate change, and the change rates from Knutson et al. (2015) are within the ranges per ocean basin predicted in the IPCC's 5th Assessment Report (Christensen et al., 2013). However, there are other relevant projected changes in TC characteristics neglected by this approach, as listed above. For the representation of these complex responses in TC characteristics to climate change, future TC risk modeling efforts should aim at incorporating modeled future TC hazard sets (e.g., Emanuel et al., 2006; Emanuel, 2013; Lee et al., 2018, 2020) instead of manually adjusting parameters of historically recorded events. Attention should be paid to biases and discontinuities when historical hazard sets based on observed TC events are compared to modeled TC event sets.

A TC represents a weather system associated to a number of possible disastrous outcomes (associated with so-called sub-hazards), including strong winds, flooding due to storm surge (e.g., Bloemendaal et al., 2019) and torrential rain, as defined in the typology of compound weather and climate events by Zscheischler et al. (2020). With regard to further calibration and fitting of the vulnerability component, the representation of sub-hazards is one of the most decisive next steps, as it also affects impact functions, as discussed in Chapter Three: "For TC impact models, we echo the call for a more refined representation of TC hazards as a combination of wind-, surge-, and rain-induced flood and landslide events. When modeling multiple TC sub-perils, aggregated reported damage data are not sufficient to constrain impact function calibration. This might be resolved by consulting socio-economic- and engineering-type data and knowledge. Furthermore, our case study for the Philippines suggests that model accuracy could be improved by differentiating between urban and rural asset exposure, considering topography in wind speed estimations, and including exposed agricultural assets" (Eberenz et al., 2021b). When applying the calibrated impact functions presented here, it should always be kept in mind that they were fit to represent aggregated damage in an area, integrated across building types. For the development of improved building type specific impact functions, future research could start from the basis provided by previous TC impact modeling projects (Federal Emergency Management Authority [FEMA], 2010; Yamin et al., 2014), however keeping limitations for local applications in mind that arise irrespective of the chosen impact function when not adapted to local conditions. As for heuristics, one might refer to commercial buildings being about half, and industrial sites about a quarter as vulnerable as common residential ones (oral communication by David N. Bresch, supervisor of this thesis, summarizing more than thirty years of industry experience by him and fellow applied catastrophe modelers) and hence seek ways to evaluate this rule-of-thumb as often applied in industry catastrophe modeling with proper data analysis.

Further research and development could also focus on a better representation of compound events related to TC weather systems. On the one hand, this requires simulating an adequate impact for multiple TCs hitting the same area or asset in a short period of time. On the other hand, the interaction of several sub-hazards associated with the same TC could be represented explicitly; for example, wind-induced damage to roofs can amplify rain-induced losses, or agricultural land flooding with saltwater can render simultaneous wind-induced impacts to the same area irrelevant. The possibility to combine TC impacts with crop yield simulations to assess multi-hazard risk to agricultural production is further discussed in the following subsection.

5.5.3 Assessing climate-related risk to agricultural production

In Chapter Four, we developed a framework that integrates current and future generations of climate-crop model ensemble output in CLIMADA for use in a probabilistic risk assessment. Possible outlooks about the particular choice of detrending techniques and, more importantly, the selecting risk metrics and underlying thresholds are presented in the discussion section of Chapter Four. Most relevant for increasing the robustness of crop production risk assessments such as the one presented here, future studies should explore alternative risk metrics to assess variability-induced crop production risk, as measured by the probability P_r in the present study. The latest generation of GGCMs, as run for GC6 (ISIMIP3b) used in Chapter Four entails soil moisture and temperature memory effects (Jägermeyr et al., under review), enabling the model setup to represent pre-conditioned events to a certain extent. Probabilities of consecutive extreme years and spatial interconnectedness could be analyzed further in the present setup, thereby expanding the scope of crop risk modeling. Furthermore, extreme years identified in the crop yield hazard could be attributed to causal climate variables in the driving climate simulations.

Recent literature also offers new opportunities for crop risk modeling approaches based directly on climate model output for the hazard component. In 2020, Franke et al. presented the first version of spatially calibrated emulator functions representing crop yield responses to changes in CO_2, temperature, water, and nitrogen (Franke et al., 2020a). These crop yield response emulators are derived from an ensemble of climate-crop simulations comparable to the one used in Chapter

Four. Müller et al. (2021) used these emulators to explore uncertainties in global climate-crop projections driven by climate model simulations from both CMIP5 and CMIP6. The study benefited from the resource-effectiveness of using emulators instead of running process-based crop models for each ensemble member. Likewise, such emulators could be used as impact functions in risk assessments with hazard sets comprising temperature, water availability, and CO_2 concentrations based on climate model output. It should be noted however, that the emulators by Franke et al. (2020a) represent yield responses to yearly mean values of driving climate variables (e.g., temperature or water availability) and are thus not well suited to represent the response to extreme events at a higher temporal resolution relevant for risk to crop production due to extreme events.

Yearly crop production derived from climate-crop model simulations consider multiple hazard types. The crop models simulate crop yield response to climatic extremes in the driving climate data. The most relevant environmental drivers include temperature and water availability, but also fertilizing factors such as CO_2 concentration and nitrogen availability (Elliott et al., 2014; Franke et al., 2020a; Müller et al., 2017; Rosenzweig et al., 2014). While crop yields are simulated per year, the climate model output driving them comes at a higher temporal resolution. Simulating the interaction of multiple drivers on different time scales (short time events like heat waves, mean weather conditions during a growing season, long term CO_2 trends, etc.) is at the very core of what GGCMs are developed for.

Furthermore, there are weather and climate hazards putting crop production at risk that most crop models do not resolve, e.g., gusts of wind knocking down plants and flooding of agricultural area caused by TC surge, as well as pluvial and fluvial flooding, but also slow-onset factors such as soil depletion, erosion, and salination. The case study on TC impacts in the Philippines (Chapter Three) highlighted the relevance of TC impacts on the agricultural area for subnational TC risk assessments. The integration of a crop production exposure layer in CLIMADA is opening up the arena for the combination of crop yield simulations with the impacts not only from multiple drivers represented by crop models but also from other natural hazards. For a physically consistent multi-hazard and compound assessment of current and future weather and climate risks for crop production, simulations from the ISIMIP framework driven by the same climate model runs could be exploited. This can be illustrated by a though experiment. Consider the scenario of the following climate impact simulations to be available, all driven by the same selection of benchmarked and bias-corrected climate model runs as specified by the experimental protocol of the respective round of ISIMIP: (1) an ensemble of climate-crop simulations such as the one used in Chapter Four; (2) Hydrological model output and / or flood hazard data from a fluvial routing model such as CaMa-Flood (Yamazaki et al., 2011) used in the river flood study by Sauer et al. (in press); (3) TC hazard footprints for wind and possibly also storm surge and torrential rain driven by the same climate model runs, e.g., based on downscaling experiments. This would allow a multi-hazard impact assessment for each year simulated by the driving climate models. For example, such a setup could be used to analyze probability and impact of a fluvial flood or strong wind gusts ruining the harvest in an area coinciding with an otherwise good or bad simulated crop yield. Using harmonized climate simulations, this could be done not only for selected years, but for a whole climate-crop model ensemble with hundreds of years simulated. Currently, (1) and (2) are available for ISIMIP2 and should become available for ISIMIP3 soon. Sauer et al. (in press) processed output from ISIMIP2 in CLIMADA to assess damages caused by fluvial flooding. Currently, TC tracks (above) based on the same harmonized set of climate model simulations are not yet available openly. However, recent scientific progress in the field is promising (see Section 5.5.2). In a recent multi-hazard study, Lange et al. (2020) already combined the analysis of ISIMIP2 simulations with future projections of TC exposure implemented in CLIMADA, using a TC hazard based on dynamical downscaling by Emanuel (2013). In the future, the harmonization of climate data driving TC simulations and crop models, could allow assessments of crop production risks to consider combined effects of impacts represented by GGCM simulations, river floods, TCs, and possibly additional hazards like wild fires, on a yearly basis. By doing so, the diverse communities developing sectoral climate impact models and probabilistic risk models would move even closer and provide information of crucial relevance for society to navigate in increasingly turbulent times.

5.6 Conclusion

This thesis resulted in globally consistent yet regionally specific quantifications of asset value distribution, tropical cyclone impact functions, and future crop production risk, as well as guidance, metrics, and open-source and -access tools for future assessments of global climate impacts and risk in academia and beyond. Set in the context of a joint research and development project, its focus is on building and evaluating methods and datasets for the spatially explicit modeling of climate-related economic risk on a global scale. Main objectives were to conduct research and to develop tools that contribute both to the academic debate and practical use, with the goal to extend research and tools for science-based climate adaptation efforts across sectors. Both conceptually and methodologically, the research and its applications presented here are situated in a wider framework of climate risk, where risk is expressed as a function of hazard, exposure, and vulnerability, and implemented with the open-source and -access risk modeling platform CLIMADA. The scientific papers forming the main chapters of this thesis combine diverse data sets and methodologies to quantify and integrate selected hazard, exposure, and vulnerability components for global-scale risk assessments. Chapter Two develops a method to estimate global gridded asset value exposures by disaggregating country-level asset values with a combination of gridded nightlight intensity and population data (LitPop method). In Chapter Three, these exposures are used for the regional calibration of tropical cyclone impact functions by fitting simulated impact functions against reported damage data. In Chapter Four, we use gridded crop yield simulations from a large climate-crop model ensemble facilitated by ISIMIP3b for a global assessment of country-level crop production risk under 21st century climate change. The latter study required a flexible conceptualization of what represents hazard, exposures, and vulnerability, providing a starting point both to reflect upon this traditional framework and to explore its flexibility in applications using input from diverse sources, including complex modeling chains.

Going forward, the integration of impact model output from ISIMIP in CLIMADA offers great potential for probabilistic multi-hazard risk modeling, building on the effort the ISIMIP community puts into the harmonization, benchmarking, and evaluation of process-oriented climate and impact models. Not a process-oriented model itself, CLIMADA can benefit from the integration of statistical emulators, for example for a resource-efficient simulation of crop yield responses to climatic conditions, similar to the TC impact functions calibrated in Chapter Three. The discussion presented here further offers outlook and guidance for pragmatic approaches to communicate and mitigate the manifold uncertainties entailed in complex risk modeling chains, demonstrated in its own modeling with quantitative ranges for single components that can be used in future uncertainty analyses.

In addition to the research presented in Chapters Two to Four, the joint project required mediation of differences in pace, priority, and measures of success. Working in an applied context allowed for and guided research and development that would have been much harder to achieve without an implementing partner, not least daring to build end-to-end impact modeling chains without getting lost in every single detail. We managed this while adhering to and promoting scientific standards and a pragmatic yet transparent treatment of uncertainties. For a rigorous and science-based assessment of climate-related physical risk as fostered by initiatives such as the TCFD, there is no way back from the standards set by this thesis and the open-source and -access modeling platform CLIMADA, with regard to both the spatially explicit and globally consistent modeling of climate risk.

Code and data availability

The CLIMADA repository (Aznar-Siguan and Bresch, 2019; Bresch and Aznar-Siguan, 2021; CLIMADA-Project, 2019) implemented in Python is openly available online at https://github.com/CLIMADA-project/climada_python (Bresch et al., 2020) under the GNU GPL license version 3 (Free Software Foundation, Inc., 2007, gnu.org/licenses/gpl-3.0.en.html). The repository includes the LitPop asset exposure module (CLIMADA v1.2.0+), regionally calibrated TC impact functions, crop hazard and exposure module, and low flow hazard module (all CLIMADA v.1.5.1+), as developed as part of this project. The code repository of CLIMADA v1.4.1, as used for the calibration in Chapter Three, is archived at http://doi.org/10.5905/ethz-1007-252 (Bresch et al., 2020). The documentation of CLIMADA is hosted on Read the Docs (https://climada-python.readthedocs.io/en/stable/), including a link to the interactive tutorial of CLIMADA.

Python scripts reproducing the main results and figures of Chapters Two and Three are available at https://github.com/CLIMADA-project/climada_papers (Aznar-Siguan et al., 2020; https://doi.org/10.5281/zenodo.4467858, Eberenz et al., 2021a). The scripts reproducing the main results and figures of Chapter 4 are available at https://github.com/sameberenz/climada_papers_crop_production_risk_isimip (Eberenz and Steinmann, 2021, http://doi.org/10.5281/zenodo.4549259).

Further material is permanently available online in the supplements published alongside the two peer-reviewed publications (Eberenz et al., 2020, 2021b). Furthermore, LitPop asset exposure data (in US dollars, value of 2015) at a resolution of 30 arcsec for 224 countries (see Chapter Two) are archived in the ETH Research Repository with link https://doi.org/10.3929/ethz-b-000331316 (Eberenz et al., 2019).

Gridded output from crop models and hydrological models used as input for computing relative crop yield, baseline crop production, and the low river flow hazard have been (ISIMIP2) or will inshallah be (ISIMIP3) made available under a Creative Commons 4.0 license via ISIMIP (ISIMIP, online, https://esg.pik-potsdam.de/search/isimip/). Readily prepared hazard and exposure sets for TC, crop production, and low flow hazards are planned to be made available for download via the CLIMADA project in the near future.

Financial support

This research has been supported by ETH Zurich and the Innosuisse – Schweizerische Agentur für Innovationsförderung (grants no. 26792.1 PFES-ES and 37861.1 IP-SBM).

Disclaimer

The focus on quantifiable economic impacts of natural hazard and climate change proliferated here represents a radical simplification. While it makes sense to quantify climate risk to inform decision makers, this approach neglects that weather and climate events can damage and destroy irreplaceable values, like the life and health of affected persons, but also historical, cultural, and ecological assets (Lyubchich et al., 2020). It is often forgotten just how radical and potentially harmful the simplification is that comes with quantification. Therefore, I find it of utmost importance to keep also the risk in mind, which weather and climate events and thus climate change entail for assets that are not to be quantified and expressed in monetary terms – also and especially while conducting research that focusses on the quantifiable.

References

Abon, C. C., David, C. P. C. and Pellejera, N. E. B.: Reconstructing the Tropical Storm Ketsana flood event in Marikina River, Philippines, Hydrol. Earth Syst. Sci., 7, https://doi.org/10.5194/hess-15-1283-2011, 2011.

Ackerman, F., DeCanio, S. J., Howarth, R. B. and Sheeran, K.: Limitations of integrated assessment models of climate change, Climatic Change, 95(3–4), 297–315, https://doi.org/10.1007/s10584-009-9570-x, 2009.

Adams, R. M.: Global Climate Change and Agriculture: An Economic Perspective, American Journal of Agricultural Economics, 71(5), 1272–1279, https://doi.org/10.2307/1243120, 1989.

Altman, J., Ukhvatkina, O. N., Omelko, A. M., Macek, M., Plener, T., Pejcha, V., Cerny, T., Petrik, P., Srutek, M., Song, J.-S., Zhmerenetsky, A. A., Vozmishcheva, A. S., Krestov, P. V., Petrenko, T. Y., Treydte, K. and Dolezal, J.: Poleward migration of the destructive effects of tropical cyclones during the 20th century, PNAS, 115(45), 11543–11548, https://doi.org/10.1073/pnas.1808979115, 2018.

Andrijevic, M., Crespo Cuaresma, J., Muttarak, R. and Schleussner, C.-F.: Governance in socioeconomic pathways and its role for future adaptive capacity, Nature Sustainability, 3(1), 35–41, https://doi.org/10.1038/s41893-019-0405-0, 2020.

Arnell, N. W., Lowe, J. A., Brown, S., Gosling, S. N., Gottschalk, P., Hinkel, J., Lloyd-Hughes, B., Nicholls, R. J., Osborn, T. J., Osborne, T. M., Rose, G. A., Smith, P. and Warren, R. F.: A global assessment of the effects of climate policy on the impacts of climate change, Nature Climate Change, 3(5), 512–519, https://doi.org/10.1038/nclimate1793, 2013.

Aznar-Siguan, G. and Bresch, D. N.: CLIMADA v1: a global weather and climate risk assessment platform, Geoscientific Model Development, 12(7), 3085–3097, https://doi.org/10.5194/gmd-12-3085-2019, 2019.

Aznar-Siguan, G., Bresch, D. N., Eberenz, S. and Röösli, T.: CLIMADA-papers repository, GitHub, (202005) https://github.com/CLIMADA-project/climada_papers, last access: 9 July 2020, 2020.

Bagtasa, G.: Contribution of Tropical Cyclones to Rainfall in the Philippines, J. Climate, 30(10), 3621–3633, https://doi.org/10.1175/JCLI-D-16-0150.1, 2017.

Bakkensen, L. A., Park, D.-S. R. and Sarkar, R. S. R.: Climate costs of tropical cyclone losses also depend on rain, Environ. Res. Lett., 13(7), 074034, https://doi.org/10.1088/1748-9326/aad056, 2018a.

Bakkensen, L. A., Shi, X. and Zurita, B. D.: The Impact of Disaster Data on Estimating Damage Determinants and Climate Costs, Economics of Disasters and Climate Change, 2(1), 49–71, https://doi.org/10.1007/s41885-017-0018-x, 2018b.

Baradaranshoraka, M., Pinelli, J.-P., Gurley, K., Peng, X. and Zhao, M.: Hurricane Wind versus Storm Surge Damage in the Context of a Risk Prediction Model, Journal of Structural Engineering, 143(9), 04017103, https://doi.org/10.1061/(ASCE)ST.1943-541X.0001824, 2017.

Bertinelli, L., Mohan, P. and Strobl, E.: Hurricane damage risk assessment in the Caribbean: An analysis using synthetic hurricane events and nightlight imagery, Ecological Economics, 124, 135–144, https://doi.org/10.1016/j.ecolecon.2016.02.004, 2016.

Bhatia, K., Vecchi, G., Murakami, H., Underwood, S. and Kossin, J.: Projected Response of Tropical Cyclone Intensity and Intensification in a Global Climate Model, Journal of Climate, 31(20), 8281–8303, https://doi.org/10.1175/JCLI-D-17-0898.1, 2018.

Blanc, E. and Reilly, J.: Approaches to Assessing Climate Change Impacts on Agriculture: An Overview of the Debate, Review of Environmental Economics and Policy, 11(2), 247–257, https://doi.org/10.1093/reep/rex011, 2017.

Blanc, E. and Strobl, E.: Assessing the Impact of Typhoons on Rice Production in the Philippines, J. Appl. Meteor. Climatol., 55(4), 993–1007, https://doi.org/10.1175/JAMC-D-15-0214.1, 2016.

Bloemendaal, N., Muis, S., Haarsma, R. J., Verlaan, M., Irazoqui Apecechea, M., de Moel, H., Ward, P. J. and Aerts, J. C. J. H.: Global modeling of tropical cyclone storm surges using high-resolution forecasts, Clim Dyn, 52(7), 5031–5044, https://doi.org/10.1007/s00382-018-4430-x, 2019.

Bloemendaal, N., Haigh, I. D., Moel, H. de, Muis, S., Haarsma, R. J. and Aerts, J. C. J. H.: Generation of a global synthetic tropical cyclone hazard dataset using STORM, Sci Data, 7(1), 1–12, https://doi.org/10.1038/s41597-020-0381-2, 2020.

Bloomberg, M. R., D. Pavarina, G. Pitkethly, C. Thimann, and Y. L. Sim: Final Report: Recommendations of the Task Force on Climate-related Financial Disclosures, Task Force on Climate-Related Financial Disclosures (TCFD), Switzerland. https://assets.bbhub.io/company/sites/60/2020/10/FINAL-2017-TCFD-Report-11052018.pdf, last access: 19 February 2021, 2017.

Bokern, D.: Water Stress: A Global Risk Analysis for Financial Markets, Journal of Environmental Investing. http://www.thejei.com/wp-content/uploads/2019/09/JEI_Vol.-9-no.-1-Complete.pdf, last access: 19 February 2021, 2019.

Bresch, D. N. and Aznar-Siguan, G.: CLIMADA v1.4.1: towards a globally consistent adaptation options appraisal tool, Geoscientific Model Development, 14(1), 351–363, https://doi.org/10.5194/gmd-14-351-2021, 2021.

Bresch, D. N., Aznar-Siguan, G., Eberenz, S., Röösli, T., Stocker, D., Hartman, J., Pérus, M. and Bozzini, V.: CLIMADA v.1.2.0, ETH Data Archive, https://doi.org/10.5905/ethz-1007-226, 2019.

Bresch, D. N., Aznar-Siguan, G., Bozzini, V., Bungener, R., Eberenz, S., Hartman, J., Mühlhofer, E., Pérus, M., Röösli, T., Sauer, I., Schmid, E., Stalhandske, Z., Steinmann, C. and Stocker, D.: CLIMADA v.1.4.1, ETH Data Archive, https://doi.org/10.5905/ethz-1007-252, 2020.

Brönnimann, S. and Wintzer, J.: Climate data empathy, Wiley Interdisciplinary Reviews: Climate Change, e559, https://doi.org/10.1002/wcc.559, 2018.

Brunner, L., Pendergrass, A. G., Lehner, F., Merrifield, A. L., Lorenz, R. and Knutti, R.: Reduced global warming from CMIP6 projections when weighting models by performance and independence, Earth System Dynamics, 11(4), 995–1012, https://doi.org/10.5194/esd-11-995-2020, 2020.

Carbon Delta: Carbon Delta - an MSCI company, carbon-delta.com https://www.carbon-delta.com/, last access: 2 December 2021, 2019.

Carbon Delta: Climate Value-at-Risk, www.carbon-delta.com/climate-value-at-risk/ https://www.carbon-delta.com/climate-value-at-risk/, last access: 2 December 2021, online.

Cardona, O. D., Ordaz, M. G., Reinoso, E., Yamín, L. E. and Barbat, A. H.: CAPRA - Comprehensive Approach to Probabilistic Risk Assessment: International Initiative for

Risk Management Effectiveness, p. 11, Lisboa, https://www.researchgate.net/publication/259598259, last access: 19 February 2021, 2012a.

Cardona, O.-D., Ordaz, M. G., Mora, M. G., Salgado-Gálvez, M. A., Bernal, G. A., Zuloaga-Romero, D., Marulanda Fraume, M. C., Yamín, L. and González, D.: Global risk assessment: A fully probabilistic seismic and tropical cyclone wind risk assessment, International Journal of Disaster Risk Reduction, 10, 461–476, https://doi.org/10.1016/j.ijdrr.2014.05.006, 2014.

Cardona, O.-D., van Aalst, M. K., Birkmann, J., Fordham, M., McGregor, G., Perez, R., Pulwarty, R. S., Schipper, E. L. F., Sinh, B. T., Décamps, H., Keim, M., Davis, I., Ebi, K. L., Lavell, A., Mechler, R., Murray, V., Pelling, M., Pohl, J., Smith, A.-O. and Thomalla, F.: Determinants of Risk: Exposure and Vulnerability, in Managing the Risks of Extreme Events and Disasters to Advance Climate Change Adaptation, edited by C. B. Field, V. Barros, T. F. Stocker, and Q. Dahe, pp. 65–108, Cambridge University Press, Cambridge, https://doi.org/10.1017/CBO9781139177245.005, , 2012b.

Carleton, T. A. and Hsiang, S. M.: Social and economic impacts of climate, Science, 353(6304), aad9837, https://doi.org/10.1126/science.aad9837, 2016.

Carlowicz, M.: Out of the Blue and Into the Black. https://earthobservatory.nasa.gov/Features/IntotheBlack, last access: 10 February 2020, 2012.

Carlowicz, M.: Night Light Maps Open Up New Applications. https://earthobservatory.nasa.gov/images/90008/night-light-maps-open-up-new-applications, last access: 10 February 2020, 2017.

Cayanan, E. O., Chen, T.-C., Argete, J. C., Yen, M.-C. and Nilo, P. D.: The Effect of Tropical Cyclones on Southwest Monsoon Rainfall in the Philippines, JMSJ, 89A, 123–139, https://doi.org/10.2151/jmsj.2011-A08, 2011.

CDP: CDP Web Page, https://www.cdp.net/en/info/about-us, last access: 10 February 2021, online.

Center For International Earth Science Information Network (CIESIN), Columbia University: Documentation for the Gridded Population of the World, Version 4 (GPWv4), Revision 10 Data Sets, Palisades NY: NASA Socioeconomic Data and Applications Center (SEDAC), https://doi.org/10.7927/H4B56GPT, 2017.

Challinor, A. J., Müller, C., Asseng, S., Deva, C., Nicklin, K. J., Wallach, D., Vanuytrecht, E., Whitfield, S., Ramirez-Villegas, J. and Koehler, A.-K.: Improving the use of crop models for risk assessment and climate change adaptation, Agricultural Systems, 159, 296–306, https://doi.org/10.1016/j.agsy.2017.07.010, 2018.

Christensen, J. H., Aldrian, E., Abraham, L., Arritt, R., Biasutti, M. and Fyfe, J.: Climate Phenomena and their Relevance for Future Regional Climate Change. In: Climate Change 2013: The Physical Science Basis. Contribution of Working Group I to the Fifth Assessment Report of the Intergovernmental Panel on Climate Change [Stocker, T.F., D. Qin, G.-K. Plattner, M. Tignor, S.K. Allen, J. Boschung, A. Nauels, Y. Xia, V. Bex and P.M. Midgley (eds.)]., Cambridge University Press, Cambridge, United Kingdom and New York, NY, USA., 2013.

Cinco, T. A., Guzman, R. G. de, Ortiz, A. M. D., Delfino, R. J. P., Lasco, R. D., Hilario, F. D., Juanillo, E. L., Barba, R. and Ares, E. D.: Observed trends and impacts of tropical cyclones in the Philippines, International Journal of Climatology, 36(14), 4638–4650, https://doi.org/10.1002/joc.4659, 2016.

CLIMADA-Project: CLIMADA repository, GitHub https://github.com/CLIMADA-project/climada_python, last access: 19 February 2021, 2019.

Collins, D. and Lowe, S. P.: A Macro Validation Dataset for US Hurricane Models, Casualty Actuarial Society. https://www.casact.org/pubs/forum/01wforum/01wf217.pdf, last access: 26 January 2021, 2001.

Cooper, G. A. and Falvey, R. J.: Annual Tropical Cyclone Report, U.S. Naval Maritime Forecast Center/ Joint Typhoon Warning Center Pearl Harbor, Hawaii. https://www.metoc.navy.mil/jtwc/products/atcr/2009atcr.pdf, last access: 25 March 2020, 2009.

Cramer, W., Bondeau, A., Woodward, F. I., Prentice, I. C., Betts, R. A., Brovkin, V., Cox, P. M., Fisher, V., Foley, J. A., Friend, A. D., Kucharik, C., Lomas, M. R., Ramankutty, N., Sitch, S., Smith, B., White, A. and Young-Molling, C.: Global response of terrestrial ecosystem structure and function to CO2 and climate change: results from six dynamic global vegetation models, Global Change Biology, 7(4), 357–373, https://doi.org/10.1046/j.1365-2486.2001.00383.x, 2001.

Cramer, W., Yohe, G. W., Auffhammer, M., Huggel, C. and Molau, U.: Detection and attribution of observed impacts, in Climate Change 2014: Impacts, Adaptation, and Vulnerability. Part A: Global and Sectoral Aspects. Contribution ofWorking Group II to the Fifth Assessment Report of the Intergovernmental Panel on Climate Change [ed. CB Field, VR Barros, DJ Dokken, KJ Mach, MD Mastrandrea, et al.], pp. 979–1037, Cambridge University Press, Cambridge, United Kingdom and New York, NY, USA, https://www.ipcc.ch/report/ar5/wg2/, last access: 19 January 2021, 2014.

Creative Commons: Creative Commons — Attribution 4.0 International — CC BY 4.0, Creative Commons https://creativecommons.org/licenses/by/4.0/, last access: 12 February 2021, online.

Credit Suisse Research Institute: Global Wealth Report 2017, Credit Suisse Research Institute. https://www.credit-suisse.com/corporate/en/articles/news-and-expertise/global-wealth-report-2017-201711.html, last access: 3 July 2020, 2017.

Cruz, F. T. and Narisma, G. T.: WRF simulation of the heavy rainfall over Metropolitan Manila, Philippines during tropical cyclone Ketsana: a sensitivity study, Meteorol Atmos Phys, 128(4), 415–428, https://doi.org/10.1007/s00703-015-0425-x, 2016.

Cucchi, M., Weedon, G. P., Amici, A., Bellouin, N., Lange, S., Müller Schmied, H., Hersbach, H. and Buontempo, C.: WFDE5: bias-adjusted ERA5 reanalysis data for impact studies, Earth Syst. Sci. Data, 12(3), 2097–2120, https://doi.org/10.5194/essd-12-2097-2020, 2020.

Czajkowski, J. and Done, J.: As the Wind Blows? Understanding Hurricane Damages at the Local Level through a Case Study Analysis, Wea. Climate Soc., 6(2), 202–217, https://doi.org/10.1175/WCAS-D-13-00024.1, 2013.

De Bono, A. and Mora, M. G.: A global exposure model for disaster risk assessment, International Journal of Disaster Risk Reduction, 10, 442–451, https://doi.org/10.1016/j.ijdrr.2014.05.008, 2014.

Dietz, S., Bowen, A., Dixon, C. and Gradwell, P.: 'Climate value at risk' of global financial assets, Nature Climate Change, 6(7), 676–679, https://doi.org/10.1038/nclimate2972, 2016.

Dilley, M., Chen, R. S., Deichmann, U., Lerner-Lam, A. L. and Arnold, M.: Natural Disaster Hotspots - A Global Risk Analysis, World Bank Group, Washington DC. https://doi.org/10.1596/0-8213-5930-4, last access: 31 December 2020, 2005.

Done, J. M., Ge, M., Holland, G. J., Dima-West, I., Phibbs, S., Saville, G. R. and Wang, Y.: Modelling global tropical cyclone wind footprints, Natural Hazards and Earth System Sciences, 20(2), 567–580, https://doi.org/10.5194/nhess-20-567-2020, 2020.

Doxsey-Whitfield, E., MacManus, K., Adamo, S. B., Pistolesi, L., Squires, J., Borkovska, O. and Baptista, S. R.: Taking Advantage of the Improved Availability of Census Data: A First Look at the Gridded Population of the World, Version 4, Papers in Applied Geography, 1(3), 226–234, https://doi.org/10.1080/23754931.2015.1014272, 2015.

Eberenz, S.: Research Plan: Impact oriented top-down climate risk modeling, ETH Zürich, Zürich, Switzerland. Unpublished, 2019.

Eberenz, S.: anthropo-obscenity, Consilience Journal. SI: Geoscience https://www.consilience-journal.com/si/geoscience/anthropo-obscenity, last access: 22 February 2021, 2021.

Eberenz, S. and Steinmann, C.: climada_papers_crop_production_risk_isimip: v1.0.1, GitHub/sameberenz, https://doi.org/10.5281/zenodo.4549259, 2021.

Eberenz, S., Stocker, D., Röösli, T. and Bresch, D. N.: LitPop: Global Exposure Data for Disaster Risk Assessment, ETH Research Collection, https://doi.org/10.3929/ethz-b-000331316, 2019.

Eberenz, S., Stocker, D., Röösli, T. and Bresch, D. N.: Asset exposure data for global physical risk assessment, Earth System Science Data, 12(2), 817–833, https://doi.org/10.5194/essd-12-817-2020, 2020.

Eberenz, S., Lüthi, S. and Bresch, D. N.: climada_papers_tropical_cyclone_impact_functions: v1.1: TC impact function calibration, GitHub, https://doi.org/10.5281/zenodo.4467858, 2021a.

Eberenz, S., Lüthi, S. and Bresch, D. N.: Regional tropical cyclone impact functions for globally consistent risk assessments, Natural Hazards and Earth System Sciences, 21(1), 393–415, https://doi.org/10.5194/nhess-21-393-2021, 2021b.

Elliott, J., Deryng, D., Müller, C., Frieler, K., Konzmann, M., Gerten, D., Glotter, M., Flörke, M., Wada, Y., Best, N., Eisner, S., Fekete, B. M., Folberth, C., Foster, I., Gosling, S. N., Haddeland, I., Khabarov, N., Ludwig, F., Masaki, Y., Olin, S., Rosenzweig, C., Ruane, A. C., Satoh, Y., Schmid, E., Stacke, T., Tang, Q. and Wisser, D.: Constraints and potentials of future irrigation water availability on agricultural production under climate change, PNAS, 111(9), 3239–3244, https://doi.org/10.1073/pnas.1222474110, 2014.

Elliott, J., Müller, C., Deryng, D., Chryssanthacopoulos, J., Boote, K. J., Büchner, M., Foster, I., Glotter, M., Heinke, J., Iizumi, T., Izaurralde, R. C., Mueller, N. D., Ray, D. K., Rosenzweig, C., Ruane, A. C. and Sheffield, J.: The Global Gridded Crop Model Intercomparison: data and modeling protocols for Phase 1 (v1.0), Geoscientific Model Development, 8(2), 261–277, https://doi.org/10.5194/gmd-8-261-2015, 2015a.

Elliott, R. J. R., Strobl, E. and Sun, P.: The local impact of typhoons on economic activity in China: A view from outer space, Journal of Urban Economics, 88, 50–66, https://doi.org/10.1016/j.jue.2015.05.001, 2015b.

Elsner, J. B., Kossin, J. P. and Jagger, T. H.: The increasing intensity of the strongest tropical cyclones, Nature, 455(7209), 92–95, https://doi.org/10.1038/nature07234, 2008.

Elvidge, C., Safran, J., Nelson, I., Tuttle, B., Ruth Hobson, V., Baugh, K., Dietz, J. and Erwin, E.: Area and Positional Accuracy of DMSP Nighttime Lights Data, in Remote Sensing and GIS Accuracy Assessment, pp. 281–292, https://doi.org/10.1201/9780203497586.ch20, , 2004.

Elvidge, C. D., Cinzano, P., Pettit, D. R., Arvesen, J., Sutton, P., Small, C., Nemani, R., Longcore, T., Rich, C., Safran, J., Weeks, J. and Ebener, S.: The Nightsat mission concept, International Journal of Remote Sensing, 28(12), 2645–2670, https://doi.org/10.1080/01431160600981525, 2007.

Elvidge, C. D., Baugh, K. E., Anderson, S. J., Sutton, P. C. and Ghosh, T.: The Night Light Development Index (NLDI): a spatially explicit measure of human development from satellite data, Social Geography, 7(1), 23–35, https://doi.org/10.5194/sg-7-23-2012, 2012.

Emanuel, K.: Global Warming Effects on U.S. Hurricane Damage, Wea. Climate Soc., 3(4), 261–268, https://doi.org/10.1175/WCAS-D-11-00007.1, 2011a.

Emanuel, K.: Global Warming Effects on U.S. Hurricane Damage, Weather, Climate, and Society, 3(4), 261–268, https://doi.org/10.1175/WCAS-D-11-00007.1, 2011b.

Emanuel, K.: Assessing the present and future probability of Hurricane Harvey's rainfall, Proceedings of the National Academy of Sciences, 114(48), 12681–12684, https://doi.org/10.1073/pnas.1716222114, 2017.

Emanuel, K., Ravela, S., Vivant, E. and Risi, C.: A Statistical Deterministic Approach to Hurricane Risk Assessment, Bull. Amer. Meteor. Soc., 87(3), 299–314, https://doi.org/10.1175/BAMS-87-3-299, 2006.

Emanuel, K., Fondriest, F. and Kossin, J.: Potential Economic Value of Seasonal Hurricane Forecasts, Wea. Climate Soc., 4(2), 110–117, https://doi.org/10.1175/WCAS-D-11-00017.1, 2012.

Emanuel, K. A.: Downscaling CMIP5 climate models shows increased tropical cyclone activity over the 21st century, Proceedings of the National Academy of Sciences, 110(30), 12219–12224, https://doi.org/10.1073/pnas.1301293110, 2013.

Espada, R.: Return period and Pareto analyses of 45 years of tropical cyclone data (1970–2014) in the Philippines, Applied Geography, 97, 228–247, https://doi.org/10.1016/j.apgeog.2018.04.018, 2018.

Eyring, V., Bony, S., Meehl, G. A., Senior, C. A., Stevens, B., Stouffer, R. J. and Taylor, K. E.: Overview of the Coupled Model Intercomparison Project Phase 6 (CMIP6) experimental design and organization, Geoscientific Model Development, 9(5), 1937–1958, https://doi.org/10.5194/gmd-9-1937-2016, 2016.

Eyring, V., Cox, P. M., Flato, G. M., Gleckler, P. J., Abramowitz, G., Caldwell, P., Collins, W. D., Gier, B. K., Hall, A. D., Hoffman, F. M., Hurtt, G. C., Jahn, A., Jones, C. D., Klein, S. A., Krasting, J. P., Kwiatkowski, L., Lorenz, R., Maloney, E., Meehl, G. A., Pendergrass, A. G., Pincus, R., Ruane, A. C., Russell, J. L., Sanderson, B. M., Santer, B. D., Sherwood, S. C., Simpson, I. R., Stouffer, R. J. and Williamson, M. S.: Taking climate model evaluation to the next level, Nature Climate Change, 9(2), 102–110, https://doi.org/10.1038/s41558-018-0355-y, 2019.

Falkner, R.: The Paris Agreement and the new logic of international climate politics, International Affairs, 92(5), 1107–1125, https://doi.org/10.1111/1468-2346.12708, 2016.

FAO: FAOSTAT, http://www.fao.org/faostat/en/#home, last access: 22 December 2020, 2019.

Federal Emergency Management Authority [FEMA]: HAZUS MH MR5 Technical Manual, Washington, D.C. https://www.fema.gov/sites/default/files/2020-09/fema_hazus_hurricane-model_technical-manual_2.1.pdf, last access: 26 January 2021, 2010.

Fink, L.: Larry Fink's 2021 letter to CEOs, BlackRock https://www.blackrock.com/corporate/investor-relations/larry-fink-ceo-letter, last access: 8 February 2021, 2021.

Fischer, E. M. and Knutti, R.: Anthropogenic contribution to global occurrence of heavy-precipitation and high-temperature extremes, Nature Clim Change, 5(6), 560–564, https://doi.org/10.1038/nclimate2617, 2015.

Florczyk, A. J., Corbane, C., Ehrlich, D., Freire, S., Kemper, T., Maffenini, L., Melchiorri, M., Pesaresi, M., Politis, P., Schiavina, M., Sabo, F., Zanchetta, L., European Commission, and Joint Research Centre: GHSL data package 2019, EUR 29788 EN, JRC, Luxembourg. https://doi.org/10.2760/290498, last access: 15 February 2021, 2019.

Franke, J. A., Müller, C., Elliott, J., Ruane, A. C., Jägermeyr, J., Snyder, A., Dury, M., Falloon, P. D., Folberth, C., François, L., Hank, T., Izaurralde, R. C., Jacquemin, I., Jones, C., Li, M., Liu, W., Olin, S., Phillips, M., Pugh, T. A. M., Reddy, A., Williams, K., Wang, Z., Zabel, F. and Moyer, E. J.: The GGCMI Phase 2 emulators: global gridded crop model responses to changes in CO_2, temperature, water, and nitrogen (version 1.0), Geoscientific Model Development, 13(9), 3995–4018, https://doi.org/10.5194/gmd-13-3995-2020, 2020a.

Franke, J. A., Müller, C., Elliott, J., Ruane, A. C., Jägermeyr, J., Balkovic, J., Ciais, P., Dury, M., Falloon, P. D., Folberth, C., François, L., Hank, T., Hoffmann, M., Izaurralde, R. C., Jacquemin, I., Jones, C., Khabarov, N., Koch, M., Li, M., Liu, W., Olin, S., Phillips, M., Pugh, T. A. M., Reddy, A., Wang, X., Williams, K., Zabel, F. and Moyer, E. J.: The GGCMI Phase 2 experiment: global gridded crop model simulations under uniform changes in CO2, temperature, water, and nitrogen levels (protocol version 1.0), Geoscientific Model Development, 13(5), 2315–2336, https://doi.org/10.5194/gmd-13-2315-2020, 2020b.

Free Software Foundation, Inc.: GNU General Public License, version 3, https://www.gnu.org/licenses/gpl-3.0.en.html, last access: 19 February 2021, 2007.

Frieler, K., Lange, S., Piontek, F., Reyer, C. P. O., Schewe, J., Warszawski, L., Zhao, F., Chini, L., Denvil, S., Emanuel, K., Geiger, T., Halladay, K., Hurtt, G., Mengel, M., Murakami, D., Ostberg, S., Popp, A., Riva, R., Stevanovic, M., Suzuki, T., Volkholz, J., Burke, E., Ciais, P., Ebi, K., Eddy, T. D., Elliott, J., Galbraith, E., Gosling, S. N., Hattermann, F., Hickler, T., Hinkel, J., Hof, C., Huber, V., Jägermeyr, J., Krysanova, V., Marcé, R., Müller Schmied, H., Mouratiadou, I., Pierson, D., Tittensor, D. P., Vautard, R., Vliet, M. van, Biber, M. F., Betts, R. A., Bodirsky, B. L., Deryng, D., Frolking, S., Jones, C. D., Lotze, H. K., Lotze-Campen, H., Sahajpal, R., Thonicke, K., Tian, H. and Yamagata, Y.: Assessing the impacts of 1.5 °C global warming – simulation protocol of the Inter-Sectoral Impact Model Intercomparison Project (ISIMIP2b), Geoscientific Model Development, 10(12), 4321–4345, https://doi.org/10.5194/gmd-10-4321-2017, 2017a.

Frieler, K., Schauberger, B., Arneth, A., Balkovič, J., Chryssanthacopoulos, J., Deryng, D., Elliott, J., Folberth, C., Khabarov, N., Müller, C., Olin, S., Pugh, T. A. M., Schaphoff, S., Schewe, J., Schmid, E., Warszawski, L. and Levermann, A.: Understanding the weather signal in national crop-yield variability, Earth's Future, 5(6), 605–616, https://doi.org/10.1002/2016EF000525, 2017b.

Frisch, M.: Modeling Climate Policies: A Critical Look at Integrated Assessment Models, Philosophy & Technology, 26(2), 117–137, https://doi.org/10.1007/s13347-013-0099-6, 2013.

Füssel, H. M., Toth, F. L. and van Minnen, J. G.: Climate Impact Response Functions as Impact Tools in the Tolerable Windows Approach, Climatic Change, 56, 91–117, https://doi.org/10.1023/A:1021340513936, 2003.

Gallina, V., Torresan, S., Critto, A., Sperotto, A., Glade, T. and Marcomini, A.: A review of multi-risk methodologies for natural hazards: Consequences and challenges for a climate change impact assessment, Journal of Environmental Management, 168, 123–132, https://doi.org/10.1016/j.jenvman.2015.11.011, 2016.

Gaupp, F., Hall, J., Mitchell, D. and Dadson, S.: Increasing risks of multiple breadbasket failure under 1.5 and 2 °C global warming, Agricultural Systems, 175, 34–45, https://doi.org/10.1016/j.agsy.2019.05.010, 2019.

Gaupp, F., Hall, J., Hochrainer-Stigler, S. and Dadson, S.: Changing risks of simultaneous global breadbasket failure, Nat. Clim. Chang., 10(1), 54–57, https://doi.org/10.1038/s41558-019-0600-z, 2020.

Geiger, T.: Continuous national gross domestic product (GDP) time series for 195 countries: past observations (1850–2005) harmonized with future projections according to the Shared Socio-economic Pathways (2006–2100), Earth System Science Data, 10(2), 847–856, https://doi.org/10.5194/essd-10-847-2018, 2018.

Geiger, T., Daisuke, M., Frieler, K. and Yamagata, Y.: Spatially-explicit Gross Cell Product (GCP) time series: past observations (1850-2000) harmonized with future projections according to the Shared Socioeconomic Pathways (2010-2100), , https://doi.org/10.5880/PIK.2017.007, 2017.

Geiger, T., Frieler, K. and Bresch, D. N.: A global historical data set of tropical cyclone exposure (TCE-DAT), Earth System Science Data, 1–15, https://doi.org/10.5194/essd-10-185-2018, 2018.

Gettelman, A., Bresch, D. N., Chen, C. C., Truesdale, J. E. and Bacmeister, J. T.: Projections of future tropical cyclone damage with a high-resolution global climate model, Climatic Change, 146(3–4), 575–585, https://doi.org/10.1007/s10584-017-1902-7, 2017.

Ghosh, T., Anderson, S. J., Elvidge, C. D. and Sutton, P. C.: Using nighttime satellite imagery as a proxy measure of human well-being, Sustainability (Switzerland), 5(12), 4988–5019, https://doi.org/10.3390/su5124988, 2013.

Gordon, M. J.: Dividends, Earnings, and Stock Prices, The Review of Economics and Statistics, 41(2), 99–105, https://doi.org/10.2307/1927792, 1959.

Gordon, M. J.: The Investment, Financing, and Valuation of the Corporation, 2013 Reprint., Homewood, Ill., Irwin., 1962.

Guha-Sapir, D.: EM-DAT, CRED / UCLouvain, Brussels, Belgium, www.emdat.be, last access: 31 October 2018, 2018.

Guha-Sapir, D. and Below, R.: The quality and accuracy of disaster data: A comparative analyse of three global data sets, Disaster Management Facil., World Bank. http://www.cred.be/sites/default/files/Quality_accuracy_disaster_data.pdf, last access: 26 January 2021, 2002.

Guha-Sapir, D. and Checchi, F.: Science and politics of disaster death tolls, BMJ, 362, k4005, https://doi.org/10.1136/bmj.k4005, 2018.

Gunasekera, R., Ishizawa, O., Aubrecht, C., Blankespoor, B., Murray, S., Pomonis, A. and Daniell, J.: Developing an adaptive global exposure model to support the generation of country disaster risk profiles, Earth-Science Reviews, 150, 594–608, https://doi.org/10.1016/j.earscirev.2015.08.012, 2015.

Haddeland, I., Clark, D. B., Franssen, W., Ludwig, F., Voß, F., Arnell, N. W., Bertrand, N., Best, M., Folwell, S., Gerten, D., Gomes, S., Gosling, S. N., Hagemann, S., Hanasaki, N., Harding, R., Heinke, J., Kabat, P., Koirala, S., Oki, T., Polcher, J., Stacke, T., Viterbo, P., Weedon, G. P. and Yeh, P.: Multimodel Estimate of the Global Terrestrial Water Balance: Setup and First Results, J. Hydrometeor., 12(5), 869–884, https://doi.org/10.1175/2011JHM1324.1, 2011.

Han, J., Meng, X., Liang, H., Cao, Z., Dong, L. and Huang, C.: An improved nightlight-based method for modeling urban CO2 emissions, Environmental Modelling & Software, 107, 307–320, https://doi.org/10.1016/j.envsoft.2018.05.008, 2018.

Hansen, G., Stone, D., Auffhammer, M., Huggel, C. and Cramer, W.: Linking local impacts to changes in climate: a guide to attribution, Reg Environ Change, 16(2), 527–541, https://doi.org/10.1007/s10113-015-0760-y, 2016.

Henderson, J. V., Storeygard, A. and Weil, D. N.: Measuring Economic Growth from Outer Space, American Economic Review, 102(2), 994–1028, https://doi.org/10.1257/aer.102.2.994, 2012.

Herring, S. C., Christidis, N., Hoell, A., Hoerling, M. P. and Stott, P. A.: Explaining Extreme Events of 2018 from a Climate Perspective, Bulletin of the American Meteorological Society, 101(1), S1–S134, https://doi.org/10.1175/BAMS-ExplainingExtremeEvents2018.1, 2020.

Holland, G.: A Revised Hurricane Pressure–Wind Model, Mon. Wea. Rev., 136(9), 3432–3445, https://doi.org/10.1175/2008MWR2395.1, 2008.

Hurlbert, M., Krishnaswamy, J., Davin, E., Johnson, F. X., Fernando, C., Morton, J., Viner, D., Bailis, R., Byers, E., Calvin, K., Diaz-Chavez, R., Evans, J., Fletcher, A., Ford, J., Manialawy, Y., McElwee, P., Quan, J., Renwick, A., Thiery, W., Warner, A., Rodrigues, R., Ii, B. L. T. and Zikhali, T.: Risk management and decision-making in relation to sustainable development, in Climate Change and Land: an IPCC special report on climate change, desertification, land degradation, sustainable land management, food security, and greenhouse gas fluxes in terrestrial ecosystems [P.R. Shukla, J. Skea, E. Calvo Buendia, V. Masson-Delmotte, H.-O. Pörtner, D.C. Roberts, P. Zhai, R. Slade, S. Connors, R. van Diemen, M. Ferrat, E. Haughey, S. Luz, S. Neogi, M. Pathak, J. Petzold, J. Portugal Pereira, P. Vyas, E. Huntley, K. Kissick, M. Belkacemi, J. Malley, (eds.)], p. 128, In press, , 2019.

Hurtt, G. C., Chini, L., Sahajpal, R., Frolking, S., Bodirsky, B. L., Calvin, K., Doelman, J. C., Fisk, J., Fujimori, S., Goldewijk, K. K., Hasegawa, T., Havlik, P., Heinimann, A., Humpenöder, F., Jungclaus, J., Kaplan, J., Kennedy, J., Kristzin, T., Lawrence, D., Lawrence, P., Ma, L., Mertz, O., Pongratz, J., Popp, A., Poulter, B., Riahi, K., Shevliakova, E., Stehfest, E., Thornton, P., Tubiello, F. N., van Vuuren, D. P. and Zhang, X.: Harmonization of Global Land-Use Change and Management for the Period 850–2100 (LUH2) for CMIP6, preprint, Climate and Earth System Modeling., 2020.

ICMA Group: Green Bonds Principles – Voluntary Process Guidelines for Issuing Green Bonds, Paris, France. https://www.icmagroup.org/assets/documents/Regulatory/Green-Bonds/Green-Bonds-Principles-June-2018-270520.pdf, last access: 15 December 2020, 2018.

IFPRI, I. F. P. R. I. and IIASA, I. I. for A. S. A.: Global Spatially-Disaggregated Crop Production Statistics Data for 2005 Version 3.2, Harvard Dataverse, (V9), https://doi.org/10.7910/DVN/DHXBJX, 2016.

IFRC: Philippines: Typhoon Fengshen (Emergency appeal), MDRPH004, International Federation of the Red Cross and Red Crescent Societies. https://reliefweb.int/sites/reliefweb.int/files/resources/FB51CB092CBBC9F18525763A0058A87A-Full_Report.pdf, last access: 26 January 2021, 2009.

Inokuchi, T., Nakasu, T. and Sato, T.: Landslide Disaster around Baguio City caused by Typhoon Pepeng in 2009, Natural Disaster Research Report. https://researchmap.jp/read0139271/misc/15254764/attachment_file.pdf, last access: 26 January 2021, 2011.

IPCC: Managing the Risks of Extreme Events and Disasters to Advance Climate Change Adaptation: Special Report of the Intergovernmental Panel on Climate Change, edited by C. B. Field, V. Barros, T. F. Stocker, and Q. Dahe, Cambridge University Press, Cambridge., 2012.

IPCC: Summary for Policymakers, in Climate Change 2013: The Physical Science Basis.Contribution of Working Group I to the Fifth Assessment Report of the Intergovernmental Panel on Climate Change [Stocker, T.F., D. Qin, G.-K. Plattner, M. Tignor, S.K. Allen, J. Boschung, A. Nauels, Y. Xia, V. Bex and P.M. Midgley (eds.)], p. 28, Cambridge University Press, Cambridge, United Kingdom and New York, NY, USA, https://www.ipcc.ch/site/assets/uploads/2018/02/WG1AR5_SPM_FINAL.pdf, last access: 15 December 2020, 2013.

IPCC: Climate Change 2014: Impacts, Adaptation, and Vulnerability. Part A: Global and Sectoral Aspects. Contribution of Working Group II to the Fifth Assessment Report of the Intergovernmental Panel on Climate Change, edited by C. B. Field, V. R. Barros, D. J. Dokken, K. J. Mach, M. D. Mastrandrea, T. E. Bilir, M. Chatterjee, K. L. Ebi, Y. O. Estrada, R. C. Genova, B. Girma, E. S. Kissel, A. N. Levy, S. MacCracken, P. R. Mastrandrea, and L. L. White, Cambridge University Press, Cambridge, United Kingdom and New York, NY, USA., 2014a.

IPCC: Climate Change 2014: Mitigation of Climate Change. Contribution of Working Group III to the Fifth Assessment Report of the Intergovernmental Panel on Climate Change [Edenhofer, O., R. Pichs-Madruga, Y. Sokona, E. Farahani, S. Kadner, K. Seyboth, A. Adler, I. Baum, S. Brunner, P. Eickemeier, B. Kriemann, J. Savolainen, S. Schlömer, C. von Stechow, T. Zwickel and J.C. Minx (eds.)], Cambridge University Press, Cambridge, United Kingdom and New York, NY, USA., 2014b.

Ishizawa, O. A., Miranda, J. J. and Strobl, E.: The Impact of Hurricane Strikes on Short-Term Local Economic Activity: Evidence from Nightlight Images in the Dominican Republic, Int J Disaster Risk Sci, 10(3), 362–370, https://doi.org/10.1007/s13753-019-00226-0, 2019.

ISIMIP: ISIMIP3a/3b protocol published, The Inter-Sectoral Impact Model Intercomparison Project https://www.isimip.org/newsletter/isimip3a3b-protocol-published/, last access: 1 February 2021a, 2020.

ISIMIP: ISIMIP3b simulation round simulation protocol - Agriculture, https://protocol.isimip.org/protocol/ISIMIP3b/agriculture.html, last access: 23 December 2020b, 2020.

ISIMIP: The Inter-Sectoral Impact Model Intercomparison Project, https://www.isimip.org/, last access: 23 December 2020, online.

ISO: ISO 31000:2009(en), Risk management — Principles and guidelines, International Organization for Standardization https://www.iso.org/obp/ui/#iso:std:iso:31000:ed-1:v1:en, last access: 1 February 2021, 2009.

ISO: ISO 31000:2018(en), Risk management — Guidelines, International Organization for Standardization https://www.iso.org/obp/ui/#iso:std:iso:31000:ed-2:v1:en, last access: 1 February 2021, 2018.

Jägermeyr, J. and Frieler, K.: Spatial variations in crop growing seasons pivotal to reproduce global fluctuations in maize and wheat yields, Science Advances, 4(11), 10, https://doi.org/10.1126/sciadv.aat4517, 2018.

Jägermeyr, J., Robock, A., Elliott, J., Müller, C., Xia, L., Khabarov, N., Folberth, C., Schmid, E., Liu, W., Zabel, F., Rabin, S. S., Puma, M. J., Heslin, A., Franke, J., Foster, I., Asseng, S., Bardeen, C. G., Toon, O. B. and Rosenzweig, C.: A regional nuclear conflict would compromise global food security, PNAS, 117(13), 7071–7081, https://doi.org/10.1073/pnas.1919049117, 2020.

Jägermeyr, J., Müller, C., Ruane, A. C., Elliott, J., Balkovic, J., Faye, B., Franke, J. A., Folberth, C., Iizumi, T., Khabarov, N., Lange, S., Liu, W., Minoli, S., Okada, M., Phillips, M., Mialyk, O., Moyer, E. J., Rabin, S., Schneider, J. M., Schyns, J. F., Skalsky, R., Stella, T., Stephens, H., Webber, H., Zabel, F. and Rosenzweig, C.: Climate change signal in global agriculture emerges earlier in new generation of climate and crop models, under review.

James, R. A., Jones, R. G., Boyd, E., Young, H. R., Otto, F. E. L., Huggel, C. and Fuglestvedt, J. S.: Attribution: How Is It Relevant for Loss and Damage Policy and Practice?, in Loss and Damage from Climate Change: Concepts, Methods and Policy Options, edited by R. Mechler, L. M. Bouwer, T. Schinko, S. Surminski, and J. Linnerooth-Bayer, pp. 113–154, Springer International Publishing, Cham, https://doi.org/10.1007/978-3-319-72026-5_5, , 2019.

John Malloy, Jessica Noviello, and Jen Walsh: The Seasons of Research, Consilience Journal. SI: Geoscience https://www.consilience-journal.com/si/geoscience/the-seasons-of-research, last access: 22 February 2021, 2021.

Joint Typhoon Warning Center: Super Typhoon Angela (29W). https://web.archive.org/web/20110607011047/http://www.usno.navy.mil/NOOC/nmfc-ph/RSS/jtwc/atcr/1995atcr/pdf/wnp/29w.pdf, last access: 25 March 2020, 1995.

Jones, B. and O'Neill, B. C.: Spatially explicit global population scenarios consistent with the Shared Socioeconomic Pathways, Environ. Res. Lett., 11(8), 084003, https://doi.org/10.1088/1748-9326/11/8/084003, 2016.

Jones, J. W., Antle, J. M., Basso, B., Boote, K. J., Conant, R. T., Foster, I., Godfray, H. C. J., Herrero, M., Howitt, R. E., Janssen, S., Keating, B. A., Munoz-Carpena, R., Porter, C. H., Rosenzweig, C. and Wheeler, T. R.: Brief history of agricultural systems modeling, Agricultural Systems, 155, 240–254, https://doi.org/10.1016/j.agsy.2016.05.014, 2017.

Kamstra, M.: Pricing Firms on the Basis of Fundamentals, Federal Reserve Bank of Atlanta, Atlanta, USA. https://www.frbatlanta.org/-/media/documents/research/publications/economic-review/2003/vol88no1_kamstra.pdf, last access: 2 February 2021, 2003.

Kang, N.-Y. and Elsner, J. B.: Trade-off between intensity and frequency of global tropical cyclones, Nature Climate Change, 5(7), 661–664, https://doi.org/10.1038/nclimate2646, 2015.

Kidney, S., Veys, A., Flensborg, C. and Jones, B.: Environmental theme bonds: a new fixed income asset class, IFR Market Intelligence. https://www.climatebonds.net/files/files/SustBanking_Ch14_p219-232.pdf, last access: 1 March 2021, 2017.

King, A. and Bell, R.: Riskscape New Zealand - A Multihazard Loss Modelling Tool, p. 9, http://db.nzsee.org.nz/2006/Paper30.pdf, last access: 19 February 2021, 2006.

Klein Goldewijk, K., Beusen, A., Doelman, J. and Stehfest, E.: Anthropogenic land use estimates for the Holocene – HYDE 3.2, Earth Syst. Sci. Data, 9(2), 927–953, https://doi.org/10.5194/essd-9-927-2017, 2017.

Kleppek, S., Muccione, V., Raible, C. C., Bresch, D. N., Koellner-Heck, P. and Stocker, T. F.: Tropical cyclones in ERA-40: A detection and tracking method, Geophysical Research Letters, 35(10), https://doi.org/10.1029/2008GL033880, 2008.

Knapp, K. R., Kruk, M. C., Levinson, D. H., Diamond, H. J. and Neumann, C. J.: The International Best Track Archive for Climate Stewardship (IBTrACS): Unifying tropical cyclone best track data, Bull. Amer. Meteor. Soc., 91(3), 363–376, https://doi.org/10.1175/2009BAMS2755.1, 2010.

Knorr Cetina, K. and Preda, A.: The Sociology of Financial Markets, OUP Catalogue, Oxford University Press. https://econpapers.repec.org/bookchap/oxpobooks/9780199296927.htm, last access: 18 January 2021, 2006.

Knutson, T., Camargo, S. J., Chan, J. C. L., Emanuel, K., Ho, C.-H., Kossin, J., Mohapatra, M., Satoh, M., Sugi, M., Walsh, K. and Wu, L.: Tropical Cyclones and Climate Change Assessment: Part I: Detection and Attribution, Bulletin of the American Meteorological Society, 100(10), 1987–2007, https://doi.org/10.1175/BAMS-D-18-0189.1, 2019.

Knutson, T., Camargo, S. J., Chan, J. C. L., Emanuel, K., Ho, C.-H., Kossin, J., Mohapatra, M., Satoh, M., Sugi, M., Walsh, K. and Wu, L.: Tropical Cyclones and Climate Change Assessment: Part II: Projected Response to Anthropogenic Warming, Bulletin of the American Meteorological Society, 101(3), E303–E322, https://doi.org/10.1175/BAMS-D-18-0194.1, 2020.

Knutson, T. R., McBride, J. L., Chan, J., Emanuel, K., Holland, G., Landsea, C., Held, I., Kossin, J. P., Srivastava, A. K. and Sugi, M.: Tropical cyclones and climate change, Nature Geoscience, 3, 157, https://doi.org/10.1038/ngeo779, 2010.

Knutson, T. R., Sirutis, J. J., Zhao, M., Tuleya, R. E., Bender, M., Vecchi, G. A., Villarini, G. and Chavas, D.: Global Projections of Intense Tropical Cyclone Activity for the Late Twenty-First Century from Dynamical Downscaling of CMIP5/RCP4.5 Scenarios, Journal of Climate, 28(18), 7203–7224, https://doi.org/10.1175/JCLI-D-15-0129.1, 2015.

Korty, R. L., Emanuel, K. A., Huber, M. and Zamora, R. A.: Tropical Cyclones Downscaled from Simulations with Very High Carbon Dioxide Levels, Journal of Climate, 30(2), 649–667, https://doi.org/10.1175/JCLI-D-16-0256.1, 2017.

Kossin, J. P.: A global slowdown of tropical-cyclone translation speed, Nature, 558(7708), 104–107, https://doi.org/10.1038/s41586-018-0158-3, 2018.

Kossin, J. P., Olander, T. L. and Knapp, K. R.: Trend Analysis with a New Global Record of Tropical Cyclone Intensity, Journal of Climate, 26(24), 9960–9976, https://doi.org/10.1175/JCLI-D-13-00262.1, 2013.

Kossin, J. P., Emanuel, K. A. and Vecchi, G. A.: The poleward migration of the location of tropical cyclone maximum intensity, Nature, 509(7500), 349–352, https://doi.org/10.1038/nature13278, 2014.

Kuhn, M. and Ríos-Rull, J.-V.: 2013 Update on the U.S. Earnings, Income, and Wealth Distributional Facts: A View from Macroeconomics, Quarterly Review, 37, https://doi.org/10.21034/qr.3711, 2016.

Kulshreshtha, S. N. and Klein, K. K.: Agricultural drought impact evaluation model: A systems approach, Agricultural Systems, 30(1), 81–96, https://doi.org/10.1016/0308-521X(89)90083-8, 1989.

Kummu, M., Taka, M. and Guillaume, J. H. A.: Gridded global datasets for Gross Domestic Product and Human Development Index over 1990–2015, Sci Data, 5(1), 180004, https://doi.org/10.1038/sdata.2018.4, 2018.

Lagmay, A. M. F., Agaton, R. P., Bahala, M. A. C., Briones, J. B. L. T., Cabacaba, K. M. C., Caro, C. V. C., Dasallas, L. L., Gonzalo, L. A. L., Ladiero, C. N., Lapidez, J. P., Mungcal, M. T. F., Puno, J. V. R., Ramos, M. M. A. C., Santiago, J., Suarez, J. K. and Tablazon, J. P.: Devastating storm surges of Typhoon Haiyan, International Journal of Disaster Risk Reduction, 11, 1–12, https://doi.org/10.1016/j.ijdrr.2014.10.006, 2015.

Lange, S.: WFDE5 over land merged with ERA5 over the ocean (W5E5), GFZ Data Services, V 1.0, https://doi.org/10.5880/pik.2019.023, 2019.

Lange, S., Volkholz, J., Geiger, T., Zhao, F., Vega, I., Veldkamp, T., Reyer, C. P. O., Warszawski, L., Huber, V., Jägermeyr, J., Schewe, J., Bresch, D. N., Büchner, M., Chang, J., Ciais, P., Dury, M., Emanuel, K., Folberth, C., Gerten, D., Gosling, S. N., Grillakis, M., Hanasaki, N., Henrot, A.-J., Hickler, T., Honda, Y., Ito, A., Khabarov, N., Koutroulis, A., Liu, W., Müller, C., Nishina, K., Ostberg, S., Müller Schmied, H., Seneviratne, S. I., Stacke, T., Steinkamp, J., Thiery, W., Wada, Y., Willner, S., Yang, H., Yoshikawa, M., Yue, C. and Frieler, K.: Projecting Exposure to Extreme Climate Impact Events Across Six Event Categories and Three Spatial Scales, Earth's Future, 8(12), e2020EF001616, https://doi.org/10.1029/2020EF001616, 2020.

Lanzante, J. R.: Uncertainties in tropical-cyclone translation speed, Nature, 570(7759), E6–E15, https://doi.org/10.1038/s41586-019-1223-2, 2019.

Lark, J.: ISO31000: Risk Management: a Practical Guide for SMEs, https://www.intracen.org/publication/ISO-31000-Risk-Management-A-practical-guide-for-SMEs/, last access: 19 February 2021, 2015.

Lee, C.-Y., Tippett, M. K., Sobel, A. H. and Camargo, S. J.: An Environmentally Forced Tropical Cyclone Hazard Model, Journal of Advances in Modeling Earth Systems, 10, 223–241, https://doi.org/10.1002/ 2017MS001186, 2018.

Lee, C.-Y., Camargo, S. J., Sobel, A. H. and Tippett, M. K.: Statistical–Dynamical Downscaling Projections of Tropical Cyclone Activity in a Warming Climate: Two Diverging Genesis Scenarios, Journal of Climate, 33(11), 4815–4834, https://doi.org/10.1175/JCLI-D-19-0452.1, 2020.

Lee, S., Chiang, K., Xiong, X., Sun, C. and Anderson, S.: The S-NPP VIIRS Day-Night Band On-Orbit Calibration/Characterization and Current State of SDR Products, Remote Sensing, 6(12), 12427–12446, https://doi.org/10.3390/rs61212427, 2014.

Leng, G. and Hall, J.: Crop yield sensitivity of global major agricultural countries to droughts and the projected changes in the future, Science of The Total Environment, 654, 811–821, https://doi.org/10.1016/j.scitotenv.2018.10.434, 2019.

Leyk, S., Gaughan, A. E., Adamo, S. B., Sherbinin, A. de, Balk, D., Freire, S., Rose, A., Stevens, F. R., Blankespoor, B., Frye, C., Comenetz, J., Sorichetta, A., MacManus, K., Pistolesi, L., Levy, M., Tatem, A. J. and Pesaresi, M.: The spatial allocation of population: a review of large-scale gridded population data products and their fitness for use, Earth System Science Data, 11(3), 1385–1409, https://doi.org/10.5194/essd-11-1385-2019, 2019.

Lu, J., Carbone, G. J. and Gao, P.: Detrending crop yield data for spatial visualization of drought impacts in the United States, 1895–2014, Agricultural and Forest Meteorology, 237–238, 196–208, https://doi.org/10.1016/j.agrformet.2017.02.001, 2017.

Lüthi, S.: Applying Machine Learning Methods to the Assessment of Tropical Cyclone Impacts, ETH Zurich https://doi.org/10.3929/ethz-b-000398592, last access: 5 June 2020, 2019.

Lyons, S. W.: U.S. Tropical Cyclone Landfall Variability: 1950–2002, Wea. Forecasting, 19(2), 473–480, https://doi.org/10.1175/1520-0434(2004)019<0473:UTCLV>2.0.CO;2, 2004.

Lyubchich, V., Gel, Y. R., Kilbourne, K. H., Miller, T. J., Newlands, N. K. and Smith, A. B.: Evaluating climate change impacts, 1st ed., Taylor & Francis Group, New York. https://doi.org/10.1201/9781351190831, last access: 18 November 2020, 2020.

Maltais, A. and Nykvist, B.: Understanding the role of green bonds in advancing sustainability, Journal of Sustainable Finance & Investment, 0(0), 1–20, https://doi.org/10.1080/20430795.2020.1724864, 2020.

Marx, A., Kumar, R., Thober, S., Rakovec, O., Wanders, N., Zink, M., Wood, E. F., Pan, M., Sheffield, J. and Samaniego, L.: Climate change alters low flows in Europe under global warming of 1.5, 2, and 3 °C, Hydrology and Earth System Sciences, 22(2), 1017–1032, https://doi.org/10.5194/hess-22-1017-2018, 2018.

Mas, E., Bricker, J., Kure, S., Adriano, B., Yi, C., Suppasri, A. and Koshimura, S.: Field survey report and satellite image interpretation of the 2013 Super Typhoon Haiyan in the Philippines, Nat. Hazards Earth Syst. Sci., 15(4), 805–816, https://doi.org/10.5194/nhess-15-805-2015, 2015.

Masson-Delmotte, V., Zhai, P., Pörtner, H., Roberts, D., Skea, J., Shukla, P., Pirani, A., Moufouma-Okia, W., Péan, C., Pidcock, R., and others: Global Warming of 1.5 Degree Celsius: IPCC Special Report on the Impacts of Global Warming of 1.5 Degree Celsius, Report, Intergovernmental Panel on Climate Change, Geneva, Switzerland. https://www.ipcc.ch/sr15, last access: 15 January 2021, 2018.

Mbow, C., Rosenzweig, C., Barioni, L. G., Benton, T. G., Herrero, M., Krishnapillai, M., Liwenga, E., Pradhan, P., Rivera-Ferre, M. G., Sapkota, T., Tubiello, F. N. and Xu, Y.: Food Security, in Climate Change and Land: an IPCC special report on climate change, desertification, land degradation, sustainable land management, food security, and greenhouse gas fluxes in terrestrial ecosystems [P.R. Shukla, J. Skea, E. Calvo Buendia, V. Masson-Delmotte, H.-O. Pörtner, D.C. Roberts, P. Zhai, R. Slade, S. Connors, R. van Diemen, M. Ferrat, E. Haughey, S. Luz, S. Neogi, M. Pathak, J. Petzold, J. Portugal Pereira, P. Vyas, E. Huntley, K. Kissick, M. Belkacemi, J. Malley, (eds.)]., pp. 437–550, In press, https://www.ipcc.ch/site/assets/uploads/sites/4/2021/02/08_Chapter-5_3.pdf, last access: 24 February 2021, 2019.

Mellander, C., Lobo, J., Stolarick, K. and Matheson, Z.: Night-Time Light Data: A Good Proxy Measure for Economic Activity?, edited by G. J.-P. Schumann, PLOS ONE, 10(10), e0139779, https://doi.org/10.1371/journal.pone.0139779, 2015.

Mendelsohn, R., Emanuel, K., Chonabayashi, S. and Bakkensen, L.: The impact of climate change on global tropical cyclone damage, Nature Climate Change, 2(3), 205–209, https://doi.org/10.1038/nclimate1357, 2012.

Met Office: Cartopy: a cartographic python library with a Matplotlib interface, Python, Exeter, Devon. https://scitools.org.uk/cartopy, last access: 12 January 2019, 2010.

Meza, I., Siebert, S., Döll, P., Kusche, J., Herbert, C., Eyshi Rezaei, E., Nouri, H., Gerdener, H., Popat, E., Frischen, J., Naumann, G., Vogt, J. V., Walz, Y., Sebesvari, Z. and Hagenlocher, M.: Global-scale drought risk assessment for agricultural systems, Natural Hazards and Earth System Sciences Discussions, 1–26, https://doi.org/10.5194/nhess-2019-255, 2019.

Monfreda, C., Ramankutty, N. and Foley, J. A.: Farming the planet: 2. Geographic distribution of crop areas, yields, physiological types, and net primary production in the year 2000, Global Biogeochemical Cycles, 22(1), https://doi.org/10.1029/2007GB002947, 2008.

Moon, I.-J., Kim, S.-H. and Chan, J. C. L.: Climate change and tropical cyclone trend, Nature, 570(7759), E3–E5, https://doi.org/10.1038/s41586-019-1222-3, 2019.

Müller, C., Elliott, J., Chryssanthacopoulos, J., Arneth, A., Balkovic, J., Ciais, P., Deryng, D., Folberth, C., Glotter, M., Hoek, S., Iizumi, T., Izaurralde, R. C., Jones, C., Khabarov, N., Lawrence, P., Liu, W., Olin, S., Pugh, T., Ray, D., Reddy, A., Rosenzweig, C., Ruane, A. C., Sakurai, G., Schmid, E., Skalsky, R., Song, C. X., Wang, X., de Wit, A. and Yang, H.: Global Gridded Crop Model evaluation: benchmarking, skills, deficiencies and implications, Geoscientific Model Development Discussions, 10, 1403–1422, https://doi.org/10.5194/gmd-2016-207, 2017.

Müller, C., Franke, J., Jägermeyr, J., Ruane, A. C., Elliott, J., Moyer, E., Heinke, J., Falloon, P., Folberth, C., Francois, L., Hank, T., Izaurralde, R. C., Jacquemin, I., Liu, W., Olin, S., Pugh, T., Williams, K. E. and Zabel, F.: Exploring uncertainties in global crop yield projections in a large ensemble of crop models and CMIP5 and CMIP6 climate scenarios, Environ. Res. Lett., https://doi.org/10.1088/1748-9326/abd8fc, 2021.

Munich Re: NatCatSERVICE Methodology. https://natcatservice.munichre.com/assets/pdf/180220_NCS_Methodology_en.pdf, last access: 23 March 2020, 2018.

Murakami, D. and Yamagata, Y.: Estimation of Gridded Population and GDP Scenarios with Spatially Explicit Statistical Downscaling, Sustainability, 11(7), 2106, https://doi.org/10.3390/su11072106, 2019.

Nakasu, T., Inokuchi, T., Shimokawa, S. and Watanabe, A.: 2009 Typhoon Ondoy and Pepeng Disasters in the Phillipines, National Research Institute for Earth Science and Disaster Prevention. https://www.researchgate.net/profile/Tadashi_Nakasu/publication/287205168_2009_Typhoon_Ondoy_and_Pepeng_Disasters_in_the_Phillipines/links/56d94d5008aebe4638baa2d8/2009-Typhoon-Ondoy-and-Pepeng-Disasters-in-the-Phillipines.pdf, last access: 3 July 2020, 2011.

NASA Earth Observatory: Earth at Night: Flat Maps, earthobservatory.nasa.gov/features/NightLights/page3.php, last access: 10 February 2020, 2017.

National Research Council (U.S.). Carbon Dioxide Assessment Committee: Changing Climate: Report of the Carbon Dioxide Assessment Committee, National Academies Press., 1983.

NDCC: Final Report on Tropical Storm Ondoy and Typhoon Pepeng, National Disaster Coordination Council. http://ndrrmc.gov.ph/attachments/article/1543/Update_Final_Report_TS_Ondoy_and_Pepeng_24-27SEP2009and30SEP-20OCT2009.pdf, last access: 26 January 2021, 2009a.

NDCC: SiteRep No. 15 on Humanitarian Coordination on Tropical Storm ONDOY, National Disaster Coordination Council. https://web.archive.org/web/20110530012257/http://210.185.184.53/ndccWeb/images/ndccWeb/ndcc_advisory/TC_ONDOY/ondoy15.pdf, last access: 25 March 2020, 2009b.

NDRRMC: Effects of Typhoon Juan, Sitrep No 17, National Disaster Risk Reduction and Management Council.

http://www.ndrrmc.gov.ph/attachments/article/1554/SitRep_No_17_Typhoon_Juan_Issued_On_22OCT2010_1800H.pdf, last access: 25 March 2020, 2010.

NDRRMC: Effects of Typhoon Pedring (Nesat), SitRep No 20, National Disaster Risk Reduction and Management Council. http://www.ndrrmc.gov.ph/attachments/article/1748/SitRep_No_20_re_Effects_of_Typhoon_PEDRING_as_of_05OCT2011_0600H.pdf, last access: 26 March 2020, 2011.

NDRRMC: Effects of Typhoon Pablo (Bopha), Sitrep No 38, National Disaster Risk Reduction and Management Council. https://reliefweb.int/sites/reliefweb.int/files/resources/NDRRMC%20Update%20Sitrep%20No%2038%20re%20Effects%20of%20Typhoon%20Pablo%20Bopha.pdf, last access: 25 March 2020, 2012.

NDRRMC: Effects of Typhoon Yolanda (Haiyan), Final Report, National Disaster Risk Reduction and Management Council. http://ndrrmc.gov.ph/attachments/article/1329/FINAL_REPORT_re_Effects_of_Typhoon_YOLANDA_HAIYAN_06-09NOV2013.pdf, last access: 26 January 2021, 2013.

NDRRMC: Effects of Typhoon Glenda (Rammasun), Final Report, National Disaster Risk Reduction and Management Council. http://www.ndrrmc.gov.ph/attachments/article/1293/Effects_of_Typhoon_Glenda_(RAMMASUN)_Final_Report_16SEP2014.pdf, last access: 25 March 2020, 2014.

Newbold, S. C.: Summary of the DICE model, p. 8, U.S. EPA, National Center for Environmental Economics, Washington DC, http://assets.fiercemarkets.net/public/sites/energy/reports/yosemitereport2.pdf, last access: 19 February 2021, 2010.

NGFS: Origin of the Network for Greening the Financial System, Network for Greening the Financial System https://www.ngfs.net/en/about-us/governance/origin-and-purpose, last access: 22 September 2020, 2017.

Nordhaus, W.: Integrated Assessment Models of Climate Change, National Bureau of Economic Research (NBER), Cambridge, MA. http://hdl.handle.net/10419/178753, last access: 9 December 2020, 2017.

Nordhaus, W.: 20. Critical Assumptions in the Stern Review on Climate Change, in Economics of the Environment: Selected Readings, Seventh Edition [Editor: Robert N. Stavins], Edward Elgar Publishing, Hants, England, https://www.e-elgar.com/shop/gbp/economics-of-the-environment-9781788972079.html, 2019.

Nordhaus, W. D. and Boyer, J.: Warming the World: Economic Models of Global Warming, The MIT Press, Cambridge, MA and London, England. https://doi.org/10.7551/mitpress/7158.001.0001, 2000.

Oasis LMF: Oasis Loss Modelling Framework | Open source catastrophe modelling platform, Oasis Loss Modelling Framework https://oasislmf.org/, last access: 11 February 2021, online.

O'Neill, B. C., Tebaldi, C., van Vuuren, D. P., Eyring, V., Friedlingstein, P., Hurtt, G., Knutti, R., Kriegler, E., Lamarque, J.-F., Lowe, J., Meehl, G. A., Moss, R., Riahi, K. and Sanderson, B. M.: The Scenario Model Intercomparison Project (ScenarioMIP) for CMIP6, Geosci. Model Dev., 9(9), 3461–3482, https://doi.org/10.5194/gmd-9-3461-2016, 2016.

Oppenheimer, M., Campos, M., Warren, R., Birkmann, J., Luber, G., O'Neill, B. and Takahashi, K.: Emergent Risks and Key Vulnerabilities, in Climate Change 2014: Impacts, Adaptation, and Vulnerability. Part A: Global andSectoral Aspects. Contribution of Working Group II to the Fifth Assessment Report of the Intergovernmental Panel on

Climate Change [Field, C.B., V.R. Barros, D.J. Dokken, K.J. Mach, M.D. Mastrandrea, T.E. Bilir,M. Chatterjee, K.L. Ebi, Y.O. Estrada, R.C. Genova, B. Girma, E.S. Kissel, A.N. Levy, S. MacCracken, P.R. Mastrandrea, and L.L. White (eds.)], pp. 1039–1099, Cambridge University Press, Cambridge, United Kingdom and New York, NY, USA, https://archive.ipcc.ch/pdf/assessment-report/ar5/wg2/WGIIAR5-FrontMatterA_FINAL.pdf, last access: 19 February 2021, 2014.

Organisation for Economic Co-operation and Development: OECD.Stat, https://stats.oecd.org/, last access: 31 January 2019, 2019.

OS-CLIMATE: Open Source - CLIMATE, https://www.os-climate.org/, last access: 22 September 2020, 2020.

Ostberg, S., Schewe, J., Childers, K. and Frieler, K.: Changes in crop yields and their variability at different levels of global warming, Earth System Dynamics, 9(2), 479–496, https://doi.org/10.5194/esd-9-479-2018, 2018.

Otto, F. E. L.: Attribution of Weather and Climate Events, Annual Review of Environment and Resources, 42(1), 627–646, https://doi.org/10.1146/annurev-environ-102016-060847, 2017.

Otto, F. E. L., Harrington, L. J., Frame, D., Boyd, E., Lauta, K. C., Wehner, M., Clarke, B., Raju, E., Boda, C., Hauser, M., James, R. A. and Jones, R. G.: Towards an inventory of the impacts of human-induced climate change, Bull. Amer. Meteor. Soc., 1–17, https://doi.org/10.1175/BAMS-D-20-0027.1, 2020.

Pachauri, R. K., Mayer, L. and Intergovernmental Panel on Climate Change, Eds.: Climate change 2014: synthesis report, Intergovernmental Panel on Climate Change, Geneva, Switzerland. https://archive.ipcc.ch/pdf/assessment-report/ar5/syr/AR5_SYR_FINAL_All_Topics.pdf, last access: 19 February 2021, 2015.

Paglia, E.: The Socio-scientific Construction of Global Climate Crisis, Geopolitics, 23(1), 96–123, https://doi.org/10.1080/14650045.2017.1328407, 2018.

Park, S., van de Lindt, J. W. and Li, Y.: Application of the hybrid ABV procedure for assessing community risk to hurricanes spatially, Nat Hazards, 68(2), 981–1000, https://doi.org/10.1007/s11069-013-0674-2, 2013.

Parry, M., Arnell, N., Hulme, M., Martens, P., Nicholls, R. and White, A.: The global impact of climate change: a new assessment, Global Environmental Change. https://d1wqtxts1xzle7.cloudfront.net/57153338/Parry_etal_GEC1999.pdf?1533725291=&response-content-disposition=inline%3B+filename%3DViewpoint_The_global_impact_of_climate_c.pdf&Expires=1613751526&Signature=VyYGlFjSe~Ks~J6QKCqx~H-ZqqrLdKrJymqiBlWBJANOn3mEo9eRRiY4bNFSlJRUv7NcF0yuKmf~oSfDkuaBk~vj86AzYKmCDrztuqDJCFgYHoiY0XhgQnHP3ousqMUPK2r0XxFx6buVoI6XHMito4Bu5IiwkEtr9AjgXcGBzI8clU87ZY0D7h-woeFtR~4-CF09eBj9OHxLE7fYgv6cmlbpHOv1ZVlKcMc0qkhOTHI9sJJH1BnVOwrwMbL2bdakPTj-y~TXVrV-4Nif6AIVLqwr7F0hqgVNys8QAJ69Im3l3ASZo3TzzdynFMMgMhorWRfv14R9LePmP1-IV~azSA__&Key-Pair-Id=APKAJLOHF5GGSLRBV4ZA, last access: 3 January 2021, 1999.

PCAF: Partnership for Carbon Accounting Financials, PCAF https://carbonaccountingfinancials.com/12/08/2019, last access: 22 September 2020, 2015.

Pielke, R. A.: Future economic damage from tropical cyclones: sensitivities to societal and climate changes, Philosophical Transactions of the Royal Society A: Mathematical, Physical and

Engineering Sciences, 365(1860), 2717–2729, https://doi.org/10.1098/rsta.2007.2086, 2007.

Pielke, R. A., Gratz, J., Landsea, C. W., Collins, D., Saunders, M. A. and Musulin, R.: Normalized Hurricane Damage in the United States: 1900–2005, Natural Hazards Review, 9(1), 29–42, https://doi.org/10.1061/(ASCE)1527-6988(2008)9:1(29), 2008.

Pinkovskiy, M. L.: Economic Discontinuities at Borders: Evidence from Satellite Data on Lights at Night, Working paper. http://citeseerx.ist.psu.edu/viewdoc/download?doi=10.1.1.800.2067&rep=rep1&type=pdf, last access: 3 January 2021, 2014.

Pittore, M., Wieland, M. and Fleming, K.: Perspectives on global dynamic exposure modelling for geo-risk assessment, Nat Hazards, 86(1), 7–30, https://doi.org/10.1007/s11069-016-2437-3, 2017.

Porio, E.: Vulnerability, Adaptation, and Resilience to Floods and Climate Change-Related Risks among Marginal, Riverine Communities in Metro Manila, Asian Journal of Social Science, 39(4), 425–445, https://doi.org/10.1163/156853111X597260, 2011.

Portmann, F. T., Siebert, S. and Döll, P.: MIRCA2000 - global monthly irrigated and rainfed crop areas around the year 2000: A new high-resolution data set for agricultural and hydrological modeling, Global Biogeochem. Cycles, 24(1), 1–24, https://doi.org/10.1029/2008GB003435, 2010.

Ramankutty, N., Evan, A. T., Monfreda, C. and Foley, J. A.: Farming the planet: 1. Geographic distribution of global agricultural lands in the year 2000, Global Biogeochemical Cycles, 22(1), https://doi.org/10.1029/2007GB002952, 2008.

Ray, D. K., Ramankutty, N., Mueller, N. D., West, P. C. and Foley, J. A.: Recent patterns of crop yield growth and stagnation, Nat Commun, 3, 1293, https://doi.org/10.1038/ncomms2296, 2012.

Ray, D. K., Gerber, J. S., MacDonald, G. K. and West, P. C.: Climate variation explains a third of global crop yield variability, Nature Communications, 6(1), 5989, https://doi.org/10.1038/ncomms6989, 2015.

Ray, D. K., West, P. C., Clark, M., Gerber, J. S., Prishchepov, A. V. and Chatterjee, S.: Climate change has likely already affected global food production, edited by Y. H. Jung, PLoS ONE, 14(5), e0217148, https://doi.org/10.1371/journal.pone.0217148, 2019.

Rendall, M.: Discounting, Climate Change, and the Ecological Fallacy, Ethics, 129(3), 441–463, https://doi.org/10.1086/701481, 2019.

Riahi, K., van Vuuren, D. P., Kriegler, E., Edmonds, J., O'Neill, B. C., Fujimori, S., Bauer, N., Calvin, K., Dellink, R., Fricko, O., Lutz, W., Popp, A., Cuaresma, J. C., Kc, S., Leimbach, M., Jiang, L., Kram, T., Rao, S., Emmerling, J., Ebi, K., Hasegawa, T., Havlik, P., Humpenöder, F., Da Silva, L. A., Smith, S., Stehfest, E., Bosetti, V., Eom, J., Gernaat, D., Masui, T., Rogelj, J., Strefler, J., Drouet, L., Krey, V., Luderer, G., Harmsen, M., Takahashi, K., Baumstark, L., Doelman, J. C., Kainuma, M., Klimont, Z., Marangoni, G., Lotze-Campen, H., Obersteiner, M., Tabeau, A. and Tavoni, M.: The Shared Socioeconomic Pathways and their energy, land use, and greenhouse gas emissions implications: An overview, Global Environmental Change, 42, 153–168, https://doi.org/10.1016/j.gloenvcha.2016.05.009, 2017.

Ridder, N. N., Pitman, A. J. and Ukkola, A. M.: Do CMIP6 Climate Models Simulate Global or Regional Compound Events Skillfully?, Geophysical Research Letters, 48(2), 1–11, https://doi.org/10.1029/2020GL091152, 2021.

Rigaud, K., Kanta, A. de S., Jones, B., Bergmann, J., Clement, V., Ober, K., Schewe, J., Adamo, S. B., McCusker, B., Heuser, S. and Midgley, A.: Groundswell: Preparing for Internal Climate Migration, The Worldbank, Washington, DC. http://hdl.handle.net/10986/29461, last access: 2 February 2021, 2018.

Risser, M. D. and Wehner, M. F.: Attributable Human-Induced Changes in the Likelihood and Magnitude of the Observed Extreme Precipitation during Hurricane Harvey, Geophysical Research Letters, 44(24), 12,457-12,464, https://doi.org/10.1002/2017GL075888, 2017.

Roberts, M. J., Camp, J., Seddon, J., Vidale, P. L., Hodges, K., Vanniere, B., Mecking, J., Haarsma, R., Bellucci, A., Scoccimarro, E., Caron, L.-P., Chauvin, F., Terray, L., Valcke, S., Moine, M.-P., Putrasahan, D., Roberts, C., Senan, R., Zarzycki, C. and Ullrich, P.: Impact of Model Resolution on Tropical Cyclone Simulation Using the HighResMIP–PRIMAVERA Multimodel Ensemble, J. Climate, 33(7), 2557–2583, https://doi.org/10.1175/JCLI-D-19-0639.1, 2020a.

Roberts, M. J., Camp, J., Seddon, J., Vidale, P. L., Hodges, K., Vannière, B., Mecking, J., Haarsma, R., Bellucci, A., Scoccimarro, E., Caron, L.-P., Chauvin, F., Terray, L., Valcke, S., Moine, M.-P., Putrasahan, D., Roberts, C. D., Senan, R., Zarzycki, C., Ullrich, P., Yamada, Y., Mizuta, R., Kodama, C., Fu, D., Zhang, Q., Danabasoglu, G., Rosenbloom, N., Wang, H. and Wu, L.: Projected Future Changes in Tropical Cyclones Using the CMIP6 HighResMIP Multimodel Ensemble, Geophysical Research Letters, 47(14), e2020GL088662, https://doi.org/10.1029/2020GL088662, 2020b.

Román, M. O., Wang, Z., Sun, Q., Kalb, V., Miller, S. D., Molthan, A., Schultz, L., Bell, J., Stokes, E. C., Pandey, B., Seto, K. C., Hall, D., Oda, T., Wolfe, R. E., Lin, G., Golpayegani, N., Devadiga, S., Davidson, C., Sarkar, S., Praderas, C., Schmaltz, J., Boller, R., Stevens, J., Ramos González, O. M., Padilla, E., Alonso, J., Detrés, Y., Armstrong, R., Miranda, I., Conte, Y., Marrero, N., MacManus, K., Esch, T. and Masuoka, E. J.: NASA's Black Marble nighttime lights product suite, Remote Sensing of Environment, 210, 113–143, https://doi.org/10.1016/j.rse.2018.03.017, 2018.

Rosenzweig, C. and Neofotis, P.: Detection and attribution of anthropogenic climate change impacts: Anthropogenic climate change impacts, WIREs Clim Change, 4(2), 121–150, https://doi.org/10.1002/wcc.209, 2013.

Rosenzweig, C., Jones, J. W., Hatfield, J. L., Ruane, A. C., Boote, K. J., Thorburn, P., Antle, J. M., Nelson, G. C., Porter, C., Janssen, S., Asseng, S., Basso, B., Ewert, F., Wallach, D., Baigorria, G. and Winter, J. M.: The Agricultural Model Intercomparison and Improvement Project (AgMIP): Protocols and pilot studies, Agricultural and Forest Meteorology, 170, 166–182, https://doi.org/10.1016/j.agrformet.2012.09.011, 2013.

Rosenzweig, C., Elliott, J., Deryng, D., Ruane, A. C., Müller, C., Arneth, A., Boote, K. J., Folberth, C., Glotter, M., Khabarov, N., Neumann, K., Piontek, F., Pugh, T. A. M., Schmid, E., Stehfest, E., Yang, H. and Jones, J. W.: Assessing agricultural risks of climate change in the 21st century in a global gridded crop model intercomparison, PNAS, 111(9), 3268–3273, https://doi.org/10.1073/pnas.1222463110, 2014.

Rosenzweig, C., Arnell, N. W., Ebi, K. L., Lotze-Campen, H., Raes, F., Rapley, C., Smith, M. S., Cramer, W., Frieler, K., Reyer, C. P. O., Schewe, J., van Vuuren, D. and Warszawski, L.: Assessing inter-sectoral climate change risks: the role of ISIMIP, Environ. Res. Lett., 12(1), 010301, https://doi.org/10.1088/1748-9326/12/1/010301, 2017.

Saltelli, A.: Sensitivity Analysis for Importance Assessment, Risk Analysis, 22(3), 579–590, https://doi.org/10.1111/0272-4332.00040, 2002.

SASB: Sustainability Accounting Standards Board (SASB), SASB https://www.sasb.org/about/, last access: 10 February 2021, online.

Sauer, I., Reese, R., Otto, C., Geiger, T., Willner, S. N., Guillod, B., Bresch, D. N. and Frieler, K.: Climate Signals in River Flood Damages Emerge under Sound Regional Disaggregation, Nature Communications, https://doi.org/10.21203/rs.3.rs-37259/v1, in press.

SBTi: Foundations of Science-based Target Setting, https://sciencebasedtargets.org/resources/files/foundations-of-SBT-setting.pdf, last access: 2 February 2021, 2019.

Schauberger, B., Archontoulis, S., Arneth, A., Balkovic, J., Ciais, P., Deryng, D., Elliott, J., Folberth, C., Khabarov, N., Müller, C., Pugh, T. A. M., Rolinski, S., Schaphoff, S., Schmid, E., Wang, X., Schlenker, W. and Frieler, K.: Consistent negative response of US crops to high temperatures in observations and crop models, Nature Communications, 8, 13931, https://doi.org/10.1038/ncomms13931, 2017.

Schleussner, C.-F., Deryng, D., Müller, C., Elliott, J., Saeed, F., Folberth, C., Liu, W., Wang, X., Pugh, T. A. M., Thiery, W., Seneviratne, S. I. and Rogelj, J.: Crop productivity changes in 1.5 °C and 2 °C worlds under climate sensitivity uncertainty, Environ. Res. Lett., 13(6), 064007, https://doi.org/10.1088/1748-9326/aab63b, 2018.

Schneider, P. J. and Schauer, B. A.: HAZUS—Its Development and Its Future, Natural Hazards Review, 7(2), 40–44, https://doi.org/10.1061/(ASCE)1527-6988(2006)7:2(40), 2006.

Schreck, C. J., Knapp, K. R. and Kossin, J. P.: The Impact of Best Track Discrepancies on Global Tropical Cyclone Climatologies using IBTrACS, Mon. Wea. Rev., 142(10), 3881–3899, https://doi.org/10.1175/MWR-D-14-00021.1, 2014.

Sealy, K. S. and Strobl, E.: A hurricane loss risk assessment of coastal properties in the caribbean: Evidence from the Bahamas, Ocean & Coastal Management, 149, 42–51, https://doi.org/10.1016/j.ocecoaman.2017.09.013, 2017.

Sharmila, S. and Walsh, K. J. E.: Recent poleward shift of tropical cyclone formation linked to Hadley cell expansion, Nature Climate Change, 8(8), 730–736, https://doi.org/10.1038/s41558-018-0227-5, 2018.

Shishlov, I., Morel, R. and Cochran, I.: Beyond transparency: unlocking the full potential of green bonds, Institute for Climate Economics I4CE. https://www.i4ce.org/download/unlocking-the-potential-of-green-bonds/, last access: 2 February 2021, 2016.

Sitch, S., Huntingford, C., Gedney, N., Levy, P. E., Lomas, M., Piao, S. L., Betts, R., Ciais, P., Cox, P., Friedlingstein, P., Jones, C. D., Prentice, I. C. and Woodward, F. I.: Evaluation of the terrestrial carbon cycle, future plant geography and climate-carbon cycle feedbacks using five Dynamic Global Vegetation Models (DGVMs), Global Change Biology, 14(9), 2015–2039, https://doi.org/10.1111/j.1365-2486.2008.01626.x, 2008.

Skelton, M., Fischer, A. M., Liniger, M. A. and Bresch, D. N.: Who is 'the user' of climate services? Unpacking the use of national climate scenarios in Switzerland beyond sectors, numeracy and the research–practice binary, Climate Services, 15, 100113, https://doi.org/10.1016/j.cliser.2019.100113, 2019.

Small, C., Pozzi, F. and Elvidge, C. D.: Spatial analysis of global urban extent from DMSP-OLS night lights, Remote Sensing of Environment, 96(3), 277–291, https://doi.org/10.1016/j.rse.2005.02.002, 2005.

Socioeconomic Data and Applications Center (SEDAC): Country-level Information and Sources Revision 10. http://sedac.ciesin.columbia.edu/data/collection/gpw-v4/documentation, last access: 4 April 2020, 2017.

Soria, J. L. A., Switzer, A. D., Villanoy, C. L., Fritz, H. M., Bilgera, P. H. T., Cabrera, O. C., Siringan, F. P., Maria, Y. Y.-Sta., Ramos, R. D. and Fernandez, I. Q.: Repeat Storm Surge Disasters of Typhoon Haiyan and Its 1897 Predecessor in the Philippines, Bull. Amer. Meteor. Soc., 97(1), 31–48, https://doi.org/10.1175/BAMS-D-14-00245.1, 2015.

Stevanović, M., Popp, A., Lotze-Campen, H., Dietrich, J. P., Müller, C., Bonsch, M., Schmitz, C., Bodirsky, B. L., Humpenöder, F. and Weindl, I.: The impact of high-end climate change on agricultural welfare, Science Advances, 2(8), e1501452, https://doi.org/10.1126/sciadv.1501452, 2016.

Stott, P. A., Stone, D. A. and Allen, M. R.: Human contribution to the European heatwave of 2003, Nature, 432(7017), 610–614, https://doi.org/10.1038/nature03089, 2004.

Stott, P. A., Christidis, N., Otto, F. E. L., Sun, Y., Vanderlinden, J.-P., Oldenborgh, G. J. van, Vautard, R., Storch, H. von, Walton, P., Yiou, P. and Zwiers, F. W.: Attribution of extreme weather and climate-related events, WIREs Climate Change, 7(1), 23–41, https://doi.org/10.1002/wcc.380, 2016.

Strobl, E.: The Impact of Typhoons on Economic Activity in the Philippines: Evidence from Nightlight Intensity, ADB Economics Working Papers Series, (589), 28, https://doi.org/10.22617/WPS190278-2, 2019.

Sutton, P., Elvidge, C. and Ghosh, T.: Estimation of gross domestic product at sub-national scales using nighttime satellite imagery, International Journal of Ecological Economics & Statistics. http://urizen-geography.nsm.du.edu/psutton/AAA_Sutton_WebPage/Sutton/Publications/Sut_Pub_13.pdf, last access: 15 January 2021, 2007.

Sutton, P. C. and Costanza, R.: Global estimates of market and non-market values derived from nighttime satellite imagery, land cover, and ecosystem service valuation, Ecological Economics, 41(3), 509–527, https://doi.org/10.1016/S0921-8009(02)00097-6, 2002.

Swiss Re Institute: SIGMA - Natural catastrophes in times of economic accumulation and climate change, 02/2020. https://www.swissre.com/dam/jcr:85598d6e-b5b5-4d4b-971e-5fc9eee143fb/sigma-2-2020-en.pdf, last access: 29 May 2020, 2020.

Taylor, K. E., Stouffer, R. J. and Meehl, G. A.: An Overview of CMIP5 and the Experiment Design, Bulletin of the American Meteorological Society, 93(4), 485–498, https://doi.org/10.1175/BAMS-D-11-00094.1, 2012.

TCFD: Annex - Implementing the Recommendations of the Task Force on Climate-related Financial Disclosures, TCFD. https://www.fsb-tcfd.org/wp-content/uploads/2017/12/FINAL-TCFD-Annex-Amended-121517.pdf, last access: 8 November 2018, 2017.

TCFD: Task Force on Climate-related Financial Disclosures - Web Page, Task Force on Climate-Related Financial Disclosures https://www.fsb-tcfd.org/about/, last access: 10 February 2021, online.

The Linux Foundation: New LF Climate Finance Foundation to Host Open Source Initiative to Address Climate Risk and Opportunity in Financial Sector, LF Climate Finance Foundation https://www.linuxfoundation.org/press-release/2020/09/new-lf-climate-finance-foundation-to-host-open-source-initiative-to-address-climate-risk-and-opportunity-in-financial-sector/, last access: 22 September 2020, 2020.

Thiery, W., Visser, A. J., Fischer, E. M., Hauser, M., Hirsch, A. L., Lawrence, D. M., Lejeune, Q., Davin, E. L. and Seneviratne, S. I.: Warming of hot extremes alleviated by expanding irrigation, Nat Commun, 11(1), 1–7, https://doi.org/10.1038/s41467-019-14075-4, 2020.

Tigchelaar, M., Battisti, D. S., Naylor, R. L. and Ray, D. K.: Future warming increases probability of globally synchronized maize production shocks, PNAS, 115(26), 6644–6649, https://doi.org/10.1073/pnas.1718031115, 2018.

UNDRR: GAR 2013. From Shared Risk to Shared Value: the Business Case for Disaster Risk Reduction, UN Office for Disaster Risk Reduction, Geneva, Switzerland. https://www.preventionweb.net/english/hyogo/gar/2013/en/home/index.html, last access: 6 May 2020, 2013.

UNEPFI: United Nations Environment – Finance Initiative Statement, https://www.unepfi.org/about/unep-fi-statement/, last access: 22 September 2020, 1992.

UNEPFI: United Nations-convened Net-Zero Asset Owner Alliance, https://www.unepfi.org/net-zero-alliance/, last access: 22 September 2020, 2019.

UNISDR: Terminology on Disaster Risk Reduction, United Nations Publications, Geneva, Switzerland., 2009.

Van Oldenborgh, G. J., Wiel, K. van der, Sebastian, A., Singh, R., Arrighi, J., Otto, F., Haustein, K., Li, S., Vecchi, G. and Cullen, H.: Attribution of extreme rainfall from Hurricane Harvey, August 2017, Environ. Res. Lett., 12(12), 124009, https://doi.org/10.1088/1748-9326/aa9ef2, 2017.

Vanuytrecht, E. and Thorburn, P. J.: Responses to atmospheric CO2 concentrations in crop simulation models: a review of current simple and semicomplex representations and options for model development, Global Change Biology, 23(5), 1806–1820, https://doi.org/10.1111/gcb.13600, 2017.

van Vliet, M. T. H., Wiberg, D., Leduc, S. and Riahi, K.: Power-generation system vulnerability and adaptation to changes in climate and water resources, Nature Clim Change, 6(4), 375–380, https://doi.org/10.1038/nclimate2903, 2016.

Vogel, M. M., Zscheischler, J., Wartenburger, R., Dee, D. and Seneviratne, S. I.: Concurrent 2018 Hot Extremes Across Northern Hemisphere Due to Human-Induced Climate Change, Earth's Future, 7(7), 692–703, https://doi.org/10.1029/2019EF001189, 2019.

Wahiduzzaman, M., Oliver, E. C. J., Wotherspoon, S. J. and Holbrook, N. J.: A climatological model of North Indian Ocean tropical cyclone genesis, tracks and landfall, Clim Dyn, 49(7), 2585–2603, https://doi.org/10.1007/s00382-016-3461-4, 2017.

Walsh, K. J. E., Camargo, S. J., Vecchi, G. A., Daloz, A. S., Elsner, J., Emanuel, K., Horn, M., Lim, Y.-K., Roberts, M., Patricola, C., Scoccimarro, E., Sobel, A. H., Strazzo, S., Villarini, G., Wehner, M., Zhao, M., Kossin, J. P., LaRow, T., Oouchi, K., Schubert, S., Wang, H., Bacmeister, J., Chang, P., Chauvin, F., Jablonowski, C., Kumar, A., Murakami, H., Ose, T., Reed, K. A., Saravanan, R., Yamada, Y., Zarzycki, C. M., Vidale, P. L., Jonas, J. A. and Henderson, N.: Hurricanes and Climate: The U.S. CLIVAR Working Group on Hurricanes, Bulletin of the American Meteorological Society, 96(6), 997–1017, https://doi.org/10.1175/BAMS-D-13-00242.1, 2015.

Walsh, K. J. E., McBride, J. L., Klotzbach, P. J., Balachandran, S., Camargo, S. J., Holland, G., Knutson, T. R., Kossin, J. P., Lee, T., Sobel, A. and Sugi, M.: Tropical cyclones and climate change, Wiley Interdisciplinary Reviews: Climate Change, 7(1), 65–89, https://doi.org/10.1002/wcc.371, 2016.

Ward, P. J., Blauhut, V., Bloemendaal, N., Daniell, J. E., Ruiter, M. C. de, Duncan, M. J., Emberson, R., Jenkins, S. F., Kirschbaum, D., Kunz, M., Mohr, S., Muis, S., Riddell, G. A., Schäfer, A., Stanley, T., Veldkamp, T. I. E. and Winsemius, H. C.: Review article: Natural hazard risk assessments at the global scale, Natural Hazards and Earth System Sciences, 20(4), 1069–1096, https://doi.org/10.5194/nhess-20-1069-2020, 2020.

Warszawski, L., Frieler, K., Huber, V., Piontek, F., Serdeczny, O. and Schewe, J.: The Inter-Sectoral Impact Model Intercomparison Project (ISI–MIP): Project framework, Proceedings of the National Academy of Sciences, 111(9), 3228–3232, https://doi.org/10.1073/pnas.1312330110, 2014.

Weinkle, J., Landsea, C., Collins, D., Musulin, R., Crompton, R. P., Klotzbach, P. J. and Pielke, R.: Normalized hurricane damage in the continental United States 1900–2017, Nat Sustain, 1(12), 808–813, https://doi.org/10.1038/s41893-018-0165-2, 2018.

Wiebe, K., Lotze-Campen, H., Sands, R., Tabeau, A., Mensbrugghe, D. van der, Biewald, A., Bodirsky, B., Islam, S., Kavallari, A., Mason-D'Croz, D., Müller, C., Popp, A., Robertson, R., Robinson, S., Meijl, H. van and Willenbockel, D.: Climate change impacts on agriculture in 2050 under a range of plausible socioeconomic and emissions scenarios, Environ. Res. Lett., 10(8), 085010, https://doi.org/10.1088/1748-9326/10/8/085010, 2015.

World Bank: Building the World Bank's Wealth Accounts: Methods and Data, Environment and Natural Resources Global Practice, World Bank. https://development-data-hub-s3-public.s3.amazonaws.com/ddhfiles/94641/wealth-methodology-january-30-2018_4_0.pdf, last access: 14 January 2019, 2018.

World Bank: Wealth Accounting, https://datacatalog.worldbank.org/dataset/wealth-accounting, last access: 2 February 2021, 2019.

World Bank: World Bank Open Data, https://data.worldbank.org/, last access: 10 February 2020, online.

WRI: Global Power Plant Database, https://datasets.wri.org/dataset/globalpowerplantdatabase, last access: 2 February 2021, 2018.

Yamazaki, D., Kanae, S., Kim, H. and Oki, T.: A physically based description of floodplain inundation dynamics in a global river routing model, Water Resources Research, 47(4), https://doi.org/10.1029/2010WR009726, 2011.

Yamin, L. E., Hurtado, A. I., Barbat, A. H. and Cardona, O. D.: Seismic and wind vulnerability assessment for the GAR-13 global risk assessment, International Journal of Disaster Risk Reduction, 10, 452–460, https://doi.org/10.1016/j.ijdrr.2014.05.007, 2014.

Yumul, G. P., Cruz, N. A., Servando, N. T. and Dimalanta, and C. B.: The meteorologically abnormal year of 2006 and natural disasters in the Philippines, Episodes Journal of International Geoscience, 31(4), 378–383, https://doi.org/10.18814/epiiugs/2008/v31i4/002, 2008.

Yumul, G. P., Cruz, N. A., Servando, N. T. and Dimalanta, C. B.: Extreme weather events and related disasters in the Philippines, 2004–08: a sign of what climate change will mean?, Disasters, 35(2), 362–382, https://doi.org/10.1111/j.1467-7717.2010.01216.x, 2011.

Yumul, G. P., Servando, N. T., Suerte, L. O., Magarzo, M. Y., Juguan, L. V. V. and Dimalanta, C. B.: Tropical cyclone–southwest monsoon interaction and the 2008 floods and landslides in Panay island, central Philippines: meteorological and geological factors, Nat Hazards, 62(3), 827–840, https://doi.org/10.1007/s11069-012-0109-5, 2012.

Zhang, Q., Wu, L. and Liu, Q.: Tropical Cyclone Damages in China 1983–2006, Bull. Amer. Meteor. Soc., 90(4), 489–496, https://doi.org/10.1175/2008BAMS2631.1, 2009.

Zhao, N., Samson, E. L. and Currit, N. A.: Nighttime-Lights-Derived Fossil Fuel Carbon Dioxide Emission Maps and Their Limitations, Photogram Engng Rem Sens, 81(12), 935–943, https://doi.org/10.14358/PERS.81.12.935, 2015.

Zhao, N., Liu, Y., Cao, G., Samson, E. L. and Zhang, J.: Forecasting China's GDP at the pixel level using nighttime lights time series and population images, GIScience & Remote Sensing, 54(3), 407–425, https://doi.org/10.1080/15481603.2016.1276705, 2017.

Zscheischler, J., Westra, S., Hurk, B. J. J. M. van den, Seneviratne, S. I., Ward, P. J., Pitman, A., AghaKouchak, A., Bresch, D. N., Leonard, M., Wahl, T. and Zhang, X.: Future climate risk from compound events, Nature Clim Change, 8(6), 469–477, https://doi.org/10.1038/s41558-018-0156-3, 2018.

Zscheischler, J., Martius, O., Westra, S., Bevacqua, E., Raymond, C., Horton, R. M., van den Hurk, B., AghaKouchak, A., Jézéquel, A., Mahecha, M. D., Maraun, D., Ramos, A. M., Ridder, N. N., Thiery, W. and Vignotto, E.: A typology of compound weather and climate events, Nat Rev Earth Environ, https://doi.org/10.1038/s43017-020-0060-z, 2020.

Zumwald, M., Knüsel, B., Baumberger, C., Hadorn, G. H., Bresch, D. N. and Knutti, R.: Understanding and assessing uncertainty of observational climate datasets for model evaluation using ensembles, WIREs Climate Change, 11(5), e654, https://doi.org/10.1002/wcc.654, 2020.

A. Supplementary Material to Chapter 2

Table A1: List of countries used for evaluation with the number of regions on the administrative level 1, the World Bank income group 2016, and GRP data source with URLs as accessed in January 2019. The income groups are low income (1), lower-middle income (2), upper-middle income (3), and high income (4). In total, GRP data for 507 regions in 14 countries were used.

Country	Regions	Income group	Data source	Reference year
Australia	8	4	Australian Bureau of Statistics, http://www.abs.gov.au/AUSSTATS/abs@.nsf/DetailsPage/5220.02016-17?OpenDocument (last access: 5 February 2019)	2016
Brazil	27	3	OECD.Stat, https://stats.oecd.org/ (last access: 5 February 2019)	2015
Canada	14	4	OECD.Stat, https://stats.oecd.org/	2016
Switzerland	26	4	Swiss Federal Statistical Office, https://www.bfs.admin.ch/bfs/en/home/statistics/national-economy/national-accounts/gross-domestic-product-canton.assetdetail.6369918.html (last access: 5 February 2019)	2014
China	31	3	National Bureau of Statistics China, http://data.stats.gov.cn/english/easyquery.htm?cn=E0103 (last access: 5 February 2019)	2015
Germany	16	4	Statistische Ämter des Bundes und der Länder, https://web.archive.org/web/20110717065817/http://www.statistik-portal.de/Statistik-Portal/en/en_jb27_jahrtab65.asp (last access: 5 February 2019)	2017
France	101	4	Eurostat, http://ec.europa.eu/eurostat/web/regions/data/database (last access: 5 February 2019)	2015
Indonesia	33	2	OECD.Stat, https://stats.oecd.org/	2012
India	30	2	Open Government Data Platform India, https://data.gov.in/catalog/capita-state-domestic-product-current-prices#web_catalog_tabs_block_10 (last access: 5 February 2019)	2013/14
Japan	47	4	Cabinet Office Government of Japan, http://www.esri.cao.go.jp/jp/sna/data/data_list/kenmin/files/contents/main_h26.html (last access: 5 February 2019)	2014
Mexico	32	3	National Institute of Statistics and Geography of Mexico, https://www.inegi.org.mx/sistemas/bie/?idserPadre=10200070#D10200070 (last access: 5 February 2019)	2016
Turkey	81	3	OECD.Stat, https://stats.oecd.org/	2014
USA	52	4	US Bureau of Economic Analysis, https://www.bea.gov/data/gdp/gdp-state (last access: 12 February 2019)	2016
South Africa	9	3	OECD.Stat, https://stats.oecd.org/	2013

Table A2: (a) Comparison of ρ for 10 exponent combinations and 14 countries: Australia (AUS), Brazil (BRA), Canada (CAN), Switzerland (CHE), China (CHN), Germany (DEU), France (FRA), Indonesia (IDN), India (IND), Japan (JPN), Mexico (MEX), Turkey (TUR), the United States of America (USA), and South Africa (ZAF). Best fit would mean $\rho = 1$. Linear correlation is statistically significant with a p value lower than 0.05 for all shown countries and combinations. (b) Comparison of β for 10 exponent combinations and 14 countries: Australia (AUS), Brazil (BRA), Canada (CAN), Switzerland (CHE), China (CHN), Germany (DEU), France (FRA), Indonesia (IDN), India (IND), Japan (JPN), Mexico (MEX), Turkey (TUR), the United States of America (USA), and South Africa (ZAF). Best fit would mean $\beta = 1$. Linear correlation is statistically significant with a p value lower than 0.05 for all shown countries and combinations. (c) Comparison of RMSF for 10 exponent combinations and 14 countries: Australia (AUS), Brazil (BRA), Canada (CAN), Switzerland (CHE), China (CHN), Germany (DEU), France (FRA), Indonesia (IDN), India (IND), Japan (JPN), Mexico (MEX), Turkey (TUR), the United States of America (USA), and South Africa (ZAF). Best fit would mean RMSF $= 1$.

(a) ρ	AUS	BRA	CAN	CHE	CHN	DEU	FRA	IDN	IND	JPN	MEX	TUR	USA	ZAF
Lit^{1}Pop^1	0.99	0.98	0.99	0.94	0.93	0.90	0.92	0.90	0.82	0.93	0.76	0.99	0.98	0.99
Lit^1	0.92	0.92	0.99	0.81	0.95	0.96	0.37	0.75	0.81	0.59	0.36	0.53	0.76	0.85
Lit^2	0.93	0.96	0.99	0.89	0.96	0.94	0.47	0.79	0.82	0.73	0.47	0.66	0.78	0.95
Lit^3	0.94	0.96	1.00	0.91	0.95	0.93	0.51	0.83	0.83	0.79	0.53	0.72	0.79	0.97
Lit^4	0.94	0.97	1.00	0.93	0.95	0.92	0.54	0.85	0.84	0.82	0.57	0.76	0.80	0.97
Lit^5	0.94	0.97	1.00	0.93	0.95	0.91	0.56	0.87	0.84	0.84	0.60	0.79	0.81	0.97
Pop^1	0.99	0.96	1.00	0.97	0.85	0.98	0.84	0.80	0.79	0.92	0.66	0.98	0.98	0.92
Pop^2	0.97	0.97	0.98	0.81	0.82	0.88	0.86	0.86	0.80	0.96	0.85	0.96	0.86	0.97
Lit^{2}Pop^1	0.99	0.99	0.99	0.89	0.90	0.86	0.92	0.90	0.87	0.94	0.78	0.99	0.98	0.99
Lit^{3}Pop^1	0.99	0.99	0.99	0.86	0.89	0.84	0.93	0.89	0.88	0.95	0.79	0.99	0.98	0.98

(b) β	AUS	BRA	CAN	CHE	CHN	DEU	FRA	IDN	IND	JPN	MEX	TUR	USA	ZAF
Lit^{1}Pop^1	1.02	0.79	1.10	1.07	1.05	1.01	0.96	1.21	0.96	1.28	0.76	1.49	1.01	1.07
Lit^1	0.82	0.55	0.90	0.67	0.93	0.89	0.22	0.76	0.84	0.33	0.22	0.17	0.57	0.54
Lit^2	0.82	0.61	0.96	0.77	1.03	0.89	0.32	0.83	0.82	0.52	0.32	0.26	0.62	0.87
Lit^3	0.82	0.63	0.99	0.84	1.06	0.88	0.38	0.86	0.82	0.64	0.38	0.32	0.65	1.05
Lit^4	0.82	0.64	1.01	0.89	1.07	0.86	0.41	0.88	0.81	0.73	0.42	0.36	0.66	1.17
Lit^5	0.82	0.64	1.02	0.93	1.07	0.85	0.44	0.90	0.81	0.80	0.45	0.39	0.67	1.26
Pop^1	1.01	0.66	1.01	0.87	0.68	0.92	0.47	0.77	0.84	0.66	0.55	0.61	0.88	0.65
Pop^2	1.23	0.97	1.21	1.16	0.82	1.01	2.42	1.40	1.19	1.91	1.26	2.37	1.52	1.40
Lit^{2}Pop^1	1.03	0.81	1.12	1.12	1.04	0.99	1.09	1.26	1.01	1.45	0.82	1.70	1.04	1.22
Lit^{3}Pop^1	1.03	0.82	1.13	1.15	1.03	0.96	1.16	1.29	1.04	1.55	0.86	1.80	1.06	1.32

(c) RMSF	AUS	BRA	CAN	CHE	CHN	DEU	FRA	IDN	IND	JPN	MEX	TUR	USA	ZAF
Lit^{1}Pop^1	1.31	1.54	1.80	2.70	1.37	1.44	1.93	5.30	2.61	2.86	1.55	3.76	1.37	1.11
Lit^1	1.28	1.93	1.69	1.74	1.50	1.44	1.89	2.00	2.10	1.52	1.93	2.03	1.94	1.58
Lit^2	1.28	1.83	1.51	1.85	1.42	1.36	1.68	1.86	2.03	1.41	1.77	1.77	1.81	1.37
Lit^3	1.32	1.80	1.48	2.18	1.40	1.38	1.63	1.81	2.02	1.47	1.69	1.68	1.77	1.27
Lit^4	1.34	1.79	1.49	2.65	1.40	1.40	1.63	1.79	2.04	1.58	1.64	1.64	1.77	1.24
Lit^5	1.37	1.78	1.53	3.25	1.40	1.42	1.66	1.79	2.06	1.70	1.60	1.63	1.77	1.23
Pop^1	1.27	1.72	1.29	1.36	1.48	1.32	1.38	2.04	1.73	1.21	1.69	1.59	1.32	1.28
Pop^2	1.67	1.73	3.50	3.18	1.61	1.64	4.73	5.93	4.01	5.34	1.81	22.4	2.12	1.54
Lit^{2}Pop^1	1.37	1.53	2.07	4.18	1.40	1.60	2.41	6.80	3.00	4.16	1.53	6.36	1.44	1.22
Lit^{3}Pop^1	1.41	1.53	2.27	5.74	1.41	1.69	2.75	7.64	3.23	5.29	1.52	8.31	1.50	1.32

Table A3: Comparison of three skill metrics measuring the fit between modeled and reference nGRP. The table shows the median and IQR over 14 countries computed from the data in Table A2.2a–c. Perfect fit would mean a value of 1 for each metric.

	ρ		β		RMSF	
	Median	IQR	Median	IQR	Median	IQR
Lit^1Pop^1	0.94	0.09	1.03	0.12	1.67	1.29
Lit^1	0.81	0.29	0.62	0.44	1.82	0.40
Lit^2	0.85	0.21	0.80	0.32	1.72	0.41
Lit^3	0.87	0.16	0.82	0.24	1.65	0.38
Lit^4	0.89	0.14	0.82	0.24	1.64	0.36
Lit^5	0.89	0.13	0.82	0.27	1.65	0.33
Pop^1	0.94	0.14	0.73	0.22	1.37	0.37
Pop^2	0.87	0.12	1.24	0.33	2.65	2.87
Lit^2Pop^1	0.93	0.09	1.07	0.18	1.83	2.41
Lit^3Pop^1	0.94	0.10	1.10	0.23	1.98	3.27

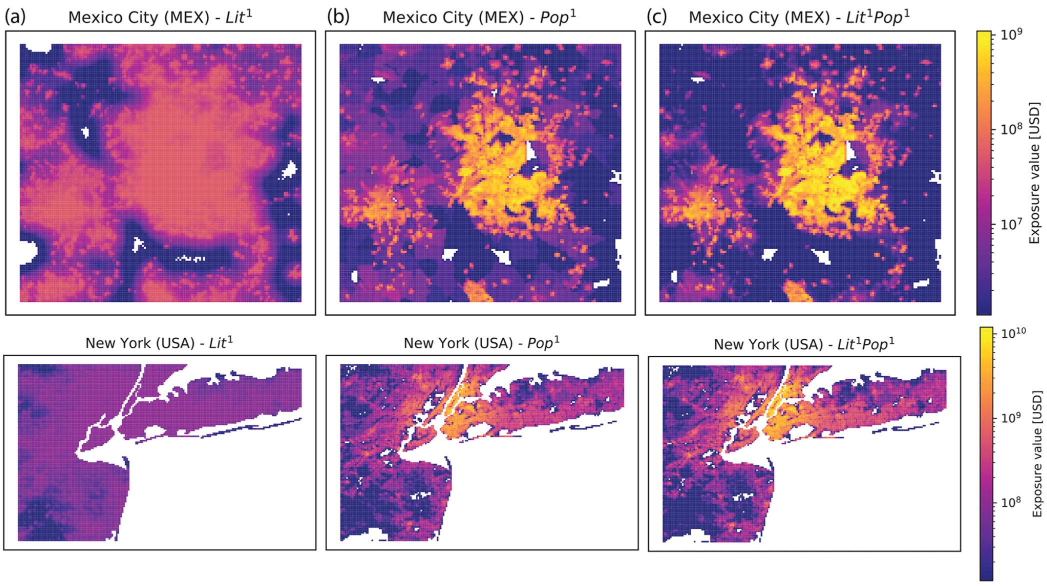

Figure A1: Maps of disaggregated asset exposure value. Values are spatially distributed proportionally to nightlight intensity of 2016 (Lit^1, a), population count as of 2015 (Pop^1, b), and the product of both (Lit^1Pop^1, c) for Mexico City (MEX) and New York (USA). The maps are restricted to the wider metropolitan areas of Mexico City (18.9–20° N, 99.8–98.6° W) and New York (40–41° N, 74.6–73° W). The color bar shows asset exposure values in current US dollars in 2014.

Supplement

The supplement related to this article (including Tables S1 & S2 mentioned in Chapter Two) is available online at: https://doi.org/10.5194/essd-12-817-2020-supplement.

Author contributions

DS, SE, and DNB developed the method collaboratively. The programming code was written by DS, TR, and SE. Evaluation and visualization was carried out by TR and SE. SE prepared the manuscript with contributions from all co-authors.

Competing interests

The authors declare that they have no conflict of interest.

Acknowledgements

We would like to thank Lea Müller for her initial implementation of gridded nightlight as a proxy for global asset exposure, Gabriela Aznar-Siguan for her input regarding the platform CLIMADA, and all members of the Weather and Climate Risks Group at ETH Zurich for their input and discussions shaping this publication. We would like to thank the two anonymous referees for their thorough and valuable reviews.

Review statement

This paper (Chapter Two) was edited by David Carlson and reviewed by two anonymous referees.

B. Supplementary Material to Chapter 3

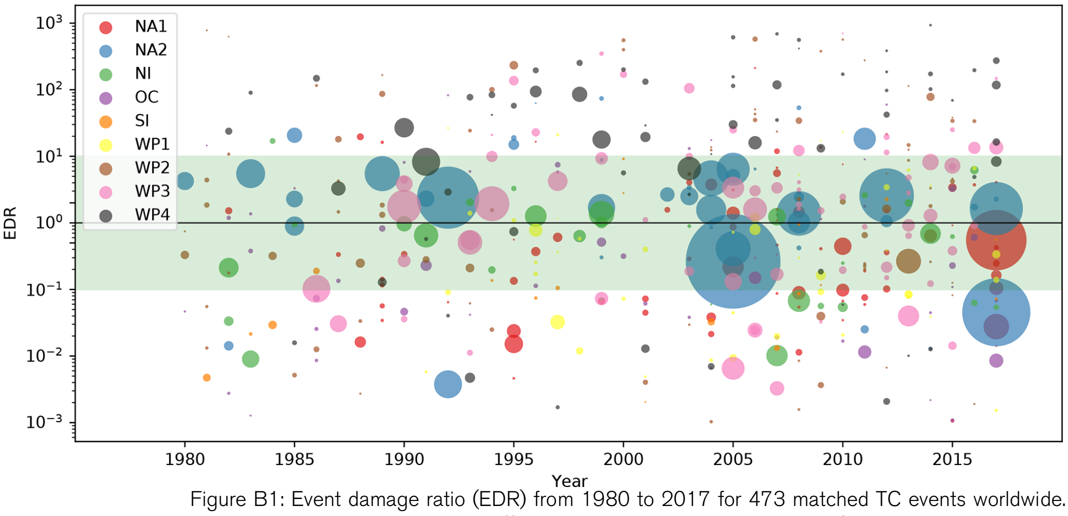

Figure B1: Event damage ratio (EDR) from 1980 to 2017 for 473 matched TC events worldwide. The nine calibration regions are differentiated by color. The area size of the dots represents the absolute normalized reported damage (NRD) per event. The green shading demarcates the range from EDR = 0.1 to 10. Regions by color: red: the Caribbean with Central America and Mexico (NA1); blue: the USA and Canada (NA2); green: North Indian Ocean (NI); purple: Oceania with Australia (OC); orange: South Indian Ocean (SI); yellow: South East Asia (WP1), brown: the Philippines (WP2); rose: mainland China (WP3); black: the rest of the north West Pacific Ocean (WP4).

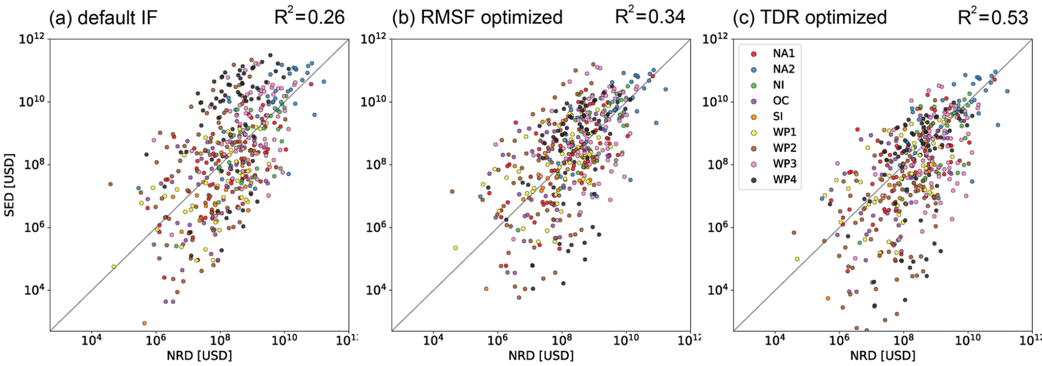

Figure B2: Simulated event damage (SED) vs. normalized reported damage (NRD) for 473 TC events worldwide computed with three different sets of impact functions: (a) uncalibrated default (V_{half} = 74.7 m s^{-1}), (b) RMSF optimized, and (c) TDR optimized. The nine calibration regions are differentiated by color.

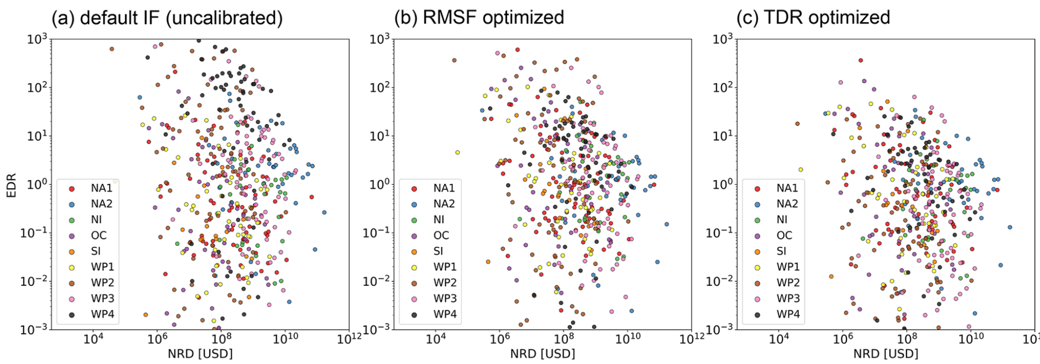

Figure B3: No significant correlation between event damage ratio (EDR) and normalized reported damage (NRD) was found. The scatter plots show the relationship for 473 TC events worldwide computed with three different sets of impact functions: (a) uncalibrated default (V_{half} = 74.7 m s^{-1}), (b) RMSF optimized, and (c) TDR optimized. The nine calibration regions are differentiated by color.

Table B1: List of countries per calibration region. Countries marked with an asterisk (*) are considered for calibration (53 in total).

Region	N countries (calibration)	Countries
North Atlantic 1 (NA1)	48 (21)	Anguilla; Antigua and Barbuda*; Argentina; Aruba; Bahamas*; Barbados; Belize*; Bermuda*; Plurinational State of Bolivia; Cabo Verde*; Cayman Islands; Chile; Colombia; Costa Rica; Cuba*; Dominica*; Dominican Republic*; Ecuador; El Salvador; Falkland Islands (Malvinas); French Guiana; Grenada; Guadeloupe; Guatemala; Guyana; Haiti; Honduras*; Jamaica*; Martinique; Mexico*; Montserrat*; Nicaragua*; Panama; Paraguay; Peru; Puerto Rico*; Saint Helena, Ascension and Tristan da Cunha; Saint Kitts and Nevis*; Saint Lucia*; Saint Vincent and the Grenadines*; Sint Maarten (Dutch part); Suriname; Trinidad and Tobago*; Turks and Caicos Islands*; Uruguay; Bolivarian Republic of Venezuela; British Virgin Islands*; US Virgin Islands*
North Atlantic 2 (NA2)	2 (2)	Canada*; United States of America*
North Indian (NI)	36 (6)	Afghanistan; Armenia; Azerbaijan; Bahrain; Bangladesh*; Bhutan; Djibouti; Eritrea; Ethiopia; Georgia; India*; Islamic Republic of Iran; Iraq; Israel; Jordan; Kazakhstan; Kuwait; Kyrgyzstan; Lebanon; Maldives; Mongolia; Myanmar*; Nepal; Oman*; Pakistan; Qatar; Saudi Arabia; Somalia; Sri Lanka*; Syrian Arab Republic; Tajikistan; Turkmenistan; Uganda; United Arab Emirates; Uzbekistan; Yemen*
Oceania (OC)	26 (11)	American Samoa; Australia*; Cook Islands; Fiji*; French Polynesia*; Guam*; Kiribati; Marshall Islands; Federated States of Micronesia*; Nauru; New Caledonia*; New Zealand; Niue; Norfolk Island; northern Mariana Islands; Palau; Papua New Guinea*; Pitcairn; Samoa*; Solomon Islands*; Timor-Leste; Tokelau; Tonga*; Tuvalu; Vanuatu*; Wallis and Futuna
South Indian (SI)	11 (2)	Comoros; Democratic Republic of the Congo; Eswatini; Madagascar*; Malawi; Mali; Mauritius; Mozambique*; South Africa; United Republic of Tanzania; Zimbabwe
North West Pacific 1 (WP1)	6 (4)	Cambodia*; Indonesia; Lao People's Democratic Republic; Malaysia*; Thailand*; Viet Nam*
North West Pacific 2 (WP2)	1 (1)	Philippines*
North West Pacific 3 (WP3)	1 (1)	Mainland China*
North West Pacific 4 (WP4)	5 (5)	Hong Kong*; Japan*; Republic of Korea*; Macao*; Taiwan*

Table B2: Resulting impact function slope parameter V_{half} and optimization metrics RMSF and TDR per region for (a) the global default impact function (uncalibrated), (b) calibrated by optimizing RMSF, and (c) calibrated by optimizing TDR. The regions NA1 to WP4 are defined in Table B1. The row "combined" summarizes results for all regions combined based on the regionalized calibration; the row "global calibration" is based on one unified global calibration based on all matched TC 473 events. RMSF: root-mean-squared fraction; TDR: total damage ratio.

Region	Number of		V_{half} (m s^{-1})			RMSF			TDR		
	countries	events	**(a)**	**(b)**	**(c)**	**(a)**	**(b)**	**(c)**	**(a)**	**(b)**	**(c)**
NA1	21	73	74.7	59.6	66.3	11.8	9.8	10.3	0.68	1.44	1.0
NA2	2	43	74.7	86	89.2	9.5	8.7	8.7	2.11	1.16	1.0
NI	6	31	74.7	58.7	70.8	7.8	6	7.2	0.85	2.03	1.0
OC	11	48	74.7	49.7	64.1	22.5	14.7	17.7	0.6	2.31	1.0
SI	2	19	74.7	46.8	52.4	20.1	8.6	9.1	0.2	1.8	1.0
WP1	4	43	74.7	56.7	66.4	15.2	11.3	12.6	0.62	2.05	1.0
WP2	1	83	74.7	84.7	188.4	38.2	36.7	104.9	25.89	16.44	1.0
WP3	1	69	74.7	80.2	112.8	15.2	14.8	20.5	5.32	3.83	1.0
WP4	5	64	74.7	135.6	190.5	73.8	35.9	43.8	35.56	3.35	1.0
Combined	53	473	74.7	–	–	22.2	16.8	24.4	4.69	2.15	1.0
Global calibration	53	473	74.7	73.4	110.1	22.2	22.2	33.1	4.69	4.84	1.0

Table B3: Total asset exposure values (TAVs) per region. First column: TAV based on Eberenz et al. (2020) as used in this study. Second and third columns: reference values of TAV from GAR 2013 and Gettelman et al. (2017). The unit is 10^{12} US dollars ($T) valued according to the year noted in brackets. AAD relative to TAV is reported in Table 1. * USA and Bermuda.

Region	TAV Eberenz et al. (2020) $T of 2014	TAV GAR 2013 $T of 2005	TAV Gettelman et al. (2017) $T of 2015
NA1	4.66	2.19	8.6
NA2	62.19	24.06	73.3*
NI	6.32	1.64	
OC	5.94	1.85	
SI	0.04	0.01	
WP1	2.27	0.83	
WP2	0.63	0.19	
WP3	31.40	4.51	
WP4	26.98	19.51	
WP	61.28	25.04	58.8
World	250.88	96.45	155.9

Table B4 (next page): Detailed information on the 21 TCs in the matched events list with the largest normalized reported damage: storm name (local name in brackets) and year, normalized reported damage (NRD), simulated event damage (SED; simulated with V_{half}= 84.7 m s^{-1}), event damage ratio (EDR), simulated intensity for the capital city Manila (at 14.5°N, 121.0°E), and associated disasters according to the literature and EM-DAT, as well as affected sectors and asset types as reported by the literature. Sources of information: [1] peer-reviewed study; [2] public report; [3] data field "associated disasters" in EM-DAT. (References in Table: Abon et al., 2011; Blanc and Strobl, 2016; Cooper and Falvey, 2009; Cruz and Narisma, 2016; Espada, 2018; IFRC, 2009; Inokuchi et al., 2011; Joint Typhoon Warning Center, 1995; Lagmay et al., 2015; Mas et al., 2015; Nakasu et al., 2011; NDCC, 2009a, 2009b; NDRRMC, 2010, 2011, 2012, 2013, 2014; Soria et al., 2015; Yumul et al., 2008, 2012)

Event	SED (million USD)	NRD[3] (million USD)	EDR $\left(\frac{\text{SED}}{\text{NRD}}\right)$	V_{wind} Manila ($\text{m}\,\text{s}^{-1}$)	Associated disasters	Affected sectors & assets	Reference
Rammasun (Glenda), 2014	39 528	821	48.17	52.8	Wind[1], flood[3]	Agriculture[2], buildings (664 000)[2], power supply[2], roads, and bridges[2]	Espada (2018); NDRRMC (2014)
Haiyan (Yolanda), 2013	1804	10 469	0.17	–	Wind[1], surge[1,2,3]	Agriculture[2], buildings (1.1 million)[1,2], airport[1,2], power supply[2], roads[2], bridges[2], and ports[2]	Blanc and Strobl (2016); Espada (2018); Lagmay et al. (2015); Mas et al. (2015); NDRRMC (2013); Soria et al. (2015)
Bopha (Pablo), 2012	1060	1022	1.04	–	Wind[2], flood[2]	Agriculture[2], buildings (217 000)[2], power and water supply[2], roads, and bridges[2]	NDRRMC (2012)
Nesat (Pedring), 2011	172	437	0.39	–	Wind[2], flood[2], surge[2], slide[2,3]	Agriculture[2], buildings (44 000)[2], power supply[2], dikes[2], roads, and bridges[2]	NDRRMC (2011)
Megi (Juan), 2010	526	393	1.34	–	Wind[2], flood[2], slide[2]	Agriculture[2], buildings (104 000)[2], power supply[2], roads, and bridges[2]	NDRRMC (2010)
Parma (Pepeng), 2009	23	990	0.02	–	Flood[1,3], slides[1]	Agriculture[2], buildings (61 000)[2], power supply[2], dikes[2], roads, and bridges[2]	Abon et al. (2011); Cooper and Falvey (2009); Cruz and Narisma (2016); Espada (2018); Inokuchi et al. (2011); Nakasu et al. (2011); NDCC (2009a, b)
Ketsana (Ondoy), 2009	1	401	0.002	–	Flood[1,3] (Manila), slides[3]	Agriculture[2], buildings (185 000)[2], power supply[2], dikes[2], roads, and bridges[2]	
Fengshen (Frank), 2008	9286	465	19.96	41.2	Flood[1,2,3], surge[2], slides[1,2]	Agriculture[2], buildings (407 000)[2], power and water supply[2], roads, and bridges[2]	Espada (2018); IFRC (2009); Yumul et al. (2012)
Xangsane (Milenyo), 2006	100 440	263	381.70	63.9	Flood[1,3], slides[1]	Dikes[1] and power supply[1]	Yumul et al. (2008)
Angela (Rosing), 1995	156 750	937	167.32	77.2	Flood[2], surge[2], slides[2]	Agriculture[2], buildings (> 96 000)[2], power supply[2], dams[2], roads, and bridges[2]	Joint Typhoon Warning Center (1995)
Teresa (Katring), 1994	17 731	299	59.24	46.5	Flood[3]	No report evaluated	
Flo (Kadiang), 1993	120	984	0.12	–	Slide[3]	No report evaluated	
Ruth (Trining), 1991	95	564	0.17	–		No report evaluated	
Gordon (Goring), 1989	347	408	0.85	–		No report evaluated	
Dan (Saling), 1989	20 398	396	51.55	48.6		No report evaluated	
Skip (Yoning), 1988	182	1120	0.16	–		No report evaluated	
Nina (Sisang), 1987	5643	480	11.75	29.8		No report evaluated	Espada (2018)
Georgia (Ruping), 1986	2	343	0.01	–		No report evaluated	
Agnes (Undang), 1984	174	875	0.20	–		No report evaluated	
Irma (Anding), 1981	305	279	1.09	22.8		No report evaluated	
Betty (Aring), 1980	173	897	0.19	18.3	Slide[3]	No report evaluated	Espada (2018)

Code availability and data availability

The full array of fitted impact function parameters can be found in the Supplement of this paper. The scripts reproducing the main results of the paper and the figures are available at https://github.com/CLIMADA-project/climada_papers (Aznar-Siguan et al., 2020; https://doi.org/10.5281/zenodo.4467858, Eberenz et al., 2021a). The CLIMADA repository (Aznar-Siguan and Bresch, 2019; CLIMADA-Project, 2019) is openly available (https://github.com/CLIMADA-project/climada_python, Bresch et al., 2020) under the GNU GPL license (Free Software Foundation, Inc., 2007). The documentation is hosted on Read the Docs (https://climada-python.readthedocs.io/en/stable/), including a link to the interactive tutorial of CLIMADA. CLIMADA v1.4.1 was used for this publication, which is permanently available at the ETH Data Archive: http://doi.org/10.5905/ethz-1007-252 (Bresch et al., 2020).

Supplement

The supplement related to this article (including Table S1 and Figures S1-S4 mentioned in Chapter Two) is available online at: https://doi.org/10.5194/nhess-21-393-2021-supplement.

Author contributions

SE and DNB developed the idea and basic methodology of the paper. Coding and analysis were the work of SE and SL. SE prepared the manuscript with contributions from all co-authors.

Competing interests

The authors declare that they have no conflict of interest.

Acknowledgements

We would like to thank Gabriela Aznar-Siguan for her input regarding the platform CLIMADA and the implementation of the TC impact model in Python. Together with Benedikt Knüsel, she also supervised the master thesis of Samuel Lüthi that was a contribution to the methods of this paper. Furthermore, our thanks go to Thomas Röösli, Benoît Guillod, and Boris Prahl who helped shape the calibration methodology, as well as Thomas Röösli, Maurice Skelton, and Jamie McCaughey for their substantial inputs during the internal review of the paper. Finally, we want to thank all members of the Weather and Climate Risks Group at ETH Zurich for their input and discussions that shaped this publication. We would like to thank the two anonymous referees for their thorough and valuable reviews.

Review statement

This paper (Chapter Three) was edited by Paolo Tarolli and reviewed by two anonymous referees.

C. Supplementary Material to Chapter 4

Table C1: Production risk changes for single crops. Baseline mean crop production and probability of crop production to fall short of the historical and the relative threshold for maize (a), rice (b), soybean (c), and wheat (d) under historical (5°C) and future (2°C and 4°C) levels of global warming. Values are provided on a globally aggregated level and for twelve major crop producing countries. Multi-model median probabilities are shown with the inter-quartile range of single crop model results provided in brackets. Blue shading marks a decrease in probability as compared to 0.5°C levels. Orange shading marks an increase in probability as compared to 0.5°C levels. The asterisk (*) implies more than 70% crop model agreement on the sign of probability change compared to 0.5°C of global warming.The countries are USA, China (CHN), Brazil (BRA), Argentina (ARG), Mexico (MEX), India (IND), Ukraine (UKR), France (FRA), Canada (CAN), South Africa (ZAF), Romania (ROU), Thailand (THA), Myanmar (MMR), Philippines (PHL), Japan (JPN), Pakistan (PAK), Paraguay (PRY), Bolivia (BOL), Russia (RUS), Uruguay (URY), Indonesia (IDN), Bangladesh (BGD), Australia (AUS), Germany (DEU), Turkey (TUR), and Kazakhstan (KAZ).

(a) Maize:

Country (ISO3)	Mean production 0.5°C		Probability (IQR) [%]					
			Historical threshold: 2.5th pctl			Relative threshold: mean-10%		
	10^{12} kcal/y	mio. t/y	0.5°C	2.0°C	4.0°C	0.5°C	2.0°C	4.0°C
global	**3524**	**990**	**2.5**	**5.0* (36.4)**	**82.1* (58.9)**	**1.6 (1.6)**	**3.6 (6.1)**	**3.0 (5.1)**
USA	1233	346	2.5	7.0* (15.3)	36.9* (59.2)	15.6 (8.7)	20.6* (10.7)	24.0* (11.1)
CHN	794	223	2.5	5.4* (18.8)	55.0* (54.8)	6.6 (5.0)	7.4 (5.9)	4.4* (10.3)
BRA	260	73	2.5	4.1* (26.0)	7.5 (33.7)	9.8 (16.8)	14.3 (16.2)	13.3 (10.6)
ARG	106	30	2.5	1.1 (2.7)	0.0* (0.7)	19.6 (14.2)	19.0 (13.4)	16.4 (19.7)
MEX	85	24	2.5	3.4 (7.7)	63.0* (79.4)	5.9 (10.0)	4.9* (5.9)	4.8 (4.1)
IND	84	24	2.5	2.2 (27.9)	4.8 (81.5)	16.3 (14.3)	14.0* (13.8)	7.5 (14.5)
UKR	80	22	2.5	3.6 (8.9)	8.2 (31.7)	21.3 (22.9)	20.6 (23.4)	30.8 (20.1)
IDN	74	21	2.5	10.8 (63.4)	93.2* (86.9)	0.7 (3.6)	0.5 (3.9)	0.7 (3.4)
FRA	51	14	2.5	3.1 (8.4)	4.1 (45.8)	24.0 (10.0)	27.4* (12.2)	29.6* (17.1)
CAN	44	12	2.5	1.3* (4.7)	15.8* (33.4)	16.3 (11.4)	17.9 (14.1)	23.3* (14.1)
ZAF	42	12	2.5	0.6* (2.4)	0.0* (0.3)	29.7 (21.4)	27.2* (17.1)	21.9* (16.8)
ROU	38	11	2.5	3.1 (2.8)	10.3 (30.0)	24.4 (21.3)	25.9* (14.6)	34.9 (14.6)

(b) Rice

Country (ISO3)	Mean production 0.5°C		Probability (IQR) [%]					
			Historical threshold: 2.5th pctl			Relative threshold: mean-10%		
	10^{12} kcal/y	mio. t/y	0.5°C	2.0°C	4.0°C	0.5°C	2.0°C	4.0°C
global	**2031**	**725**	**2.5**	0.0* (0.4)	2.1 (12.3)	0.0 (0.1)	0.4 (0.7)	0.7 (2.4)
CHN	578	207	2.5	0.1* (0.3)	0.0 (20.5)	1.4 (2.1)	2.1 (2.9)	0.0* (1.0)
IND	433	155	2.5	0.6* (0.6)	1.4 (3.8)	6.8 (6.9)	5.7 (7.3)	8.2 (3.8)
IDN	191	68	2.5	0.0* (0.0)	1.4 (3.1)	0.4 (0.5)	0.4 (0.9)	0.7 (2.4)
BGD	139	50	2.5	0.4* (1.1)	5.5 (34.9)	13.3 (4.6)	11.1 (3.8)	13.0 (2.4)
VNM	117	42	2.5	0.6* (2.0)	5.5 (10.3)	4.2 (2.2)	4.9 (2.0)	5.5 (7.9)
THA	90	32	2.5	3.4 (3.9)	32.2 (51.0)	12.9 (5.3)	17.4 (10.7)	18.5* (16.4)
MMR	77	28	2.5	0.8* (0.8)	5.5 (13.0)	1.9 (2.7)	2.5 (3.6)	2.1 (1.4)
PHL	47	17	2.5	0.4* (0.7)	1.4 (2.7)	1.2 (1.2)	1.3 (1.8)	3.4 (2.4)
BRA	32	12	2.5	0.1* (0.3)	3.4 (5.1)	0.1 (0.5)	0.6 (0.8)	3.4 (5.5)
JPN	28	10	2.5	0.0* (0.0)	0.0* (0.0)	4.1 (1.2)	1.4* (1.5)	2.1* (3.4)
PAK	27	10	2.5	5.3 (5.6)	70.5 (68.5)	17.0 (12.7)	23.0* (15.0)	30.1* (21.6)
USA	25	9	2.5	0.3* (0.4)	1.4 (7.2)	12.6 (4.5)	14.6 (6.6)	15.8* (4.5)

(c)
Soybean

Country (ISO3)	Mean production 0.5°C		Probability (IQR) [%]					
			Historical threshold: 2.5th pctl			Relative threshold: mean-10%		
	10^{12} kcal/y	mio. t/y	0.5°C	2.0°C	4.0°C	0.5°C	2.0°C	4.0°C
global	**913**	**272**	**2.5**	0.0* (0.3)	0.0* (3.4)	2.0 (2.0)	2.5 (3.5)	6.8* (2.3)
USA	322	96	2.5	0.0 (2.7)	2.7 (11.6)	12.0 (5.5)	21.0* (5.8)	17.8* (13.7)
BRA	273	81	2.5	1.3* (2.1)	19.2 (33.6)	1.8 (3.8)	5.0* (7.7)	12.9* (11.6)
ARG	150	45	2.5	0.0* (0.3)	0.0* (0.0)	22.3 (6.7)	24.1 (6.7)	24.7 (10.8)
CHN	44	13	2.5	0.0* (0.0)	0.0* (0.0)	6.3 (3.3)	7.0 (8.8)	4.1 (11.0)
IND	37	11	2.5	0.3* (0.7)	0.0* (1.4)	13.5 (5.9)	12.3* (6.8)	8.2* (9.0)
PRY	26	8	2.5	0.3* (1.8)	1.4* (3.4)	17.8 (5.7)	18.5* (5.0)	19.2* (6.3)
CAN	17	5	2.5	0.0* (1.1)	0.0 (3.4)	17.6 (11.5)	17.6 (9.5)	19.2* (11.0)
UKR	9	3	2.5	0.0* (0.5)	0.0* (2.3)	27.8 (11.1)	26.6 (12.9)	28.8 (14.4)
BOL	8	2	2.5	1.4 (3.1)	17.8 (24.7)	7.7 (4.4)	13.2* (9.2)	15.1* (15.7)
RUS	7	2	2.5	0.0* (0.0)	0.0* (0.0)	11.0 (11.9)	8.4 (8.1)	15.1 (13.7)
URY	6	2	2.5	0.0* (0.3)	0.0* (0.7)	18.6 (7.7)	19.9* (6.3)	12.3* (15.1)
IDN	3	1	2.5	0.0* (0.4)	0.0* (1.4)	10.8 (6.7)	9.2 (11.6)	8.2* (11.3)

(d) Wheat

Country (ISO3)	Mean production 0.5°C		Probability (IQR) [%]					
			Historical threshold: 2.5th pctl			Relative threshold: mean-10%		
	10^{12} kcal/y	mio. t/y	0.5°C	2.0°C	4.0°C	0.5°C	2.0°C	4.0°C
global	**2312**	**692**	**2.5**	**0.8* (1.8)**	**0.0 (8.2)**	**1.0 (3.7)**	**1.1 (4.1)**	**2.7 (2.1)**
CHN	402	120	2.5	0.8* (1.4)	2.7 (13.0)	9.8 (10.6)	10.4* (10.1)	11.0* (11.6)
IND	297	89	2.5	0.0* (0.7)	0.0* (0.7)	8.8 (7.7)	7.3* (5.0)	5.5* (6.8)
RUS	196	59	2.5	0.8* (1.0)	2.7 (3.4)	12.6 (10.9)	13.2 (13.2)	13.7 (12.3)
USA	184	55	2.5	0.8 (2.9)	2.7 (8.2)	16.3 (18.9)	14.3 (20.6)	15.1 (26.0)
FRA	119	36	2.5	0.8 (6.9)	2.7 (6.8)	23.0 (14.6)	25.5 (23.0)	27.4 (20.5)
CAN	94	28	2.5	0.3* (0.7)	1.4* (2.1)	18.3 (9.7)	20.4 (13.3)	23.3 (13.0)
PAK	87	26	2.5	1.1 (17.2)	8.2 (78.1)	40.3 (28.3)	24.1 (35.3)	26.0 (27.4)
AUS	78	23	2.5	0.6* (0.8)	0.0* (0.7)	33.9 (26.1)	31.4* (26.2)	27.4* (16.4)
DEU	77	23	2.5	0.8 (3.2)	0.0 (6.8)	18.3 (19.1)	21.8* (8.8)	21.9 (14.4)
UKR	73	22	2.5	0.8* (3.4)	4.1 (11.6)	24.8 (21.1)	23.0 (23.7)	26.0 (17.1)
TUR	64	19	2.5	0.8* (1.1)	1.4 (3.4)	26.5 (16.1)	27.5 (23.2)	26.0* (22.6)
KAZ	47	14	2.5	0.8* (1.1)	0.0* (0.0)	33.6 (18.7)	31.9 (21.7)	28.8 (11.6)

Table C2: Global gridded crop model (GGCMs) providing ensemble members to GC6 (ISIMIP, 2020b). Table adapted from Jägermeyr et al. (under review, Table S3).

Crop model (version)	Model type	Crops simulated[1]	Heat/ cold stress	Other stresses[2]	Phenology response to temperature increase	CO_2 effects
LPJmL (5t)	Ecosystem	Mai, wwh, swh, soy, ri1, ri2	Cold stress	N, W	Linear (Tbase)	[CO_2] increase affects stomatal conductance, Rubisco/PEP Carboxylation (Calvin Cycle), Photorespiration
EPIC-IIASA	Site-based	Mai, wwh, swh, soy, ri1, ri2	Both	N, W, aeration	Linear	RUE
PEPIC	Site-based	Mai, wwh, swh, soy, ri1, ri2	Both	N, W	Linear	RUE and plant transpiration
CROVER	Ecosystem	Mai, wwh, swh, soy, ri1	Both	W	Linear (Tbase)	Stomatal conductance, carboxylation, photorespiration, dark respiration
GYGMA (1p74)	Site-based	Mai, wwh, swh, soy, ri1, ri2	Both	N, W, water excess	Linear (Tbase, Topt, Tmax)	RUE and plant transpiration
SIMPLACE-LINTUL5+	Site-based	Mai, wwh, swh	Heat stress	W	Linear	Reduction in potential transpiration rates and increase in RUE under elevated [CO_2]
PROMET	Site-based	Mai, wwh, swh, soy, ri1	Both	N, W	Curvlinear (Tbase, Topt, Tmax)	[CO_2] increase affects stomatal conductance, Rubisco/PEP Carboxylation (Calvin Cycle), Photorespiration
AquaCrop-ACEA	Biophysical based on water productivity	Mai, soy	Both	W	Curvlinear (Tbase, Topt, Tmax)	Water productivity is adjusted to [CO_2]

[1] Crop codes: mai (maize); ri1 (rice first season); ri2 (rice second season); soy (soybean), swh (spring wheat), wwh (winter wheat). [2] Stresses codes: N (nitrogen deficit), W (water deficit).

Table C3: Global climate model (GCM) simulations used to drive crop models for GC6. Original GCM data was extracted from the CMIP6 archive for ISIMIP3b. The bias-adjustment of the GCM output for ISIMIP3b, please refer to Cucchi et al. (2020) and Lange et al. (2019). Table adapted from the ISIMIP3b simulation round protocol (ISIMIP, 2020b). End-of-century change in global mean temperature (ΔGMT) is the global multi-year mean near-surface temperature difference between 2069-2099 and pre-industrial control run.

Title	Institution	Ensemble member	End-of-century ΔGMT SSP126 [°C]	End-of-century ΔGMT SSP585 [°C]
GFDL-ESM4	National Oceanic and Atmospheric Administration, Geophysical Fluid Dynamics Laboratory, Princeton, NJ 08540, USA	r1i1p1f1	1.4	3.7
UKESM1-0-LL	Met Office Hadley Centre, Fitzroy Road, Exeter, Devon, EX1 3PB, UK	r1i1p1f2	2.7	6.5
MPI-ESM1-2-HR	Max Planck Institute for Meteorology, Hamburg 20146, Germany	r1i1p1f1	1.5	3.8
IPSL-CM6A-LR	Institut Pierre Simon Laplace, Paris 75252, France	r1i1p1f1	2.4	6.0
MRI-ESM2-0	Meteorological Research Institute, Tsukuba, Ibaraki 305-0052, Japan	r1i1p1f1	1.7	4.3

Table C4: Crop type coverage per climate model (columns) and crop model (rows) in the crop yield simulation ensemble used for this study. Crop codes: mai (maize); ri1 (rice first season); ri2 (rice second season); soy (soybean), swh (spring wheat), wwh (winter wheat).

	GFDL-ESM4	UKESM1-0-LL	MPI-ESM1-2-HR	IPSL-CM6A-LR	MRI-ESM2-0
LPJmL (5t)	Mai, wwh, swh, soy, ri1, ri2	Mai, wwh, swh, soy, ri1, ri2	Mai, wwh, swh, soy, ri1, ri2	Mai, wwh, swh, soy, ri1, ri2	Mai, wwh, swh, soy, ri1, ri2
EPIC-IIASA	Mai, wwh, swh, soy, ri1, ri2	Mai, wwh, swh, soy, ri1, ri2	Mai, wwh, swh, soy, ri1, ri2	Mai, wwh, swh, soy, ri1, ri2	Mai, wwh, swh, soy, ri1, ri2
PEPIC	Mai, wwh, swh, soy, ri1, ri2	Mai, wwh, swh, soy, ri1, ri2	Mai, wwh, swh, soy, ri1, ri2	Mai, wwh, swh, soy, ri1, ri2	Mai, wwh, swh, soy, ri1, ri2
CROVER	Mai, wwh, swh, soy, ri1	Mai, wwh, swh, soy, ri1	Mai, wwh, swh, soy, ri1	Mai, wwh, swh, soy, ri1	Mai, wwh, swh, soy, ri1
GYGMA (1p74)	Mai, wwh, swh, soy, ri1, ri2	Mai, wwh, swh, soy, ri1, ri2	Mai, wwh, swh, soy, ri1, ri2	Mai, wwh, swh, soy, ri1, ri2	Mai, wwh, swh, soy, ri1, ri2
SIMPLACE-LINTUL5+	Mai, wwh, swh, soy	Mai, wwh, swh, soy	Mai, wwh, swh, soy	Mai, wwh, swh, soy	Mai, wwh, swh, soy
PROMET	Mai, wwh, swh, soy, ri1	Mai, wwh, swh, soy, ri1	Mai, wwh, swh, soy, ri1	Mai, wwh, swh, soy, ri1	Mai, wwh, swh, soy, ri1
AquaCrop-ACEA	-	Mai, soy	-	-	Mai, soy

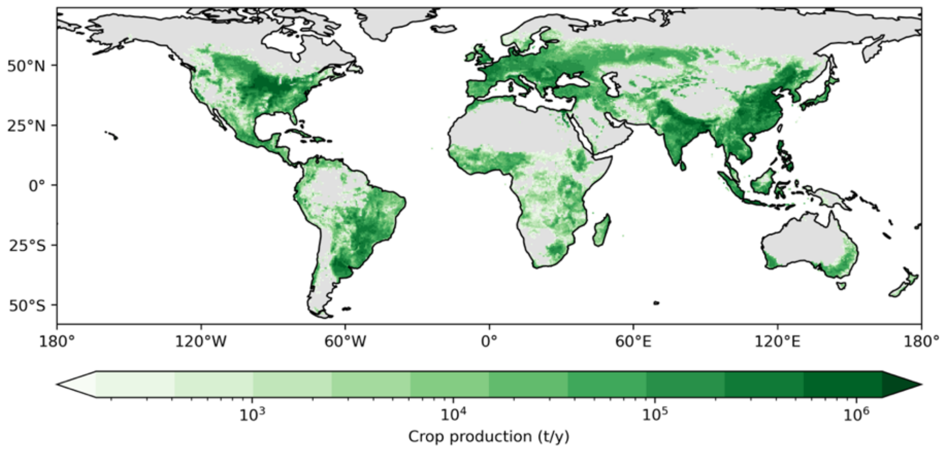

Figure C1: Baseline crop production per 0.5° x 0.5° pixel in tons per year for maize, rice, soybean, and wheat combined. The map shows mean values at 0.5°C ± 0.5°C of global warming, bias corrected with FAO statistics (see Section 2.3).

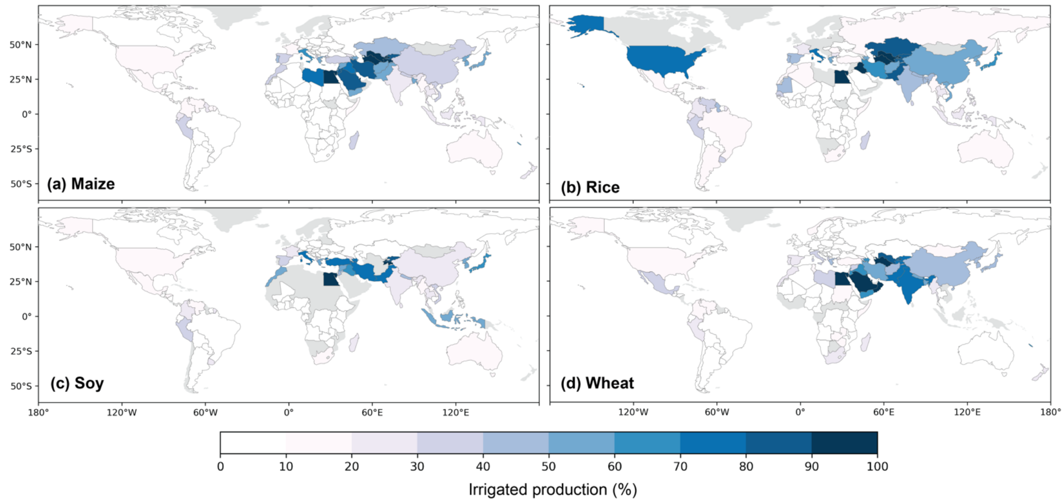

Figure C2: Share of irrigated crop production per country for maize (a), rice (b), soybean (c), and wheat (d) based on 'Farming the planet' for the year 2000 (Monfreda et al., 2008; Ramankutty et al., 2008). Countries with zero production of the respective crop in the dataset are shaded grey.

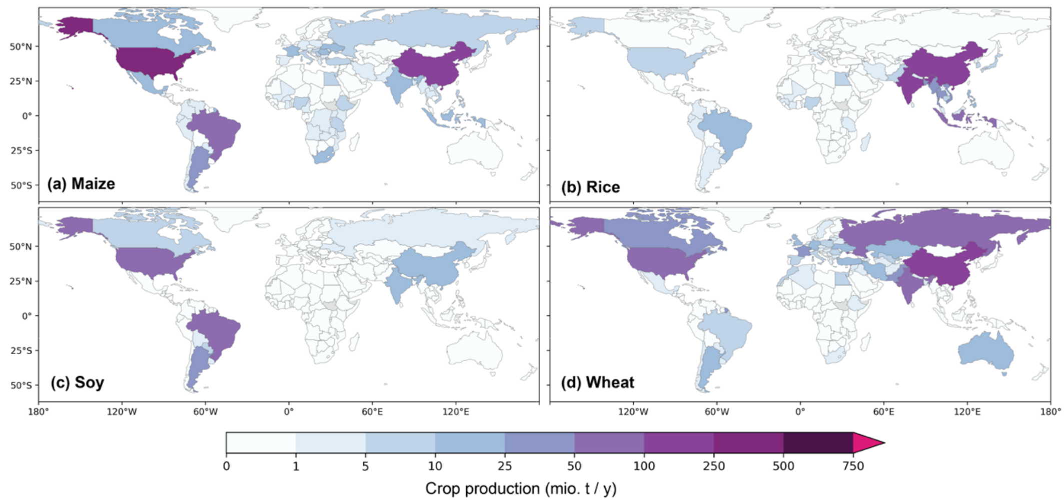

Figure C3: Multi-model median crop production per country at 0.5°C global warming (historical reference bin, $\Delta GMT = 0.5°C \pm 0.5°C$). Absolute crop production per year bias corrected with FAO statistics is shown in mio. tons for (a) maize, (b) rice, (c) soybean, and (d) wheat.

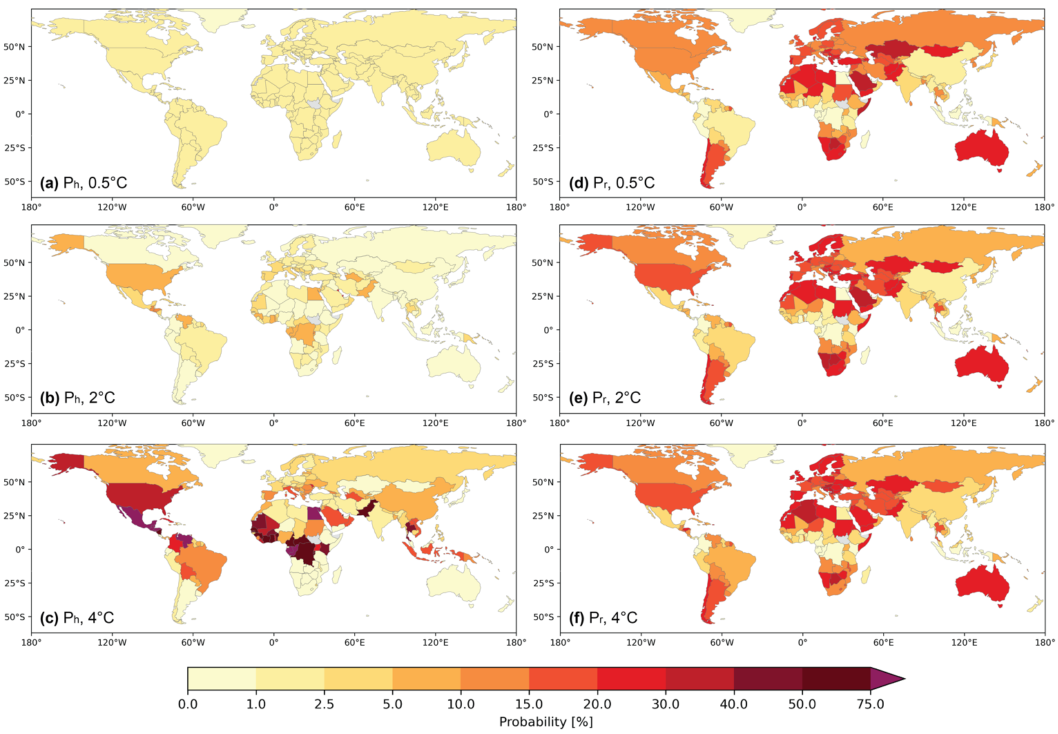

Figure C4: Multi-model median probability of any given year that crop production falls below a given threshold per country, for maize, rice, soybean, and wheat combined. The historical threshold (left, a-c) is defined as the 2.5th percentile of production at 0.5°C global warming. The relative threshold (right, d-f) is defined as 10% below the mean production for each level of global warming (GMT bins of width 1°C).

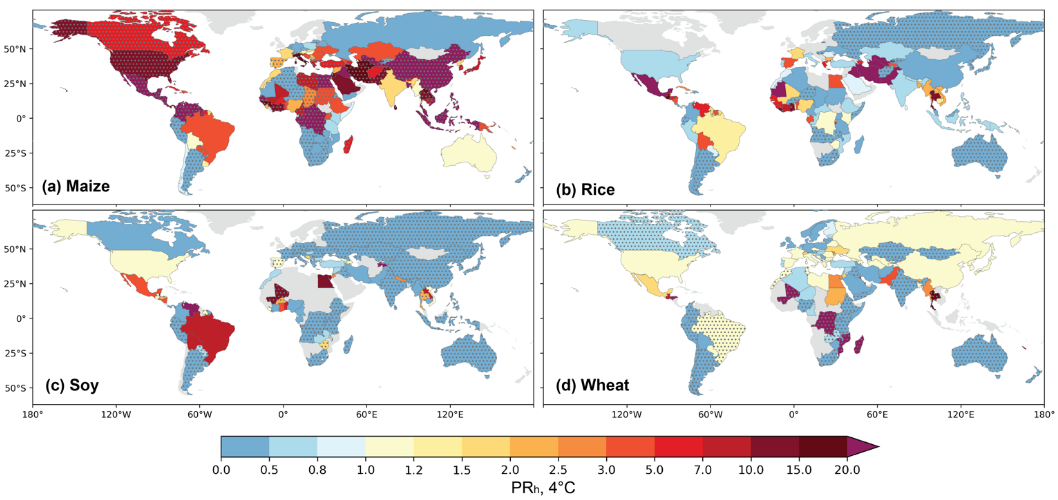

Figure C5: Probability ratio PR_h at 4°C per country for for maize (a), rice (b), soybean (c), and wheat (d). PR_h is calculated as he ratio of P_h at 4°C to P_h at 0.5°C of global warming (historical reference). P_h is the probability of crop production in any given year to fall short of the 2.5th percentile of crop production at 0.5°C (historical threshold). Blue colors (PR<1) indicate a decrease in probability. For PR>1 probability is increased compared to 0.5°C. Countries are colored in grey if the respective crop is not grown there. Stippling indicates a crop model agreement above 70% on the sign of probability change.

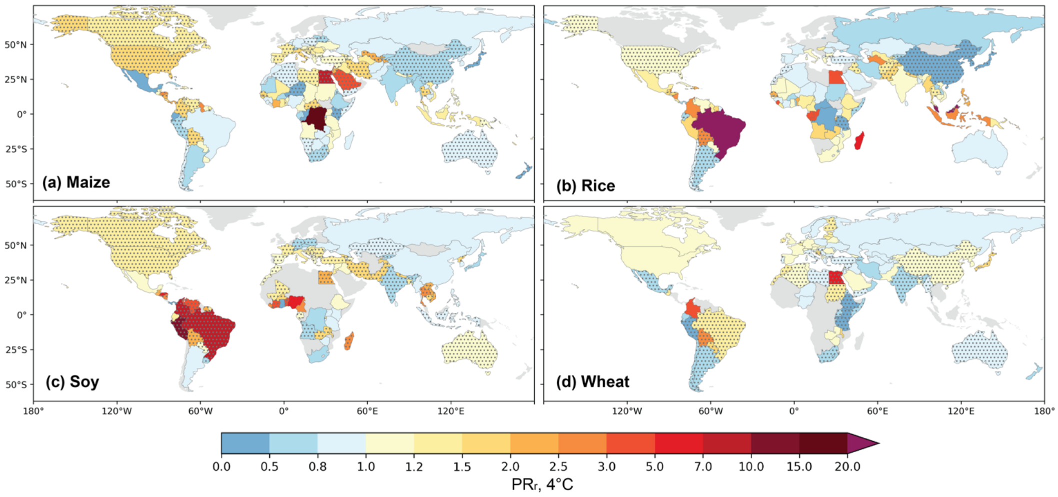

Figure C6: Probability ratio PR_r at 4°C per country for for maize (a), rice (b), soybean (c), and wheat (d). PR_r is calulcated as he ratio of P_r at 4°C to P_r at 0.5°C of global warming (historical reference). P_r is probability that crop production in a given year falls more than 10% short of the mean of the given warming level (relative threshold). Blue colors (PR<1) indicate a decrease in probability. For PR>1 probability is increased compared to 0.5°C. Countries are colored in grey if the respective crop is not grown there or if P_r is equal to 0 % at 0.5°C, making it impossible to calculate PR_r. Stippling indicates a crop model agreement above 70% on the sign of probability change.

All crop types combined:

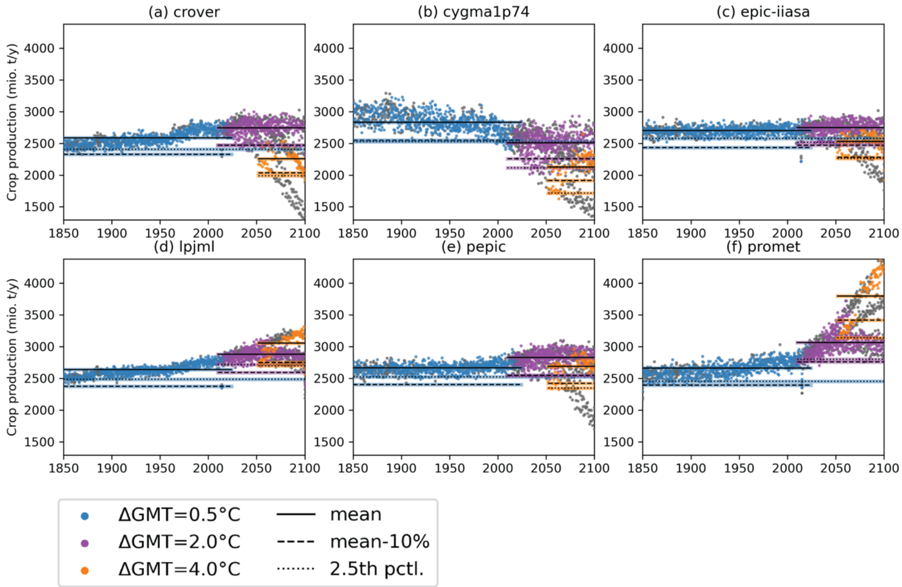

Figure C7 (all crops combined): Simulated global yearly crop production for maize, rice, soybean, and wheat combined in million tons. Color demarcates the ΔGMT bins of 0.5°C (blue), 2°C (purple), and 4°C (orange), each bin with a width of 1°C. The black lines demarcate mean (solid line), mean-10% (dashed line), and 2.5th percentile (dotted line) of each ΔGMT bin. Each subplot shows crop production based on one individual crop model (a-f).

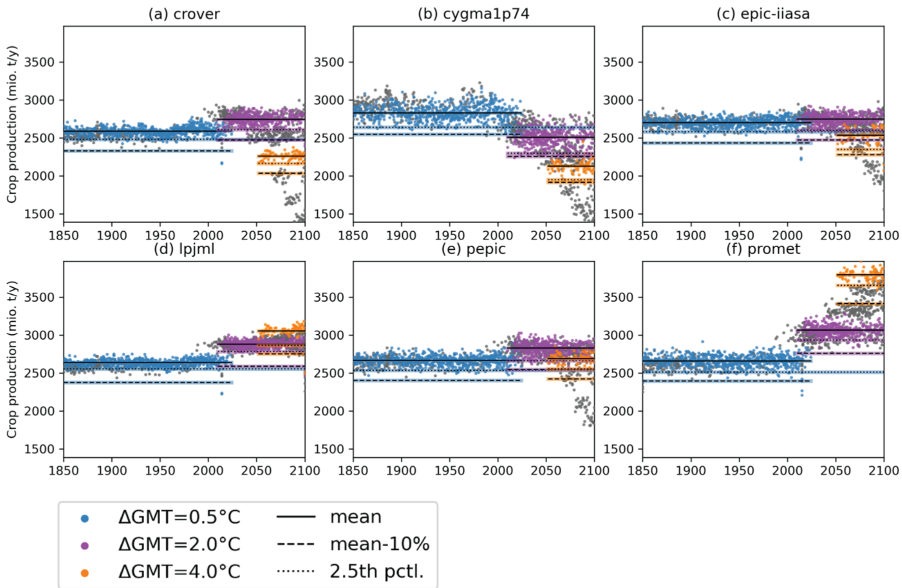

Figure C8 (all crops combined): Detrended and mean-corrected simulated yearly crop production aggregated globally for maize, rice, soybean, and wheat combined in million tons. Color demarcates the ΔGMT bins of 0.5°C (blue), 2°C (purple), and 4°C (orange), each bin with a width of 1°C. Values are detrended over time and subsequently the original mean production per ΔGMT bin is added to sustain the same mean values per bin as before detrending. The black lines demarcate mean (solid line), mean-10% (relative threshold, dashed line), and 2.5th percentile (dotted line) of each ΔGMT bin. The historical threshold is equal to the 2.5th percentile of the 0.5°C bin (dotted line with blue shading). Each subplot shows crop production based on one individual crop model (a-h).

Maize:

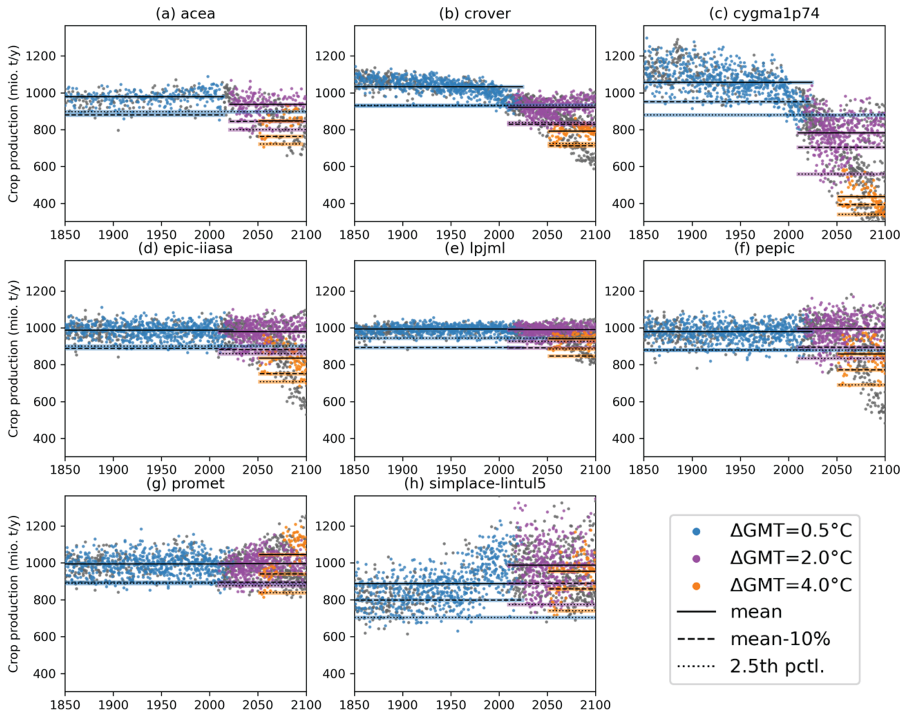

Figure C9 (maize): same as Fig. C7 for maize.

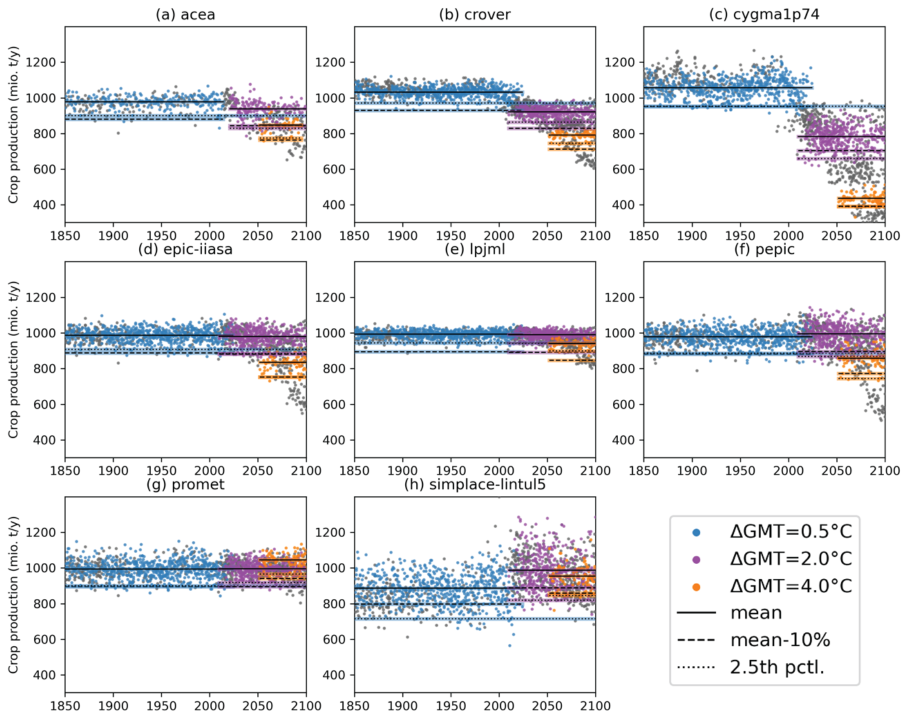

Figure C10 (maize, detrended): same as Fig. C8 for maize.

Rice:

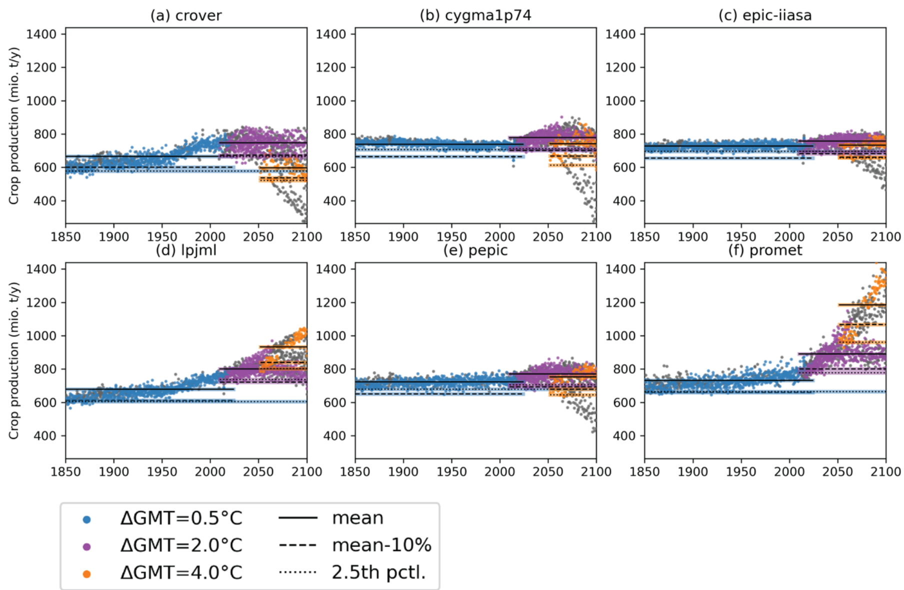

Figure C11 (rice): same as Fig. C7 for rice.

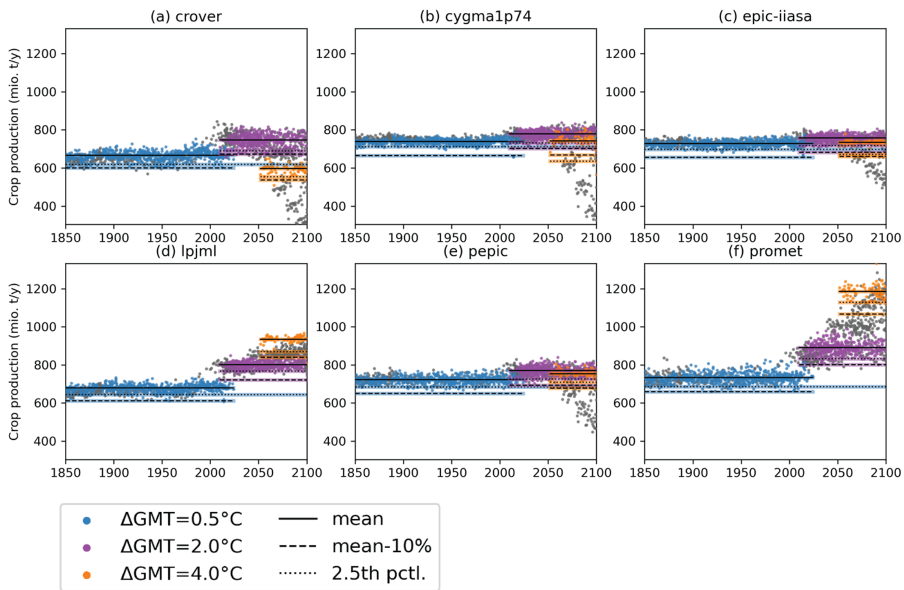

Figure C12 (rice, detrended): same as Fig. C8 for rice.

Soybean:

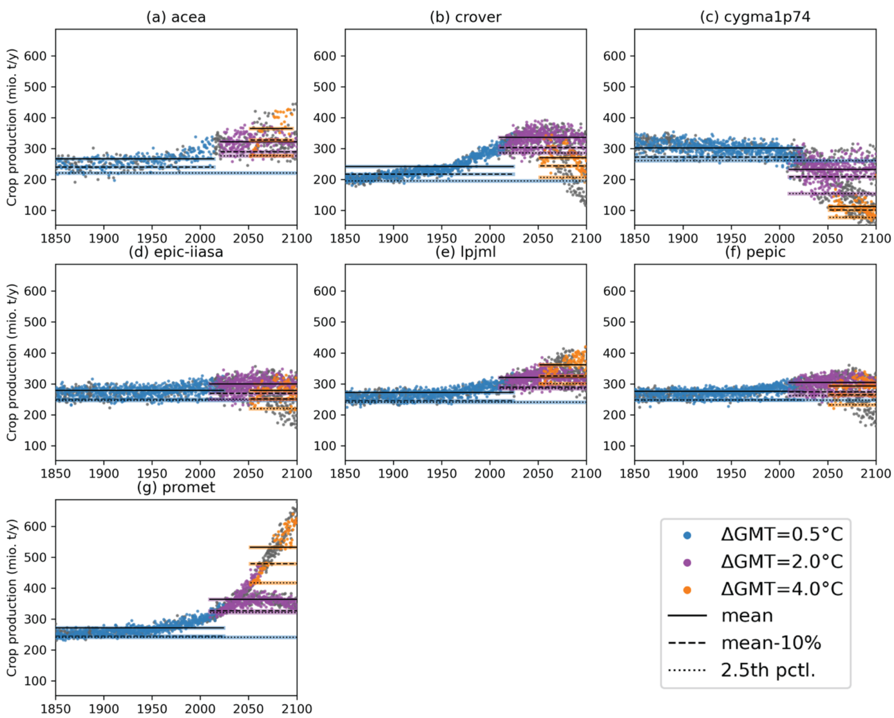

Figure C13 (soybean): same as Fig. C7 for soybean.

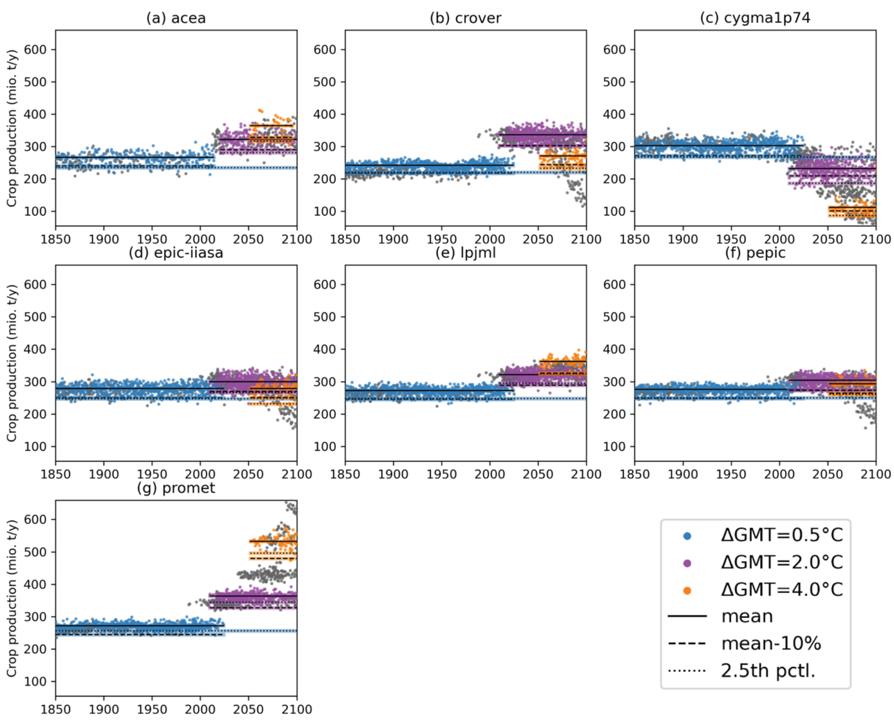

Figure C14 (soybean, detrended): same as Fig. C8 for soybean.

Wheat:

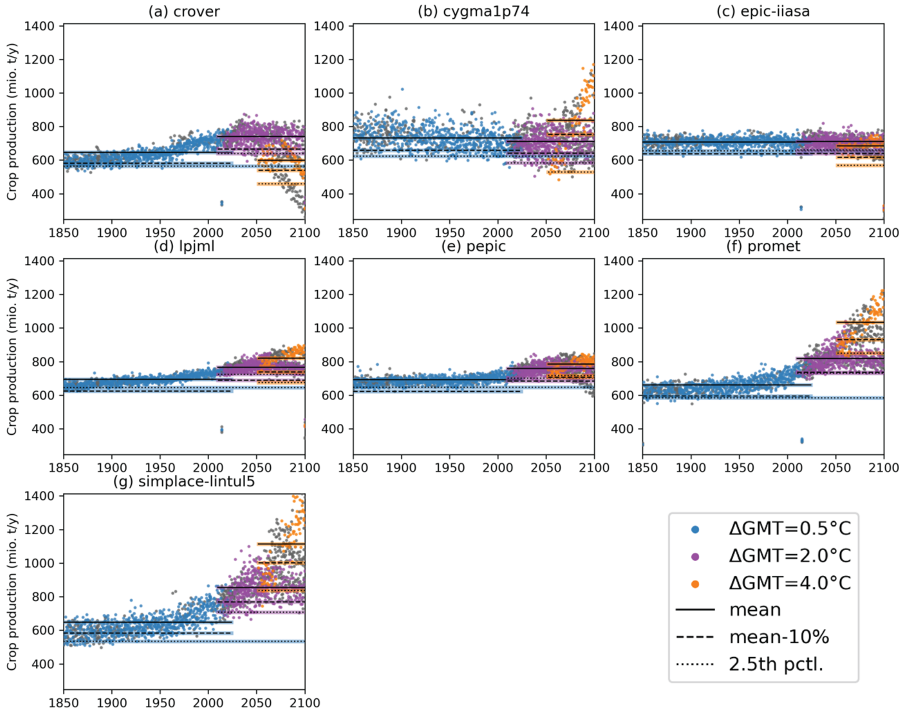

Figure C15 (wheat): same as Fig. C7 for wheat.

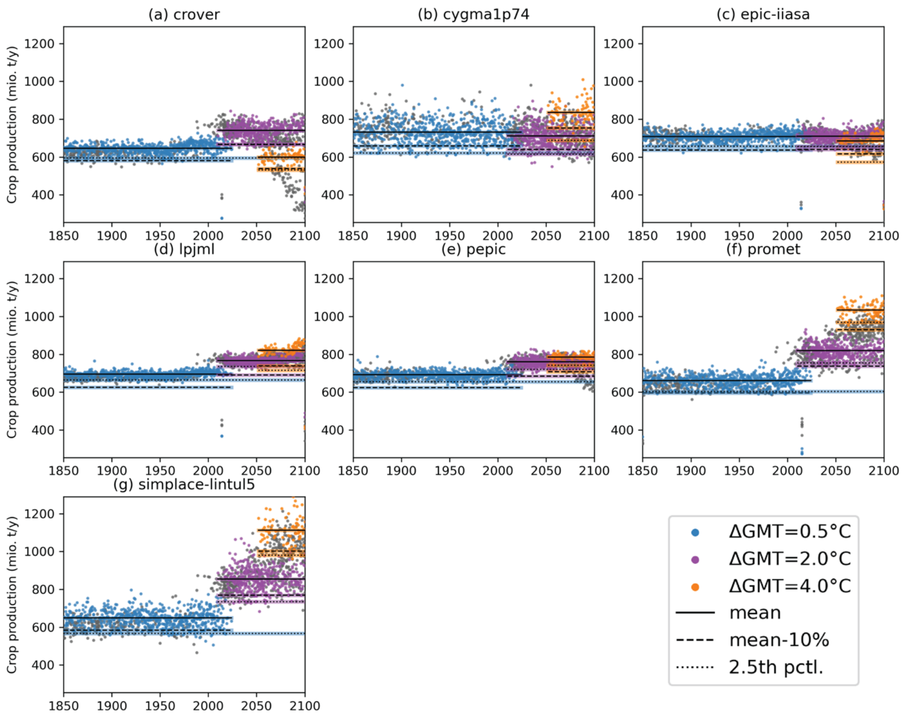

Figure C16 (wheat, detrended): same as Fig. C8 for wheat.

Maize production – relative deviation from historical mean production

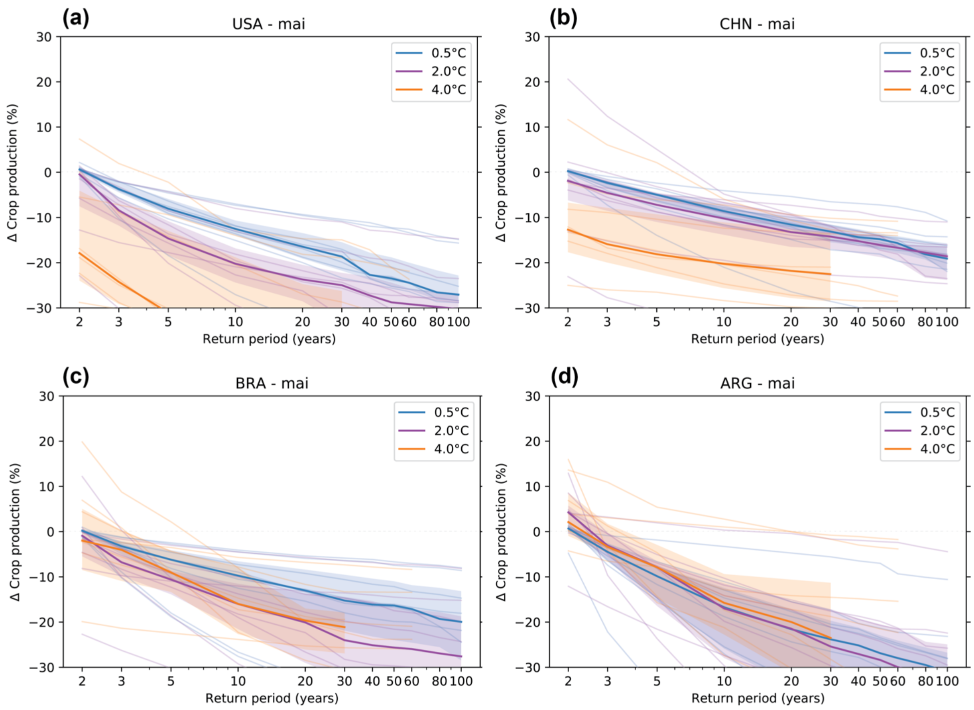

Figure C17: Country-level relative deviation of maize production from the historical mean for a global warming of 0.5° (historical reference bin, blue), 2°C (purple) and 4°C (orange) for the major maize producing countries USA (a), China (b), Brazil (c) and Argentina (d). Solid lines demarcate the multi-crop-model median, thin lines the individual crop models, and shading the inter-quartile range of the individual models.

Maize production – relative deviation from mean production

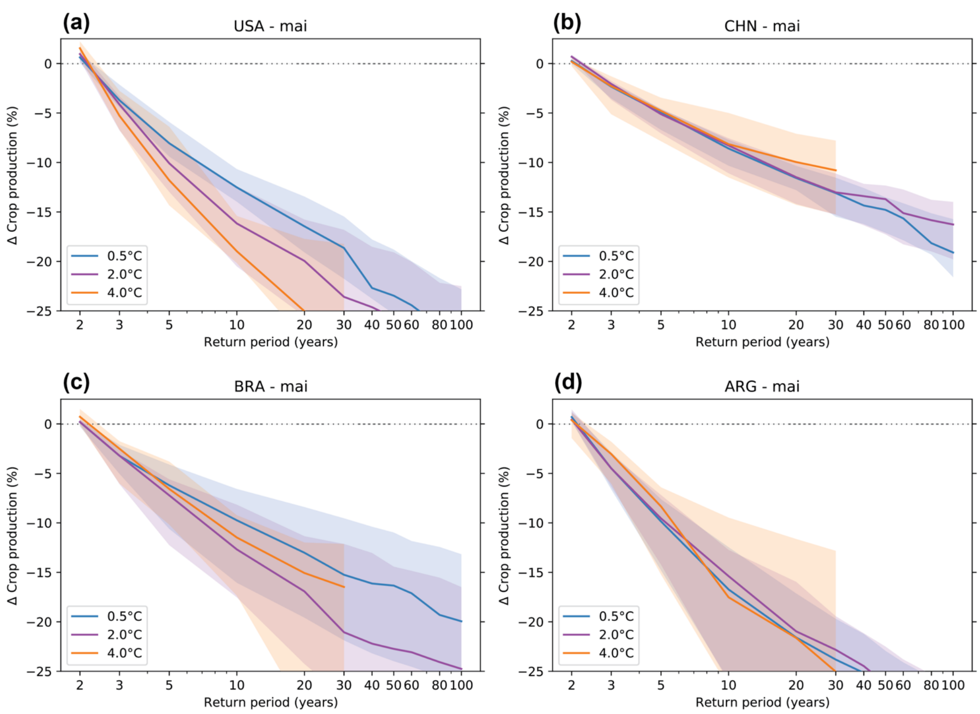

Figure C18: Country-level relative deviation of maize production from the mean within each global warming bin for 0.5° (blue), 2°C (purple) and 4°C (orange) for the major maize producing countries USA (a), China (b), Brazil (c) and Argentina (d). Solid lines demarcate the multi-crop-model median and shading the inter-quartile range of the individual models.

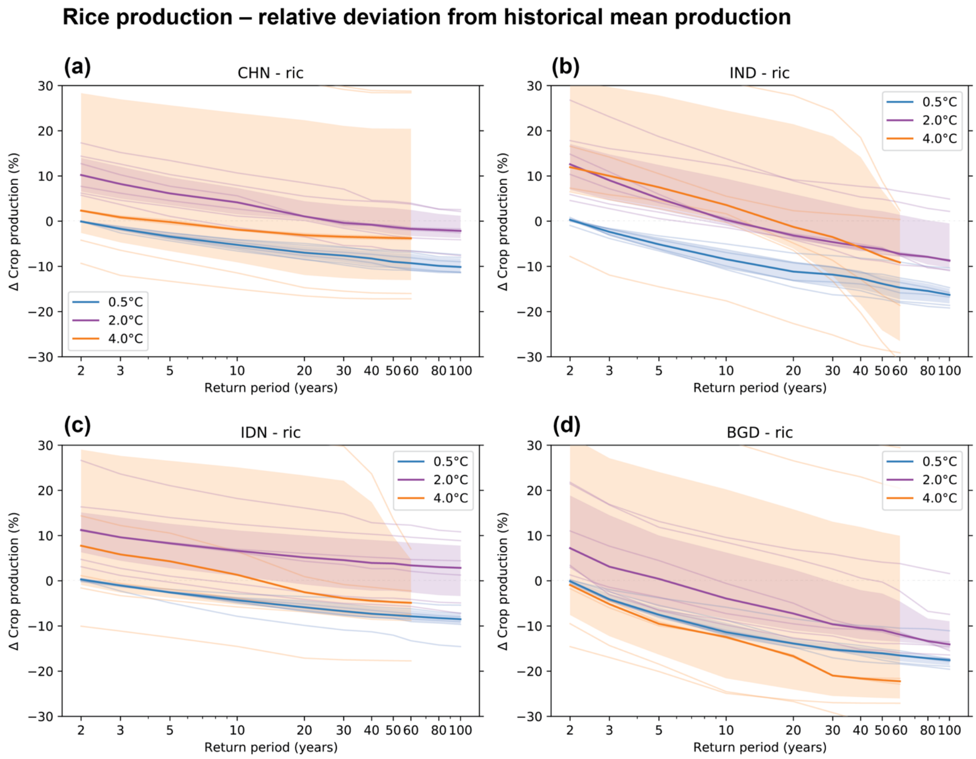

Figure C19: Country-level relative deviation of rice production from the historical mean for a global warming of 0.5° (historical reference bin, blue), 2°C (purple) and 4°C (orange) for the major rice producing countries China (a), India (b), Indonesia (c) and Bangladesh (d). Solid lines demarcate the multi-crop-model median, thin lines the individual crop models, and shading the inter-quartile range of the individual models.

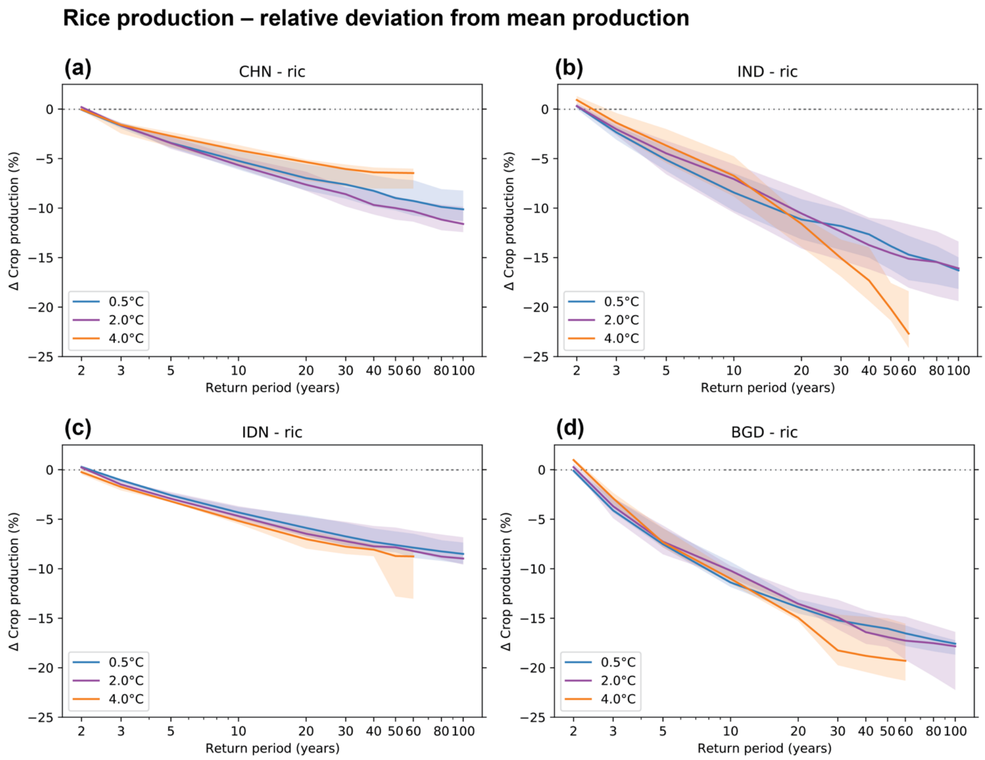

Figure C20: Country-level relative deviation of rice production from the mean within each global warming bin for 0.5° (blue), 2°C (purple) and 4°C (orange) for the major rice producing countries China (a), India (b), Indonesia (c) and Bangladesh (d). Solid lines demarcate the multi-crop-model median and shading the inter-quartile range of the individual models.

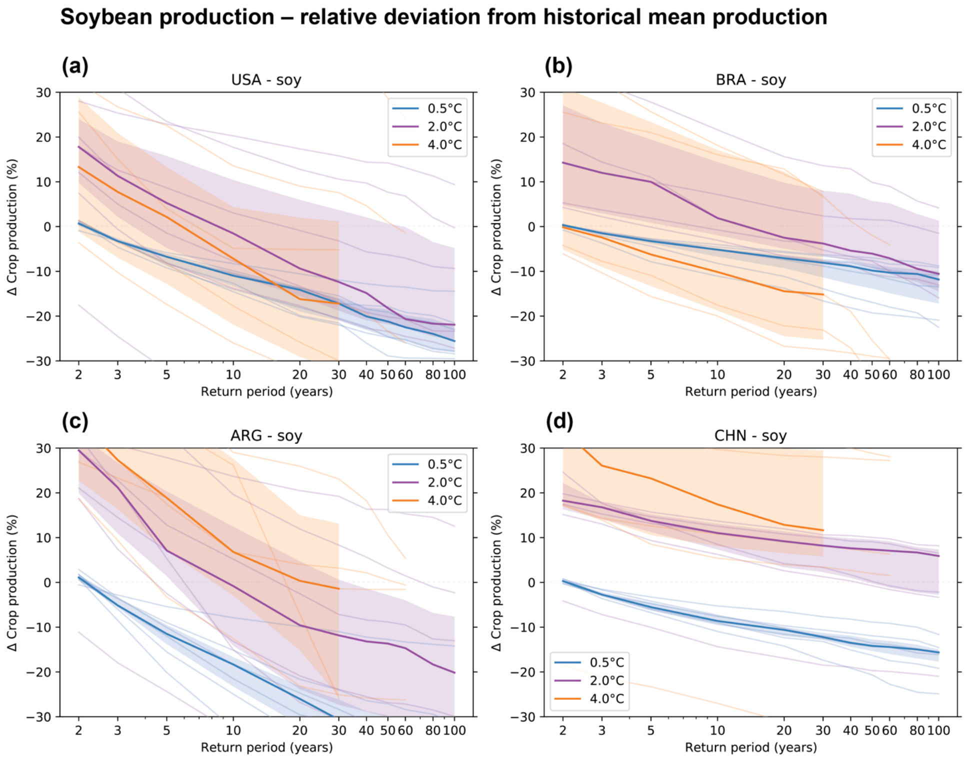

Figure C21: Country-level relative deviation of soybean production from the historical mean for a global warming of 0.5° (historical reference bin, blue), 2°C (purple) and 4°C (orange) for the major soybean producing countries USA (a), Brazil (b), Argentina (c) and China (d). Solid lines demarcate the multi-crop-model median, thin lines the individual crop models, and shading the inter-quartile range of the individual models.

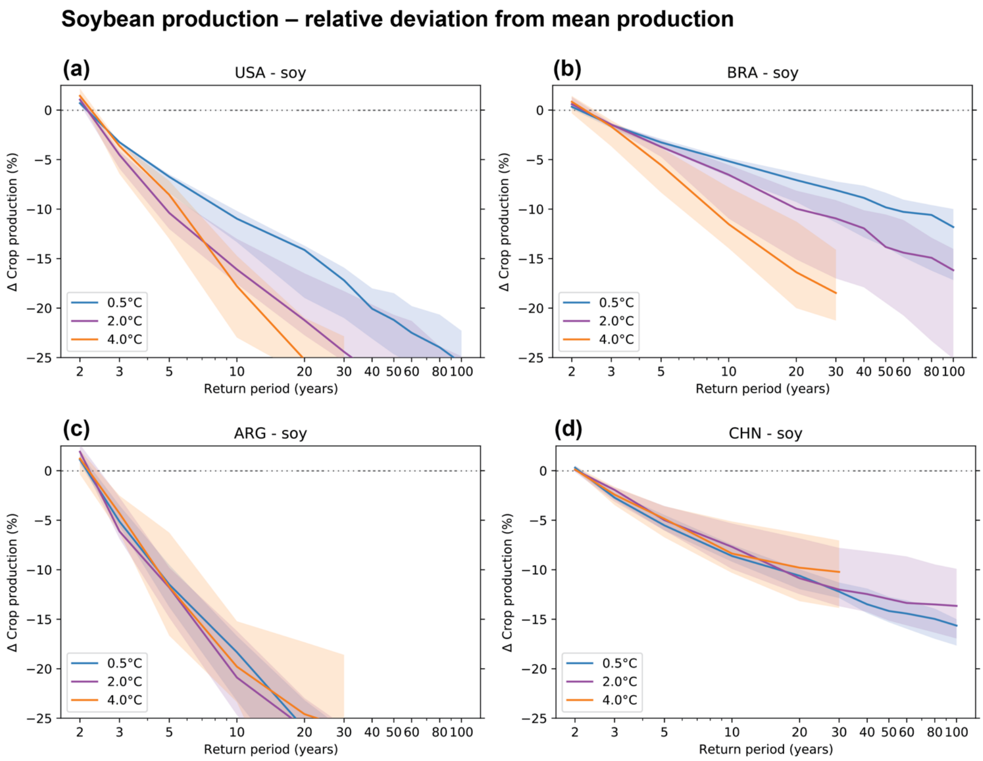

Figure C22: Country-level relative deviation of soybean production from the mean within each global warming bin for 0.5° (blue), 2°C (purple) and 4°C (orange) for the major soybean producing countries USA (a), Brazil (b), Argentina (c) and China (d). Solid lines demarcate the multi-crop-model median and shading the inter-quartile range of the individual models.

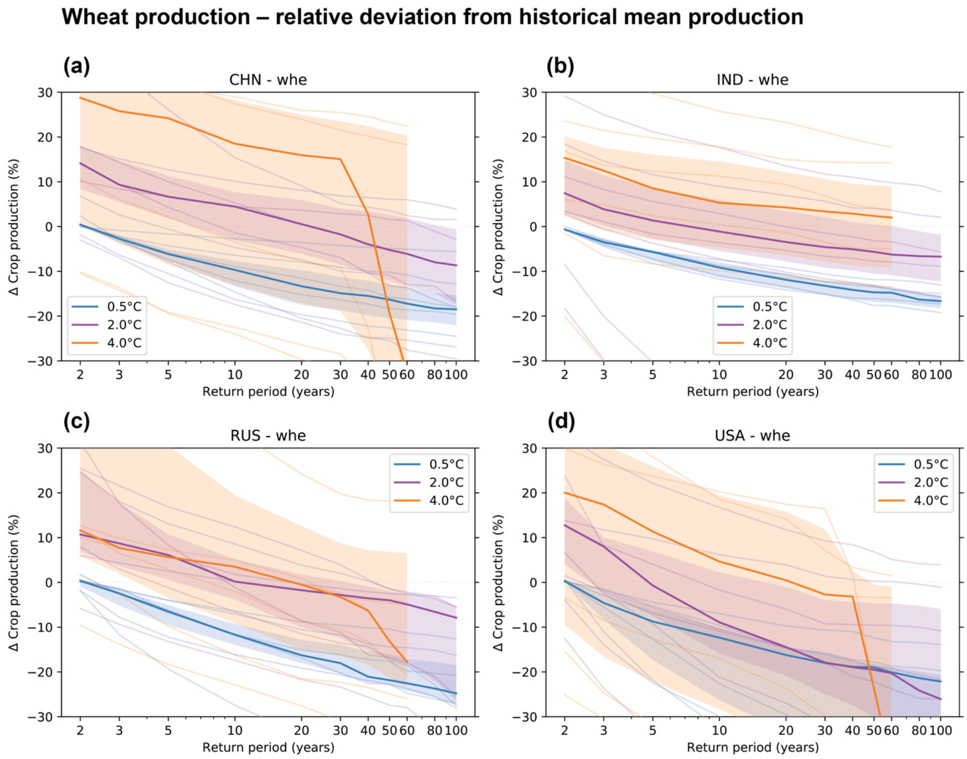

Figure C23: Country-level relative deviation of wheat production from the historical mean for a global warming of 0.5° (historical reference bin, blue), 2°C (purple) and 4°C (orange) for the major wheat producing countries China (a), India (b), Russia (c) and USA (d). Solid lines demarcate the multi-crop-model median, thin lines the individual crop models, and shading the inter-quartile range of the individual models.

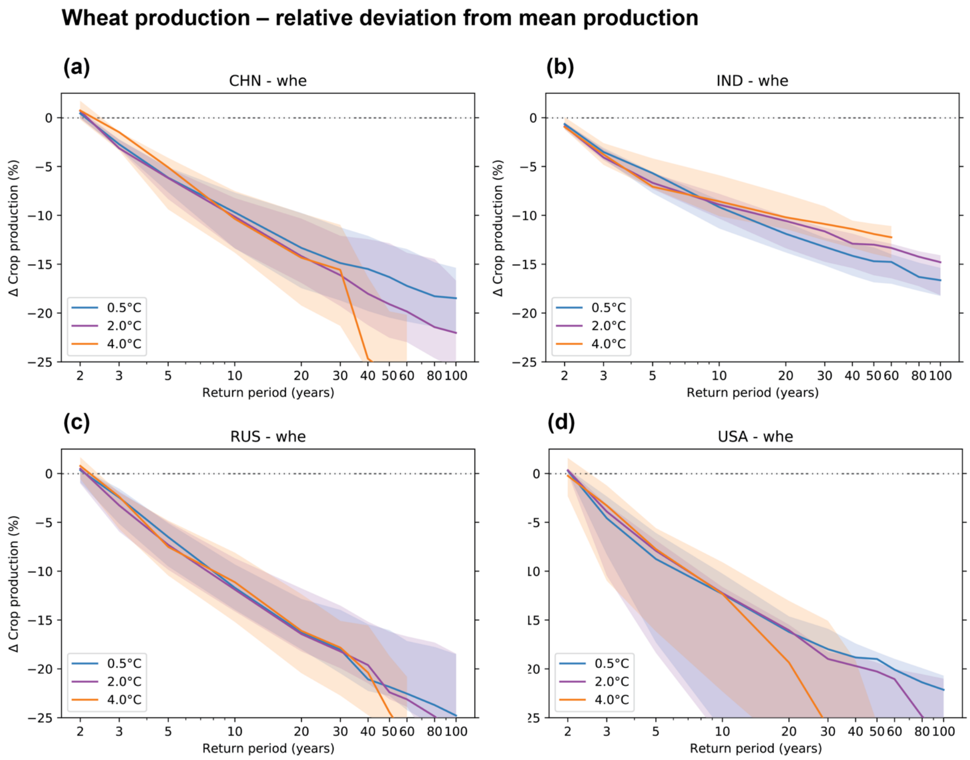

Figure C24: Country-level relative deviation of wheat production from the mean within each global warming bin for 0.5° (blue), 2°C (purple) and 4°C (orange) for the major wheat producing countries China (a), India (b), Russia (c) and USA (d). Solid lines demarcate the multi-crop-model median and shading the inter-quartile range of the individual models.

Author contributions

SE and CS developed and implemented the method collaboratively in exchange with JJ, WT, and DNB. Evaluation and visualization were carried out by SE. SE prepared the manuscript with contributions from all co-authors.

Code and data availability

The scripts reproducing the main results of the paper and the figures are available at https://github.com/sameberenz/climada_papers_crop_production_risk_isimip (Eberenz and Steinmann, 2021, http://doi.org/10.5281/zenodo.4549259). The CLIMADA repository (Aznar-Siguan and Bresch, 2019; Bresch and Aznar-Siguan, 2021; CLIMADA-Project, 2019) implemented in Python is openly available online at https://github.com/CLIMADA-project/climada_python (Bresch et al., 2020) under the GNU GPL license version 3 (Free Software Foundation, Inc., 2007). The repository includes the modules *relative_cropyield* (hazard) and *crop_production* (exposures) (CLIMADA v.1.5.1 and later) developed as part of this study. The documentation of CLIMADA is hosted on Read the Docs (https://climada-python.readthedocs.io/en/stable/), including a link to the interactive tutorial of CLIMADA.

Gridded output from crop models used as input for computing relative crop yield and baseline crop production have been (ISIMIP2) or will be (ISIMIP3) made available under a Creative Commons license via ISIMIP (ISIMIP, online, https://esg.pik-potsdam.de/search/isimip/).

Acknowledgements

This study would not have been possible without the GC6 ensemble of crop yield ensembles, which is the output of countless efforts in research, model development, and coordination by multiple research groups around the world. Therefore, we would like to thank everyone who contributed to GC6, especially Katja Frieler, Christoph Müller, Cynthia Rosenzweig, and our co-author Jonas Jägermeyr, for their groundbreaking work in fostering collaboration and a coordinated model intercomparison within the frameworks of GGCMI and ISIMIP; and to everyone else who contributed to the GC6 ensemble directly, especially Alex C. Ruane, Joshua Elliott, Juraj Balkovic, Babacar Faye, James A. Franke, Christian Folberth, Toshichika Iizumi, Nikolay Khabarov, Stefan Lange, Wenfeng Liu, Sara Minoli, Masashi Okada, Meridel Phillips, Oleksandr Mialyk, Elisabeth J. Moyer, Sam Rabin, Julia M. Schneider, Joep F. Schyns, Rastislav Skalsky, Tommaso Stella, Haynes Stephens, Heidi Webber, and Florian Zabel. For their valuable support and input, helping to shape and improve both method and manuscript, we are grateful to Thomas Röösli, David Bokern, Patric Kellermann, Stefan Lange, Christoph Müller, Katja Frieler, and Christopher Fairless.